

Springer Tracts in Advanced Robotics

Volume 40

Editors: Bruno Siciliano · Oussama Khatib · Frans Groen

Lionel Birglen, Thierry Laliberté,
Clément Gosselin

Underactuated Robotic Hands



Springer

Professor Bruno Siciliano, Dipartimento di Informatica e Sistemistica, Università di Napoli Federico II, Via Claudio 21, 80125 Napoli, Italy, E-mail: siciliano@unina.it

Professor Oussama Khatib, Robotics Laboratory, Department of Computer Science, Stanford University, Stanford, CA 94305-9010, USA, E-mail: khatib@cs.stanford.edu

Professor Frans Groen, Department of Computer Science, Universiteit van Amsterdam, Kruislaan 403, 1098 SJ Amsterdam, The Netherlands, E-mail: groen@science.uva.nl

Authors

Prof. Lionel Birglen
École Polytechnique de Montréal
Département de génie mécanique
P.O. Box 6079 Succ. Centre-Ville
Montréal, Québec,
H3C 3A7
Canada
Email: lionel.birglen@polymtl.ca

Prof. Clément Gosselin
Université Laval
Département de génie mécanique
Pavillon Adrien-Pouliot
1065 avenue de la médecine
Québec, Québec, G1V 0A6
Canada
Email: gosselin@gmc.ulaval.ca

Thierry Laliberté
Université Laval
Département de génie mécanique
Pavillon Adrien-Pouliot
1065 avenue de la médecine
Québec, Québec, G1V 0A6
Canada
Email: thierry@gmc.ulaval.ca

ISBN 978-3-540-77458-7

e-ISBN 978-3-540-77459-4

Springer Tracts in Advanced Robotics ISSN 1610-7438

Library of Congress Control Number: 2007941942

©2008 Springer-Verlag Berlin Heidelberg

This work is subject to copyright. All rights are reserved, whether the whole or part of the material is concerned, specifically the rights of translation, reprinting, reuse of illustrations, recitation, broadcasting, reproduction on microfilm or in any other way, and storage in data banks. Duplication of this publication or parts thereof is permitted only under the provisions of the German Copyright Law of September 9, 1965, in its current version, and permission for use must always be obtained from Springer. Violations are liable for prosecution under the German Copyright Law.

The use of general descriptive names, registered names, trademarks, etc. in this publication does not imply, even in the absence of a specific statement, that such names are exempt from the relevant protective laws and regulations and therefore free for general use.

Typesetting by the authors and Scientific Publishing Services Pvt. Ltd.

Printed in acid-free paper

5 4 3 2 1 0

springer.com

Editorial Advisory Board

Herman Bruyninckx, KU Leuven, Belgium
Raja Chatila, LAAS, France
Henrik Christensen, Georgia Institute of Technology, USA
Peter Corke, CSIRO, Australia
Paolo Dario, Scuola Superiore Sant'Anna Pisa, Italy
Rüdiger Dillmann, Universität Karlsruhe, Germany
Ken Goldberg, UC Berkeley, USA
John Hollerbach, University of Utah, USA
Makoto Kaneko, Osaka University, Japan
Lydia Kavraki, Rice University, USA
Sukhan Lee, Sungkyunkwan University, Korea
Tim Salcudean, University of British Columbia, Canada
Sebastian Thrun, Stanford University, USA
Yangsheng Xu, Chinese University of Hong Kong, PRC
Shin'ichi Yuta, Tsukuba University, Japan

STAR (Springer Tracts in Advanced Robotics) has been promoted under the auspices of EURON (European Robotics Research Network)



Preface

Research on underactuated robotic hands at Université Laval began in 1994 when Clément Gosselin received a grant from the *Institut de Recherche en Santé et Sécurité du Travail du Québec* (IRSST) to develop robotic grippers/hands with which robots would be capable of replacing human operators in hazardous tasks. Until then, the Robotics Laboratory at Université Laval had been focusing mainly on parallel robotic manipulators and the work on underactuated hands represented a new research thrust for the laboratory. In the early stages of this project, Clément Gosselin and Thierry Laliberté began to build cardboard models of underactuated fingers and soon realized their potential for robotic grasping. Indeed, it was clear that the gap between industrial robotic grippers and advanced fully actuated hands needed to be bridged and that underactuation was a promising avenue to reach this objective. The literature on underactuation provided the necessary inspiration. Among others, the pioneer work of Shimojima (Shimojima, Yamamoto, and Kawakita 1987), Hirose (Hirose and Umetani 1978) and Bartholet (Bartholet 1992) were the main catalysts in the inception of the first Laval designs and developments.

However, although it was soon discovered that the literature on underactuated hands included several clever designs, it was also evident that there was an open avenue for new research initiatives. Several other projects followed the IRSST research programme and a variety of prototypes were built at Laval University since 1996 until now. Most of these prototypes were designed by Thierry Laliberté and some of them are presented in Chapter 7 of this book. Funding for these research projects came from the *Natural Sciences and Engineering Research Council of Canada* (NSERC), *MacDonald Dettwiler and Associates* (MDA), the *Canadian Space Agency* (CSA), *Precarn Incorporated* and the *United Kingdom Atomic Energy Authority* (UKAEA). The authors are very grateful to all of these partners for their continued support and trust.

Concurrently with the development of the above mentioned prototypes, more fundamental research on underactuation and its application to robot hands was also performed at Laval. This book stems from Lionel Birglen's Ph.D. dissertation, which emphasized the theoretical aspects in the research on underactuated

fingers. The completion of this thesis work appeared to the authors as an appropriate moment to present the state of the art of the research completed at Laval and to consider it in the context of the international robotics community.

The research on underactuated hands completed in the Robotics Laboratory at Université Laval over the last decade is the result of the work of several individuals. The authors are gratefully acknowledging their valuable contribution to the knowledge and expertise that made this book possible. These individuals include several students and researchers, namely, Sylvain Lemieux, Éric Dégou lange, Serge Montambault, Laura Sie, Mathieu Myrand, Bruno Massa, François Deschênes, Jean-Philippe Jobin, Frédéric Pelletier and Éric Boudreault as well as Jean-Claude Gariépy, the machinist who built most of the prototypes.

Several laboratories around the world are currently very active in the area of underactuated hands. New fundamental results are published regularly and new designs are revealed. Several open issues may need significant work before they can be resolved satisfactorily. It is therefore expected that research in the area will continue to grow. To the best of the authors' knowledge, this book is the first one to specifically address the topic of underactuated robotic hands. As such, it represents a first attempt at crystallizing a body of knowledge that has so far been disseminated through publications and patents. Consequently, this monograph does not claim to present a complete picture of the research on the topic. It is rather intended as a first step in formalizing the most important research issues pertaining to underactuated hands. It is hoped that this book will be useful to many researchers and students and that it will be followed by others.

Lionel Birglen
Thierry Laliberté
Clément Gosselin

Note: some of the material presented in this book originally appeared in journal and conference publications by the authors over the last twelve years. These papers include:

- Birglen, L. and C. Gosselin (2003, September). On the force capabilities of underactuated fingers. In *Proceedings of the 2003 IEEE International Conference on Robotics and Automation*, Taipei, Taiwan, pp.1139-1145.
- Birglen, L. and C. Gosselin (2004, April). Kinetostatic analysis of underactuated fingers. *IEEE Transactions on Robotics and Automation* 20 (2), 211-221.
- Birglen, L. and C. Gosselin (2005, April). Fuzzy enhanced control of an underactuated finger using tactile and position sensors. In *Proceedings of the 2005 IEEE International Conference on Robotics and Automation*, Barcelona, Spain, pp. 2331-2336.
- Birglen, L. and C. Gosselin (2006, March). Geometric design of three-phalanx underactuated fingers. *ASME Journal of Mechanical Design* 128 (2), 356-364.
- Birglen, L. and C. Gosselin (2006, September). Optimally unstable underactuated gripper: Synthesis and applications. In *2006 ASME International Design Engineering Technical Conferences*, Philadelphia, PA, USA.

The authors would like to thank the ASME and the IEEE for granting them permission to reproduce this material.

Foreword

At the dawn of the new millennium, robotics is undergoing a major transformation in scope and dimension. From a largely dominant industrial focus, robotics is rapidly expanding into the challenges of unstructured environments. Interacting with, assisting, serving, and exploring with humans, the emerging robots will increasingly touch people and their lives.

The goal of the new series of Springer Tracts in Advanced Robotics (STAR) is to bring, in a timely fashion, the latest advances and developments in robotics on the basis of their significance and quality. It is our hope that the wider dissemination of research developments will stimulate more exchanges and collaborations among the research community and contribute to further advancement of this rapidly growing field.

The monograph written by Lionel Birglen, Thierry Laliberté and Clément Gosselin is the outcome of a decade of work by the authors and stems from the doctoral thesis of the first author. Underactuation is recognised as a promising avenue to bridge the gap between traditional industrial robotic grippers and advanced fully actuated hands.

The main contribution of this book is the theoretical analysis of underactuated hands with a particular interest in the distribution of the forces. The pursued approach can be used for a wide range of devices, e.g., compliant fingers, snake-like robots, tentacle manipulators, and others. A solid grasp stability analysis is developed which allows understanding the influence of the design parameters and the contact properties for a number of typical two- and three-phalanx fingers. The principle of underactuation is extended from the fingers to the hand itself, leading to the minimalist design of a mechanical architecture of robotic hands with a large number of degrees-of-freedom, driven by only one actuator. Remarkably, the theoretical work is supported by the mechanical design of actual prototypes, for which outstanding results have been obtained with a simple controller.

The STAR series is proud to welcome the first focused book on underactuated hands in the international literature!

Naples, Italy
October 2007

Bruno Siciliano
STAR Editor

Contents

1	Introduction	1
1.1	Underactuation	1
1.2	Contributions of the Book	2
1.3	Overview of the Book	4
2	Grasping vs. Manipulating	7
2.1	Robotic Hands: Aims and Functions	7
2.2	Underactuation in Robotic Hands	13
2.2.1	Underactuation as a Solution to Grasping	13
2.2.2	Literature Review	17
3	Kinetostatic Analysis of Robotic Fingers	33
3.1	Introduction	33
3.2	General Static Model	34
3.3	Computation of the Transmission Matrix	41
3.4	Expressions of the Contact Forces	43
3.5	Positive Definiteness of the Forces	44
3.6	Other Transmission Mechanisms	50
3.6.1	Double-Stage Mechanism	50
3.6.2	Tendon-Pulley Transmission	51
3.6.3	Gears	54
3.6.4	Da Vinci's Mechanism	55
3.6.5	Comparison	58
3.7	Less-than- n -phalanx Grasps	59
3.8	Conclusions	59
4	Grasp Stability of Underactuated Fingers	61
4.1	Introduction	61
4.2	Grasp Stability of Two-Phalanx Underactuated Fingers	63
4.2.1	Grasp Stability for Single Point Contact	63
4.2.2	Contact Trajectories	70
4.2.3	Equation of the Equilibrium Point	77

4.2.4	Linear and Circular Contact	82
4.2.5	Application: Synthesis of an Optimally Unstable Finger	89
4.2.6	Application: Design Validation	95
4.2.7	On the Grasp-State Plane Necessity	96
4.3	Grasp Stability of Three-Phalanx Underactuated Fingers	98
4.3.1	Three-Phalanx Underactuated Fingers Ejection Theory	98
4.3.2	Loss of One Contact	102
4.3.3	Degeneracy Analysis	108
4.3.4	On the Validation Surfaces	112
4.3.5	Loss of Two Contacts	113
4.4	Conclusions	114
5	Optimal Design of Underactuated Fingers	117
5.1	Introduction	117
5.2	Optimal Design of Two-Phalanx Underactuated Fingers	118
5.2.1	Force Properties and Ejection	118
5.2.2	Force Isotropic Design	121
5.2.3	Guidelines to Prevent Ejection	125
5.3	Optimal Design of Three-Phalanx Underactuated Fingers	130
5.3.1	Force Properties and Ejection	130
5.3.2	Dimensional Analysis	132
5.3.3	Grasp-Stability Analysis	136
5.4	Conclusions	137
6	Underactuation between the Fingers	139
6.1	Introduction	139
6.2	Design Solutions	140
6.2.1	Movable Pulley	140
6.2.2	Seesaw Mechanism	143
6.2.3	Fluidic T-Pipe	144
6.2.4	Planetary and Bevel Gear Differentials	146
6.3	Combining Multiple Stages	148
6.3.1	Transmission Tree Analysis	148
6.3.2	Performance Evaluation of the Transmission Tree	154
6.4	Exchanging Inputs and Outputs	155
6.5	Applications	156
6.5.1	Underactuated Gripper	156
6.5.2	Multiple Pulley Routing	160
6.5.3	Serial Routing	162
6.5.4	Symmetrical Routing	164
6.6	Other Transmission Solutions	165
6.6.1	The Floating Platform	165
6.6.2	The Spring-Loaded Slider	166
6.7	Conclusions	168

7	Design and Control of the Laval Underactuated Hands	171
7.1	Introduction	171
7.2	Design of Laval Underactuated Hands	172
7.2.1	Location and Orientation of the Fingers	172
7.2.2	Pinch Grasp Mechanism	175
7.2.3	The MARS Hand	177
7.2.4	The SARAH Hands	178
7.3	Control and Experimentation of the Laval Underactuated Hands	190
7.3.1	Hybrid Control of the MARS Hand	190
7.3.2	Force Control of the MARS Hand	194
7.3.3	Control of the SARAH hands	206
7.4	Conclusions	207
8	Conclusion	209
8.1	Summary and Contributions of the Book	209
8.2	Perspectives	211
A	Mathematical Proofs	215
A.1	Influence of the Base Joint Spring	215
A.2	Influence of k_1	216
A.3	Relationship between Proximal and Intermediate Forces	218
A.4	Transmission Tree Formulae	218
A.4.1	Serial Transmission Tree	218
A.4.2	Symmetrical Transmission Tree	221
References		227
Index		237

1 Introduction

Mais que ne fait point la main? [...] cet organe extraordinaire en quoi réside presque toute la puissance de l'humanité, et par quoi elle s'oppose si curieusement à la nature, de laquelle cependant elle procède.

But what does the hand not do? [...] this extraordinary organ in which resides almost all the power of human kind, and through which the latter so peculiarly opposes nature, from which it nevertheless proceeds.

Paul Valéry, *Discours aux chirurgiens*, 1938.

in which the aim of the book is stated. Underactuation as a general concept is put into perspective with its application to grasping. Thereupon, the main results of the book are presented and, finally, an overview of the structure of this document is proposed.

1.1 Underactuation

Underactuation is a widely used and a relatively old concept in robotics. Basically, it expresses the property of a system to have an input vector of smaller dimension than the output vector. Practically, in robotics, it means having fewer actuators than degrees of freedom (DOF). Applying this concept to robotic grasping arises from a simple fact: it is desirable to be able to grasp objects using a simple control rather than having to command and coordinate several actions. The idea behind underactuation in grasping is to use an ingenious mechanical system that can adapt to the shape of the object automatically. This mechanical intelligence, embedded in the hand, is based on the principle of differential systems. The latter devices automatically distribute one input to several outputs, the ratio between the different outputs being determined by the design parameters and the output states themselves. The same philosophy of intelligent design is commonly found in mechanical linkages where the different link lengths

and joint types are determined at the design stage in order to follow a particular trajectory. If this trajectory is entirely predetermined, then only one DOF suffices to follow it. Yet, if this trajectory is too complex, a multi-DOF mechanism capable of following any trajectory is often chosen. Similarly, in robotic grasping, anthropomorphic hands have been predominant for years in research laboratories while industrial needs were often satisfied by a few simple grippers. The postulate behind the use of underactuation in grasping can be stated as follows: if the task to be performed is grasping, it should be possible to accomplish this one action using one single actuator.

Several—and yet not that many—underactuated hands were built around the world during the past three decades. However, little attention has been paid to the fundamental behaviour of such devices as well as to their characteristics. For instance, to the best of the authors' knowledge, their grasping stability has never been thoroughly studied. Indeed, little is known about these systems and research initiatives addressing theoretical issues are rare exceptions.

This book is an attempt to lay the foundations of underactuated grasping theory, to provide dedicated tools, and to shed some light on peculiar and previously unexplained behaviour. Like any first attempt, this work is by far not exhaustive and as the new theory will be developed, the limitations of our knowledge will clearly appear. Yet, significant progress has been made with many open problems remaining to be explored in the future. This book is an instantaneous snapshot of the work performed by the authors over the past twelve years.

1.2 Contributions of the Book

The main contribution of this book is the theoretical analysis of underactuated hands with a particular interest in the distribution of the forces. Two matrices obtained respectively with screw theory and mechanical transmission analysis are defined that completely describe the contact forces generated by a robotic finger—even fully actuated—with an arbitrary number of phalanges. Thus, the proposed approach can be used for a wide range of devices, e.g., compliant fingers, snake-like robots, tentacle manipulators, and others. Although, in this book the focus is placed on underactuated fingers with a limited number of phalanges, the results presented only correspond to a special case of the theory. The aforementioned two matrices, referred to as \mathbf{J} for the Jacobian and \mathbf{T} for the Transmission matrix are very simple and yet very powerful. Their analytical form is established, allowing to obtain the exact analytical expressions of the contact forces. Several indices are proposed to compare the performances of underactuated fingers driven by arbitrary types of mechanisms and having an arbitrary number of phalanges. Examples are given in the case of two- and three-phalanx fingers driven either by linkages, pulleys, or gears.

One key issue in the analysis of underactuated fingers and hands is stability. The latter can be studied based on the determination of the contact forces on the different phalanges. When computing these forces using a static model, some contact forces generated by underactuated fingers can sometimes become

negative—pulling on the object, which is clearly impossible. Although negative contact forces do not have a physical meaning, this concept is useful in the kinetostatic analysis of the fingers. The important question that arises then is the determination of the phenomena that occur when one or more phalanges do not exert any forces on the object. The answer to this question leads to the next contribution of the book: a grasp stability analysis based on a grasp-state space where contact trajectories and equilibrium or unstable surfaces can be visualized and analyzed. This grasp-state space is presented, along with typical results, for common two- and three-phalanx fingers. Unstable designs and peculiar equilibrium configurations are discussed. The influence of the design parameters and the contact properties on the grasp-state space is studied in order to allow an accurate modelling of complex situations.

The above mentioned formulation is then used for the optimal design of underactuated two- and three-phalanx fingers. Two issues are considered, namely the contact force distribution of the grasp and the overall grasp stability of the finger. In the past, the design of underactuated fingers has been driven mainly by the intuition of the designer, leading to very good designs in some cases but to poor results in others. The rules presented in this chapter ensure the optimality of the design with respect to the grasping characteristics. With two-phalanx fingers, the latter are well-known and well-described allowing a thorough analysis of the optimization problem. On the other hand, with three-phalanx fingers, the complexity of the equations of both the contact forces and grasp-state space elements does not yet allow the derivation of similar results. However, two approaches are proposed to obtain design parameters based on either a performance index composed of several sub-indices or a grasp-stability analysis.

From the optimal design of underactuated fingers, a methodology is then proposed for the analysis of the force capabilities of common differential mechanisms used to extend the principle of underactuation from the fingers to the hand itself. This approach leads to a mechanical architecture of robotic hands with a large number of DOF, driven by only one actuator. In the first part of Chapter 6, several differential elements—most noticeably used in robotic hands to provide underactuation between a certain number of fingers—are presented. A simple matrix formulation is developed to obtain the relationship between the actuation and output forces of the devices. Then, a mathematical method to obtain the output force capabilities of connected differential mechanisms is presented. The mathematical expressions of the transmission tree characterizing the underactuated system considered are fundamentally different from the Transmission matrix arising when one considers underactuation in the fingers instead of between them.

Finally, the last contribution of this book consists in addressing the mechanical design and control of actual prototypes. The design of some of the underactuated hands developed at Université Laval is presented in Chapter 7. To increase the range of possible grasps, a parallel precision pinch mechanism is added to the fingers. This mechanism keeps the distal phalanx of the fingers perpendicular

to the palm, thereby allowing pinch grasps. During power grasps, this mechanism is automatically disengaged without any controller or sensor to properly envelop the object seized. Therefore, for most applications these prototypes lead to outstanding results with a very simple control scheme. If a more precise force control is required, tactile sensors can be used. It can be observed that promising experiments have been conducted and that the behaviour of underactuated fingers can be enhanced using tactile information. Underactuated hands may even be a predilection type of hands for the use of tactile sensing since the simplicity of the initial controller leaves significant computation time available to process the tactile data in real-time. Experimental force control is implemented using a fuzzy logic controller and prevention of slippage is built on top of the basic controller.

1.3 Overview of the Book

In Chapter 2, a fundamental dilemma in robotic prehension—particularly apparent with underactuated devices—is discussed and a brief state of the art is given for both fully-actuated and underactuated robotic hands. It is shown that underactuation has been known for—literally—hundreds of years! Nevertheless, even today, patents are filed that claim to have invented the most common architectures. In the robotics community, underactuation in grasping has only recently been brought under the spotlight. Prior to that, the development of fully actuated anthropomorphic hands overshadowed the progress made with underactuated hands, and only the failure of the former to achieve commercial and practical success allowed the revival of research on underactuation. Chapter 3 presents and analyzes the force capabilities of any robotic finger, based on the introduction of two new matrices. According to the results of this chapter, it can be shown that under certain conditions, some phalanx forces may become negative, implying a loss of contact. This loss of contact is acknowledged and formalized in the book. This fundamental drawback may come as a surprise, even for researchers dealing with underactuated prototypes. Yet, this crucial phenomenon can lead to unstable grasps with a finger sliding along the object and ejecting the latter. It is therefore of the utmost importance to understand and to prevent such degeneration of the grasp. It is futile and of little use to build a finger that can adapt to the shape of the object seized if it can never actually grasp it.

Furthermore, it is shown in Chapter 4 that it is actually *impossible* to design a two-phalanx underactuated finger that will not exhibit any ejection in its whole workspace. In this chapter, the sliding motion of two-phalanx fingers is analyzed and the influence of the design parameters as well as contact properties is presented with two- and three-phalanx underactuated fingers. Despite the impossibility of designing a two-phalanx underactuated finger that is ejection-free in its whole workspace, it is shown in Chapter 5 that under certain reasonable assumptions, one can design fingers that will never lead to ejection in parts of their workspace. These parts might even correspond to the commonly used workspace

of the finger, for all practical purposes. Therefore, practical and useful rules to ensure the grasp stability are discussed. The ejection theory is then extended to the three-phalanx case. However, it is shown that adding one phalanx to an underactuated finger yields a substantial increase in the complexity of the analysis. Nevertheless, significant breakthroughs are presented that make the analysis of such fingers possible.

In Chapter 6 a methodology is proposed for the analysis of the force capabilities of mechanisms used to extend the principle of underactuation from the fingers to the hand itself. This extension opens the avenue for multi-DOF robotic hands with several fingers that are driven by a single actuator.

Finally, the design and control of several prototypes of underactuated hands developed at Université Laval is presented in Chapter 7. While the first six chapters of the book address mainly theoretical issues, this last chapter presents practical contributions that naturally complement the results of the first chapters. The material introduced in Chapter 7 may be of great value to designers and may help the reader to apply the theory exposed in the first chapters of the book.

2 Grasping vs. Manipulating

Finger-wise, boll-wise. Jes' move along talkin', an' maybe singin' till the bag gets heavy. Fingers go right to it. Fingers know. Eyes see the work—and don't see it.

John Steinbeck, *The Grapes of Wrath*, 1939.

in which an introduction to the state of the art robotic hands is presented with a particular emphasis placed on the grasping/manipulating dilemma. Several characteristics of the best known robotic hands are presented and discussed. Common issues on grasping and manipulation are reviewed as well as different solutions proposed in the literature. Finally, the concept of underactuation in robotic fingers, a powerful and “novel” technique—leading to shape adaptation through the use of ingenious designs—is introduced to conclude this chapter.

2.1 Robotic Hands: Aims and Functions

grasp. *Function: verb. Etymology: Middle English grasper. Intransitive senses: to make the motion of seizing: clutch. Transitive senses, 1: to take or seize eagerly, 2: to clasp or embrace especially with the fingers or arms, 3: to lay hold of with the mind.*

manipulate. *Function: transitive verb. Etymology: back-formation from manipulation, from French, from manipuler to handle an apparatus in chemistry, ultimately from Latin manipulus. 1: to treat or operate with the hands or by mechanical means especially in a skillful manner, 2a: to manage or utilize skillfully, b: to control or play upon by artful, unfair, or insidious means especially to one's own advantage, 3: to change by artful or unfair means so as to serve one's purpose.*

Merriam Webster's Collegiate Dictionary, tenth edition, 2000.

In this chapter, an introduction to the current state of the art of robotic hands and some background on the grasping/manipulation theory is proposed. Most robots are nowadays based on a serial architecture with six or seven axes that allow them to perform numerous tasks such as pick-and-place, camera inspection, or assembly. These robots can work in hazardous and/or hostile environments without putting human lives in jeopardy. Nevertheless, the dexterity of robots, i.e., their ability to perform highly precise operations with visual/perceptual/tactile feedback, has always been clearly more limited than that of a well-trained human being. To overcome this limitation, numerous research initiatives have been conducted in the past to create robotic end-effectors that can match the human hand in terms of performance and versatility. These devices have been referred to as *robotic hands* and many research laboratories around the world have developed prototypes of such hands as early as in the mid 1980's when the foundations of these studies were laid (Mason and Salisbury 1985). However, the idea of copying the human hand is actually much older and may be contemporary of the first automata in the 18th century, e.g., *La Musicienne* of the inventor Jacquet-Droz (Rosheim 1994). This automate was able to play a wide variety of organ partitions with two five-finger hands actuated with steel cables connected to a programming cam shaft. More recent developments followed the first telemanipulators of the Argonne Laboratory, dedicated to nuclear material handling (Goertz 1952). This laboratory developed several mechanical gripping devices, or grippers, mostly based on a pinching motion of the jaws. However, each gripper was developed for a specific task, a drawback that still burdens the design of modern mechanical grippers.

It is clear that the adaptability of the human hand can be thought of as the *Holy Grail* of robotic end-effectors. The first robot hand, as it is commonly referred to, was perhaps the end-effector of the *Handyman*, a robot developed by Ralph Mosher for General Electric in 1960 (Mosher 1960). This hand included only two fingers similarly to the then usual grippers (Chen 1982), but each finger had three degrees of freedom (DOF) and a wrist providing two additional DOF directly controlled by the operator. Around 1969, the first research projects on robotic hands with three fingers including a "thumb" in opposition—hence an anthropomorphic design—began in the United States and in Japan.

In this book, a robotic hand refers to a particular type of end-effector with an anthropomorphic inspiration. By contrast, robotic grippers have a simpler design and are much less versatile with respect to the variety of tasks that they can perform. However, the distinction between these definitions remains rather vague and depends mostly on the authors. To match the performance of the human hand is a formidable challenge. Indeed, the latter includes more than 19 muscles, 17 joints, 19 bones, not counting ligaments, nerves, and thousands of various sensors (Tubiana and Thomine 1990). Pioneer designs of robotic hands include: the Okada hand (Okada 1982), the Stanford/JPL (Salisbury's) hand (Salisbury and Craig 1982), the Utah/MIT hand (Jacobsen et al. 1986), the BarrettHand (Ulrich 1988), the Belgrade/USC hand (Rakic 1989), the AMADEUS hand (Lane et al. 1997), the hands of Karlsruhe University (Fischer and Woern 1998;

Table 2.1. Characteristics of some robotic hands

Name	Fingers	DOF	Drive	Underactuated	Fig.
AMADEUS	3	n. a.	hydraulic	Y	2.8(c)
ASI Gripper	3	3	mechanical	N	2.2(b)
BarrettHand BH8	3	7	mechanical	Y	2.7(a)
Belgrade/USC	5	6	mechanical	Y	2.7(c)
Bologna University	3	10	tendons	N	2.1(a)
DLR Hand 1	4	12	mechanical	N	2.1(g)
DLR Hand 2	4	13	mechanical	N	2.1(h)
Goldfinger	4	12	mechanical	N	2.2(a)
HIT/DLR Hand	4	13	mechanical	N	2.1(i)
Karlsruhe Hand 2	4	12	mechanical	N	-
Karlsruhe RC	5	n. a.	fluid	Y	2.8(a)
LMS	4	16	tendons	N	2.1(e)
MARS	3	12	mechanical	Y	2.7(d)
NASA Robonaut	4	12	tendons	N	2.1(d)
Okada	3	11	tendons	N	-
Omni-Hand	3	n. a.	mechanical	N	2.1(c)
RTR Hand 1	3	6	mechanical	N	2.6(a)
RTR Hand 2	3	9	tendons	Y	2.6(b)
Salisbury	3	9	tendons	N	2.1(b)
SARAH	3	10	mechanical	Y	2.7(e)
Shadow C3 Hand	5	24	pneumatic	N	2.1(f)
Soft Gripper 1	2	10	tendons	Y	2.6(d)
Soft Gripper 3	3	10	tendons	Y	2.6(e)
SPRING Hand	3	8	tendons	Y	2.6(c)
Utah/MIT	4	16	tendons	N	-

Schulz et al. 2001), the hands from DLR (Liu et al. 1998; Butterfass et al. 2001; Jiang et al. 2003), the chopstick (!) hand of the MEL (Tanikawa and Arai 1999), the LAR-DEIS hands (Biagiotti et al. 2001), the LMS hand (Gazeau et al. 2001), the hand from the University of Beijing (Zhang et al. 2001), NASA's Johnson Space Center Robonaut hand (Diftler and Ambrose 2001), and the Gifu Hand II

(Kawasaki et al. 2002). A brief summary is presented in Table 2.1, and then-exhaustive lists can be found in (Kato 1982; Reynaerts 1995).

It was pointed out in the literature (Ceccarelli 2001) that the research on robotic hands has recently come to a crossroad. Indeed, several papers proposed to reorient the research in the field to overcome the difficulties encountered and to establish new research directions (Paulos 1998; Bicchi and Kumar 2000). Until very recently, most prototypes aimed at emulating the human hand, using mostly tendons. However, only one of these hands was successfully commercialized. This lack of success, mainly due to the cost of complex architectures including a plethora of actuators and sensors, raised questions about the relevance of the human mimetism approach (Bicchi 2000). Also, it should be noted that complex hands may lead to poor grasping performances due to a demanding control. In fact, although a gripper is generally unable to manipulate an object, it is very effective for grasping. This is what is referred to here as the “grasping vs. manipulating” dilemma, i.e., a device intended for grasping is generally unable to manipulate while a device designed for manipulation usually performs poorly in grasping. Indeed, complex robotic hands while capable of efficient grasping are overdesigned for this task and suffer from high costs and overall lack of robustness. Grasping is defined as the property of a system to prevent motion of an object while manipulating is defined as the capability of a system to control the position and orientation of an object.

Many of the existing prototypes of robotic hands use tendons to propagate the actuation to the joints. This approach tends to enhance the compactness of the devices as well as to imitate the human muscular principles. However, it presents an important drawback, namely the uni-directionality of the actuation. Indeed, a tendon can only pull, not push, therefore $2n$ actuators are theoretically required to control n DOFs, as for the Utah/MIT Hand. The control architecture required becomes very complicated and costly. Passive return systems can be adopted to reduce the number of actuators. In fact, it was established (Mason and Salisbury 1985) that the number of actuators can be reduced to $n + 1$ to control n DOFs with tendons, as in Salisbury’s Hand. Furthermore, tendon transmissions are limited to small forces and exhibit large internal friction. These major drawbacks have slowly but surely reduced the predominance of tendon drives in fully actuated hands. Recently, linkage and gear transmissions attracted the attention of laboratories, because of two important advances, namely, the miniaturization of electric motors and sensor systems (e.g. in the DLR Hands), and a new concept of mechanical design: underactuation (e.g. in the SARAH Hands). The latter principle consists in using fewer actuators than the number of DOFs in the system while passive mechanical devices—usually springs and mechanical limits—allow to fully constrain the hand. Mechanisms can be categorized in three classes with respect to the number of their DOF (n_{dof}) relatively to the number of actuators (n_{act}):

- fully actuated mechanisms: $n_{dof} = n_{act}$;
- redundantly actuated mechanisms: $n_{dof} < n_{act}$;
- underactuated mechanisms: $n_{dof} > n_{act}$.

The number of actuators is sometimes referred to as the degree of actuation (DOA). The latter definitions should be clearly understood since they are often mistaken, particularly with coupled phalanx fingers. Indeed, a finger where the motion of all the phalanges is coupled is **not** underactuated since it has only one DOF. The motion of the phalanges of such a finger may be complex but can be kinematically described with only one free parameter. Hence $n_{dof} = n_{act}$ and the finger is fully actuated. In this book, fully actuated fingers can be briefly acknowledged but the focus is placed on underactuated mechanisms.

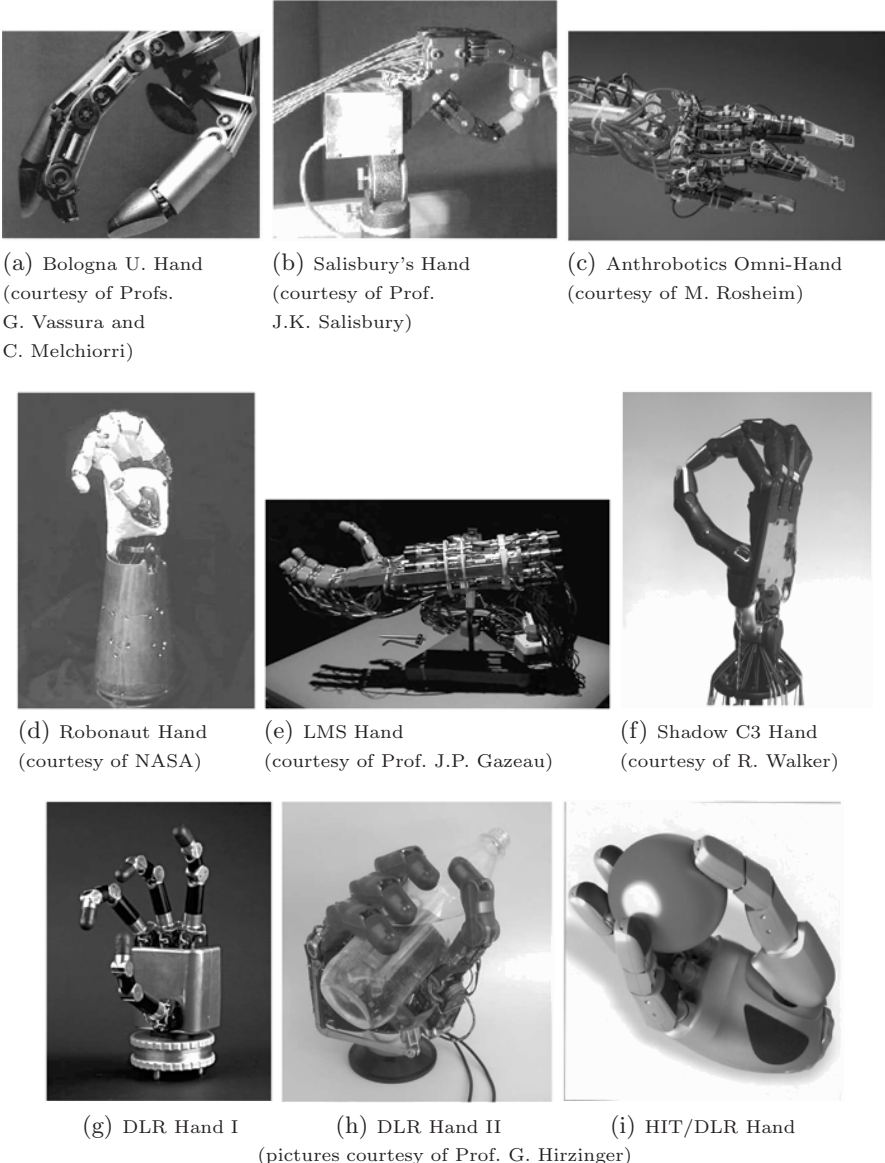
In (Krut 2005), a classification of underactuated fingers was proposed based on the concept of “configuration variables” (Olfati-Saber 2001). According to the International Federation for the Theory of Machines and Mechanisms (IFToMM) terminology (IFToMM 1991), the DOF of a mechanism is:

“the number of independent generalized coordinates required to define completely the configuration of a system at any instant of time.”

However, this definition becomes unclear in the case of compliant mechanisms for instance. Hence, “configuration variables” were introduced to reflect the number of independent parameters that is sufficient to characterize all the feasible motions of the mechanism. With compliant mechanisms for example, they are related to the number of machined joints in the structure. In (Krut 2005), three classes of underactuated mechanisms are proposed: differential mechanisms, compliant mechanisms, and triggered mechanisms. It should be noted that a system may belong to several of these classes and the list itself is presumably not exhaustive. The analysis technique developed in this book is focused on underactuated systems based on differential mechanisms. In fact, it is still debated by some authors whether compliant and triggered mechanisms are truly underactuated and belong to the same family as the designs based on differential mechanisms.

Robotic hands are mostly categorized by their function, namely either for manipulating or grasping an object. To obtain both functions is almost exclusive to the human hand. However it has been suggested (Bicchi 2000) that using an anthropomorphic design approach is restrictive and ambitious since one tends to copy what nature has produced in millions of years of evolution. Furthermore, if the general aspect of a human hand is highly desirable in prosthetics, for a robotic hand it is not always necessary. This additional and often unnecessary constraint has been a rather common trend in robotics, namely to create devices matching the human: “more human than human is our motto” is often an implicit rule in robotics, or more specifically, in biologically-inspired robotics. However, even amongst those who have supported this idea, some voices have raised to claim that one must look at nature for inspiration, not for systematic copy, since nature and robotics do not share the same constraints¹. Indeed, some devices can largely outperform the human hand in dedicated applications, while copies of the human hand have not been very successful due to their complexity. The

¹ As suggested by Prof. S. Hirose during his plenary speech in the 2003 IEEE International Conference on Robotics and Automation.

**Fig. 2.1.** Anthropomorphic robotic hands

main lessons that have been learned from biology and actual prototypes can be summarized in two words: *versatility* and *simplicity*. The idea being to approach the versatility of the human hand, i.e., the ability to achieve multiple tasks, with a device as simple as possible.

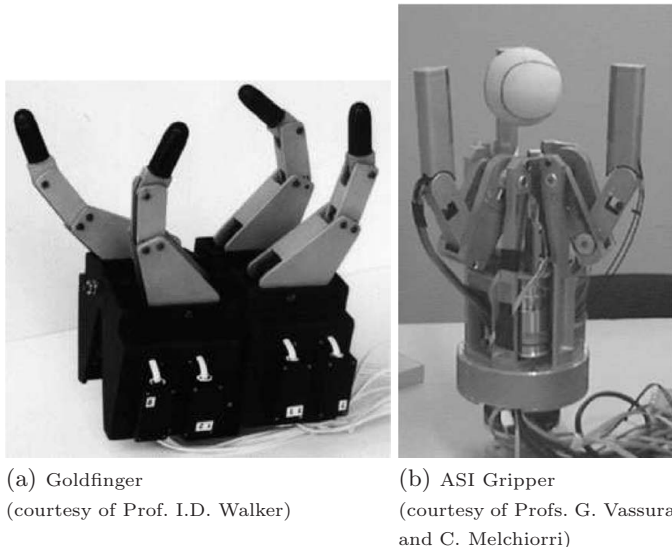


Fig. 2.2. Other dexterous pinching robot hands

Copying the human hand leads to complex systems and should be seen as it really is: one of the many possible solutions to the manipulation issue, but perhaps not *the* best solution in robotics. To manipulate an object in Cartesian space, the fully actuated hands try to emulate the human hand, and end up with solutions that sometimes have even greater capabilities than the latter. Indeed, it is physiologically very difficult to control one particular joint of one's finger without moving the others, an operation that fully actuated fingers perform without problem. Another solution to manipulate an object, or maybe another point of view, consists in grasping that object—preventing it to move—and thereupon, use an articulated system (e.g. a robot on which the hand is mounted) to perform the required manipulation task. This approach focuses on grasping and allows to cut the Gordian knot of the grasping vs. manipulating dilemma: they are accomplished using different devices.

2.2 Underactuation in Robotic Hands

2.2.1 Underactuation as a Solution to Grasping

As stated before, the lack of success of complex robotic hands is mainly due to the cost of the control architecture needed, with often more than ten actuators plus numerous sensors. This complexity arises from the attempt to copy the human hand. This wonder of Nature features approximately 20 DOFs (Tubiana and Thomine 1990) with twice the number of muscles, more than 17,000 tactile sensors in the skin, and its control architecture accounts for 30 – 40% of the motor cortex of the brain. To match such characteristics is impossible with the

current technological limitations, even if it is natural to aim at that goal. In order to overcome the complexity of modern mechanical hands, a particular emphasis has been placed on the reduction of the number of DOFs, thereby decreasing the number of actuators. In particular, the SSL hand (Akin et al. 2002), the ASI gripper (Biagiotti et al. 2001), and the Cassino finger (Figliolini and Ceccarelli 2002) followed this path, using coupling between the joints, etc. On the other hand, few prototypes involve a smaller number of actuators without decreasing the number of DOF. This approach, referred to as *underactuation* can be implemented through the use of passive elements like mechanical limits and springs leading to a mechanical adaptation of the finger to the shape of the object to be grasped (Hirose and Umetani 1978; Rovetta 1981; Rakic 1989; Laliberté and Gosselin 1998; Carrozza et al. 2003). In the recent years, the need for evolved grasping systems has dramatically increased with the automation of the manufacturing industry to reduce cost and time. Furthermore, shape adaptive hands can be used to distribute the actuation torque to a larger contact surface which allows the combination of secure grasps with delicate handling. This property is especially important for food processing (Chua et al. 2004) or even mandatory in medical robotics. However, grasping using mechanical systems is no more than one solution to these issues and other approaches can be considered (Koustoumpardis and Aspragathos 2004): vacuum and air flow, glue, cryofreeze, electrostatic adherence, etc.

Underactuated robotic hands are the intermediate solution between robotic hands for manipulation and simple grippers. It takes advantage of the *mechanical intelligence* (Gosselin 2006) embedded into the design of the hand allowing the shape adaptation of the fingers. The idea to approach the spatial complement of the shape of an object to ensure a distributed grasp is rather common in biologically-inspired robotics: e.g. snake robots (Hirose 1993), elephant trunks (Hannan and Walker 2001), or tentacle manipulators (Antonelli and Immega 1997). They belong to what has been defined as the Frenet-Serret manipulators (Mochiyama et al. 2001) intended for whole-arm manipulation (Salisbury 1987). A similar approach consists in using elastic phalanges, which increases the adaptation capability but can decrease the strength of the grasp (Schulz et al. 2001; Choi and Koc 2006). Underactuation in robotic fingers is different from the concept of underactuation usually presented in robotic systems and both notions should not be confused. An underactuated robot is generally defined as a manipulator with one or more unactuated joints. On the other hand, underactuated fingers use elastic elements in the design of their “unactuated” joints, combined to a transmission system distributing the actuation torque to the latter joints. Thus, one should rather think of these joints as uncontrollable or passively driven instead of unactuated. In an underactuated finger, the actuation torque (or more generally wrench) T_a is applied to the input of the finger and is transmitted to the phalanges through suitable mechanical design, e.g. linkages, pulleys and tendons, gears, etc. Since underactuated fingers have many DOFs, say n , and fewer than n actuators, passive elements, e.g. springs, are used to kinematically constrain the finger and ensure the shape adaptation of the finger to the object grasped. A particular class of underactuated hands are

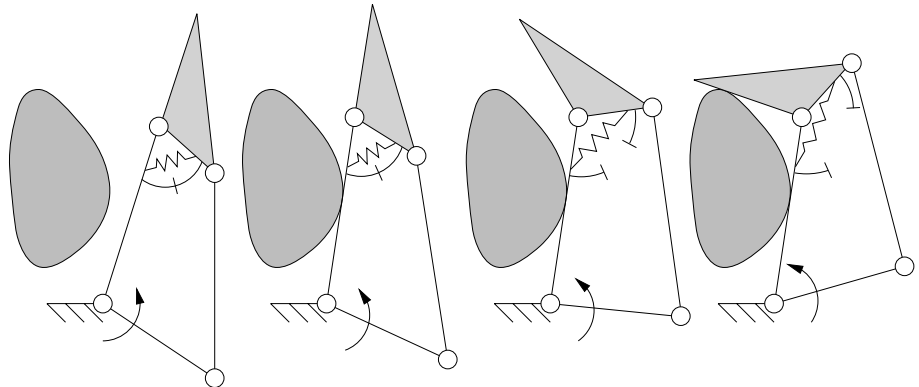


Fig. 2.3. Closing sequence of a two-phalanx underactuated finger

triggered mechanisms, as defined in (Krut 2005). They usually require complicated mechanical designs relying on friction to switch the actuation torque from one output to the other (Ulrich 1988; Ulrich and Kumar 1988; Townsend 2000; Saliba and de Silva 1991). Such devices use mechanisms equivalent in principle to clutches and are not detailed in this book.

An example of underactuated two-phalanx finger using linkages performing a typical closing sequence is illustrated in Fig. 2.3. The finger is actuated through the lower link, as shown by the arrow in the figure. Since there are two DOFs and one actuator, one (two minus one) elastic element is used. In the first two steps of the Figure, the finger behaves as a single rigid body in rotation about a fixed pivot. When the proximal phalanx makes contact with the object, the second phalanx is rotated away from the mechanical limit, and the finger is closing on the object since the proximal phalanx is constrained. During this phase, the actuator has to produce the force required to extend the spring. Finally, both phalanges are in contact with the object and the finger has completed the shape adaptation phase. The actuator force is distributed among the two phalanges in contact with the object. It should be noted that this sequence occurs with a continuous motion of the actuator. Notice also the mechanical limit that allows a pre-loading of the spring to prevent any undesirable motion of the second phalanx due to its own weight and/or inertial effects, and to prevent hyperextension of the finger. Springs are useful for keeping the finger from incoherent motion, but when the grasp sequence is complete, they still oppose the actuator force. Thus, they should be designed with the smallest stiffness possible, however sufficient to keep the finger from collapsing.

The basic property of the transmission system of an underactuated finger is to offer $n > 1$ DOF produced with fewer than n actuators. In Fig. 2.3, the transmission stage consists of a five-bar linkage (the base joint is a double pivot) with two DOFs but one angle is initially constrained to a particular value with the spring and the mechanical limit. The important class of mechanisms used in underactuation as detailed in this book and providing 2 outputs for one input is the

differential mechanisms. According to the IFToMM terminology, a differential mechanism is a

“mechanism for which the degree of freedom is two and which may accept two inputs to produce one output or, may resolve a single input into two outputs.”

Since these mechanisms have only two outputs, it is necessary to connect them in order to achieve n DOF (Hirose 1985), as illustrated in Fig. 2.4. In the latter figure, the input variable is noted θ_a while the outputs (the angles of a finger's joints for instance but not necessarily) are noted θ_i for $i = 1, \dots, n$, and internal actuation angles are noted θ_{a_i} for $i = 2, \dots, n - 1$. However, any connection tree can be used to distribute the actuation. In fact, these mechanisms are usually connected in series, perhaps because of the serial nature of the system to be driven (the fingers). Also, it is worth noting that fluid transmissions have the advantage of being capable of providing multiple outputs for a single input very simply whereas seesaw and pulley transmissions require more complicated designs. Furthermore, one should note that, in order to obtain three outputs, a three-dimensional plate instead of two combined planar seesaw mechanisms can be used (Herder and de Visser 2000). A plate has also been proposed in (Guo et al. 1995) to drive three fingers but it was equivalent to a single seesaw mechanism due to the restricted motion of the plate. More details on the analysis of connected differential mechanisms are presented in Chapter 6.

Underactuation in robotic hands generates intriguing properties that have never been studied, as discussed in Chapters 3 and 4. An ideal grasping sequence such as the one illustrated in Fig. 2.3 does not always occur. For instance, in the final configuration—a configuration is defined as the set of finger joint angles

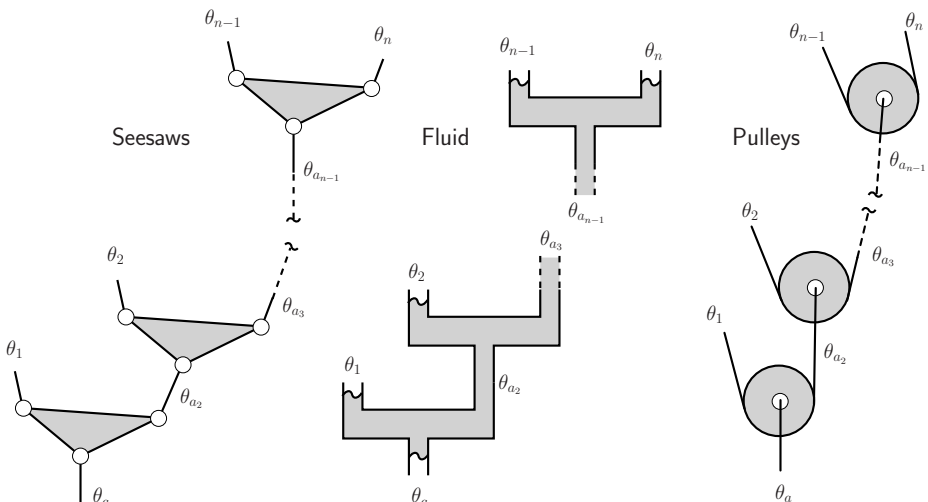


Fig. 2.4. Examples of differential mechanisms connected in series

and contact locations—some phalanx forces may be negative. If this case arises, a sliding motion of the finger on the object will take place. This property is not only theoretical. For instance, it can be observed in a video released to illustrate the JPL LEMUR 1 underactuated end-effector. What happens during this sliding motion and its causes will be studied in Chapters 3 and 4. Understanding such phenomena is critical in order to design optimal underactuated fingers and hands as discussed in Chapters 5 and 7.

2.2.2 Literature Review

An ideal grasping sequence has always been taken for granted and it is intriguing that no one ever studied the grasp properties of underactuated fingers while prototypes have existed since the late 1970's. To the best of the authors' knowledge, a prototype of robotic finger explicitly describing underactuation was presented for the first time in (Hirose and Umetani 1978). In the latter reference, the *Soft Gripper*, a ten-phalanx two-finger gripper, was presented. This prototype used pulleys and was driven by two cables, one for closing the finger and the other with a constant tension for pulling back the finger (equivalently to using springs). The same author then proposed in (Hirose 1985) a very comprehensive and complete survey of the application of differential mechanisms to grasping and wrist-bracing that can adapt to various shapes of objects. Most interestingly, this paper presents all the underactuation techniques that are still in use today, especially those used to distribute the actuation between the fingers. For example, the movable pulley used in the RTR2 Hand (Carrozza et al. 2002) was illustrated, the planetary gear technique of the SARAH prototypes (Laliberté and Gosselin 2003), the T-pipe connected circuit used in the pneumatic version of the latter hands, the connected seesaw circuit of the TUAT Hand (Fukaya et al. 2000) or the Belgrade/USC Hand (Bekey et al. 1999), and others. The *Soft Gripper* is probably the best-known underactuated hand and also the most copied. Indeed, two- (Kaneko et al. 2003), three- (Greiner 1990; Zecca et al. 2003) and five- (Yoshida and Nakanishi 2001) phalanx versions of the *Soft Gripper* exist.

The RTR1 Hand (Carrozza et al. 2002) was the first prototype from the Scuola Superiore Sant'Anna in Italy. It consisted of three fingers made of ABS (built using a fused deposition modelling technique) and was fully actuated. The next generation prototype, the RTR2 Hand (Zecca et al. 2003) used underactuation in the fingers and also between them. The underactuation technique used in the finger is exactly the same as the one used in the *Soft Gripper*, while the underactuation between the fingers used a technique similar to the movable pulley introduced in (Hirose 1985). Two DC actuators move the hand, one for the thumb, and one for the other two three-phalanx fingers. This hand was designed as a first attempt towards an intelligent mechatronic hand dedicated to prosthetics. The third generation RTR Hand or SPRING Hand (Carrozza et al. 2004) also uses underactuation but with a technique different from the one used in the *Soft Gripper*. Another third generation hand was also built, in fact an improvement of the RTR2 Hand with all phalanges having a cylindrical shape without sharp edges and dimensions closer to the human finger. The *Cyberhand* consortium was created, regrouping the

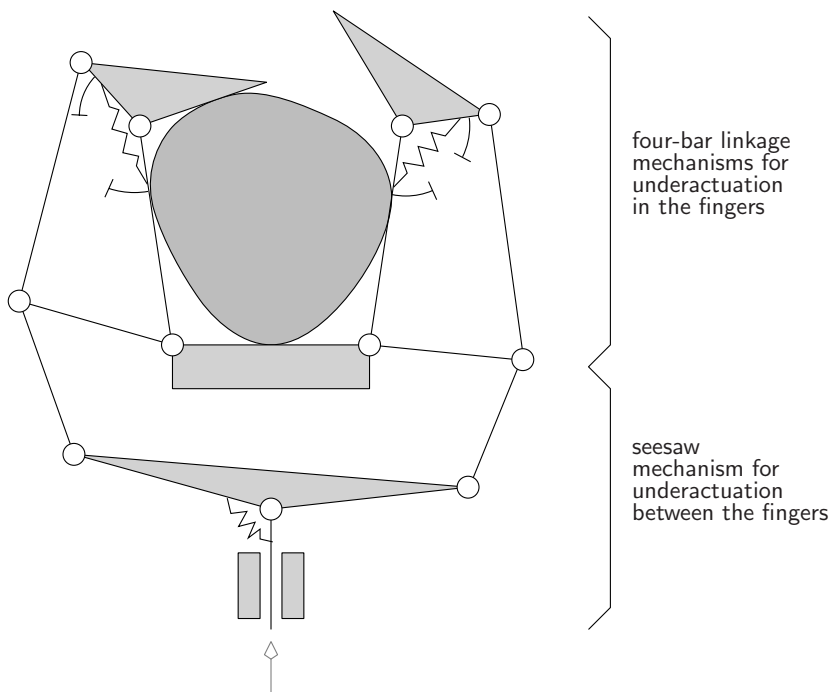


Fig. 2.5. Underactuation in and between the fingers

Scuola Superiore Sant’Anna (Pisa, Italy), the Inail RTR Centre (Pisa, Italy), the Centro Nacional de Microelectronica (Barcelona, Spain), the Fraunhofer-Institut für Biomedizinische Technik (St. Ingbert, Germany), the Universidad Autonoma de Barcelona (Barcelona, Spain), and the Centre for Sensory-Motor Interaction (Aalborg, Denmark), with the intention of developing and commercialize these “cybernetic prosthetic hands.”

Similarly, using the *Soft Gripper* technology, the Space Robotics Laboratory of Tohoku University built the *TAKO*, Japanese word for octopus, illustrated in Fig. 2.8(e) (Yoshida and Nakanishi 2001). This prototype is a five-phalanx three-finger gripper intended for satellite servicing and rendez-vous. Another prototype of this gripper was used by the Robotic Systems Laboratory of Santa Clara University, in the submarine remotely operated vehicle (ROV) *Triton* (Bulich et al. 2004). Finally, a modified version with a two six-phalanx design using pneumatic bellows instead of the tendon-driven mechanism, was designed (Yoshida and Nakanishi 2001).

The underactuation technique of the *Soft Gripper* has also been used in the 100 G Hand (Kaneko et al. 2003), a high speed gripper with two fingers (each one having two phalanges) capable of seizing an object within the blink of an eye. To achieve such speed, an Arm/Gripper Coupling Mechanism (AGCM) was developed, where the potential energy initially accumulated in the arm is transformed into kinetic energy to the arm and, continuously, to close the gripper

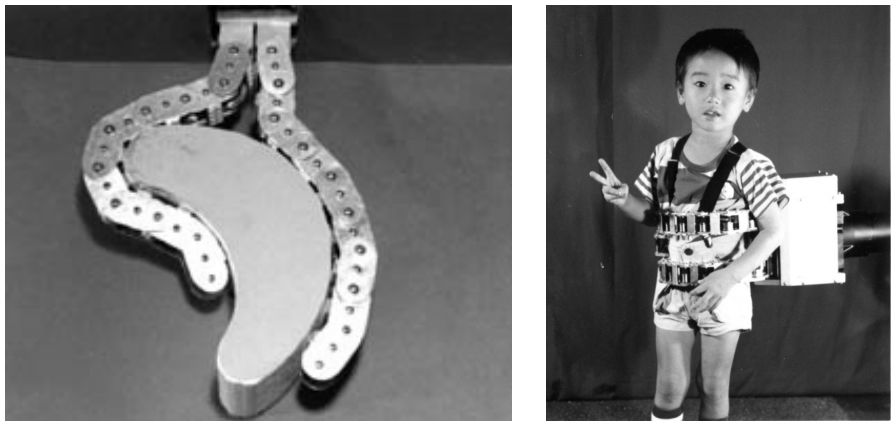


(a) RTR Hand I

(b) RTR Hand II

(c) SPRING Hand

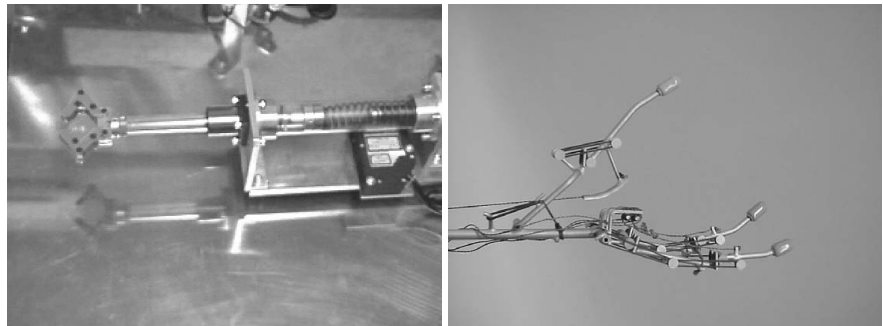
(pictures courtesy of Prof. M.C. Carrozza)



(d) Soft Gripper I

(e) Soft Gripper III

(pictures courtesy of Prof. S. Hirose)



(f) 100 G Hand

(courtesy of Prof. M. Kaneko)

(g) TU Delft Hand

(courtesy of Prof. J.L. Herder)

Fig. 2.6. Tendon-driven underactuated robotic hands

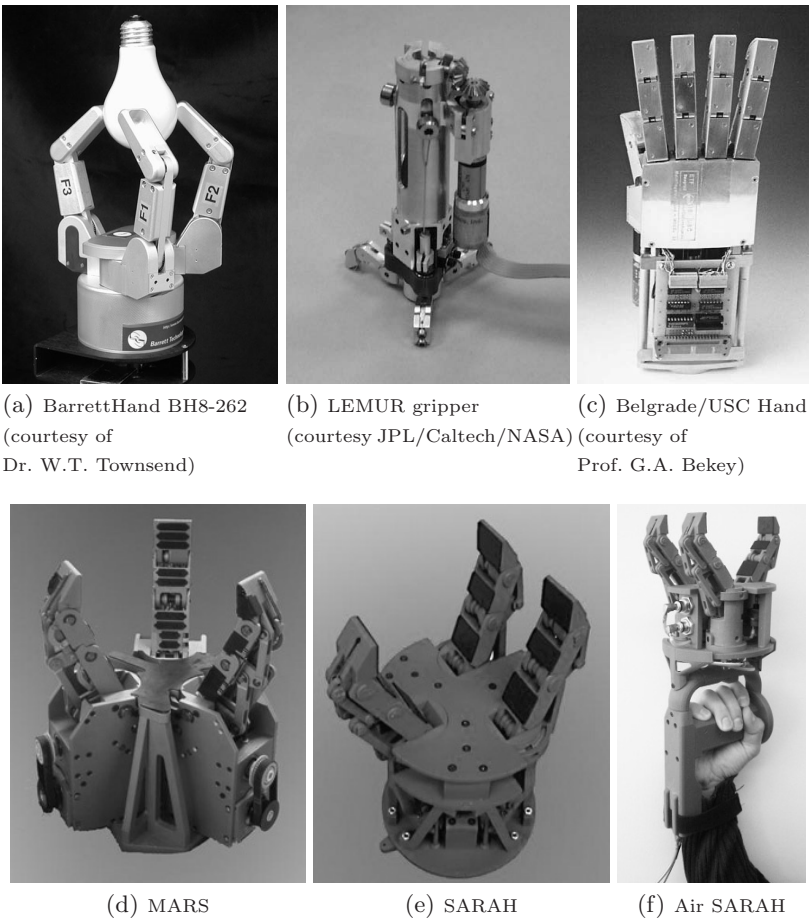


Fig. 2.7. Underactuated robotic hands driven by mechanisms

at the capturing point, without any time lag. The experimental results showed a maximum acceleration of 91 G, and a total capturing time of 0.03 s.

Prosthetics is an application where underactuation can greatly extend the capabilities of existing systems without requiring a complete re-design. Indeed, if one actuator was already used, one just has to replace the finger and mechanically connect it to the motor. No additional actuators, sensors or electronics is required. Prosthetics can also benefit from the light weight of tendons used in underactuated fingers. In (Herder and de Visser 2000; Herder 2001), a prosthetic prototype using tendons was presented and analyzed. Important contributions of the latter references include the highlighting of a design approach based on force rather than kinematics as well as the idea of a negative-stiffness spring mechanism to compensate the stiffness of the cosmetic glove. Similar designs have also been proposed in (Mullen 1972) and (Rovetta 1981; Rovetta et al. 1982). In (Rovetta et al. 1982) a pinching gripper consisting of two four-phalanx fingers working in opposition

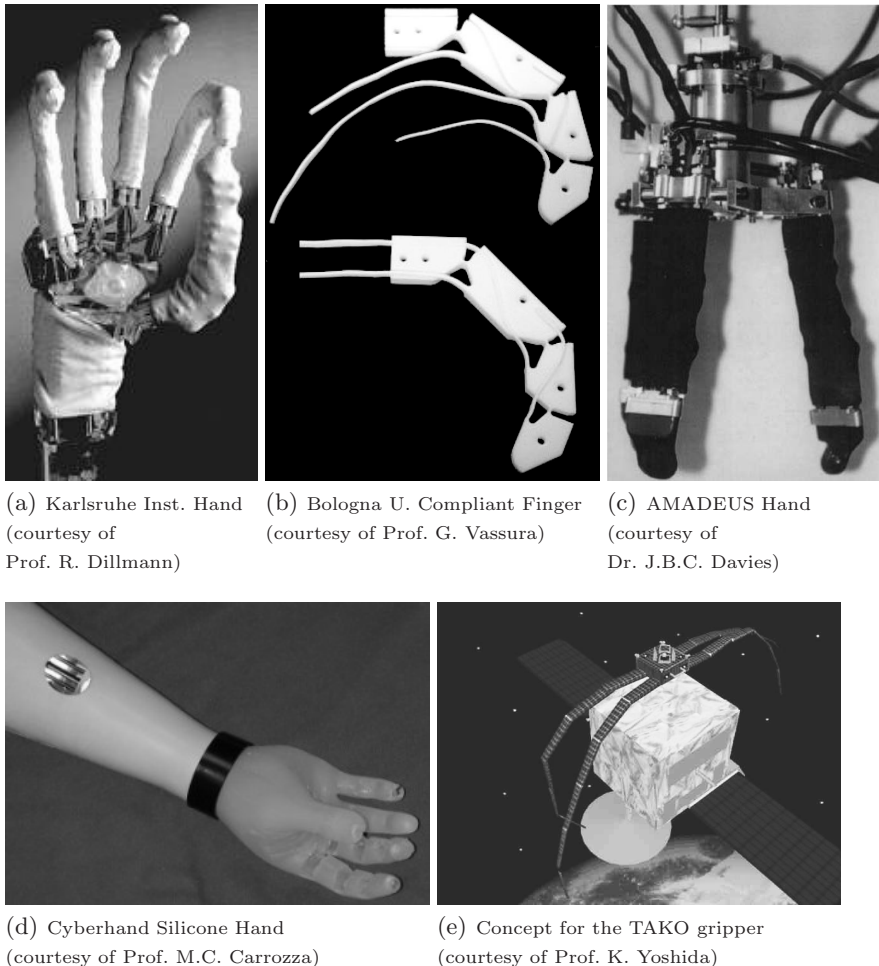


Fig. 2.8. Elastic robotic hands²

was presented. Each of these fingers was actuated with a single tendon, while mechanical limits and springs were used in the different joints of the system. Interestingly, a brief introduction to the grasp stability using an energy based approach was proposed, however with no explicit results. Other tendon-based designs of underactuated fingers with similar architectures include (Crisman et al. 1996; Dollar and Howe 2006; Cabas et al. 2006). Another solution, intended for prosthetic applications is to use elastic fingers (Schulz et al. 2001; Robinson and Davies 1997; Dilibal et al. 2002) to conform to the shape of the object. This technique is not

² Fig. 2.8(a) is from the Collaborative Research Center SFB 588 “Humanoid Robots,” Karlsruhe (Germany) and the Forschungszentrum Karlsruhe, Institut für Angewandte Informatik IAI, Professor Brethauer (project partner).

usually considered to belong to the same family as underactuation but the method is definitely a close relative, considering the idea of shape adaptation to perform enveloping grasps.

Still based on an elastic approach, compliant joints have been proposed in (Doshi et al. 1998; Lotti and Vassura 2002; Ullmann et al. 2004; Carrozza et al. 2005; Boudreault and Gosselin 2005; Birglen 2006). In (Lotti and Vassura 2002) several architectures are proposed with various tendon routings to drive a three-phalanx finger with one, two or three actuators (an example is shown if Fig. 2.8(b)). The compliant action of the joints is used either to pull back the finger or to provide the grasping forces themselves. Thus, this action compensates for the uni-directionality of tendon actuation. The mechanical architecture of the fingers is similar to that proposed in (Rovetta et al. 1982) and is in fact, perhaps the oldest of all architectures of three-phalanx systems, as will be discussed at the end of the present section. It is worth noting that while several underactuated architectures were proposed in (Lotti and Vassura 2002), the actuation pattern finally selected coupled the last two phalanges of the finger and therefore, eliminated underactuation. The authors argued that this choice was made to allow variable approach trajectories. However, in that case, the automatic shape adaptation capability is lost. Another version of the finger (Lotti et al. 2005), the UB Hand 3, using a polyurethane external shell and embedded sensors to mimic the human skin is under development. The total DOF of this hand is 20, of which 15 are actuated, three are coupled, and two are locked. Also one two-DOF joint is redundantly actuated with three tendons. Therefore, this new version is again not underactuated to allow manipulation experiments, but self-adapting grasping can be obtained by changing the tendon routing as noted in (Lotti et al. 2005). A similar finger design based on compliant joints and tendons was proposed by the Rehabilitation Research and Development Center of Palo Alto Department of Veterans Affairs (Doshi et al. 1998) for an endoskeletal prosthetic hand with a soft polyurethane foam shell. However, the latter design is underactuated with one tendon driving the three joints of each finger. However, the hand does not embed any sensor, since it is aiming at minimizing cost. This type of hand supposedly originates from the “Collin Hand,” a prosthetic hand for amputees designed by an engineer from the English Health Ministry (Alfieri 1970). However the authors were not able to verify this information. Another prototype, the “Silicone Hand” (Carrozza et al. 2005), illustrated in Fig. 2.8(d), was also developed. It consists of a silicone prosthetic hand with one actuator embedded in the stump, used to close all the five fingers. This hand is anthropomorphic with an opposable thumb with two DOFs facing four fingers with three DOFs each. The compliant joints are directly machined in the structure of the hand, moulded as a single part which further reduces the cost of the device. A similar design was proposed in (Ullmann et al. 2004) for developing countries. In (Fite et al. 2006), an anthropomorphic hand also based on a similar design was presented featuring underactuation between a set of fingers and driven with liquid-fuel actuators.

The compliance of the joints can be extended to compliance in the whole finger. In (Yang et al. 2004; Yang et al. 2004), a spring is used as a finger with a closing motion driven by a tendon attached to the distal end of the finger.

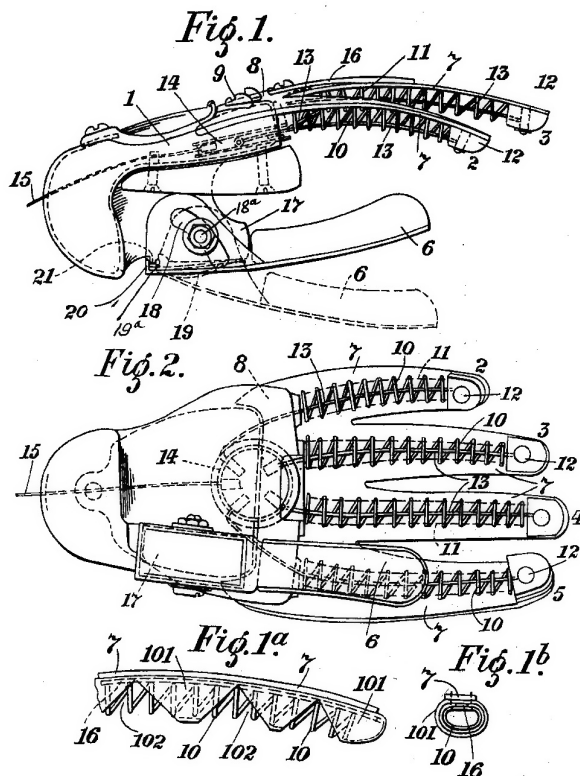


Fig. 2.9. Artificial hand by A. Pringle (1919)

This design is actually very similar to a design patented almost one century ago in (Pringle 1919), illustrated in Fig. 2.9. In the latter patent, self-adaptation to the object seized is obtained using elastic fingers, simply constituted by a linear spring and underactuation between the fingers by a mobile element:

"The ring 14 is accommodated within the hollow body part of the hand and, being free to turn and move within limits in any direction, it enables the fingers to adjust themselves to the object being gripped by them."

It should be noted that the inventor, Alexander Pringle, also proposed to use compliant material in replacement of the springs:

"The finger may be made of rubber or other flexible and resilient material instead of the spiral springs above described, the rubber or equivalent being suitably stiffened at one side so as to insure the bending or flexing movement in one direction only, as hereinbefore described."

Another technique of underactuation consists in using linkages instead of tendons. This is usually the preferred solution when large grasping forces are required or when very compact designs are mandatory. One example is the end-effector of

the Limbed Excursion Mobile Utility Robot 1 or *LEMUR 1* (Kennedy et al. 2001) which consists of three two-phalanx fingers of small dimension: when fully open, it spans a diameter of approximately 5 cm. The *LEMUR 1* is a small six-legged walking robot that has been built at the Jet Propulsion Laboratory to perform dexterous small-scale assembly, inspection and maintenance of macro space facilities. JPL describes it as “*a robotic instantiation of a six-limbed primate with Swiss Army knife tendencies.*” The three fingers are spring-loaded into planes of action 120° apart, and during the grasp, this relative orientation is mechanically (through the springs) adapted to the object seized. The Odetics Hand (Bartholet 1992) is another example of underactuation using linkages. This hand has two phalanges and uses a parallelogram linkage mechanism to allow pinch grasp in addition to the shape adaptation capability. A cam mechanism allows to disengage this parallelogram linkage during enveloping grasps. The digits of the hand also feature a mechanism to allow a reconfigurable disposition of the fingers with respect to the palm plane, as discussed in Chapter 7.

In the Robotics Laboratory of Université Laval, several underactuated robotic hands have been developed in the past decade. The first prototype (Gosselin and Laliberté 1996), named MARS, an acronym for “Main Articulée Robuste Sous-actionnée” or “Minimally Actuated Robotic System” was built in 1996. It consists of three underactuated three-phalanx fingers. The hand has twelve DOF and is actuated by three brushless DC motors for closing/opening the fingers and three DC motors for orienting the fingers. It is nearly twice the size of a human hand and weighs 9 kg. Yet, its maximum payload is 70 kg. The hand is capable of performing cylindrical, spherical, and planar grasps with both power and precision grips. In a precision grip, the object enters into contact only with the distal phalanges, which automatically stay parallel to the axis of the hand. In 1999, another version was built: SARAH (Laliberté and Gosselin 2003) for “Self Adaptive Robotic Auxiliary Hand.” In this prototype, the principle of underactuation was pushed further, by using the latter between the fingers. This was achieved through an innovative gear differential mechanism. The result was a highly underactuated self-adaptive ten-DOF robotic hand having nearly the same functionality as the MARS Hand, yet driven by only two external motors. The current version is adapted as an end-effector to the SPDM of the Canadian Space Arm (Canadarm, a.k.a. SSRMS/SPDM) for the International Space Station and was developed as a collaborative project with the company MDA (formerly known as MD Robotics, Brampton, ON, Canada). A second version has also been built, differing from the previous one in the actuator placement and its overall size, the SARAH CSA hand. In the latter version, two DC motors were incorporated inside the base of the robotic hand. The hand is smaller than its predecessor and is presently mounted on the CART (the SPDM simulator) of the Canadian Space Agency. Finally, the last prototype of this type developed in the laboratory uses ordinary pneumatic actuators, replacing the gear differential mechanism that provides the underactuation between the three fingers, with a T-pipe scheme. This robotic hand, built with a rapid prototyping machine, is a relatively low-cost multi-functional self-adaptive robotic hand

that can fit onto any industrial robot that can use pneumatic grippers with minimal modifications. Another version, SARAH UKAEA, was developed for the retrieval of contaminated material. Its design was modified to be able to lift heavy loads in a confined and radioactive environment. In a completely different design, underactuation using tendons was applied in a prosthetic device with five fingers, 15 DOFs and only one actuation. Finally, sub-centimetre prototypes of underactuated fingers with flexible joints have been developed for surgery.

The underactuation technique used in the fingers of the Laval hands was subsequently used in (Figliolini et al. 2003; Nasser et al. 2006) while a replica of SARAH was built by the Chinese Academy of Science (Luo et al. 2004). A five-fingered prosthetic hand (Zhao et al. 2005) developed by the Chinese Harbin Institute of Technology in collaboration with the Deutschen Zentrum für Luft- und Raumfahrt (DLR, German Aerospace Centre) similarly uses three-phalanx fingers driven by only one actuator through the same transmission linkage.

The idea of combining underactuation in the fingers and between them has also been used in (Fukaya et al. 2000) in the design of a humanoid hand consisting of four three-phalanx fingers plus a thumb. The underactuation between the fingers is accomplished using with a multiple stage seesaw mechanism. In order to mimic the kinematics of the human finger even more closely, the last two joints of each finger have been coupled. The grand total for this hand is 20 DOFs with a single actuator. One of the pioneer designs of a robotic hand featuring underactuation between the fingers is the Belgrade/USC Hand (Rakic 1989; Bekey et al. 1999) (illustrated in Fig. 2.7(c)). While the phalanges of this hand were rigidly coupled in each digit, four of the fingers (all except the thumb) were driven with only two actuators through a seesaw mechanism.

It is noted that although tendon transmission seems to be the preferred choice in prosthetics, linkages have also been used in a handful of prototypes, e.g. the hands of the University of Southampton (Crowder 1991; Kyberd et al. 2001; Dubey and Crowder 2002) and the University of Toronto (Dechev et al. 2001). In the latter prototype, referred to as the TBM Hand, the joints of the fingers are coupled but a differential spring-loaded seesaw mechanism is used to distribute the actuation force to the five fingers of the hand. Considerable efforts have been made to reduce the size of the hand until achieving a child-sized prosthesis. Note that coupling between the last two phalanges of a finger is often used in robotics since it mimics the inability of most people to independently control each of these rotations individually. This coupling can be used even if underactuation between the first phalanges is used as for example in (Koganezawa 2004). In this reference, a three-phalanx finger is presented, the first two phalanges are underactuated using a planetary gear differential mechanism while the distal phalanx is coupled to the intermediate phalanx through a four-bar linkage.

Finally, beside the authors' own research described in this book, the theoretical studies of the grasp properties of underactuated fingers can be reduced to only two papers, to the best of the authors' knowledge: (Hirose and Umetani 1978)

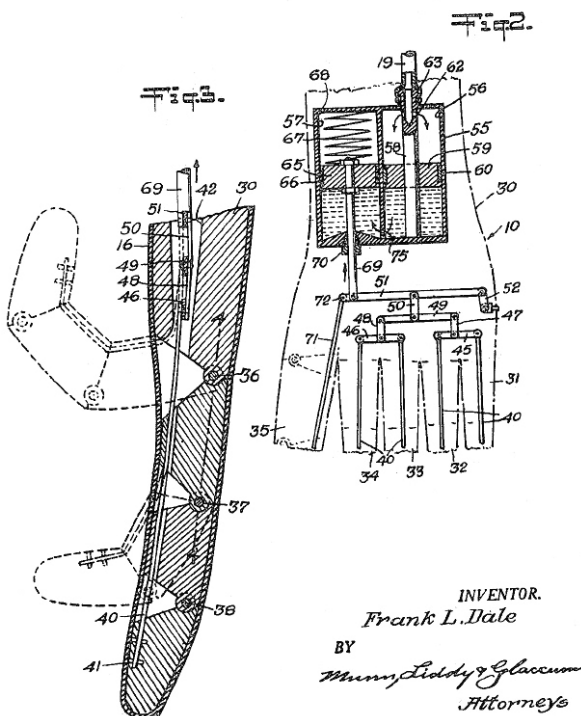


Fig. 2.10. Illustration of the 1946 artificial hand from F.L. Dale

and (Shimojima et al. 1987). In (Shimojima et al. 1987) the synthesis of underactuated fingers was presented considering mobility of the finger and the grasping contact forces were experimentally measured. It should be noted that this paper was the first attempt with (Hirose and Umetani 1978) to formalize underactuation from a theoretical point of view. In (Hirose and Umetani 1978), the *Soft Gripper* was presented along with a method to achieve a design generating a uniform pressure grasp based on the stress analysis of cantilever beams.

Although (Hirose and Umetani 1978) was the first paper introducing the concept of underactuation, much older patents making use of underactuation should be acknowledged in order to make this literature review complete. For instance, a patent (Itoh 1975) was filed a few years before (Hirose and Umetani 1978) concerning a “mechanical hand” with two fingers comprising two and three phalanges. This patent presented an underactuation technique in the fingers almost identical to other more recent prototypes and patents. Furthermore, the very same patent presented a technique to implement underactuation between the fingers. However, it is not known if a prototype of the invention was built (the patent only shows schematic illustrations). In 1946, a patent (Dale 1948) claimed an artificial hand, illustrated³ in Fig. 2.10, featuring underactuation between the

³ All patent illustrations are from the United States Patent and Trademark Office.

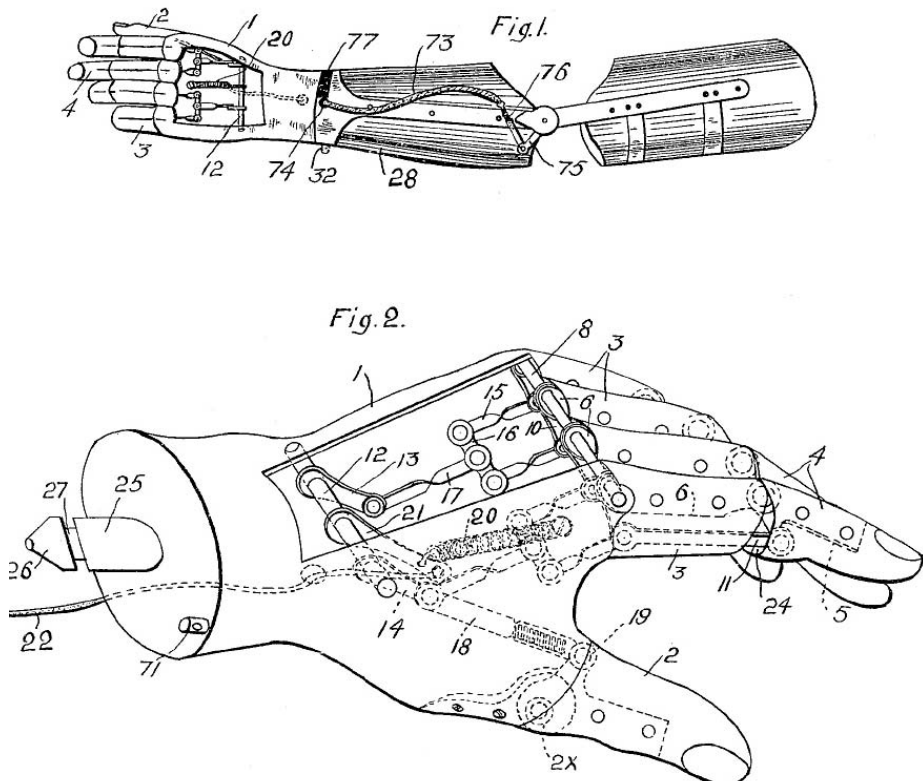


Fig. 2.11. Illustration of the 1918 artificial hand from F.C. Henning

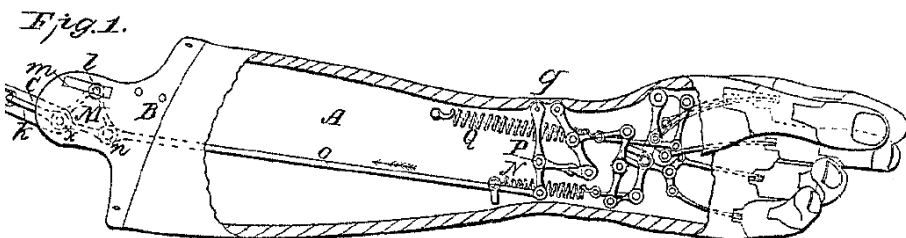


Fig. 2.12. The 1864 artificial arm from E. Spellerberg

fingers using a seesaw mechanism identical to the 2003 TUAT hand, and also underactuated fingers with tendons. Another patent (Henning 1919) filed in 1919 and illustrated in Fig. 2.11, also used a seesaw linkage as a solution to drive the five digits of the hand. Each of these fingers was underactuated with a four-bar linkage identical to the one used in (Itoh 1975).

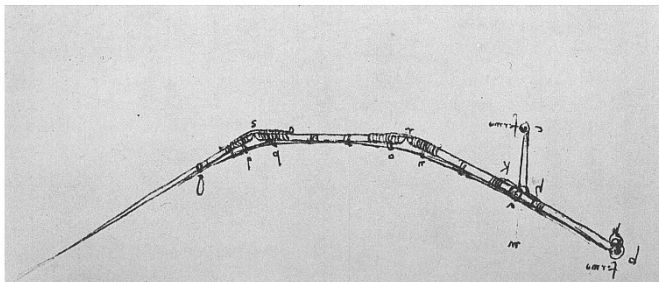
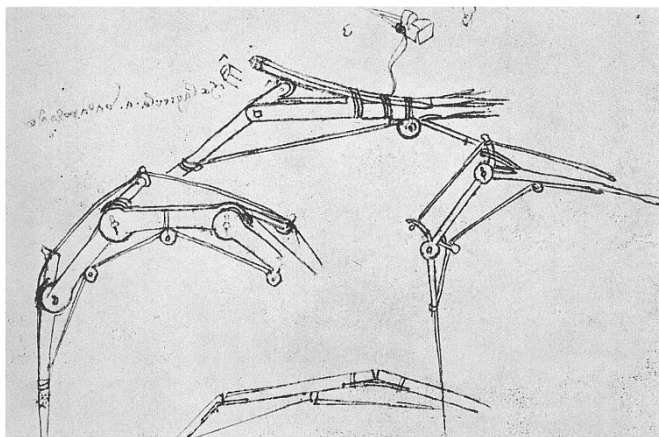
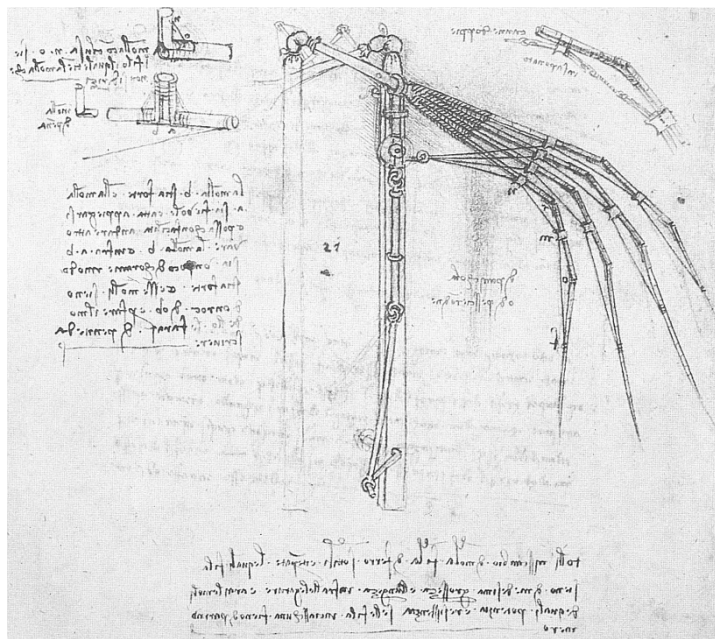


Fig. 2.13. Da Vinci's articulated wing, *Codex Atlanticus* (ca. 1496)

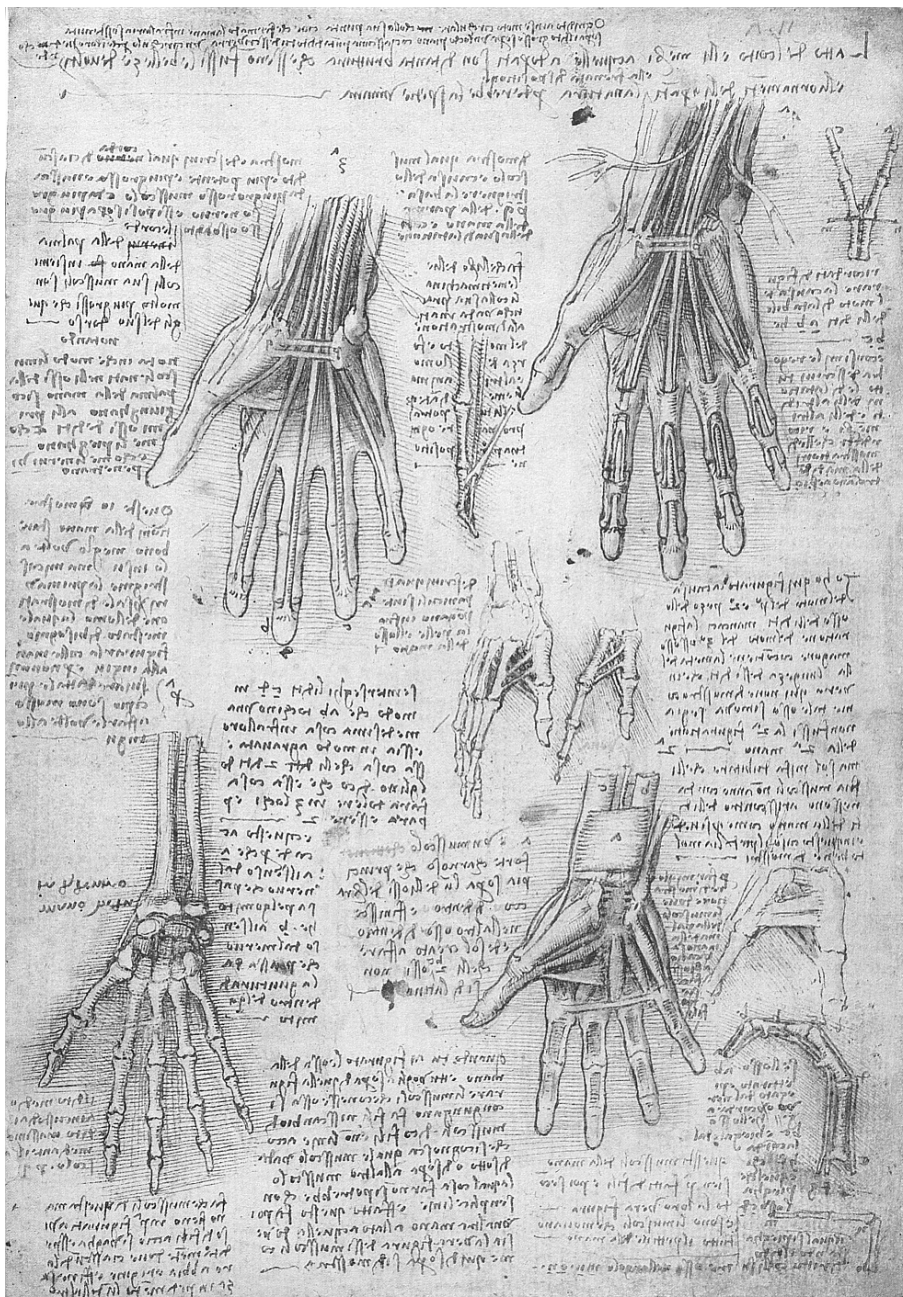


Fig. 2.14. Da Vinci's anatomic study, *Windsor Royal Collection Folios*

Even before, one of the first US patents (Spellerberg 1864), filed in 1864 and illustrated in Fig. 2.12 clearly showed seesaw underactuation between the fingers linked to elastic digits. And this technique was not even claimed:

“The arrangement of the finger-joints and of the levers and links in immediate connection therewith and contained in the interior of the hand are not part of my invention, as they are substantially similar to those already in common use, and will, therefore, (as they are, moreover, clearly shown in Figs. 1 and 2 of the drawings,) not require a more minute description here than is requisite in explaining the operation of my improvement.”

(Quoted⁴ from (Spellerberg 1864))

So, even in 1864, these techniques were commonly used. This is in fact not surprising since in those days, prosthetic hands could not have been fully actuated, electric motors having been invented only a few years before by Michael Faraday.

Furthermore, the oldest mechanism using underactuation between phalanges—at least to the best of the authors’ knowledge—was proposed by Leonardo da Vinci himself! The Renaissance genius did not design an artificial hand per se but underactuated articulated wings, which are part of one of his well-known flying machines. Each of these wings, illustrated in Fig. 2.13, consists of four “fingers” with three phalanges. Each finger is driven by a single cable to flex the wing and deformable elements are used as springs to stretch the latter (although a “return cable” was considered). A similar mechanism was patented almost 500 years later in (Rovetta et al. 1982) for a four-phalanx finger. The authors were unsuccessful at determining whether underactuation between the so-called fingers or coupled motion was used in da Vinci’s wings. One should note that in this case, the shape adaptation property was not intended for grasping but rather to ensure good aerodynamic performances. However, it seems that Leonardo was inspired by the anatomy of the human hand to design this system. Indeed, one of Leonardo’s anatomic studies showing the mechanical principle of the human fingers (especially the bottom rightmost illustration of Fig. 2.14), is strikingly similar to the design of his articulated wing.

Nevertheless, even today, patents are filed that claim what has been known for hundreds of years! It is not the intention of the authors to imply plagiarism: da Vinci’s designs, Alexander Pringle’s patent and other ancient inventions described in this section have been long forgotten. The similarity between the present research directions and these precursory works should incite humility, and acknowledgment of self-adaptive mechanisms developed in the past. In the research community, (Hirose and Umetani 1978) is usually acknowledged as the corner stone of underactuation in robotic fingers and it is not the intention of the authors to belittle this work: it was and remains an outstanding scientific contribution that should be praised. The only criticism that could be made is that this paper was 30 years ahead of its time. However, as clearly presented, underactuation is an old technique that has only recently been brought under

⁴ Typo from the original document.

the spotlight in the robotics community. Before that, the development of fully actuated anthropomorphic hands has kept it in the shadows, and only the failure of the latter devices to achieve commercial and practical success has allowed the revival of research on underactuation. In the next chapters, we propose to study the properties of underactuated fingers from a thorough theoretical point of view. These studies will reveal surprising behaviours that have been either unknown or dismissed. It is also one of the goals of the authors to prevent a repetition of the recurring re-invention of the wheel that took place over the last half century, when “new” designs are claimed that have been invented on several occasions in the past. It is hoped that the dissemination of this book in the robotics community will help in that respect.

3 Kinetostatic Analysis of Robotic Fingers

*Quapropter bono christiano siue mathematici siue quilibet in pie diuinantium,
maxime dicentes uera, cauendi sunt, ne consortio daemoniorum animam deceptam
pacto quodam societatis inretiant.*

The good Christian should beware of mathematicians and all those who make empty prophecies. The danger already exists that mathematicians have made a covenant with the devil to darken the spirit and confine man in the bonds of Hell.

Saint Augustine, *De Genesi ad Litteram*, Book II-xviii-37, 401-415.

in which a fundamental basis for the analysis of underactuated robotic fingers is established. A method to determine the ability of an underactuated finger to generate an external wrench onto a fixed object is presented. This method is based on the introduction of two new matrices which completely describe the relationship between the input torque of the finger actuator and the contact forces on the phalanges.

3.1 Introduction

Two main approaches dominate the literature on robotic grasping, namely, on one hand purely theoretical work on grasping and manipulation and, on the other hand, the rather intuitive design of functional prototypes. This chapter attempts to bridge this gap for the special case of underactuated fingers. Indeed, although the development of underactuated fingers aims at overcoming the theoretical difficulties of general manipulation issues and at obtaining prototypes of practical relevance, the capabilities of these fingers remain not well known. Prototypes have often been built through intuitive design, without a generic knowledge of the resulting behaviour and based mainly on special purpose computer-aided simulation. This chapter presents an effort to establish a common framework using simple theoretical bases to analyze the contact forces generated by robotic fingers during enveloping grasps. The fundamental goal of underactuation being simplicity, the objective of this work is to provide practical tools for the analysis

and comparison of underactuated fingers. Indeed, some issues have been overlooked in previous work and should be systematically addressed. For instance, the grasp force distribution, the capability of the finger to actually exert forces on a grasped object, the stability of the grasp and others will be covered in this chapter. Underactuation in robotic hands generates intriguing properties, e.g. underactuated hands cannot always ensure full *whole-hand grasping*. Indeed, the distribution of the forces between the different phalanges is governed by the mechanical design of the hand since only one actuator is used and some phalanges may not be able to actually exert any effort in certain configurations. This uncontrollable force distribution can also lead to unstable grasps: a continuous closing motion of the actuator tending to eject the object, as discussed in more details in Chapter 4. A new method to study the capabilities of underactuated fingers is presented that allows rigorous comparison of different transmission mechanisms through the definition of indices that are similar to the dexterity in kinematics. In this chapter:

- two matrices that completely characterize the contact forces are defined;
- using these matrices, configurations leading to stable grasps are presented;
- indices to quantify the ability of the finger to generate these stable grasps are introduced;
- different mechanisms used in underactuated hands are compared using the latter indices;

The first part of the chapter (Section 3.2) establishes the fundamental background of our analysis and requires knowledge in screw theory and mechanical transmission design. It is then demonstrated in the second part (Section 3.6), how these results can be used to characterize underactuated fingers. Throughout the first part of this chapter, linkage-driven fingers using a mechanical architecture similar to the SARAH hands are used as an example but the methodology is general and other transmission techniques are presented in Section 3.6. Also, the methodology used in the subsequent sections to develop a general static model of underactuated fingers remains valid, even if the finger is fully actuated. Hence, the title of this chapter does not contain the word “underactuated.”

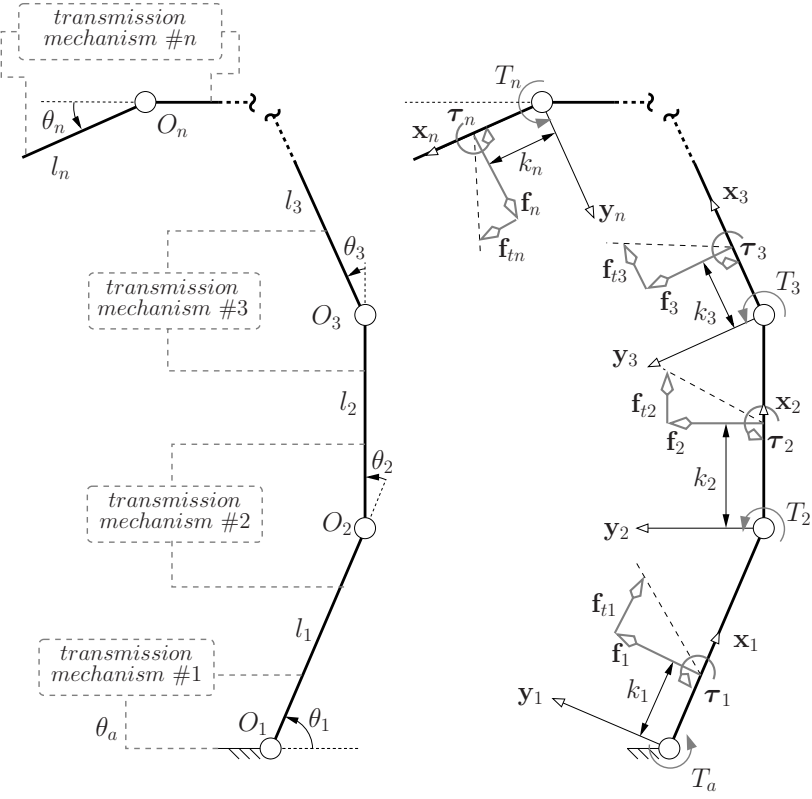
3.2 General Static Model

The model of underactuated finger used in this book is presented in Fig. 3.1, the finger is planar (no abduction/adduction motion) and all phalanges are connected through revolute joints. Only one actuator is used to drive all the phalanges of the fingers.

Equating the input and output virtual powers of this system, one obtains

$$\mathbf{t}^T \boldsymbol{\omega}_a = \sum_{i=1}^n \boldsymbol{\xi}_i \circ \boldsymbol{\zeta}_i \quad (3.1)$$

where \mathbf{t} is the input torque vector exerted by the actuator and the springs located between the phalanges, $\boldsymbol{\omega}_a$ is the corresponding joint velocity vector, $\boldsymbol{\xi}_i$



Geometry/design

Forces

Fig. 3.1. Conceptual underactuated finger

is the twist of the i^{th} contact point on the i^{th} phalanx (assuming one contact per phalanx) with a corresponding wrench ζ_i , and the operator \circ stands for the reciprocal product of screws in the plane, i.e.,

$$\mathbf{t} = \begin{bmatrix} T_a \\ T_2 = -K_2 \Delta\theta_2 \\ T_3 = -K_3 \Delta\theta_3 \\ \dots \\ T_n = -K_n \Delta\theta_n \end{bmatrix}, \quad \boldsymbol{\omega}_a = \begin{bmatrix} \dot{\theta}_a \\ \dot{\theta}_2 \\ \dot{\theta}_3 \\ \dots \\ \dot{\theta}_n \end{bmatrix}, \quad (3.2)$$

where T_a is the actuation torque applied at the base of the finger (Fig. 3.1), T_i is the torque at the i^{th} joint, K_i is the stiffness of the i^{th} spring¹, $\Delta\theta_i$ is the

¹ For the sake of simplicity, a linear elastic model is used for the springs. However, in practice, the spring torque is not zero at the rest configuration (pre-loading is used). This effect is easily included when computations or simulations are performed.

i^{th} joint coordinate relative to the rest configuration (usually associated with a mechanical stop) and

$$\boldsymbol{\xi}_i = \begin{bmatrix} \omega_i \\ v_i^x \\ v_i^y \end{bmatrix} \quad \boldsymbol{\zeta}_i = \begin{bmatrix} f_{ti} \\ f_i \\ \tau_i \end{bmatrix} \quad (3.3)$$

where ω_i , v_i^x and v_i^y are respectively the angular velocity of the i^{th} phalanx, and the x and y components of the velocity at the i^{th} contact point while f_{ti} , f_i and τ_i are the tangential force, the normal force and the torque applied by the i^{th} phalanx (Fig. 3.1). One can define $\boldsymbol{\xi}_i$ more precisely, i.e.,

$$\boldsymbol{\xi}_i = \sum_{k=1}^i \dot{\theta}_k \boldsymbol{\xi}_i^{O_k} \quad (3.4)$$

where $\boldsymbol{\xi}_i^{O_k}$ is the joint twist associated to O_k with respect to C_i , the contact point considered (Hunt 1978). The latter twist can be written as

$$\boldsymbol{\xi}_i^{O_k} = \begin{bmatrix} 1 \\ \mathbf{E}\mathbf{r}_{ki} \end{bmatrix} \quad (3.5)$$

since every joint connecting two phalanges is assumed to be of the revolute type, and where \mathbf{r}_{ki} is the vector from O_k to the contact point on the i^{th} phalanx. \mathbf{E} is the matrix representation of the cross product in the plane, i.e.,

$$\mathbf{E} = \begin{bmatrix} 0 & -1 \\ 1 & 0 \end{bmatrix}. \quad (3.6)$$

On the edge of the friction cone (if considered) of the i^{th} phalanx, which corresponds to the limit case of equilibrium—a case in which we are most interested in order to ensure the stability of the grasp—one has $f_{ti} = \pm \mu_{i-static} f_i$ where $\mu_{i-static}$ is the static coefficient of friction at the i^{th} contact. Generalizing this notation, one obtains $\mathbf{f}_t = \boldsymbol{\mu} \mathbf{f}$, where:

$$\mathbf{f} = \begin{bmatrix} f_1 \\ f_2 \\ \dots \\ f_n \end{bmatrix}, \quad \mathbf{f}_t = \begin{bmatrix} f_{t1} \\ f_{t2} \\ \dots \\ f_{tn} \end{bmatrix} \quad (3.7)$$

and

$$\boldsymbol{\mu} = \begin{bmatrix} \mu_1 & 0 & \dots & 0 \\ 0 & \mu_2 & \dots & 0 \\ \dots & \dots & \dots & \dots \\ 0 & 0 & \dots & \mu_n \end{bmatrix}. \quad (3.8)$$

Note that μ_i can be negative and is not necessarily the static coefficient of friction. In general, one is not on the edge of the static friction cone—especially not simultaneously at all the phalanges—and hence generally $\mu_i \neq \mu_{i-static}$. Matrix $\boldsymbol{\mu}$ simply allows us to relate \mathbf{f}_t and \mathbf{f} , but the exact value of its components is usually unknown.

Similarly, for τ_i , one can write $\boldsymbol{\tau} = \boldsymbol{\eta}\mathbf{f}$, with

$$\boldsymbol{\tau} = \begin{bmatrix} \tau_1 \\ \tau_2 \\ \vdots \\ \tau_n \end{bmatrix} \quad (3.9)$$

and

$$\boldsymbol{\eta} = \begin{bmatrix} \eta_1 & 0 & \dots & 0 \\ 0 & \eta_2 & \dots & 0 \\ \dots & \dots & \dots & \dots \\ 0 & 0 & \dots & \eta_n \end{bmatrix}. \quad (3.10)$$

Therefore one can write ζ_i as

$$\zeta_i = f_{ti}\mathbf{x}_i^* + f_i\mathbf{y}_i^* + \tau_i\mathbf{z}_i^* = f_i(\mathbf{y}_i^* + \mu_i\mathbf{x}_i^* + \eta_i\mathbf{z}_i^*) \quad (3.11)$$

where $\mathbf{y}_i^* = [\mathbf{y}_i^T \ 0]^T$ is the unit wrench corresponding to a pure force along \mathbf{y}_i , the latter being a unit vector orthogonal to the i^{th} phalanx. Similarly, $\mathbf{x}_i^* = [\mathbf{x}_i^T \ 0]^T$ is the unit wrench corresponding to a pure force along \mathbf{x}_i and $\mathbf{z}_i^* = [0 \ 0 \ 1]^T$ is the unit wrench corresponding to a pure torque along the out-of-the-plane axis \mathbf{z} . Thus,

$$\boldsymbol{\xi}_i \circ \zeta_i = \sum_{k=1}^i \dot{\theta}_k \boldsymbol{\xi}_i^{O_k} \circ f_i(\mathbf{y}_i^* + \mu_i\mathbf{x}_i^* + \eta_i\mathbf{z}_i^*) \quad (3.12)$$

$$\boldsymbol{\xi}_i \circ \zeta_i = f_i \left(\sum_{k=1}^i \dot{\theta}_k \mathbf{r}_{ki}^T \mathbf{x}_i - \mu_i \sum_{k=1}^i \dot{\theta}_k \mathbf{r}_{ki}^T \mathbf{y}_i + \eta_i \sum_{k=1}^i \dot{\theta}_k \right) \quad (3.13)$$

and hence,

$$\mathbf{t}^T \boldsymbol{\omega}_a = \mathbf{f}^T(\mathbf{J}\dot{\boldsymbol{\theta}}) = \mathbf{f}^T(\mathbf{J}\mathbf{T}\boldsymbol{\omega}_a) \quad (3.14)$$

with

$$\mathbf{J} = \mathbf{J}_1 - \boldsymbol{\mu}\mathbf{J}_2 + \boldsymbol{\eta}\mathbf{J}_3. \quad (3.15)$$

Matrix \mathbf{J} depends only on the location of the contacts on the phalanges, the relative orientation of the phalanges, and the friction coefficients (if modelled), while \mathbf{T} depends on the transmission mechanism used to propagate the actuation

torque to the phalanges. Matrix \mathbf{T} relates vector $\boldsymbol{\omega}_a$ to the time derivatives of the phalanx joint coordinates, i.e.,

$$\dot{\boldsymbol{\theta}} = \mathbf{T}\boldsymbol{\omega}_a. \quad (3.16)$$

Matrices \mathbf{J}_1 , \mathbf{J}_2 and \mathbf{J}_3 can now be defined by identification of eqs. (3.13) and (3.15). One obtains

$$\mathbf{J}_1 = \begin{bmatrix} k_1 & 0 & 0 & \dots & 0 \\ \mathbf{r}_{12}^T \mathbf{x}_2 & k_2 & 0 & \dots & 0 \\ \dots & \dots & \dots & \dots & \dots \\ \mathbf{r}_{1n}^T \mathbf{x}_n & \mathbf{r}_{2n}^T \mathbf{x}_n & \mathbf{r}_{3n}^T \mathbf{x}_n & \dots & k_n \end{bmatrix} \quad (3.17)$$

where it was used that $\mathbf{r}_{ii}^T \mathbf{x}_i = k_i$, the distance between the i^{th} joint and the i^{th} contact point (Fig. 3.1). One also has,

$$\mathbf{J}_2 = \begin{bmatrix} 0 & 0 & 0 & \dots & 0 \\ \mathbf{r}_{12}^T \mathbf{y}_2 & 0 & 0 & \dots & 0 \\ \dots & \dots & \dots & \dots & \dots \\ \mathbf{r}_{1n}^T \mathbf{y}_n & \mathbf{r}_{2n}^T \mathbf{y}_n & \mathbf{r}_{3n}^T \mathbf{y}_n & \dots & 0 \end{bmatrix} \quad (3.18)$$

where the following relationship was used: $\mathbf{r}_{ii}^T \mathbf{y}_i = 0$. And finally,

$$\mathbf{J}_3 = \begin{bmatrix} 1 & 0 & 0 & \dots & 0 \\ 1 & 1 & 0 & \dots & 0 \\ \dots & \dots & \dots & \dots & \dots \\ 1 & 1 & 1 & \dots & 1 \end{bmatrix}. \quad (3.19)$$

The components of matrices \mathbf{J}_1 and \mathbf{J}_2 can also be expressed as

$$\mathbf{r}_{ij}^T \mathbf{x}_j = k_j + \sum_{k=i}^{j-1} l_k \cos \left(\sum_{m=k+1}^j \theta_m \right), \quad i < j \quad (3.20)$$

$$\mathbf{r}_{ij}^T \mathbf{y}_j = - \sum_{k=i}^{j-1} l_k \sin \left(\sum_{m=k+1}^j \theta_m \right), \quad i < j \quad (3.21)$$

where l_i is the length of the i^{th} phalanx (Fig. 3.1). Finally,

$$\mathbf{J}^T = \begin{bmatrix} k_1 + \eta_1 & \mathbf{r}_{12}^T(\mathbf{x}_2 - \mu_2 \mathbf{y}_2) + \eta_2 & \dots & \mathbf{r}_{1n}^T(\mathbf{x}_n - \mu_n \mathbf{y}_n) + \eta_n \\ 0 & k_2 + \eta_2 & \dots & \mathbf{r}_{2n}^T(\mathbf{x}_n - \mu_n \mathbf{y}_n) + \eta_n \\ \dots & 0 & \dots & \mathbf{r}_{3n}^T(\mathbf{x}_n - \mu_n \mathbf{y}_n) + \eta_n \\ \dots & \dots & \dots & \dots \\ 0 & 0 & \dots & 0 & k_n + \eta_n \end{bmatrix}. \quad (3.22)$$

Obviously, the coefficient of friction μ_1 of the first phalanx does not appear since this phalanx cannot slide on the object due to kinematic constraints. Coefficients η_i are usually small and will hereafter be neglected. However these coefficients will be useful if friction is considered and the phalanges have a non-negligible thickness as will be discussed in Section 4.2.6. Note that the expression of matrix \mathbf{J} is not specific to underactuated fingers and still holds in more general cases such as fully actuated fingers performing enveloping grasps, provided that abduction/adduction is not considered. One also has to establish matrix \mathbf{T} which relates vector ω_a to the time derivatives of the phalanx joint coordinates as defined in eq. (3.16) or

$$\begin{bmatrix} \dot{\theta}_1 \\ \dot{\theta}_2 \\ \dot{\theta}_3 \\ \dots \\ \dot{\theta}_n \end{bmatrix} = \begin{bmatrix} X_1 & X_2 & X_3 & \dots & X_n \\ 0 & 1 & 0 & \dots & 0 \\ 0 & 0 & 1 & \dots & 0 \\ \dots & \dots & \dots & \dots & \dots \\ 0 & 0 & 0 & \dots & 1 \end{bmatrix} \begin{bmatrix} \dot{\theta}_{a_1} \\ \dot{\theta}_2 \\ \dot{\theta}_3 \\ \dots \\ \dot{\theta}_n \end{bmatrix}. \quad (3.23)$$

Note that the form of this matrix is characteristic of underactuation. If the finger is fully actuated, \mathbf{T} becomes the identity matrix of dimension n (with $\theta_{a_1} = \theta_1$).

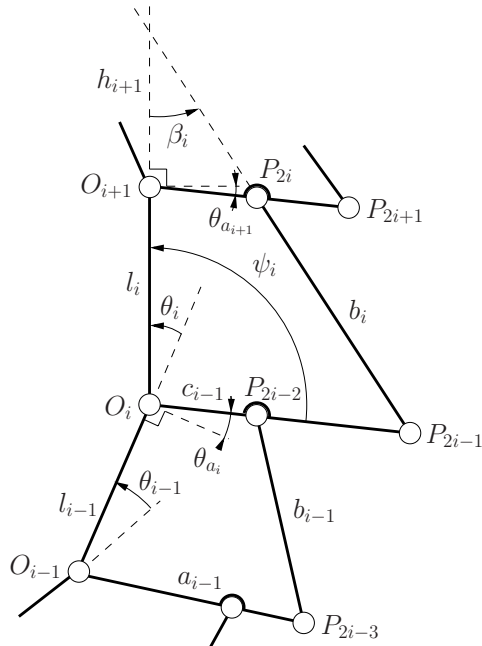


Fig. 3.2. Detailed modelling of a stage of a linkage-driven finger

Indeed, the method proposed in this chapter can be used with fully actuated fingers, a particular and simplified case of this derivation. Each coefficient X_i is a function of the transmission mechanism used to propagate the actuator torque to the i^{th} phalanx. For instance, if four-bar linkages are considered in the model, the principle of transmission, also known as *Kennedy's Theorem* (Norton 1992; McCarthy 2000), gives the angular velocity ratio of this linkage (consider $O_{i-1}O_iP_{2i-2}P_{2i-3}$ with θ_{i-1} constant, in Fig. 3.2). By superposition, one obtains

$$\dot{\theta}_{a_{i-1}} = \dot{\theta}_{i-1} + \frac{h_i}{h_i + l_{i-1}} \dot{\theta}_{a_i} \quad (3.24)$$

since the velocity output of each stage is the input of the next stage, the transmission stages are assumed to be connected in series. One also has

$$h_i = c_{i-1} (\cos(\theta_i - \psi_i) - \sin(\theta_i - \psi_i) \cot \beta_{i-1}), \quad (3.25)$$

where angles β_i and ψ_i are defined in Fig. 3.2. Distance h_i is the signed distance between point O_i and the intersection of lines $(O_{i-1}O_i)$ and $(P_{2i-2}P_{2i-3})$. This distance can be negative if the intersection point is on the same side as O_{i-1} with respect to O_i . Thus, $h_i + l_{i-1}$ can also vanish. Geometrically, it corresponds to the case where links a_{i-1} and b_{i-1} are aligned. In such a configuration, it is easy to see that power cannot be properly transmitted and an infinitesimal motion $\Delta\theta_{a_{i-1}}$ is possible with $\Delta\theta_{a_i} = 0$. One can also obtain $\cot \beta_{i-1}$ as a function of the parameters of the system, i.e.,

$$\cot \beta_{i-1} = \frac{c_{i-1} \sin(\theta_i - \psi_i) \sqrt{4a_{i-1}^2 b_{i-1}^2 - N_i^2} + M_i(l_{i-1} + c_{i-1} \cos(\theta_i - \psi_i))}{-(l_{i-1} + c_{i-1} \cos(\theta_i - \psi_i)) \sqrt{4a_{i-1}^2 b_{i-1}^2 - N_i^2} + M_i c_{i-1} \sin(\theta_i - \psi_i)} \quad (3.26)$$

with

$$M_i = -l_{i-1}(l_{i-1} + 2c_{i-1} \cos(\theta_i - \psi_i)) + a_{i-1}^2 - b_{i-1}^2 - c_{i-1}^2, \quad (3.27)$$

$$N_i = l_{i-1}(l_{i-1} + 2c_{i-1} \cos(\theta_i - \psi_i)) - a_{i-1}^2 - b_{i-1}^2 + c_{i-1}^2, \quad (3.28)$$

where ψ_i can be expressed as a function of ψ_{i-1} and θ_i , namely

$$\begin{aligned} \psi_i = & \arctan \left[\frac{-c_i \sin(\theta_{i+1} - \psi_{i+1})}{l_i + c_i \cos(\theta_{i+1} - \psi_{i+1})} \right] \\ & + \arccos \left[\frac{l_i^2 + a_i^2 + c_i^2 - b_i^2 + 2c_i l_i \cos(\theta_{i+1} - \psi_{i+1})}{2a_i \sqrt{c_i^2 + 2c_i l_i \cos(\theta_{i+1} - \psi_{i+1}) + l_i^2}} \right]. \end{aligned} \quad (3.29)$$

Thus, one can obtain the expressions of angles ψ_i recursively. Eq. (3.24) can be used recursively to obtain $\dot{\theta}_{a_1}$ as a function of vector $\dot{\theta}$, i.e.:

$$\begin{aligned} \dot{\theta}_{a_1} &= \dot{\theta}_1 + \frac{h_2}{h_2 + l_1} \dot{\theta}_{a_2} \\ &= \dot{\theta}_1 + \frac{h_2}{h_2 + l_1} \left(\dot{\theta}_2 + \frac{h_3}{h_3 + l_2} \dot{\theta}_{a_3} \right) \\ &= \dots \end{aligned} \quad (3.30)$$

For the last phalanx, one has

$$\dot{\theta}_{a_{n-1}} = \dot{\theta}_{n-1} + \frac{h_n}{h_n + l_{n-1}} \dot{\theta}_n. \quad (3.31)$$

Therefore, one obtains

$$\dot{\theta}_{a_1} = \dot{\theta}_1 + \frac{h_2}{h_2 + l_1} \dot{\theta}_2 + \dots + \prod_{i=2}^n \frac{h_i}{h_i + l_{i-1}} \dot{\theta}_n \quad (3.32)$$

and, by observation of eqs. (3.32) and (3.23), one finally obtains,

$$\mathbf{T}^T = \begin{bmatrix} 1 & \mathbf{0}_{n-1}^T \\ -\frac{h_2}{h_2 + l_1} & \\ -\frac{h_2 h_3}{(h_2 + l_1)(h_3 + l_2)} & \\ \dots & \mathbf{1}_{n-1} \\ -\prod_{i=2}^n \frac{h_i}{h_i + l_{i-1}} & \end{bmatrix} \quad (3.33)$$

where $\mathbf{1}_{n-1}$ and $\mathbf{0}_{n-1}$ are respectively the identity matrix and the zero vector of dimension $n - 1$. This method can also be used to obtain the components of matrix \mathbf{T} with different types of transmission mechanisms, as will be presented in Section 3.3. The benefit of the method presented in this chapter is that it allows to obtain very quickly the expression of the contact forces developed by an underactuated finger. This can be especially useful if different mechanisms are considered: matrix \mathbf{J} is independent of the type of transmission used and only the components of matrix \mathbf{T} need to be modified. Two methods to obtain the components of \mathbf{T} follow.

3.3 Computation of the Transmission Matrix

To compute the different components of matrix \mathbf{T} , the general form of eq. (3.24), obtained by superposition is recalled, namely

$$\dot{\theta}_{a_{i-1}} = \dot{\theta}_{i-1} + x_i \dot{\theta}_{a_i}, \quad (3.34)$$

where x_i is the transmission ratio of the i^{th} stage. The latter equation means that the velocity output of each stage is the input of the next stage (Figs. 2.4, 3.1, and 3.2 illustrate this concept). The i^{th} ratio x_i is readily obtained by “locking” the joint associated with angle θ_{i-1} and determining the ratio between $\dot{\theta}_{a_i}$ and $\dot{\theta}_{a_{i-1}}$, which can be obtained for any mechanism. These ratios are already well-known for most usual transmissions (e.g. gears, pulleys). Once an expression for the transmission ratio is obtained, a recursive scheme can be easily derived from

eq. (3.24) and therefore the components of the first line of matrix \mathbf{T} , noted X_i in eq. (3.23), can be written as:

$$\begin{cases} X_1 = 1 \\ X_j = -\prod_{i=1}^j x_i \quad j = 2, \dots, n \end{cases} \quad (3.35)$$

For instance, if tendons are considered, one has

$$x_1 = 1 \quad \text{and} \quad x_i = \frac{r_{2i}}{r_{2i-1}} \quad i > 1, \quad (3.36)$$

and thus,

$$\mathbf{T}^T = \begin{bmatrix} 1 & \mathbf{0}_{n-1}^T \\ -\frac{r_2}{r_1} & \\ -\frac{r_2 r_4}{r_1 r_3} & \\ \dots & \mathbf{1}_{n-1} \\ -\prod_{i=1}^n \frac{r_{2i}}{r_{2i-1}} & \end{bmatrix} \quad (3.37)$$

where r_{2i-1} and r_{2i} for $i > 0$ are respectively the radius of the pulley located at the base and the end of the i^{th} phalanx. Further examples will be given in Section 3.6. However, eq. (3.35) is only useful if eq. (3.34) can be easily obtained, which is not always the case (see Section 3.6.4 for an example). A more general but slightly less straightforward method to obtain the components X_i consists in using simple differential calculus. Based on eq. (3.23), one has

$$\dot{\theta}_1 = X_1 \dot{\theta}_{a_1} + \sum_{i=2}^n X_i \dot{\theta}_i \quad (3.38)$$

which is equivalent to

$$\dot{\theta}_1 = \frac{\partial \theta_1}{\partial \theta_{a_1}} \dot{\theta}_{a_1} + \sum_{i=2}^n \frac{\partial \theta_1}{\partial \theta_i} \dot{\theta}_i. \quad (3.39)$$

Hence, it is readily observed that the components X_i are equal to the partial derivatives of angle θ_1 with respect to the other angles. A more convenient form of eq. (3.39) is

$$\dot{\theta}_1 = \frac{\partial \theta_1}{\partial \theta_{a_1}} \left[\dot{\theta}_{a_1} + \sum_{i=2}^n \frac{\partial \theta_{a_1}}{\partial \theta_i} \dot{\theta}_i \right]. \quad (3.40)$$

This form factors the term $\partial \theta_1 / \partial \theta_{a_1}$ which is equal to 1 with the mechanisms discussed in this chapter, and emphasizes the partial derivative of the input actuation angle θ_{a_1} with respect to angle θ_i . The latter derivative has an obvious physical meaning; it is the inverse ratio of the instantaneous angular velocities $\dot{\theta}_i$ and $\dot{\theta}_{a_1}$. Therefore, to compute this coefficient, one simply has to lock all

the joints of the finger except the one corresponding to θ_i and compute the instantaneous velocity $\dot{\theta}_i$ when $\dot{\theta}_{a_1} = 1$. Once this ratio (noted X_i^*) is found, the coefficient X_i can be very easily be expressed as

$$X_i = \frac{\partial \theta_1}{\partial \theta_{a_1}} \frac{1}{X_i^*} = \frac{1}{X_i^*}. \quad (3.41)$$

Thus, the relationship between X_i and X_i^* (the velocity ratio between the input actuation angle and the output angles of the phalanges) is trivial.

3.4 Expressions of the Contact Forces

From eq. (3.14) one obtains

$$\mathbf{f} = \mathbf{J}^{-T} \mathbf{T}^{-T} \mathbf{t}, \quad (3.42)$$

which is the equation that provides a practical relationship between the actuator torques and the contact forces. One should note that $\mathbf{T}^{-T} = -\mathbf{T}^T + 2\mathbf{1}_n$, due to the particular form of matrix \mathbf{T} . Thus, this inverse is not computationally costly and specific inversion procedures exist for triangular matrices like \mathbf{J} .

The previous equation can also be written

$$\mathbf{J}^* \mathbf{f} = \mathbf{T}^* \mathbf{t} \quad (3.43)$$

with

$$\mathbf{J}^* = \mathbf{J}^T \quad \text{and} \quad \mathbf{T}^* = \mathbf{T}^{-T} \quad (3.44)$$

It is readily observed that eq. (3.43) is in fact a relationship similar to the velocity equation of parallel manipulators (Gosselin and Angeles 1990). The similarity does not end here, since $\mathbf{T}^* = \mathbf{1}$ for fully-actuated fingers, as one of the two Jacobian matrices defined in (Gosselin and Angeles 1990) becomes the identity matrix for serial manipulators. This formulation is therefore very well suited for both analytical derivations and numerical calculations. Furthermore, if the finger is fully actuated, i.e., $\mathbf{T} = \mathbf{1}_n$, one has $\mathbf{f} = \mathbf{J}^{-T} \mathbf{t}$, a relationship similar to the grasp matrix linking fingertips to object wrenches or the Jacobian matrix that maps joint torques to fingertip forces, both usually presented in papers on grasping (Mason and Salisbury 1985; Yoshikawa 2000). The validity of eq. (3.42) can be verified by considering the conditions for the existence of the inverses which are written as

$$\det(\mathbf{T}) = 1 \neq 0 \quad (3.45)$$

$$\det(\mathbf{J}) = \prod_{i=1}^n k_i \neq 0 \quad (3.46)$$

Eqs. (3.45) and (3.46) mean that contacts should exist with all phalanges and that \mathbf{T} should exist (if it does, the latter is always invertible), i.e.,

$$\prod_{i=2}^n (h_i + l_{i-1}) \neq 0, \quad (3.47)$$

for linkage-driven fingers, meaning geometrically that points O_{i-1} , P_{2i-2} and P_{2i-3} are not on the same line. If this is not true, no effort can be transmitted to upper stages of the mechanism in the current configuration. Another interesting case arises if $h_k = 0$, then $X_j = 0$, $j \geq k$ because of the particular form of ratio X_j :

$$X_j = - \prod_{i=2}^j \frac{h_i}{h_i + l_{i-1}}, \quad j > 1 \quad \text{and} \quad X_1 = 1. \quad (3.48)$$

This case has a simple physical interpretation: $h_k = 0$ means that the distance between point O_k and the intersection of lines $(O_{k-1}O_k)$ and $(P_{2k-2}P_{2k-3})$ is zero. Thus both lines intersect in O_k . If one assumes that $c_{k-1} \neq 0$, it means that points O_k , P_{2k-2} and P_{2k-3} are on the same line. Since the actuator torque is usually transmitted to upper stages of the mechanism through link b_{k-1} and since in this particular configuration such transmission is impossible (link b_{k-1} cannot generate any actuation torque about O_k), no motion is transmitted and hence no torque except for the springs, which usually generate negligible torques. Consequently, an infinitesimal rotation is possible around O_k , and if the springs are neglected, one also has that $f_j = 0$ $j \geq k$. In consequence, the finger cannot grasp any object with the upper phalanges since they cannot apply forces. This situation is similar to the condition of existence of matrix \mathbf{T} . Such situations should be avoided through suitable design, so that h_i , $i > 1$ will always be positive and therefore $h_i + l_{i-1} \neq 0$, $i > 1$.

This analysis illustrates the physical meaning of the components of the transmission matrix. It should be performed for any other transmission type. Indeed, it allows the derivation of analytical expressions of the contact forces generated by underactuated fingers and provides practical insights.

3.5 Positive Definiteness of the Forces

The most usual cases, i.e., linkage-driven fingers with two and three phalanges, shall now be explicitly studied. The following contact force expressions results have been verified using classical static analysis (Birglen 2004). Neglecting friction, for linkage-driven fingers and $n = 2$, one has,

$$\mathbf{J} = \begin{bmatrix} k_1 & 0 \\ k_2 + l_1 \cos \theta_2 & k_2 \end{bmatrix}, \quad (3.49)$$

$$\mathbf{T} = \begin{bmatrix} 1 - \frac{h}{h+l_1} \\ 0 & 1 \end{bmatrix}, \quad (3.50)$$

$$\mathbf{f} = \begin{bmatrix} \frac{l_1(k_2 - h \cos \theta_2)Ta}{k_1 k_2 (h+l_1)} - \frac{(k_2 + l_1 \cos \theta_2)T_2}{k_1 k_2} \\ \frac{h T_a}{k_2 (h+l_1)} + \frac{T_2}{k_2} \end{bmatrix}. \quad (3.51)$$

For $n = 3$, still neglecting friction,

$$\mathbf{J} = \begin{bmatrix} k_1 & 0 & 0 \\ k_2 + l_1 \cos \theta_2 & k_2 & 0 \\ k_3 + l_1 \cos(\theta_2 + \theta_3) + l_2 \cos \theta_3 & k_3 + l_2 \cos \theta_3 & k_3 \end{bmatrix}, \quad (3.52)$$

$$\mathbf{T} = \begin{bmatrix} 1 - \frac{h_2}{h_2 + l_1} - \frac{h_2 h_3}{(h_2 + l_1)(h_3 + l_2)} \\ 0 & 1 & 0 \\ 0 & 0 & 1 \end{bmatrix}, \quad (3.53)$$

$$\mathbf{f} = \begin{bmatrix} \frac{l_1 U T_a}{k_1 k_2 k_3 (h_2 + l_1)(h_3 + l_2)} - \frac{(k_2 + l_1 \cos \theta_2) T_2}{k_1 k_2} + \frac{l_1 V T_3}{k_1 k_2 k_3} \\ \frac{h_2 l_2 (k_3 - h_3 \cos \theta_3) T_a}{k_2 k_3 (h_2 + l_1)(h_3 + l_2)} + \frac{T_2}{k_2} - \frac{(k_3 + l_2 \cos \theta_3) T_3}{k_2 k_3} \\ \frac{h_2 h_3 T_a}{k_3 (h_2 + l_1)(h_3 + l_2)} + \frac{T_3}{k_3} \end{bmatrix} \quad (3.54)$$

where the coefficients in eq. (3.54) are defined as

$$\begin{aligned} U &= k_2 k_3 h_3 + k_2 k_3 l_2 - h_2 k_3 l_2 \cos \theta_2 + h_2 h_3 l_2 \cos \theta_2 \cos \theta_3 \\ &\quad - h_2 h_3 k_2 \cos(\theta_2 + \theta_3) \end{aligned} \quad (3.55)$$

$$V = l_2 \cos \theta_2 \cos \theta_3 + k_3 \cos \theta_2 - k_2 \cos(\theta_2 + \theta_3). \quad (3.56)$$

These expressions allow the determination, for a set of geometric parameters, of the contact situations defined by the pair $(\mathbf{k}^*, \boldsymbol{\theta}^*)$ with

$$\mathbf{k}^* = \begin{bmatrix} k_2 \\ k_3 \\ \dots \\ k_n \end{bmatrix} \quad \text{and} \quad \boldsymbol{\theta}^* = \begin{bmatrix} \theta_2 \\ \theta_3 \\ \dots \\ \theta_n \end{bmatrix}, \quad (3.57)$$

that allow full positiveness of the vector \mathbf{f} . The set of these contact situations corresponds to the stable part of the space spanned by the contact situations pair $(\mathbf{k}^*, \boldsymbol{\theta}^*)$ which will be referred to as the space of contact configurations or *grasp-state space*. Stable grasps, as we refer to them should not be confused with form- or force-closure as usually defined in the literature. In this book, a stable grasp is a contact situation pair which corresponds to a vector \mathbf{f} where no component is negative, or more precisely,

“a grasp is stable if and only if the finger is in static equilibrium.”

The above definition of stability means that the phalanges in contact with an object have a positive (or zero) corresponding contact forces. The other phalanges, that are not in contact with the object must correspond to zero contact forces.

Again, this chapter tries to characterize the finger itself, independently from the object being grasped. If springs are neglected, expressions of the latter vectors become most simple. Angle θ_1 is obviously absent from the expressions because rotation about this axis leaves the mechanism in the same kinematic configuration (the finger is rotated as one single rigid body). It can also be shown that the signs of the components of \mathbf{f} are independent from k_1 , the proof is however more cumbersome and relies on the computation of a general inverse by means of cofactors (available in Appendix A.2).

The limit between the zones where all elements of \mathbf{f} are positive and the rest of the space is a $(2n - 3)$ -hypersurface in the grasp-state space. Therefore, it is impossible to completely visualize this boundary (between the all positive component space and its complement) for $n > 2$, e.g. for a three-phalanx finger. For example, with the set of parameters presented in Table 3.1, the volume of the stable three-phalanx grasps is approximately 14% of the whole space of contact configurations. This result is obtained by assuming this space to be bounded by a hyper-parallelepiped defined by $0 < k_i < l_i$ and $-\pi < \theta_i < \pi$ for $i > 0$. An illustration of the stability regions is provided in Fig. 3.3 where a section of the configuration space is shown: each force component is shown with the plane $f_i = 0$ (intersections with the latter are outlined). The percentage obtained above can seem abnormally small but, one should remember that full-phalanx grasps correspond only to a part of the set of whole possible grasps. That is, fewer-than- n -phalanx grasps can also be stable as will be discussed in Section 3.7. Furthermore, the stable contact situations are almost always located in the intuitive useful workspace. For example, if one changes the joint limits to $0 < \theta_i < \pi/2$ for $i > 0$, the percentage of stable three-phalanx grasps jumps to approximately 32%.

One should also note that even if the contact situation allows \mathbf{f} to be fully positive definite, the ratios between the components of this vector are independent from the actuator torque. Thus, in each contact situation, $\text{span}(\mathbf{f})$ is of dimension 1 and can be parameterized by T_a . One cannot modify the ratios between the components of \mathbf{f} without changing the contact situation, this property is characteristic of underactuated fingers since a limited number of actuators is available. In comparison, with a fully actuated finger, $\text{span}(\mathbf{f})$ is of dimension n .

The conditions for f_i to become zero—which can be considered as the edges of the positive-definite regions—become more complicated as i decreases. For example:

$$f_n = 0 \Leftrightarrow \prod_{i=2}^n h_i(h_i + l_{i-1}) = 0 \quad (3.58)$$

$$f_{n-1} = 0 \Leftrightarrow \begin{cases} g_{n-1} = k_n - h_n \cos \theta_n = 0 \\ \text{or} \\ \prod_{i=2}^{n-1} h_i(h_i + l_{i-1}) = 0 \end{cases} \quad (3.59)$$

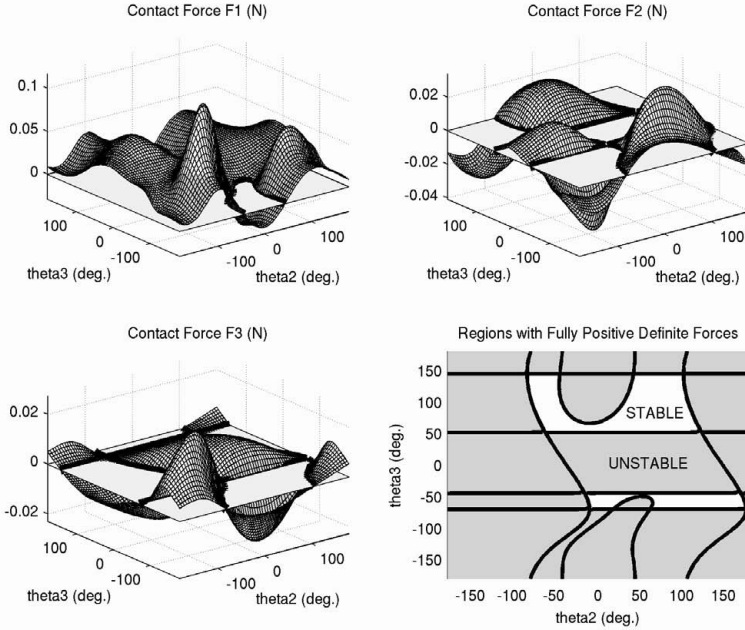


Fig. 3.3. Contact forces and associated stability loci ($k_i = l_i/2$, $i = 1, \dots, 3$)

$$f_{n-2} = 0 \Leftrightarrow \begin{cases} g_{n-2} = h_{n-1}l_{n-1}g_{n-1} \cos \theta_{n-1} \\ -k_{n-1}k_n(h_n + l_{n-1}) \\ +h_{n-1}h_nk_{n-1} \cos(\theta_{n-1} + \theta_n) = 0 \\ \text{or} \\ \prod_{i=2}^{n-2} h_i(h_i + l_{i-1}) = 0 \end{cases} \quad (3.60)$$

$$f_{n-3} = 0 \Leftrightarrow \begin{cases} g_{n-3} = 0 = \\ -h_{n-2}h_{n-1}k_{n-2}l_{n-2}g_{n-1}C_{\theta_{n-2}\theta_{n-1}} \\ -k_{n-2}k_{n-1}(h_{n-1} + l_{n-2})(h_n + l_{n-1}) \\ +h_{n-2}h_{n-3}h_nk_{n-2}k_{n-1}C_{\theta_{n-2}\theta_{n-1}\theta_n} \\ \text{or} \\ \prod_{i=2}^{n-3} h_i(h_i + l_{i-1}) = 0 \end{cases} \quad (3.61)$$

The first condition on f_{n-1} , namely g_{n-1} , has a simple geometrical meaning, i.e., the contact point lies on a particular location named the “equilibrium position” of the last phalanx (illustrated in Fig. 3.4(b)) as defined in (Laliberté and Gosselin 1998). This position corresponds to a distal phalanx in

equilibrium with no contact on the preceding phalanx. However, to the best of the knowledge of the authors, higher order cases have no simple interpretation and can correspond to situations where intuitively, one would expect that a full-phalanx grasp is stable (an example is shown in Fig. 3.4(c)). An illustration of configurations where one or more forces become negative is provided in Fig. 3.4. If k_i exists, it is assumed that $k_i = l_i/2$. Vanishing forces are indicated by dashed lines.

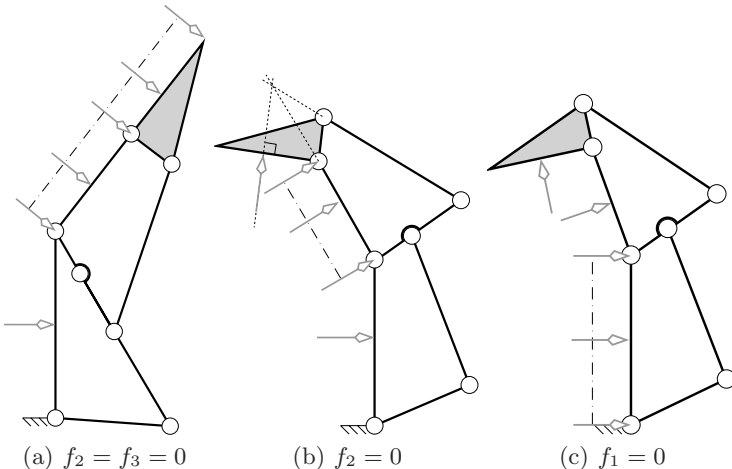


Fig. 3.4. Contact situations where one or more forces vanish (parameter set 1)

Table 3.1. Geometric parameters of a three-phalanx finger

Set	l_1	l_2	l_3	ψ	a_1	b_1	c_1	a_2	b_2	c_2
1	1	.67	.62	$\pi/2$.68	.95	.26	.68	.95	.26

A remarkable result is that the vanishing of f_n is most rare, because it can only happen when one X_i , $i > 1$ is zero which can be prevented by means of mechanical limits or careful design. One can also remark that if one and only one f_i is zero for a given θ^* , there is an implicit relationship between the contact location k_j for $j > i$ only. If more f_i 's are zero, a set of implicit equations must be satisfied by certain components of the contact situation pair. The latter can have one, many or no solutions, determining if this equilibrium configuration is possible. In order to obtain a stable grasp with the general n -phalanx finger, a contact situation (\mathbf{k}^*, θ^*) where the contact force vector \mathbf{f} has only positive components (however not strictly, a zero force component is acceptable) must be obtained. It is trivial to demonstrate that such situations are a subset of the set described by $f_n \geq 0$, meaning that the finger cannot be in equilibrium if the last phalanx is not. This simple statement yields more consequences than it

seems since, to ensure the final stability of the grasp, one has to obtain a stable last phalanx. Thus, one can design the last phalanx to obtain an optimally stable design. Using this approach, under the assumption that the variation of position of point O_{n-1} is negligible and no internal periodic mobility is possible, contact made with the last phalanx will never be lost inside the finger workspace and such an initial contact will thus tend to converge to a stable contact situation. The evolution of the contact situation trajectory can be rather complex depending on the geometry of the grasped object (cf. Section 4.2.3) and the dynamic properties of the phalanges (cf. Sections 4.3.4 and 4.3.5): contacts can be made, lost, remade, etc. during the grasping sequence. Nevertheless, an optimal last phalanx design will lead to a stable configuration under the assumptions previously stated.

Unstable designs can lead to the *roll-back phenomenon*, where the last phalanx slides against the object with a continuous closing motion resulting in a situation where the finger grasps nothing but itself (Fig. 3.5). Mechanical limits are key elements in the design of underactuated fingers considering stability issues because they limit the shape adaptation to reasonable configurations. In the worst case where all joints except the first one are locked, the finger simply act as a basic rotational gripper—with a quite complex shape of the jaw—but still, can firmly grasp the object. From that point of view, underactuated hands could be considered more like grippers with shape adaptation or deformable jaws, than like traditional robotic hands.

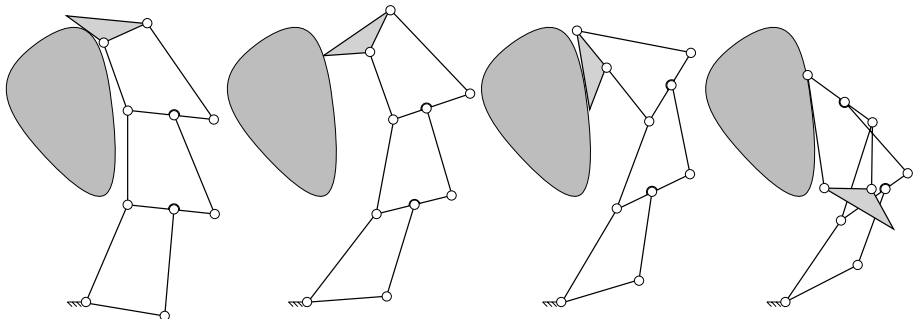


Fig. 3.5. Roll-back phenomenon

Finally, the capability of an underactuated finger to generate full-phalanx grasps can be characterized using an index χ as follows:

$$\chi = \frac{\int_W \delta(\mathbf{k}^*, \boldsymbol{\theta}^*) d\mathbf{k}^* d\boldsymbol{\theta}^*}{\int_W d\mathbf{k}^* d\boldsymbol{\theta}^*} \quad (3.62)$$

where $\delta(\mathbf{k}^*, \boldsymbol{\theta}^*)$ is a Kronecker-like symbol for the positiveness of vector \mathbf{f} that eliminates non-whole-phalanx grasps:

$$\delta(\mathbf{k}^*, \boldsymbol{\theta}^*) = \begin{cases} 1 & \text{if } f_i > 0, \forall i > 0 \\ 0 & \text{otherwise} \end{cases} \quad (3.63)$$

and W is the workspace of the finger in terms of $(\mathbf{k}^*, \boldsymbol{\theta}^*)$, i.e., the hyperbox defined by $0 < k_i < l_i$ and $-\pi < \theta_i < \pi$ for $i > 0$ or $0 < \theta_i < \pi/2$ for $i > 0$. The latter workspace is generally more useful since it ensures good performances in the usual workspace of the finger and avoids having the fully positive (stable) parts of the workspace in the least used areas of the latter. This index physically represents the percentage of the workspace that is achievable by full-phalanx grasps, namely the whole-hand grasping workspace. The definition of the index can be modified to obtain a measure of how far one is to losing contact with one phalanx by including a “distance” from the vanishing of the smallest component, i.e.,

$$\sigma = \frac{\int_W \min_i(f_i) \delta(\mathbf{k}^*, \boldsymbol{\theta}^*) d\mathbf{k}^* d\boldsymbol{\theta}^*}{\int_W T_a d\mathbf{k}^* d\boldsymbol{\theta}^*} \quad (3.64)$$

An index can also be defined based on the grasp forces distribution to provide the grasp with roughly equally distributed contact forces, such as (based on (Laliberté and Gosselin 2001), slightly modified):

$$I = \frac{\int_W \frac{\sum_i^n f_i}{\max_i(f_i)} \delta(\mathbf{k}^*, \boldsymbol{\theta}^*) d\mathbf{k}^* d\boldsymbol{\theta}^*}{n \int_W d\mathbf{k}^* d\boldsymbol{\theta}^*}. \quad (3.65)$$

Numerical values of the latter indices will be presented in Section 3.6.5.

3.6 Other Transmission Mechanisms

In the following sections, examples of usual transmission mechanisms will be given. Note that different types of mechanisms mixed in the same finger can be handled without changing the procedure.

3.6.1 Double-Stage Mechanism

The so-called double-stage mechanism is a mechanism similar to the one represented in Fig. 3.2 but with two consecutive phalanges merged into a single one as illustrated in Fig. 3.6. It has been considered for compactness (Shimojima et al. 1987). Analyzing such mechanisms is very similar to the initial study: matrix \mathbf{J} remains unchanged since the finger is still planar and only revolute joints are used, keeping in mind that phalanx lengths should be adjusted.

Matrix \mathbf{T} becomes:

$$\mathbf{T}^T = \begin{bmatrix} 1 & \mathbf{0}_{n-1}^T \\ -\frac{h_2 h_3}{(h_2 + l_1)(h_3 + l_2)} & \dots \\ \dots & \mathbf{1}_{n-1} \\ -\prod_{i=1}^n \frac{h_{2i} h_{2i+1}}{(h_{2i} + l_{2i-1})(h_{2i+1} + l_{2i})} & \end{bmatrix} \quad (3.66)$$

which corresponds simply to locking every even-numbered joint from the original single-stage design to zero degree. The expression of the matrix is straightforward and can be used to design a particular finger with a specific desired grasp force distribution. By using two stages instead of one, one can obtain specific ratios without requiring large values of a_i and c_i (link lengths). Thus, this mechanism will indeed generally lead to more compact designs. However, such designs will also have some drawbacks such as the limited space available for sensors, and a more complex architecture.

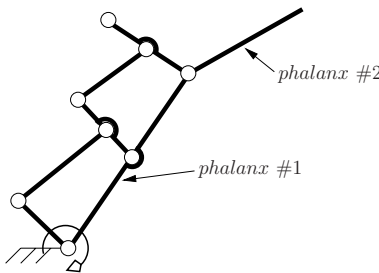


Fig. 3.6. Double-stage mechanism

3.6.2 Tendon-Pulley Transmission

A legacy of the tradition in robot finger actuation, and maybe even the first modern type of underactuated finger as discussed in Section 2.2, a tendon-driven finger is now studied. The design adopted here has already been used in underactuated fingers (Hirose and Umetani 1978; Massa et al. 2002) and is commonly available. The corresponding layout is shown in Fig. 3.7, and corresponds to the *Soft Gripper* architecture. Note that the pulleys and the respective phalanx joints share the same axis, yet, both are not rigidly attached. It is important to notice that the pulleys can freely rotate around their axes without transmitting this rotation to the phalanges. If this condition is not satisfied, the finger will not be underactuated but will rather exhibit a coupled motion of the phalanges and the finger itself will only have one DOF.

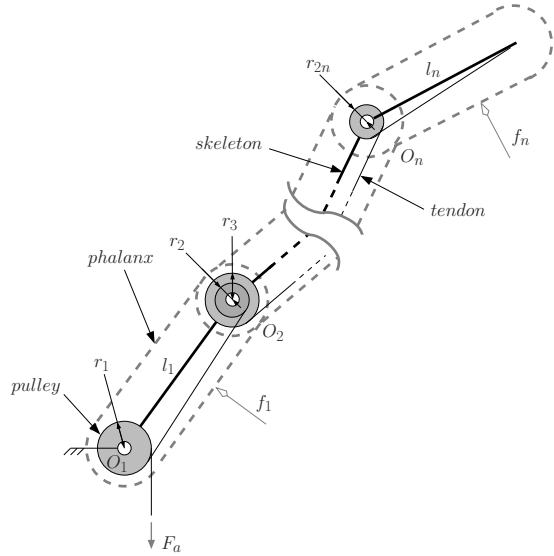


Fig. 3.7. Tendon-driven finger

The expression of matrix \mathbf{J} remains again unchanged. Matrix \mathbf{T} can be simply expressed as:

$$\mathbf{T}^T = \begin{bmatrix} 1 & \mathbf{0}_{n-1}^T \\ -\frac{r_2}{r_1} & \\ -\frac{r_2 r_4}{r_1 r_3} & \\ \dots & \mathbf{1}_{n-1} \\ -\prod_{i=1}^n \frac{r_{2i}}{r_{2i-1}} & \end{bmatrix} \quad (3.67)$$

as presented in eq. (3.37). Note that, in this case, the latter matrix is constant for any configuration of the finger as opposed to what was obtained in the analysis presented above for fingers driven with linkages. One can again proceed with the expression of the contact force vector as presented in eq. (3.42). An interesting result arises if the ratio of the pulley radii is constant, i.e.:

$$\frac{r_{2i}}{r_{2i-1}} = \alpha \quad i > 0 \quad (3.68)$$

Usually $\alpha < 1$ for compactness. Moreover, if $\alpha > 1$, the design is intrinsically unstable as will be shown in Section 4.2.3. Eq. (3.68) considerably simplifies the expression of matrix \mathbf{T} . The expression of the last phalanx forces can then be written as:

$$\begin{cases} f_n = \frac{\alpha^{n-1}}{k_n} T_a \\ f_{n-1} = -\frac{\alpha^{n-2}(k_n(\alpha-1)+\alpha l_{n-1} \cos \theta_n)}{k_{n-1} k_n} T_a \end{cases} \quad (3.69)$$

with $T_a = r_1 F_a$. Similarly to the previous study, the conditions for the forces to become zero are implicit functions that cannot be easily solved. Interestingly, the contact force on the last phalanx is only a function of the ratio α and the location of the corresponding contact k_n , and not of the configuration of the finger itself.

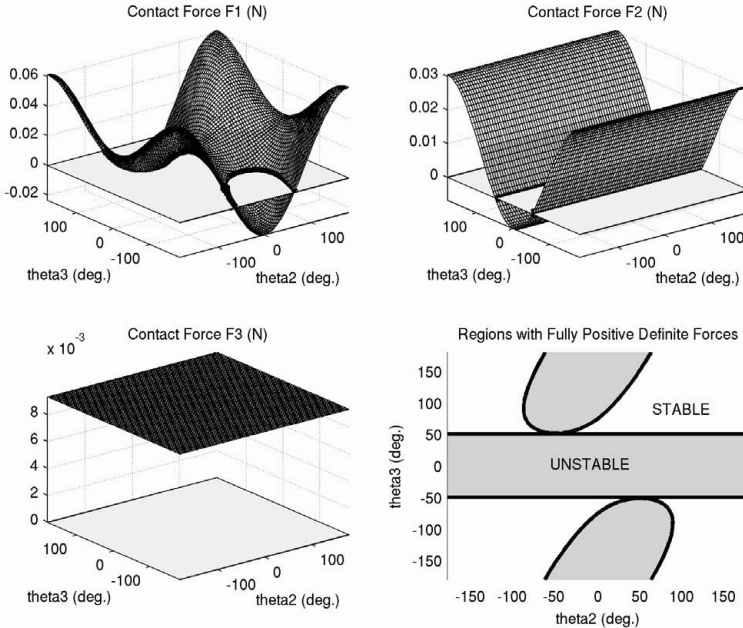


Fig. 3.8. Tendon-driven finger, contact forces and stability loci ($k_i = l_i/2$, $i = 1, \dots, 3$)

Furthermore, note that the limit case where $\alpha = 1$ is an almost always unstable design. It is equivalent to its linkage-driven “evil twin,” the parallelogram (details on this issue will be presented in Section 4.2.3): both have the exact same condition for positiveness. Similarly to what was obtained in Section 3.5, a tendon-driven finger with pulley radii equivalent to link lengths, i.e., $r_{2i-1} = a_i$ and $r_{2i} = c_i$, has a possible stable three-phalanx grasp occurrence of approximately 56% to be compared to the 14% of the mechanism first studied (a section similar to that shown in Fig. 3.3 is shown in Fig. 3.8 for $k_2 = l_2/2$ and $k_3 = l_3/2$). If limits are placed on the components of $\boldsymbol{\theta}$ similarly to what was done in Section 3.5, that percentage drops to approximately 41%, which is still larger than what was obtained for the linkage-driven finger. Thus, for small forces and with appropriate control to compensate elasticity and friction, this mechanism can be very effective, as for instance for lightweight prosthetic devices. The kinematic similarity between both mechanisms is clearly evidenced with our analysis technique, highlighting the inherent generality of the presented method. Instantaneous equivalence is illustrated in Fig. 3.9.

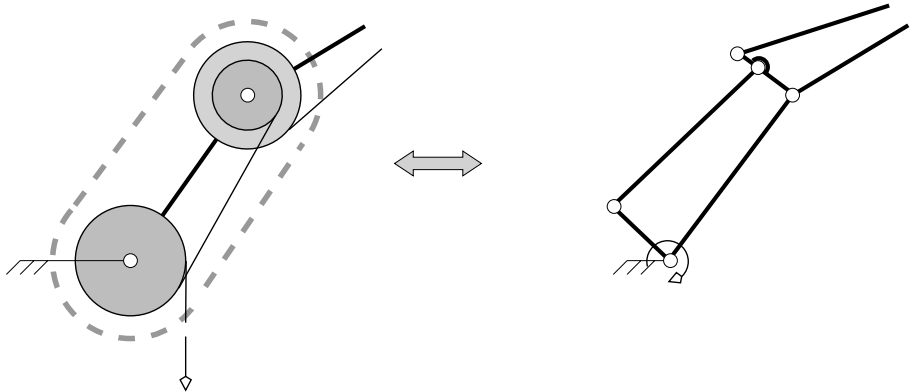


Fig. 3.9. Equivalence between pulley-tendon and four-bar transmission

3.6.3 Gears

A gear train can be used instead of tendons to connect the principal gears located on the joints of the fingers. With such a mechanism, matrix \mathbf{T} becomes:

$$\mathbf{T}^T = \begin{bmatrix} 1 & \mathbf{0}_{n-1}^T \\ -\frac{N_2 N_2^{1*}}{N_1 N_2^1} & \\ -\frac{N_2 N_2^{1*} N_4 N_4^{3*}}{N_1 N_2^1 N_3 N_4^3} & \\ \dots & \mathbf{1}_{n-1} \\ -\prod_{i=1}^n \frac{N_{2i} N_{2i}^{2i-1*}}{N_{2i-1} N_{2i}^{2i-1}} & \end{bmatrix} \quad (3.70)$$

where N_{2i-1} and N_{2i} are respectively the number of teeth of the gear located at the base and the end of the i^{th} phalanx. Both gears are connected through a train with an odd number of intermediate stages (to maintain rotation in the same direction) that can be described by two equivalent gears with tooth ratio

$$\frac{N_{2i}^{2i-1*}}{N_{2i}^{2i-1}}. \quad (3.71)$$

In other words, the gear with N_{2i}^{2i-1} teeth is in contact with the gear having N_{2i-1} teeth which is rigidly connected to gear N_{2i}^{2i-1*} which in turn transmits motion to the gear having N_{2i} teeth. Note that this form is very similar to the double-stage mechanism presented in Section 3.6.1. In fact this mechanism is to pulleys and tendons what the double-stage mechanism is to the four-bar linkage. A comparison is again illustrated in Fig. 3.10 (gears are represented by their primitive circles).

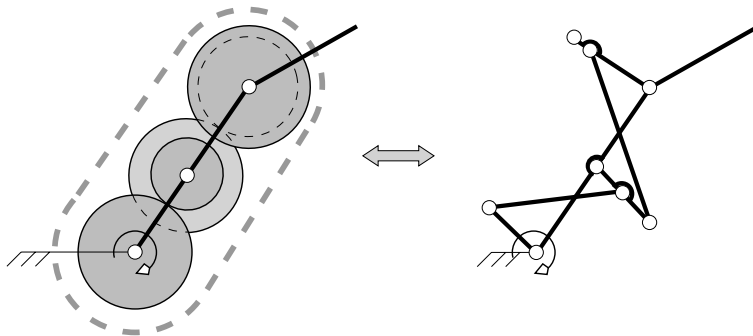


Fig. 3.10. Equivalence between gears and four-bar transmission

3.6.4 Da Vinci's Mechanism

The finger architecture invented by da Vinci and presented in Section 2.2.2 (also illustrated in Fig. 2.13) is now studied. The architecture studied in this section is shown in Fig. 3.11, and corresponds to the drawing found in the *Codex Atlanticus*. It is important to notice that the pulleys can again freely rotate around their axes without transmitting this rotation to the phalanges.

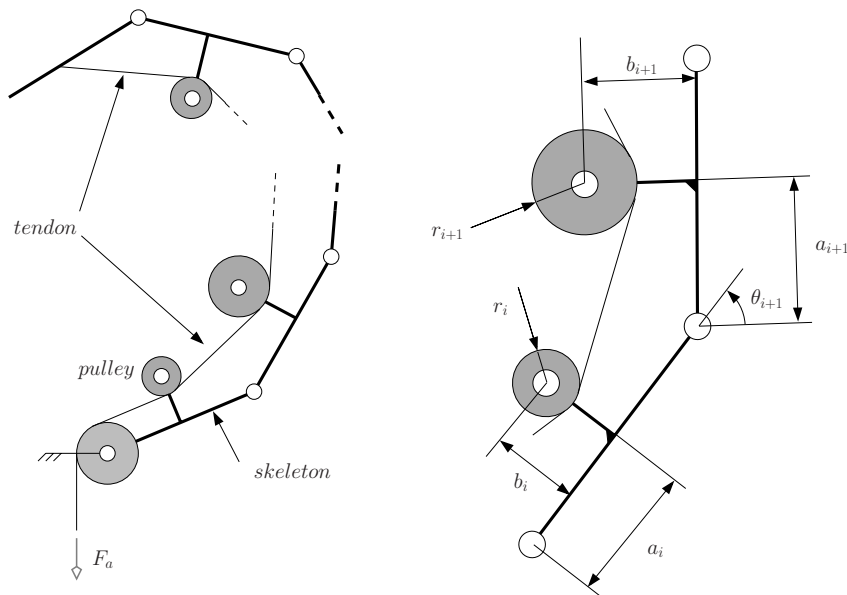


Fig. 3.11. Da Vinci's mechanism

As usual, the expression of matrix \mathbf{J} remains unchanged while matrix \mathbf{T} becomes:

$$\mathbf{T}^T = \begin{bmatrix} 1 & \mathbf{0}_{n-1}^T \\ \frac{R_1}{r_0} & \\ \dots & \\ \frac{R_{n-1}}{r_0} & \mathbf{1}_{n-1} \end{bmatrix} \quad (3.72)$$

where R_i for $i = 1, \dots, n-1$ is the radius of a pulley equivalent to the i^{th} transmission stage (illustrated in the right hand side of Fig. 3.11) and driven by the base pulley (with a radius r_0). This equivalent radius corresponds to the radius r_{2i-1} of the pulley located at the base of the i^{th} phalanx with a *Soft Gripper* architecture using a single tendon routing (i.e., $r_{2i-1} = r_{2i-2}$ for $i = 2, \dots, n$), discussed in Section 2.2.2. It can be shown that the equivalent radius of the i^{th} transmission stage is

$$R_i = r_i + \frac{b_i(rb - al) - (l_i - a_i)(ar + bl)}{a^2 + b^2} \quad (3.73)$$

with

$$r = r_{i+1} - r_i, \quad (3.74)$$

$$a = l_i - a_i + a_{i+1} \cos \theta_{i+1} - b_{i+1} \sin \theta_{i+1}, \quad (3.75)$$

$$b = -b_i + a_{i+1} \sin \theta_{i+1} + b_{i+1} \cos \theta_{i+1}, \quad (3.76)$$

$$l = \sqrt{a^2 + b^2 - r^2}. \quad (3.77)$$

$$(3.78)$$

It should be noted that the absence of a minus sign in front of the radius ratios in eq. (3.72) is not a mistake and is due to the tendon routing between the first and subsequent pulleys, which is changed from Section 3.6.2. This modification inverts the direction of rotation of the latter pulleys with respect to the first one and yields the positive signs in eq. (3.72).

Similarly to what was encountered in the analysis of the *Soft Gripper*, the conditions for the forces to become zero are implicit functions that cannot be easily solved. A section similar to that presented in Figs. 3.3 and 3.8 is shown in Fig. 3.12 for $k_2 = l_2/2$ and $k_3 = l_3/2$. The geometric parameters used in this example are shown in Table 3.2.

As opposed to what was observed for the *Soft Gripper* architecture, in the case of da Vinci's mechanism, the distal contact force can vanish. This phenomenon corresponds to a configuration where the last part of the tendon is on the same line as the distal phalanx, as illustrated in Fig. 3.13. The expression of the Transmission matrix is also far more complicated than the simple and

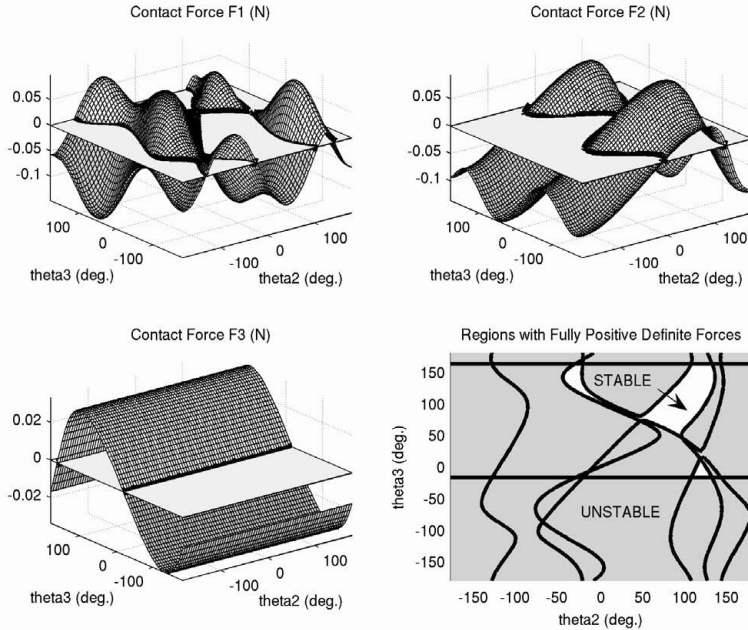


Fig. 3.12. Da Vinci’s mechanism: contact forces and stability loci ($k_i = l_i/2$, $i = 1, \dots, 3$)

Table 3.2. Geometric parameters of Da Vinci’s mechanism

Set	l_1	l_2	l_3	r_0	a_1	b_1	r_1	a_2	b_2	r_2	a_3
1	1	1	1	.15	.2	.25	.1	.45	.25	.07	.25

elegant radius ratios of the *Soft Gripper* architecture. Furthermore, da Vinci’s architecture might be difficult to implement practically because of mechanical interferences and seems to achieve poorly with respect to the positive definiteness of the contact forces as illustrated in Fig. 3.12. However, it should be taken into account that the equivalence rule used to compare linkage- and tendon-driven fingers cannot be applied here due to the amount of parameters available and therefore percentages of possible stable three-phalanx grasp occurrence are not given since they are not deemed representative.

Da Vinci’s mechanism can be seen as a generalization of the single-tendon *Soft Gripper* architecture described in Section 3.6.2 where $a_i = l_i$ and $b_i = 0$ for $i = 1, \dots, n$. However, note that the expressions obtained in this section cannot be derived directly from eq. (3.67) since the routing of the tendon between the first two pulleys is different, as discussed previously.

Finally, it is important to note that in this book, unless specifically stated otherwise, a “tendon-driven finger” denotes an architecture similar to that of

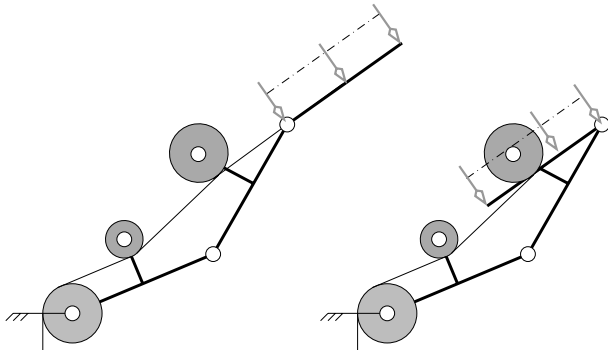


Fig. 3.13. Contact situations where the distal phalanx force vanishes

the *Soft Gripper* as described in Section 3.6.2 although da Vinci's finger is also, indeed, driven with a tendon.

3.6.5 Comparison

The indices introduced in eqs. (3.62), (3.64), and (3.65) can be used to compare some of the different mechanisms presented in the previous sections. Results are presented in Table 3.3. In order to illustrate a comparison procedure, equivalence between link lengths, pulley radii, etc. are established arbitrarily using the rule presented in Section 3.6.2 and with the parameters defined in Table 3.1. When only two phalanges are considered, geometric parameters correspond to the last two phalanges in the latter table. The workspace used is defined by $0 < k_i < l_i$ and $0 < \theta_i < \pi/2$ for $i > 0$.

It can be observed that, in general, tendon-driven fingers have better overall performances than linkage-driven fingers. This is due to the fact that they do not suffer from mechanical singular configurations (for example when three points of the transmission mechanism are aligned, see Section 3.5). This is not the

Table 3.3. Characteristic indices

Transmission	n	χ	σ	I
linkages	3	0.32	0.0011	0.17
linkages	2	0.43	0.0051	0.21
pulley-tendons	3	0.41	0.0019	0.24
pulley-tendons	2	0.53	0.0058	0.27
gears	2	0.63	0.0037	0.33
double-stage	2	0.64	0.0035	0.32

case with multiple-stage fingers because such singular configurations become most rare if they exist at all, since both stages contribute to attaining the same kinematic configuration. However, larger forces can be applied with linkages than with tendons since power transmission is performed through rigid bodies resulting in very firm grasps. With more phalanges, one tends to achieve more adaptive grasps but it becomes less likely that all phalanges simultaneously contribute to the grasp.

3.7 Less-than- n -phalanx Grasps

In order for a less-than- n -phalanx grasp to be stable, each phalanx in contact with the object should have a strictly positive contact force. For phalanges not in contact with the object, the corresponding generated forces, defined in eq. (3.42) should be zero. Indeed, the latter forces can also be seen as the external forces needed to counter the actuation torque since equilibrium is implicitly assumed by eq. (3.1). Thus, the relationships discussed in Section 3.5 for the positiveness of forces also give us the equilibrium conditions for less-than- n -phalanx grasps. For example, in order to determine under which conditions a stable grasp can be achieved with no contact on phalanx say $n - 1$, the following condition must be satisfied

$$\begin{cases} f_j > 0 & j \neq n - 1 \\ g_{n-1} = 0. \end{cases} \quad (3.79)$$

Such conditions are of greater importance than it may seem at first glance since, as it has been shown, only part of the finger contact situation space is stable with full-phalanx stable grasps. Thus, full-phalanx grasps are only a subset of the possible stable grasp contact configurations. Moreover, non-trivial less-than- n -phalanx contact equilibria are possible, non-trivial meaning without simple geometric relationships as two links on the same line. Thus, it is theoretically possible to fully constrain a general n -DOF finger with a single contact in such non-trivial configurations. It should also be noted that, in the previous example, f_j with $j < n - 1$ is a function of k_{n-1} which does not actually exist. Reasoning on the limit case of equilibrium, when the phalanx force f_{n-1} tends to zero, one can argue that f_j with $j < n - 1$ should be positive for any k_{n-1} . Hence modified force expressions should be satisfied to achieve equilibrium.

3.8 Conclusions

This chapter presented and analyzed the force capabilities of underactuated fingers. The main contribution of this chapter is the introduction of matrices \mathbf{J} (Jacobian) and \mathbf{T} (Transmission). These matrices allow immediate characterization of the finger, provide the expressions of contact forces developed by the finger, lead to considerations on equilibrium with any number of phalanges in contact and provide tools for comparison between different designs. Such comparisons

can be very useful to choose a particular design of underactuated finger. However, one shall keep in mind other considerations, that are not easily mathematically quantifiable. For example, friction and elasticity can eliminate tendon-driven fingers despite their good performance indices. Even the performance criteria themselves should be used with caution as they are context dependent. Furthermore, although an infinite number of phalanges is theoretically ideal for grasping—since such a finger would tend to approach the spatial complement of the shape of the object, which is the perfect grasper—practical considerations on cost and complexity of the design generally limit the number of phalanges to three or four at most. Hence, the authors believe that the tools presented in this chapter can help refining underactuated finger designs in terms of geometric parameters although the general layout of the finger remains application-driven. The results obtained in this chapter have been partially published in (Birglen and Gosselin 2004a).

In order to properly design underactuated fingers, one should be aware of the possible unstable grasps and also of the phalanx force distribution to avoid weak last phalanges that cannot ensure sufficient force to secure the grasp. It should be pointed out that the possibility of having negative forces on the phalanges during a grasp with an underactuated finger is a new concept for many designers of underactuated hands. Indeed, most of the time, the theoretical static analysis of the grasp is quickly performed (Dubey and Crowder 2002), is incomplete (Hirose and Umetani 1978), or relies on experimental measurements (Hirose and Umetani 1978; Shimojima et al. 1987; Carrozza et al. 2003). Once a force has been established to be negative, the sliding motion taking place afterwards should be studied to guarantee the stability of the grasp. In the next chapter, the behaviour of two- and three- phalanx fingers subjected to such motion will be studied.

4 Grasp Stability of Underactuated Fingers

Montag had done nothing. His hand had done it all, his hand, with a brain of its own, with a conscience and a curiosity in each trembling finger, had turned thief.

Ray Bradbury, *Fahrenheit 451*, 1953.

in which the grasp properties of two- and three-phalanx underactuated fingers of general architecture are presented and their ability to seize objects with a stable grasp is studied. Considerations on the local geometry of the contact and the influence of the design parameters are discussed. The finger behaviour is described using a grasp-state space representation that allows an accurate visualization of the contact state trajectory as well as equilibrium and unstable situations. With three-phalanx fingers, an i^{th} order equilibrium is defined, when the finger is in static equilibrium with i missing contacts. A particular emphasis is placed on the cases for which $i = 1$ and $i = 2$. Certain geometric configurations leading to equilibrium even with missing contacts are also shown.

4.1 Introduction

If one or more phalanx force is negative when an underactuated finger closes on an object, the corresponding phalanx will loose contact with the latter object. Then, another step in the grasping process will take place: the remaining phalanges—corresponding to positive forces—will slide on the surface of the object. This sliding process will continue until either a stable configuration is achieved (with only positive or zero phalanx forces) or joint limits are reached (usually a stable situation, but the shape adaptation is less effective) or the finger will curl away and loose contact with the object (ejection).

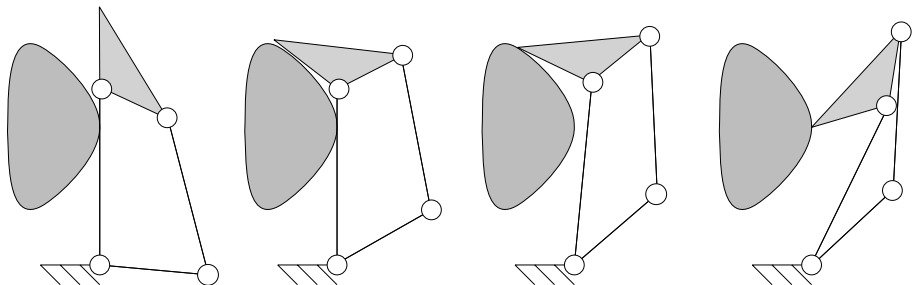


Fig. 4.1. Ejection phenomenon with a two-phalanx underactuated finger

In this book, a stable grasp means that the finger is in static equilibrium. This definition, given in Chapter 3 is fundamental to the comprehension of the book and should be re-emphasized:

“a grasp is stable if and only if the finger is in static equilibrium.”

If contact with the last phalanx is lost, a “stable” grasp can still be achieved in fact, but with surfaces of the phalanx that were not intended for this task (the back of the finger). It is also theoretically possible that ejection will then propagate itself to all lower phalanges (if they exist), ending in a catastrophic configuration where the finger does not hold the object at all (as illustrated in Fig. 3.5). An example of an ejection sequence is presented in Fig. 4.1. This phenomenon was first noticed in (Laliberté and Gosselin 1998), and is similar to the self-posture changeability described in (Kaneko and Tanie 1990). However, despite its importance, it has never been closely studied for grasping. The occurrence of these situations where one (or more) phalanx force is negative should be decreased (prevention may be impossible, as will be discussed in Section 4.2.7) and the ejection avoided. Thus, a fundamental question should be raised: “how can we guarantee that a grasp is stable?” as well as its direct corollary “how can we increase the occurrence of these situations?” The answer to these questions will allow one to elaborate design rules that can be used to obtain optimally stable fingers.

With practical prototypes, the stability of the grasps must be ensured in the sense that ejection is prevented. Significant progress has been achieved by intuitive designs from outstanding individuals, to create underactuated fingers. However, this method may overlook theoretical issues and it is one purpose of this book to lay the foundation of a theoretical background to study the performances of such fingers and to guarantee a proper “behaviour”. Biomimetic approaches have been used in the past and are usually reliable since they are based on the results of natural selection. However, understanding the qualities and drawbacks of these designs can help to overcome their limits. One should also keep in mind that designing a robot is not the same as producing robust living creatures, with distinct constraints and different objectives, as discussed in Chapter 2.

In Chapter 3, the fact that underactuated fingers cannot always apply forces with all their phalanges in all configurations was presented and the consequences were briefly discussed. In fact, even if a fully positive workspace is provided,

i.e., with a finger that can always provide positive contact forces with all its phalanges, one cannot guarantee that contact between the object and the finger will be made with all the phalanges, depending on the object size and position. Therefore, the mobility of a n -phalanx finger with less than n contacts should be studied. In this chapter, the cases for which $n = 2$ and $n = 3$ are presented and a technique to study the grasp stability is introduced.

The ideal grasping sequence illustrated in Fig. 2.3 does not always occur for in the final configuration some phalanx forces may be negative. These configurations correspond to the unstable regions of the finger workspace described in the previous chapter. The aim of this chapter is to characterize this sliding motion to predict if a stable configuration will be achieved or if ejection occurs, with two- and three-phalanx fingers of arbitrary architecture. Examples involving common transmissions, namely linkages and pulleys, are presented and discussed (described in Sections 3.2 and 3.6.2).

4.2 Grasp Stability of Two-Phalanx Underactuated Fingers

4.2.1 Grasp Stability for Single Point Contact

Using the results of the preceding chapter, one obtains, for a two-phalanx finger:

$$\mathbf{T} = \begin{bmatrix} 1 & R \\ 0 & 1 \end{bmatrix} \quad \text{and} \quad \mathbf{J} = \begin{bmatrix} k_1 & 0 \\ k_2 + l_1(\cos \theta_2 - \mu \sin \theta_2) & k_2 \end{bmatrix} \quad (4.1)$$

where R is the transmission factor characterizing the mechanism. The resulting normal forces are therefore obtained from eq. (3.42), i.e.,

$$\mathbf{f} = \mathbf{J}^{-T} \mathbf{T}^{-T} \mathbf{t} \quad (4.2)$$

which yields

$$\mathbf{f} = \begin{bmatrix} \frac{k_2(1+R)+Rl_1G}{k_1k_2} T_a - \frac{k_2+l_1G}{k_1k_2} T_2 \\ -\frac{R}{k_2} T_a + \frac{1}{k_2} T_2 \end{bmatrix}, \quad (4.3)$$

where $G = (\cos \theta_2 + \mu \sin \theta_2)$. If an additional torsional spring is located in O_1 , its effect, namely T_1/k_1 , is simply subtracted from the first component of vector \mathbf{f} (this holds for any number of phalanges, the proof is presented in Appendix A.2). This spring is not necessary to obtain a statically determined finger but it has been used in tendon-driven fingers since the actuation cannot pull the finger back. For instance, the springs presented in our model, Fig. 3.1, have been replaced with a “release wire” in (Hirose and Umetani 1978) and a “release tendon” in (Crisman et al. 1996). Note that this replacement can be extended to any transmission mechanism used to distribute the actuation torque to the phalanges.

In this section, the conditions for a two-phalanx underactuated finger to achieve a stable grasp are studied. As opposed to what is commonly used in

grasping analysis and as defined in Section 2.2, the term “stability” designates in this book a grasp situation where the finger is in static equilibrium, i.e., all phalanx forces are positive or zero. An alternative definition can be given as:

“a grasp is stable only if all phalanx forces are positive or zero.”

If a contact exists with a phalanx, the corresponding contact force should be positive or zero. If no contact exists, this force should be zero. The above definition of stability is different from form- or force-closure and is a necessary condition to be achieved in order to ensure one or the other of the previous forms of stability. Usually force-closure is defined as the property of a system to be able to withstand any external wrench, hence to be able to generate any wrench in the wrench space. This concept has been historically referred to as *form-closure* by Reuleaux in 1875 (Reuleaux 1963). Reuleaux defined another kind of force-closure when the system is stable with the help of an external wrench, “closure” came from a water wheel he studied that needed to “close” the contact between the axle and the groove to function properly. It should be noted that both definitions are often confused, which is quite understandable since what Reuleaux defined as *form-closure* is now commonly referred to as *force-closure* while the former is now used with a different meaning.

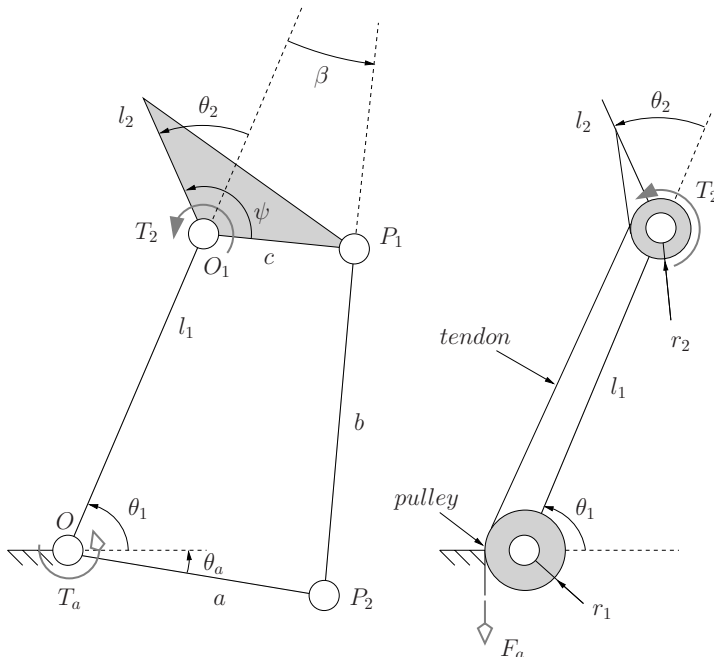


Fig. 4.2. Common transmissions: mechanical linkage and pulley-tendon

A model for the fingers under study is presented in Fig. 4.2. The results of the previous chapter allow us to obtain the expressions of the contact forces, for instance (initially without friction) for a linkage-driven finger, one has:

$$\mathbf{T} = \begin{bmatrix} 1 - \frac{h}{h+l_1} \\ 0 & 1 \end{bmatrix}, \quad (4.4)$$

$$\mathbf{f} = \begin{bmatrix} -\frac{l_1(-k_2 + h \cos \theta_2)}{k_1 k_2 (h+l_1)} T_a - \frac{k_2 + l_1 \cos \theta_2}{k_1 k_2} T_2 \\ \frac{h}{k_2(h+l_1)} T_a + \frac{1}{k_2} T_2 \end{bmatrix}, \quad (4.5)$$

where

$$h = c(\cos(\theta_2 - \psi) - \sin(\theta_2 - \psi) \cot \beta) \quad (4.6)$$

is the directed distance between point O_1 and the geometric intersection of lines (OO_1) and $(P_1 P_2)$. An expression of $\cot \beta$ can also be obtained as a function of the parameters of the system as established in eq. (3.26), namely

$$\cot \beta = \frac{c \sin(\theta_2 - \psi) \sqrt{4a^2 b^2 - N^2} + M(l_1 + c \cos(\theta_2 - \psi))}{-(l_1 + c \cos(\theta_2 - \psi)) \sqrt{4a^2 b^2 - N} + Mc \sin(\theta_2 - \psi_2)} \quad (4.7)$$

with

$$M = -l_1(l_1 + 2c \cos(\theta_2 - \psi)) + a^2 - b^2 - c^2, \quad (4.8)$$

$$N = l_1(l_1 + 2c \cos(\theta_2 - \psi)) - a^2 - b^2 + c^2. \quad (4.9)$$

For tendon-driven fingers, one has:

$$\mathbf{T} = \begin{bmatrix} 1 - \alpha \\ 0 & 1 \end{bmatrix}, \quad (4.10)$$

$$\mathbf{f} = \begin{bmatrix} -\frac{-k_2 + \alpha k_2 + \alpha l_1 \cos \theta_2}{k_1 k_2} T_a - \frac{k_2 + l_1 \cos \theta_2}{k_1 k_2} T_2 \\ \frac{\alpha}{k_2} T_a + \frac{T_2}{k_2} \end{bmatrix} \quad (4.11)$$

with $\alpha = r_2/r_1$ and $T_a = F_a/r_1$. As it can be seen, the expressions are much simpler with tendon-driven fingers because the transmission factor r_2/r_1 is constant compared to $h/(h+l_1)$ which is a complex function of the design parameters of the finger and the angle θ_2 . Then, one can study the condition under which both f_1 and f_2 are positive (or not), which depends on the contact situation, namely the pair (k_2, θ_2) , but neither on θ_1 nor on k_1 as shown in Chapter 3. This pair defines a plane, where the contact situation can be tracked. This plane will be referred to as the grasp-state plane, the associated pair is not a state vector as defined in the control literature since it is not associated with the potential energy of the system. However, this grasp-state plane can be analyzed similarly to

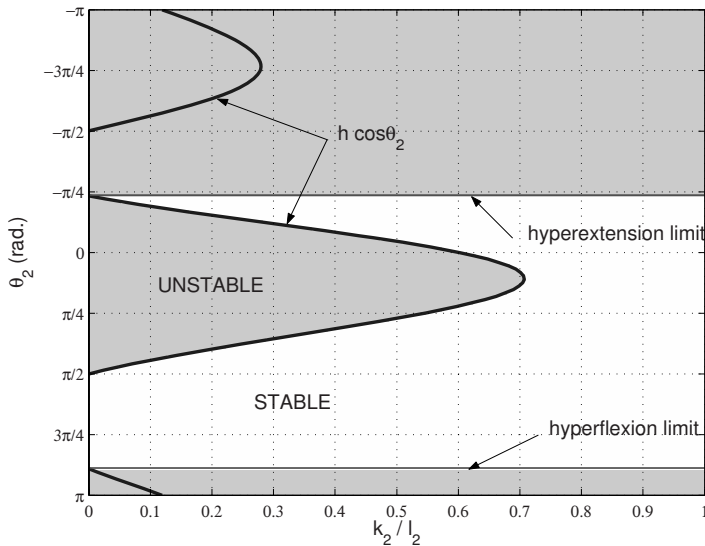


Fig. 4.3. Positive zones for f (parameter set 1)

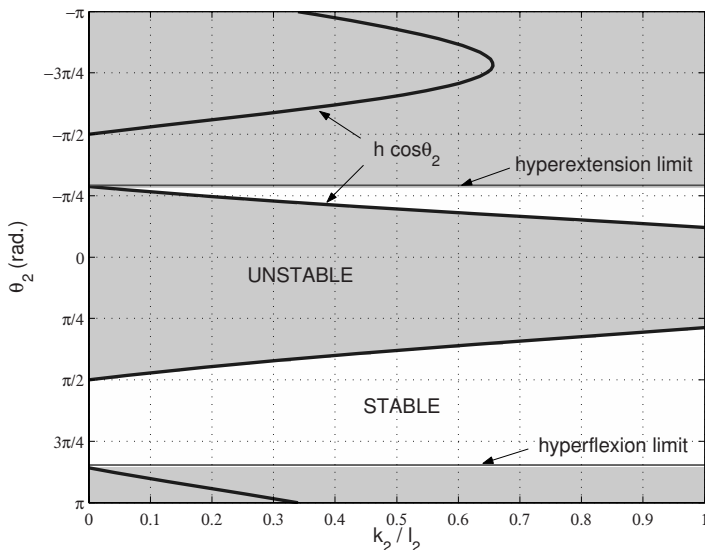


Fig. 4.4. Positive zones for f (parameter set 2)

the state plane of a dynamic system to study the grasp stability, and equilibrium situations. Grasp-state trajectories can also be defined, as will be shown.

Examples of configurations with fully positive contact forces are presented in Figs. 4.3, 4.4 and 4.5 for the sets of geometric parameters presented in

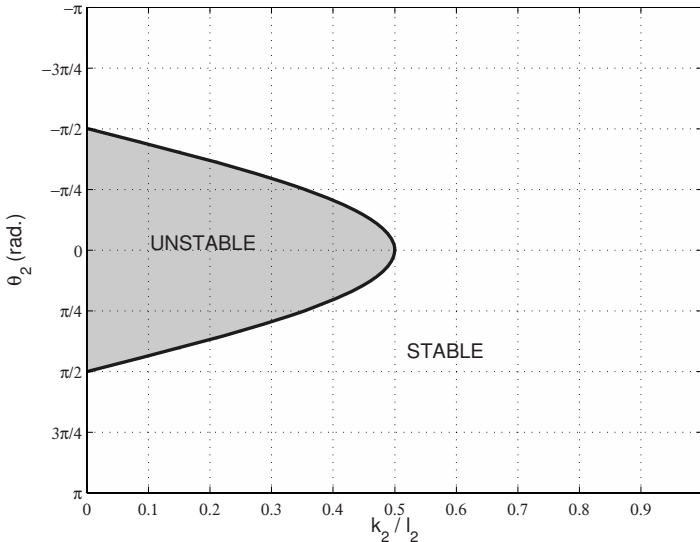


Fig. 4.5. Positive zones for f (Soft Gripper)

Table 4.1 (with neither friction nor the spring). Shaded areas are unstable contact configurations where

$$f_1 < 0 \quad \text{or} \quad f_2 < 0 \quad (4.12)$$

The *Soft Gripper* parameters have been calculated according to the formula presented in (Hirose and Umetani 1978). It should be emphasized that, with a fully actuated finger, the stable zones will be the whole workspace (the whole plane). Conversely, in Fig. 4.3—a not so particular example—situations with positive phalanx forces are minority cases.

When in an unstable configuration, the closing process will force the finger to lose contact with one of the phalanges, usually the proximal one. Then, contact will only remain with the distal phalanx (Figs. 4.6 and 4.7). In Fig. 4.6, empty arrows indicate mono-directionality of contact forces (objects grasped are fixed in space and can be merged). It should be noted that the signs of both contact forces do not change because of the local geometry of the object at the contact

Table 4.1. Geometric parameters of the two-phalanx fingers

Set	l_1	l_2	ψ	a	b	c
1	1	2/3	90°	1	1	1/3
2	1	2/3	90°	2/3	1	1/3
Soft Gripper	1	1	—	1	—	1/3

point, but only of its location on the phalanx. However, this shape is important as will be discussed in Sections 4.2.2 and 4.2.4.

If $f_1 < 0$, an equilibrium position can still be attained but only for a unique particular position of contact k_2 . This is, of course, the position corresponding to the solution of the equation $f_1(k_2) = 0$, i.e.,

$$k_2 = e = -\frac{R}{1+R}l_1(\cos \theta_2 + \mu \sin \theta_2) \quad (4.13)$$

if the spring is neglected. In the case of linkage-driven fingers, one obtains

$$e = h(\cos \theta_2 + \mu \sin \theta_2). \quad (4.14)$$

Physically, if friction is neglected, eq. (4.14) implies that the contact force should be located on the projection onto the distal phalanx of the intersection of lines (OO_1) and (P_1P_2) (dashed lines in Fig. 4.6). Indeed, the distal phalanx is subjected to three pure forces, thus equilibrium can only exist if they all intersect at a common point. However this geometric interpretation no longer holds if the spring is taken into account. Also, this is no longer valid if there is a contact on the proximal phalanx. For tendon-driven fingers, one has:

$$e = \frac{r_2}{r_1 - r_2}l_1(\cos \theta_2 + \mu \sin \theta_2). \quad (4.15)$$

The geometric construction of the equilibrium point is illustrated in Fig. 4.8 for both cases of transmission, with neither friction nor the spring. In the case of a tendon-driven finger, the construction is very similar to the previous example with the tendon between the pulleys replacing the link b .

It should be noted that the force on the distal phalanx is always positive except in hyperflexion/hyperextension configurations for mechanical transmissions (illustrated in Fig. 4.9). With pulleys and tendons, the force on the distal phalanx

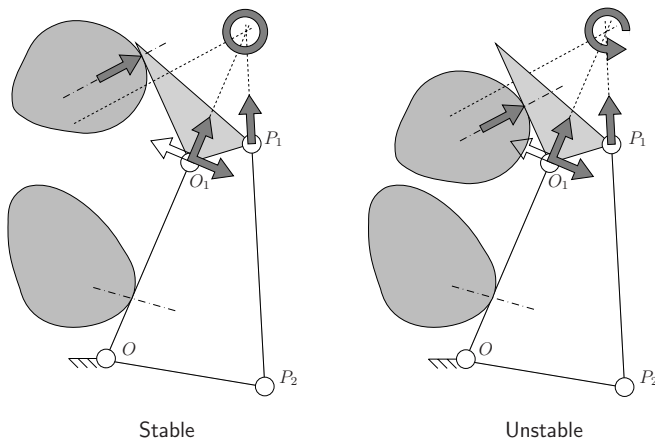


Fig. 4.6. Stable and unstable configurations with two contact points

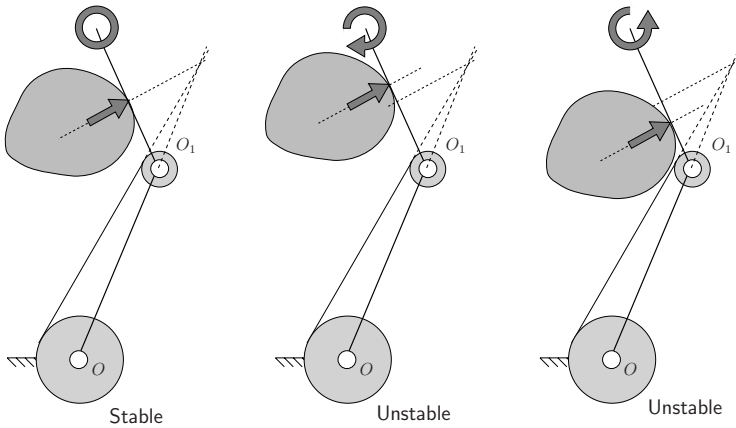


Fig. 4.7. Stable and unstable one-phalanx contact configurations

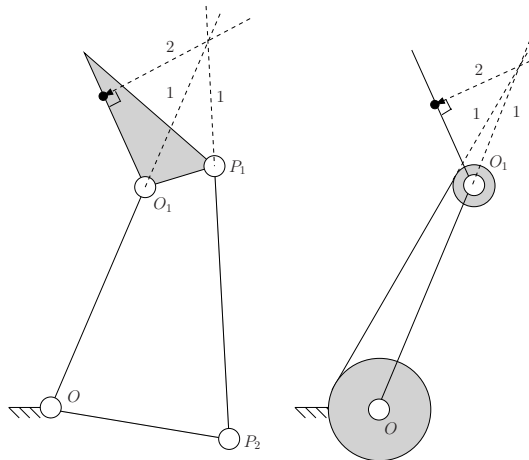


Fig. 4.8. Geometric construction of the equilibrium point

is *always* positive if the spring is neglected. The hyperflexion/hyperextension configurations are bounded by the horizontal lines at approximately $\theta_2 = -52^\circ$ and $\theta_2 = 160^\circ$ in Fig. 4.3 for that particular parameter set and are responsible for most of the large unstable areas in the latter figure, the others corresponding to a contact below the equilibrium point where $f_1 < 0$. These horizontal lines correspond to limit cases where $h = 0$. Such configurations may indicate that tendon-driven fingers should be preferred. However, it should be noted that such configurations with large values of θ_2 are usually not achievable with both kinds of transmission due to mechanical limits, common limits on θ_2 being $0 < \theta_2 < \pi/2$. Therefore, practical considerations will generally overcome this theoretical drawback. Furthermore, tendon-driven fingers do not have physically

achievable equilibrium positions with $k_2 > 0$ if $|\theta_2| > \pi/2$, and hence ejection will happen anyway. It is intriguing that these fingers which do not suffer from hyper-configurations have no equilibrium possible for large values of θ_2 whereas linkage-driven finger which do have possible equilibrium positions are eliminated because they suffer from these hyper-configurations. The limits of these configurations can be expressed analytically as functions of the design parameters, as they correspond to $h = 0$, i.e.,

$$\theta_2 = \psi \pm \arctan 2(\sqrt{-(A^2 - l_1^2)(B^2 - l_1^2)}, l_1^2 + AB), \quad (4.16)$$

$$\theta_2 = \psi \pm \arctan 2(\sqrt{-(C^2 - l_1^2)(D^2 - l_1^2)}, l_1^2 + CD), \quad (4.17)$$

with $A = a + b + c$, $B = -a + b + c$, $C = a - b + c$, and $D = -a - b + c$. Of the four solutions of the above equations only two are valid: it should be checked for each one that $f_2 = 0$. Since these limit configurations correspond to $h = 0$, they also correspond to $e(\theta_2) = 0$ which can be easily identified in Fig. 4.3, the other solution to this equation being $\theta_2 = \pm\pi/2$. These configurations are of course influenced by the stiffness of the spring located between the two phalanges if the latter is not neglected. The finger can be in a kinematic hyperextension configuration but with a spring torque overcoming the actuation torque and generating a positive contact force. It should be noted that if $c > a$ some configurations may be equivalent to the latter hyper-configurations, with $f_2 < 0$, if the link between points P_1 and P_2 actually pulls on the distal phalanx, instead of pushing. The limit case between these two types of behaviour is defined by $h + l_1 = 0$. More details on these designs will be discussed in Section 4.2.3.

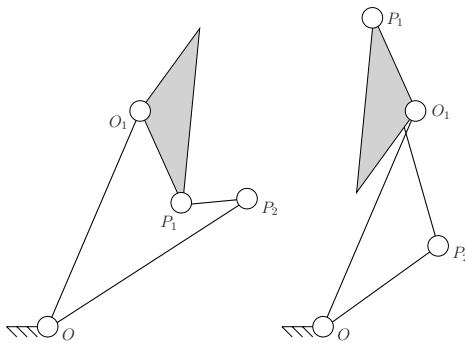


Fig. 4.9. Hyperextension/hyperflexion configurations

4.2.2 Contact Trajectories

If the proximal contact is lost, the behaviour of the finger must be studied in order to determine if a stable position will be reached or not. To obtain this evolution, the contact location as seen from the distal phalanx is introduced. It

can be easily shown that if only this contact exists and if it is a point fixed in space (illustrated in Fig. 4.10), one has

$$k_2^2 - k_{2i}^2 + 2l_1(k_2 \cos \theta_2 - k_{2i} \cos \theta_{2i}) = 0, \quad (4.18)$$

where k_{2i} and θ_{2i} are an arbitrary initial configuration, for example, the precise instant when the contact on the first phalanx is lost. This equation is actually a conic in the plane $(k_2, \cos \theta_2)$, namely a hyperbola, centred in $(0, 0)$ and with principal axes:

$$\begin{cases} k_2 = 0 \\ \cos \theta_2 = -\frac{k_2}{2l_1}. \end{cases} \quad (4.19)$$

This hyperbola degenerates into two intersecting lines corresponding to the above two axes when the location of the contact point is on the circle centred at the base joint of the finger and of radius l_1 . Each quadrant corresponds to a combination of a contact point inside/outside this circle and a positive/negative value of the contact location. Note that for the finger studied in this chapter, a negative value of the contact location is dismissed. It is however possible to extend the distal phalanx below its base joint. A single point of contact is not simply a theoretical abstraction, it can be the edge of a polygon for instance. Also, for the contact to be maintained, the sign of the distal phalanx force should be considered, i.e., if f_2 is positive, the contact should be located in front of the phalanx. On the contrary, if this force is negative, the contact should be physically made with the back of the phalanx frontline. Note that this part of the phalanx may not be accessible, or present a complex shape invalidating our analysis. Furthermore, for most grippers, contact is not suitable on these surfaces.

The contact hyperbola corresponds to a complex curve in the (k_2, θ_2) plane which is similar to a hyperbola with centres $\cos \theta_2 = 0$, i.e., $\theta_2 = \pm\pi/2$ and with

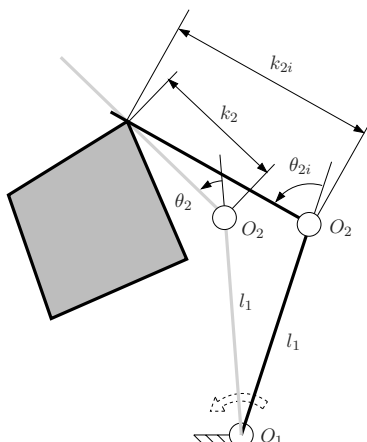


Fig. 4.10. Grasp-state illustration

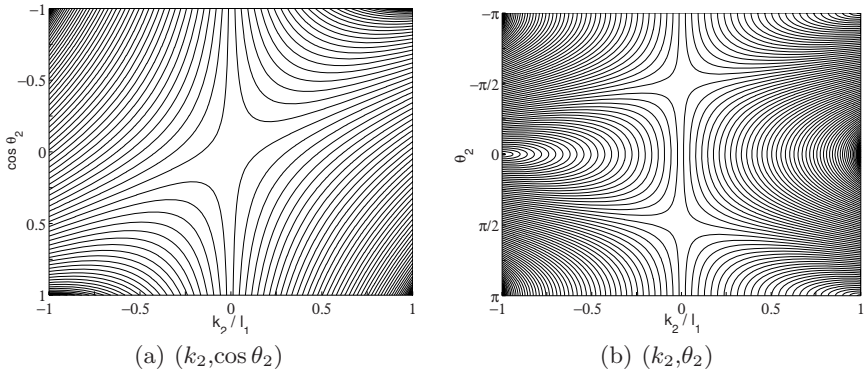


Fig. 4.11. Contact trajectories in the $(k_2, \cos \theta_2)$ and (k_2, θ_2) planes

a principal axis defined as $k_2 = 0$. The contact curves in their respective plane are illustrated in Figs. 4.11(a) and 4.11(b). Note that in the (k_2, θ_2) plane there is only one axis ($k_2 = 0$). Although it seems that each centre has another axis, this other asymptote is actually a curve and not a straight line.

Eq. (4.18) allows us to obtain the precise evolution of the contact position with respect to the evolution of θ_2 since the finger now has one degree of freedom while keeping contact with the object. This motion has been referred to as self-posture changing motion (Kaneko and Hayashi 1993) and used for haptic exploration. This evolution is determined by the location of the contact with respect to the equilibrium position, namely the sign of f_1 . Indeed, the contact trajectory is a curve in the contact (k_2, θ_2) plane, so the direction in which the contact situation travels on that curve is not immediate but can be determined by studying the sign of f_1 . For instance, in the central part of the contact trajectories (where there is an intersection with the horizontal line $\theta_2 = 0$), if the contact is located below the equilibrium point, the finger undergoes an closing motion and thus θ_2 increases (illustrated in Figs 4.6 and 4.7, indicated by arrows in Fig. 4.12). The contact state, defined by the pair (θ_2, k_2) , evolves along the trajectories defined by eq. (4.18), and then, if the contact trajectory crosses the equilibrium equation defined by eq. (4.13), the grasp is finally stable. Otherwise, contact with the object will be lost, namely one obtains the ejection phenomenon either due to the kinematic evolution ($k_2 \geq l_2$, illustrated in Fig. 4.1), or due to the hyperflexion/hyperextension configurations. Depending on the geometric parameters (Table 4.1) of the mechanism, the final stability of the grasp can be obtained for a given initial contact situation, as presented in Figs. 4.12, 4.13, and 4.14.

The contact trajectories defined above are indicated by dotted lines on the latter Figures, the arrows indicate the direction of the contact evolution, and the solid lines indicate the equilibrium equation (labeled “repulsive” and “attractive” frontiers). However, if conclusions on the final stability of the grasp can be drawn from this plane, any notion of time is missing from the analysis. If the contact situation corresponds to a stable final grasp, this stable grasp will

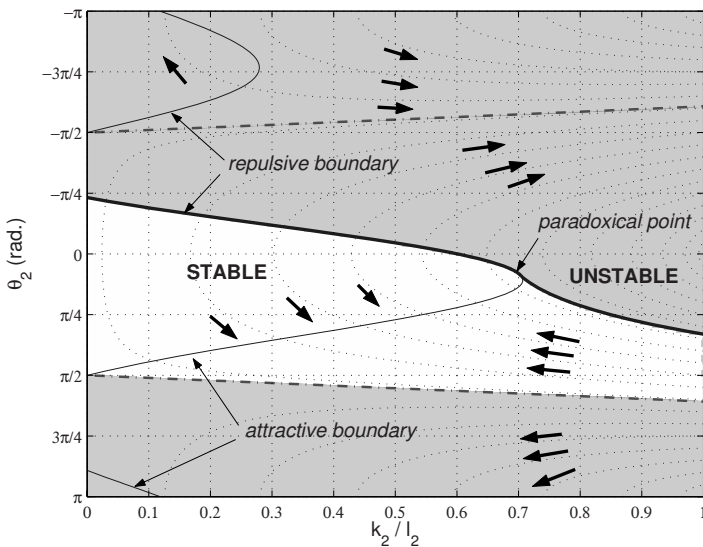


Fig. 4.12. Final stability of the grasp with one phalanx contact (parameter set 1)

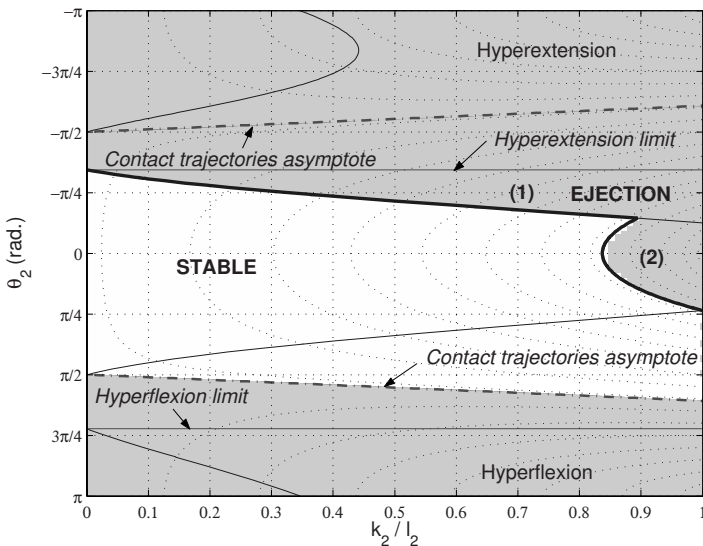


Fig. 4.13. Final stability of the grasp with one phalanx contact (parameter set 2)

be achieved, however, the time required to achieve this equilibrium situation is totally unknown and depends on the dynamics of the system (actuation torque, masses and inertias). It can take 1 ms or 1 year to “travel” on the contact trajectory until achieving either equilibrium or ejecting the object. This limit of

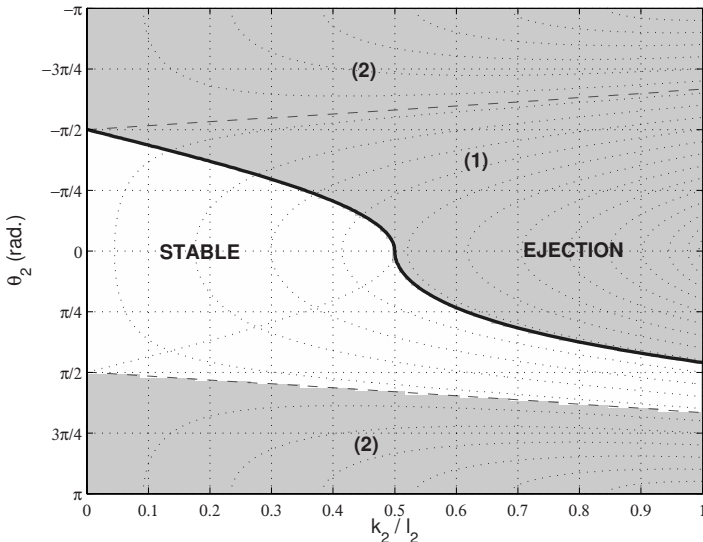


Fig. 4.14. Final stability of the grasp with one phalanx contact (Soft Gripper)

our analysis should be understood, and clearly stated. Our technique is very similar to the result of a Lyapunov stability analysis, which does not consider the time required to achieve stability. At this point one may think that using Lyapunov theory to generalize the stability concept of the present work may be a good idea. However, the authors have been unsuccessful at establishing a proper (and required) Lyapunov potential function. Indeed, such a function must be strictly varying with respect to the system state, at least in a neighbourhood of the equilibrium hypersurface (a 1D curve in our case). However, by inspection of Fig. 4.12, it can be seen that some contact trajectories (the rightmost in the Figure), which actually describe the system state evolution, may come very close of the equilibrium curve but, then suddenly tend to escape from it. This behaviour may indicate that a Lyapunov function does not exist, at least not with this state description. Nevertheless, the authors only conjecture the impossibility of such a function and do not formally exclude it.

Given the evolution of θ_2 , the equilibrium curve can be separated in two distinct stable parts, one attracting limit (the lower part on the graph) and a repulsive limit (upper part) similarly to a saddle plot. The transition between the two modes is the tangent point between the contact trajectories and the equilibrium curve. This point is labeled “paradoxical point” since it belongs to both the attractive and the repulsive boundaries, and being on the stability boundary, a small variation around this point can lead to a completely different stability behaviour. However, when the equilibrium point physically leaves the phalanx, i.e., $\exists \theta_2 | e(\theta_2) > l_2$, another unstable frontier appears, as shown for instance in Fig. 4.13. The contact situations under the equilibrium curve and on the right hand side of the stability limit (shaded area number 2) are unstable

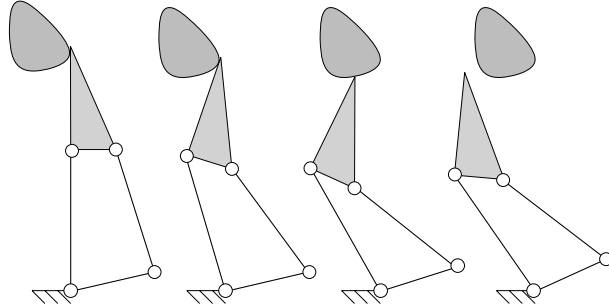


Fig. 4.15. Example of an opening-ejection sequence

because the contact trajectories cross the boundary $k_2/l_2 = 1$ before attaining an attractive equilibrium limit. The latter is not physically on the phalanx for this trajectory and this parameter set. This corresponds to the ejection phenomenon depicted in Fig. 4.1, ejection for a closing motion (θ_2 increases) of the distal phalanx. Contact situations under the equilibrium curve and on the right hand side of the stability limit are unstable because the contact trajectories cross the boundary $k_2/l_2 = 1$ before attaining the attractive limit. The latter is not physically on the phalanx for this trajectory and this parameter set. Ejection for an opening motion (θ_2 decreases) of the distal phalanx can also occur (shaded area number (1) in Fig. 4.13), illustrated in Fig. 4.15. In fact in Fig. 4.12 it is the only form of ejection possible for common ranges of angle θ_2 . If the distal phalanx tends to open, the motion of link a (and thus, the motion as seen from the actuator) is however still a closing process. Nevertheless, the contact situation will open the finger. More details on the methods to prevent ejection will be presented in Chapter 5. For tendon-driven fingers, any contact in the outer quadrant of the contact trajectory in Fig. 4.14 is unstable since no equilibrium locations physically exist on the phalanx (they correspond to $k_2 < 0$).

If the actuator is stopped on a trajectory that would lead to ejection, the grasp-state space is frozen in the local configuration. However, it should be understood that this frozen configuration is *not* an equilibrium configuration as usually shown in the figures. Indeed, if the spring is neglected, stopping the actuator also generates a zero contact force and equilibrium is achievable and corresponds to $T_a = 0$. If the spring is not negligible, the actuation torque must take the exact value that leads to equilibrium considering the spring torque in order to stop the actuator. In the latter case, a linkage-driven finger with a fixed actuation bar a can be considered as a spring-loaded four-bar linkage. However in this case, the contact force cannot be changed or controlled.

In conclusion, the equation describing the position of the equilibrium point is of the uttermost importance for the stability of the grasp and allows us to prefer two-phalanx (power) over one-phalanx (pinch) grasps. One shall then proceed with the detailed study of this function. Construction of the stability regions of an underactuated two-phalanx finger with an arbitrary equilibrium curve and contact trajectories is illustrated in Fig. 4.16.

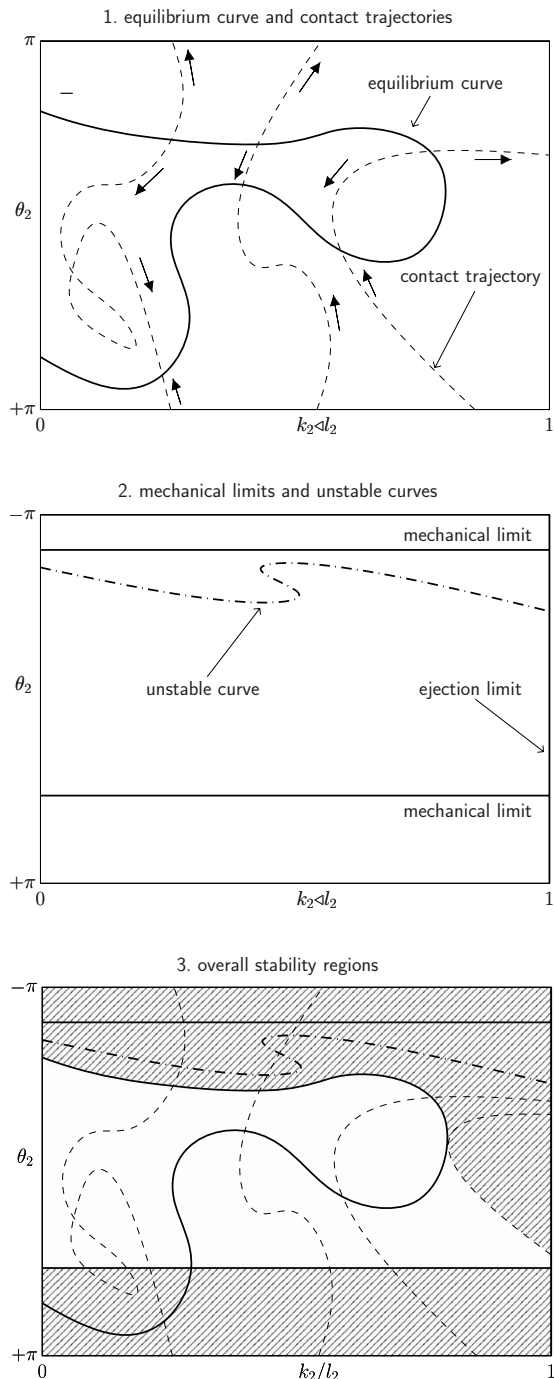


Fig. 4.16. Construction of the stability regions

4.2.3 Equation of the Equilibrium Point

Main Parameters and Spring Issues

The equilibrium locus, defined in eq. (4.13), is primarily a function of two parameters, namely the ratio c/a and the angle ψ (Fig. 4.2). The respective effect of these parameters on the equilibrium curves is shown in Fig. 4.17. It can be seen that the amplitude of the deviation of the equilibrium locus is roughly proportional to the ratio c/a while angle ψ tends to shift the curve horizontally. If the spring is not neglected, deviations are observed depending on the ratio between the input torque and the spring torque as illustrated in Fig. 4.18. Note that for the usual range of motion of θ_2 ($0 < \theta_2 < \pi/2$), the spring tends to move the equilibrium locus closer to the base of the distal phalanx. This behaviour tends to eliminate the closing-ejection presented in the previous section and therefore the spring has, for this range of motion, a stabilizing effect on the system. This only corresponds to a local behaviour over the usual range of motion of the second phalanx for moderate spring stiffness. Indeed, if the spring is too stiff, the grasp can degenerate for certain positions, with an equilibrium point pushed to infinity. If

$$\frac{T_2}{T_a} = 1 + R, \quad (4.20)$$

then the equilibrium location is not attainable, i.e., $e \rightarrow \infty$. Eq. (4.20) will be referred to as the spring-degeneracy condition (c.f. Section 4.2.3 for more details on the possible degeneracy of the equilibrium equation) and it allows to obtain the finger configuration, characterized by the angle θ_2 , corresponding to an impossible equilibrium. This degeneracy condition depends on the spring stiffness and zero-force position. Furthermore, it also depends on the transmission index which can be a function of the geometric configuration of the finger. One can obtain a condition for non-degeneration, namely that the solution of eq. (4.20) for θ_2 corresponds to an angle that is not physically possible to achieve. For instance, if tendon-driven fingers are considered with $-\pi < \theta_2 < \pi$ and a zero neutral position of the spring, if

$$K_{spring} < \left(1 - \frac{r_2}{r_1}\right) \frac{T_a}{\pi}, \quad (4.21)$$

then $e < \infty$, $\forall \theta_2$. For linkage-driven fingers the condition is much more complicated due to the complex expression of the transmission ratio as a function of θ_2 . Nevertheless, the non-degeneracy condition can be checked numerically. Furthermore, if the spring is too stiff, there will exist a range of values of angle θ_2 that will not be attainable. When the spring torque T_2 is equal to the closing torque induced by the actuator (namely RT_a), contact with the second phalanx will not be sustained. However, usually the spring torque is several orders of magnitude smaller than the closing torque and such issues remain theoretical with practical fingers.

The equilibrium locus with a single point of contact and non-negligible spring can be verified using a commercial dynamic simulation software. After numerous

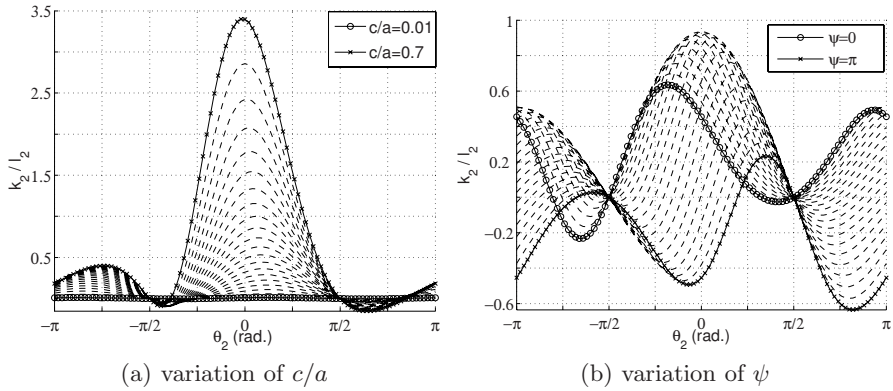


Fig. 4.17. Equilibrium curves (parameter set 1)

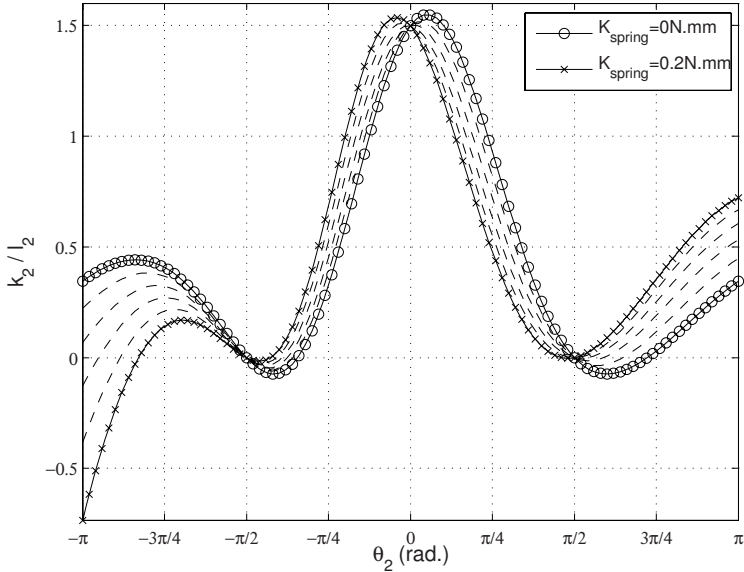


Fig. 4.18. Equilibrium curves for different spring stiffnesses (parameter set 2)

simulations performed by the authors, the final equilibrium state configuration does not differ more than 1% from what was expected, thus validating our results.

Friction

If friction is also considered during the grasp, eq. (4.13) is used to obtain the equilibrium locus. However, there is no longer a single equilibrium curve but rather two curves. The sign of μ defines these two curves in the grasp-state

plane, each corresponding to one sliding direction, i.e., $\mu = +\mu_{static}$ or $\mu = -\mu_{static}$ as described in eq. (3.8). The area between these two curves described by $\mu = \pm\mu_{static}$ —including the previous equilibrium curve, i.e., with $\mu = 0$ —corresponds to a value of the coefficient μ such that $-\mu_{static} < \mu < +\mu_{static}$. In this case, recalling the definition of this coefficient in eq. (3.8), the tangential force on the phalanx is within the static friction cone. Therefore, since a rolling motion of the phalanx around the contact point is kinematically not feasible—except infinitesimally when $\theta_2 = 0$ which explains the intersection of all equilibrium curves considering friction for this particular angle—the second phalanx is stuck and the finger will not slide anymore. Finally, the grasp is stable again, this time with $f_1 \neq 0$ but this non-zero normal force simply compensates the tangential distal phalanx force in order to achieve the overall static equilibrium of the finger.

The coefficient of friction depends on the material of the object-finger contact, numerical values¹ are 0.8 for a steel-steel contact (clean and non-lubricated) and 1 – 4 for solid-rubber (idem). This is interesting since a robotic finger surface is usually covered with rubber to increase friction or indirectly by using a tactile sensing device. Graphical illustrations of these two numerical examples are presented in Fig. 4.19. In the case of rubber contact, a conservative value of 2 has been chosen for the static coefficient of friction. The grey shaded areas correspond to a tangential distal force inside the friction cone.

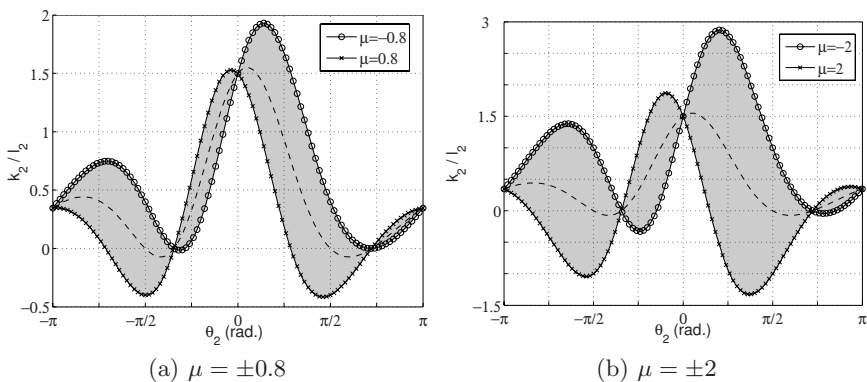


Fig. 4.19. Stable areas with friction (parameter set 2)

Phalanx Geometry

If the phalanx thickness is non-zero, the apparent value of angle θ_2 should be shifted by a quantity equal to:

$$\psi_\epsilon = \arctan \left(\frac{\epsilon}{k_2} \right), \quad (4.22)$$

¹ From *The Machinery's Handbook 23*, Industrial Press Inc.

where ϵ is the thickness of the distal phalanx (as illustrated in Fig. 4.20(a)). The contact location itself should be replaced with

$$k_2 \rightarrow k_2^* = \sqrt{k_2^2 + \epsilon^2}. \quad (4.23)$$

These substitutions should be made only in the contact eq. (4.18) and not the equilibrium eq. (4.13), since the latter is defined by considerations on the expressions of the forces which do not change with the thickness of the phalanx if friction is neglected. If the latter is not negligible, the equilibrium locus is changed because of the moment induced by the tangential force which can be modelled using the coefficient η_2 as will be discussed more thoroughly in Section 4.2.6. Note also that the substitutions are valid for a single point of contact and not a circular contact. The latter case will be discussed in the next section and, in this case, if the phalanx thickness is not negligible, the radius corresponding to the contact trajectory is simply changed from R_c to $R_c + \epsilon$ (illustrated in Fig. 4.20(b)). Furthermore, as a single point of contact is a particular case of the circular contact, the latter contact type can be used to model phalanx thickness (i.e., by replacing R_c with ϵ in the corresponding equations of Section 4.2.4). Obviously, in the above discussion, the phalanx thickness is assumed to be constant. This assumption is reasonable since it is the case in most prototypes, except maybe if teeth on the phalanges are required to increase the penetration in the object seized, but this is beyond the scope of this book.

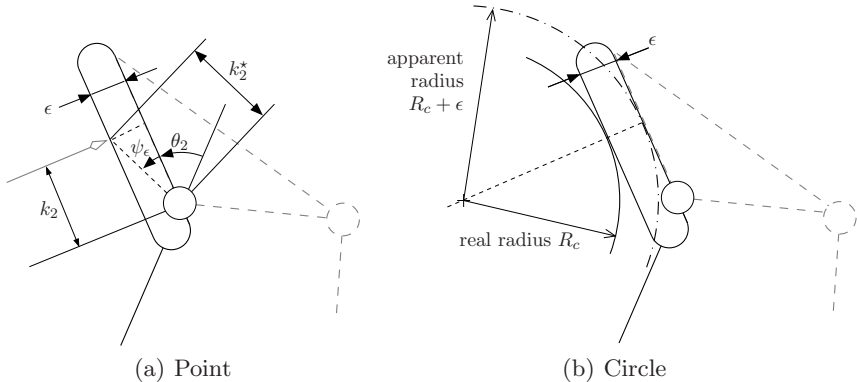


Fig. 4.20. Effect of the phalanx thickness

Unstable Designs and Other Considerations

In the previous sections, most examples have been presented using a linkage-driven finger, since tendon transmission considerably simplifies the expression of the equilibrium curve. For instance, if no friction is considered, the latter can simply be expressed as

$$e = \frac{\alpha}{1 - \alpha} l_1 \cos \theta_2, \quad (4.24)$$

with $\alpha = r_2/r_1$, therefore the equilibrium equation is defined as the cosine of angle θ_2 multiplied by a constant factor. Nevertheless, the results are very similar to those obtained with a linkage-driven finger.

Another important kind of equilibrium curve that has not yet been discussed is the mechanical limits on joint θ_2 . Indeed, if the finger is resting against a mechanical limit, is in static equilibrium since no further motion is possible. The finger in such a position acts like a simple rotational gripper with an unusual shape of the jaw. However, the shape adaptation in these situations is not optimal. In the grasp-state plane, mechanical limits on θ_2 are represented by horizontal lines. These boundaries can be either attractive or repulsive (or even both if the equilibrium curve is intersected) depending on the value of θ_2 associated with the mechanical limit. Practically, mechanical limits are of the utmost importance, most noticeably to prevent opening-ejection, as discussed in Section 5.2.3. All contact trajectories intersecting the mechanical limit line that would normally lead to an opening-ejection will converge to this line and thus, result in a stable grasp.

Another important aspect to consider about the equilibrium equation is its possible degeneracy, namely when:

$$e(\theta_2) \rightarrow \pm\infty. \quad (4.25)$$

The latter can be either local, i.e., for a particular θ_2 or architectural, for all values of θ_2 . Eq. (4.13) which expresses the equilibrium equation for any kind of transmission of our model, relates the degeneracy condition to the transmission coefficient, i.e.,

$$e(\theta_2) \rightarrow \pm\infty \iff R(\theta_2) = -1. \quad (4.26)$$

For instance, considering eq. (4.24), if $\alpha = 1$, then $e \rightarrow \infty$. What is important to notice is that in this case, the degeneracy is not local—i.e., for a particular θ_2 as introduced in the discussion on the effect of the spring—but global (for all θ_2)! For linkage-driven fingers, the same phenomenon occurs if $c = a$ and $l_1 = b$. Such designs have been referred to as *evil twins* in Chapter 3 because of their penchant to ejection. However, such designs do have equilibrium positions, namely

$$\text{if } R = -1, f_1 = 0 \text{ if and only if } G(\theta_2) = 0.$$

Therefore, if friction is neglected, the equilibrium curve degenerates into a set of two straight lines defined by $\theta_2 = \pm\pi/2$. Hence, these positions correspond to a peculiar behaviour where any contact location leads to a static equilibrium! Nevertheless, the price to pay in return is that for these fingers, only two configurations can lead to these peculiar and paradoxical equilibria, i.e., shape adaptation is not achieved. If friction is not negligible, the equilibrium curves become two equilibrium areas comprised between horizontal lines in the grasp-state plane. An illustration of a linkage-driven finger in paradoxical equilibrium with and without friction is given in Fig. 4.21.

If the degeneracy is only local, i.e., $R(\theta_2) = -1$ for a particular angle θ_2 (a configuration achievable with a linkage-driven finger), no equilibrium is possible,

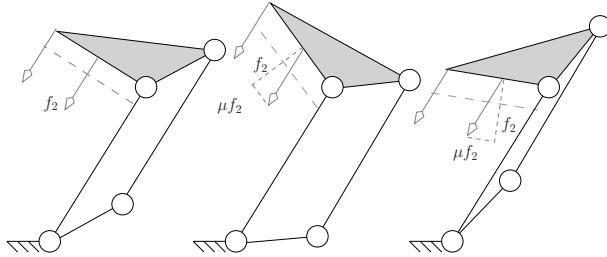


Fig. 4.21. Unstable design in a paradoxical equilibrium with (right) and without (left) friction

except if $G(\theta_2) = 0$ for the same angle, which is not likely to occur. Therefore, the equilibrium location is indeed pushed to infinity, similarly to what was described in the spring-degeneracy discussion. Hence, the configurations close to a degeneracy location should be generally avoided since, in their neighbourhood, the equilibrium locus corresponds to large values of k_2 , not physically achievable. These situations are therefore prone to closing-ejection.

If $\alpha > 1$, the equilibrium curve is negative if $-\pi/2 < \theta_2 < \pi/2$ and positive elsewhere, therefore no equilibrium position is physically on the phalanx for the common small values of θ_2 . If $c > a$, similar results are obtained for linkage-driven fingers. However, it should be noted that these designs are not *always* unstable: for example if $\theta_2 > \pi/2$ a design with $\alpha > 1$ can lead to a stable grasp since the contact point is under the equilibrium curve, a stable situation for a two-phalanx grasp in this region, i.e., both f_1 and f_2 are positive. Nevertheless such designs should be avoided since they do not have equilibrium positions in the usual range of motion of the finger.

Summary

To summarize, one can obtain the stable and unstable behaviour of an underactuated finger by establishing its equilibrium curve and contact trajectory in the defined grasp-state plane. Then, having established the direction of the contact evolution on the trajectory, the grasp-state plane can be used to determine whether this initial situation will reach an equilibrium position by intersecting either the equilibrium curve or a mechanical limit. If not, ejection will occur, either by intersection of a hyper-configuration limit (if they exist) or physically leave the phalanx ($k_2 > l_2$). Based on the behaviour of the distal phalanx, opening-and closing-ejection have been defined, respectively if the distal phalanx has an opening (θ_2 decreasing) or closing (θ_2 increasing) motion.

4.2.4 Linear and Circular Contact

If the contact geometry is no longer a single point, the results of the preceding section do not apply because the contact trajectories are no longer valid. Indeed, the contact trajectories allowed to establish a relationship between the two state

variables of the grasp, namely k_2 and θ_2 . This relationship depends on the local geometry of the object being seized. To be complete, a more general case should be studied, namely a contact with a local curvature. The two extreme cases of a curvature are the line, i.e., an infinite radius of curvature, and the single point, namely the case previously studied which accounts for a zero radius of curvature. In the case of linear and circular contact, the location of the contact point is no longer fixed in the Cartesian space. However, its motion can be predicted if the object is known and related to the grasp-state variables of the grasp. Note that this approach is driven by practical considerations since a single point of contact is less probable than a circular or planar contact.

Linear Contact

Consider first the linear contact. The mobility of the finger with a distal linear contact is 0 except in particular configurations where $\theta_2 = \pi/2$. Even in these particular cases, the mobility is only locally increased to 1. Thus, if a linear contact is established and maintained, the finger can be assumed to be in equilibrium. One can relate the linear contact with the previous section by considering the two extremities or vertices of this line segment. Consider a linear contact, made by an arbitrary closing sequence: if this contact is unstable, contact will be lost with the line but not with the vertices (the contact force is assumed to be positive). Therefore, the final grasp will be stable if the sliding motion of the phalanx converges toward an equilibrium position as previously discussed or if the motion corresponding to the contact on each one of the two vertices of the line segment tends to bring the phalanx back in contact with the line. The latter case is indeed a stable linear contact while the other guarantees a stable grasp but only with a contact on one vertex. Since studying the behaviour of the finger with respect to the vertices of the line segment is sufficient to discuss the stability issue, the grasp-state plane introduced above and the associated contact trajectories can be used directly. The representation of a linear contact in this plane is simply a line segment with a length corresponding to the ratio of its physical length with the distal phalanx length.

Examples of linear contacts are presented in Fig. 4.22: the Cartesian line segments correspond to horizontal bold lines in the grasp-state plane. Therefore, two contact trajectories are obtained, each corresponding to one vertex of the line. If both vertices belong to stable contact trajectories, the grasp will be stable anyhow. If both vertices belong to unstable contact trajectories, the finger will lose the object. The latter holds even if the equilibrium curve is intersected since any deviation around this situation will induce a motion that leads to ejection. However, if one contact trajectory is stable and the other leads to ejection, the case must be investigated. To ensure a stable linear grasp, the single force equivalent to the distributed load acting on the phalanx by the line, which is at the centroid of this load, must be located on an equilibrium position. However, this load distribution is not known and is not necessarily a hyperbolic function of k_2 —as in eq. (4.3). If the initial contact with the line is made with a vertex whose contact trajectory corresponds to a certain evolution of θ_2 and the second contact

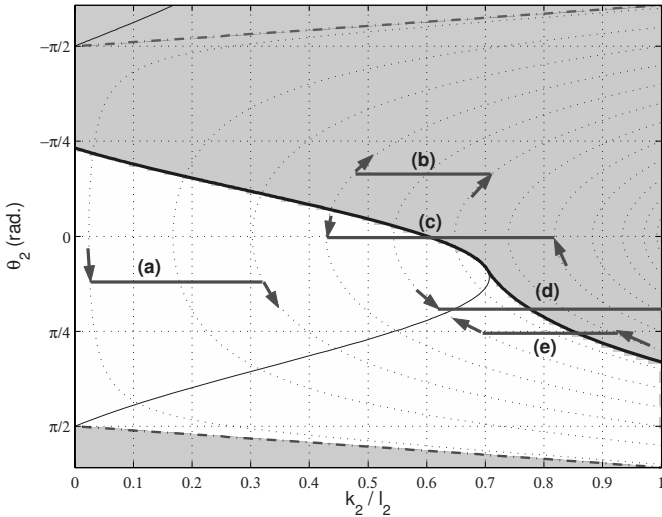


Fig. 4.22. Linear contact stability (parameter set 1)

with a vertex corresponding to the opposite evolution then the linear grasp is stable. Inspection of Figs. 4.12–4.14 reveals that, two different cases should be considered, depending on the quadrant in which the hyperbolic trajectories of the contact situation is located:

- if the latter is located between the two asymptotes (central part of the figures), this change of direction can only happen if each contact vertex is located on a different side of the equilibrium curve, i.e., the linear grasp is stable if the line intersects the equilibrium curve;
- if the contact situation is located in the other area, the contact situation cannot be stable since either there is no equilibrium position for this quadrant (tendon-driven finger), or it is past the hyperflexion/hyperextension limit.

Then, it was assumed that the contact situations of both vertices stay in the same quadrant. However, this is not obligatory since the contact trajectory asymptotes are not horizontal, a linear contact theoretically can have a grasp-state representation that intersects one of the asymptotes. The upper asymptote is not a concern since both vertices of the line are unstable. However for the lower asymptote, one vertex can be stable while the other is unstable. In this case the grasp stability has to be studied with the technique discussed previously. It can be shown that this case is similar to case (e), illustrated in Fig. 4.22.

Furthermore, one should note that only the extremity of the line physically in contact with a phalanx is to be taken into account. Obviously, if the line extends beyond the phalanx, only the last point in contact with the latter has to be considered. In a stable linear contact, the single force equivalent to the load is

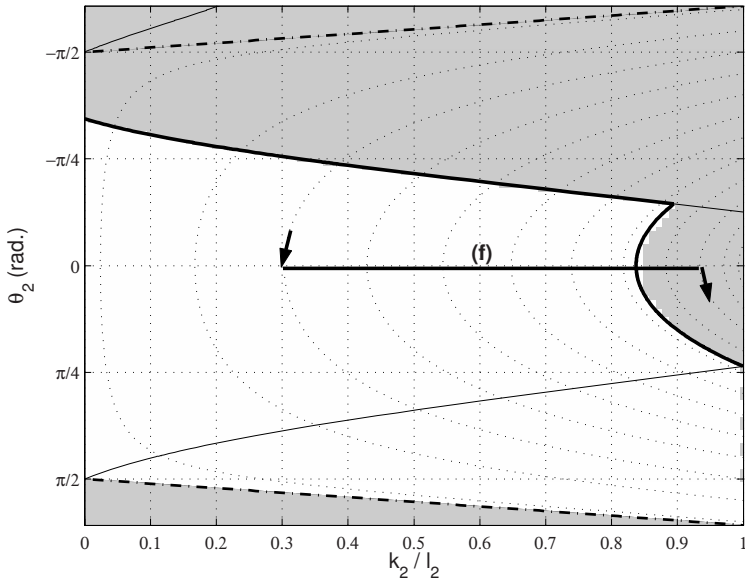


Fig. 4.23. Linear contact stability (parameter set 2)

a force located on the equilibrium location with a magnitude equal to the result of eq. (4.3). Different cases are illustrated in Figs. 4.22 and 4.23:

- (a): both vertices are stable, the grasp will be stable and contact will only remain with the (rightmost) second vertex;
- (b): both vertices are unstable, the grasp will be unstable, opening-ejection occurs by crossing the hyperextension limit;
- (c): the first vertex is stable while the second is unstable, the grasp will be stable, contact with the whole line is maintained;
- (d): the first vertex is stable while the second is unstable, the latter is not physically on the phalanx, the grasp will be stable and contact with the line is maintained;
- (e): the first vertex is unstable while the second is stable, the grasp will be stable and contact will remain only with the stable vertex;
- (f): the first vertex is stable while the second is unstable, the grasp is unstable, closing-ejection will occur!

As it can be observed, a linear contact generally has a stabilizing effect on the grasp: configurations with an unstable vertex can be stable if the other vertex is stable, except in the case where the first one belongs to a closing-ejection zone. This kind of ejection tends to destabilize the grasp, very similarly to what can be observed in the previous case: a stable vertex can be “destabilized” if the other vertex belongs to such a zone. Therefore, this kind of ejection seems to be particularly penalizing in terms of stability for the grasp and should be avoided.

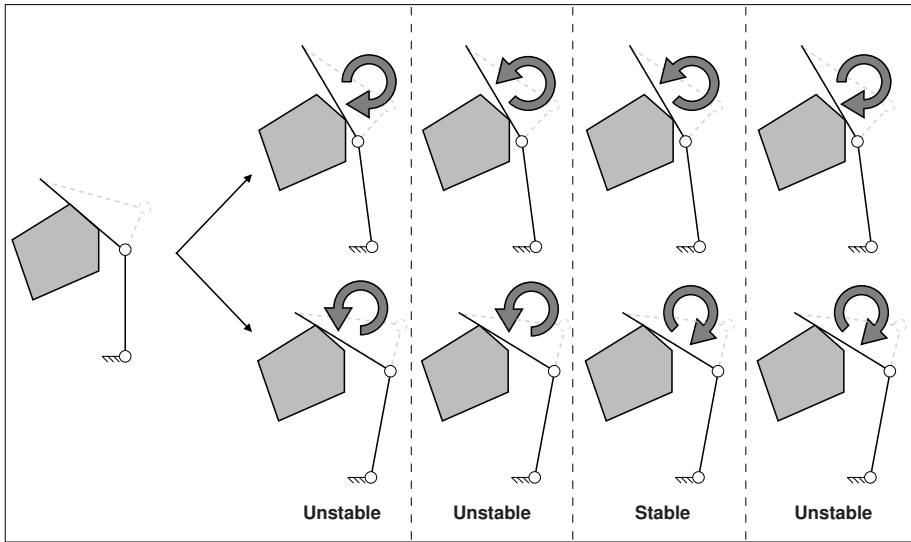


Fig. 4.24. Stability of the initial linear contact

The linear contact model can also be helpful when the finger has several points of contact with the object: by considering the extreme vertices in contact with the phalanx, one can describe a virtual line and study the stability of the grasp similarly to a linear contact. A summary of the different cases of linear contacts is provided in Fig. 4.24.

Circular Contact

In this case, the contact trajectories depend on the two parameters defining the circle, namely the position of the centre of the circle with respect to the base joint of the finger (given by two coordinates, but only the distance from this joint is important) and the radius of the circle. One has:

$$k_2^2 + R_c^2 - d^2 + l_1^2 + 2l_1(k_2 \cos \theta_2 - R_c \sin \theta_2) = 0, \quad (4.27)$$

where d is the distance between the base joint of the finger and the centre of the circle, and R_c is its radius. Using an arbitrary initial contact state, the latter equation can be rewritten as:

$$k_2^2 - k_{2i}^2 + 2l_1(R_c(\sin \theta_{2i} - \sin \theta_2) + k_2 \cos \theta_2 - k_{2i} \cos \theta_{2i}) = 0, \quad (4.28)$$

where (k_{2i}, θ_{2i}) is the initial contact situation. Eq. (4.27) is a quartic in the plane $(k_2, \tan(\theta_2/2))$ having the following form:

$$(y^2 + 1)(B + x^2) + Ax(y^2 - 1) + Cy = 0, \quad (4.29)$$

where x and y stand respectively for k_2 and $\tan(\theta_2/2)$. Coefficients A , B and C are defined as:

$$\begin{aligned} A &= -2l_1, \\ B &= l_1^2 + R_c^2 - d^2, \\ C &= -4l_1 R_c. \end{aligned} \quad (4.30)$$

One can draw the contact trajectories corresponding to a family of circles, i.e., different circle radii (illustrated in Fig. 4.25) or positions. Each contact trajectory in these plots corresponds to a particular cylinder and two parameters are required to define this trajectory. In Figs. 4.26(a) and 4.26(b), only the distance from the base joint is changed, and the radius is constant in each figure. The asymptote curves in each figure are defined by replacing $d = l_1 \pm R_c$ in eq. (4.27) and are indicated by dashed lines. Note that they intersect in the same points, namely $(0, \pm\pi/2)$, as the single point asymptotes. One should note that the smaller the radius, the more the contact trajectories tend to converge to the trajectories defined for a single point of contact. Mathematically, if $R_c = 0$, eq. (4.28) reduces to eq. (4.18). This was foreseeable and suggests that the analysis is correct. In Figs. 4.26(a) and 4.26(b), only the central part is represented since it was established in the previous sections that no equilibrium is possible outside the latter. These figures indicate that in the case of cylindrical contact, the opening-ejection is usually minimized due to the slope of the contact trajectories (illustrated in Fig. 4.26(a)). On the contrary, in the case of closing-ejection, the same slope of the curve actually increases the occurrence of ejection (illustrated in Fig. 4.26(b)). Since cylindrical contact is more likely to happen than a single point contact, closing-ejection is again particularly penalizing in terms of stability for the grasp.

Note that the circular contact can be used to study both the single point and linear contact by changing the radius of curvature accordingly. However, the contact trajectory for a single point is easier to understand and the linear contact requires the latter trajectories to describe the line vertices. Hence, it has been chosen to describe them individually.

Local Contact Geometry: Summary

By studying every possible case of local curvature of the object, one can describe the behaviour of the finger grasping an arbitrary shaped-object which can be decomposed into sequential/continuous variations of these basic shapes (Bergevin and Mokhtari 1998). For instance, varying the curvature will allow the study of an ovoid object while line and edge contacts can be used for a polygon. For example, a circular object partially cut is presented in Fig. 4.27 with its corresponding grasp-state plane equivalent. Note that the equilibrium curve does not appear since it depends on the transmission used and the latter does not influence the contact trajectory—only the phalanx lengths do. If no theoretical results about an arbitrary shaped object can be given, practical considerations

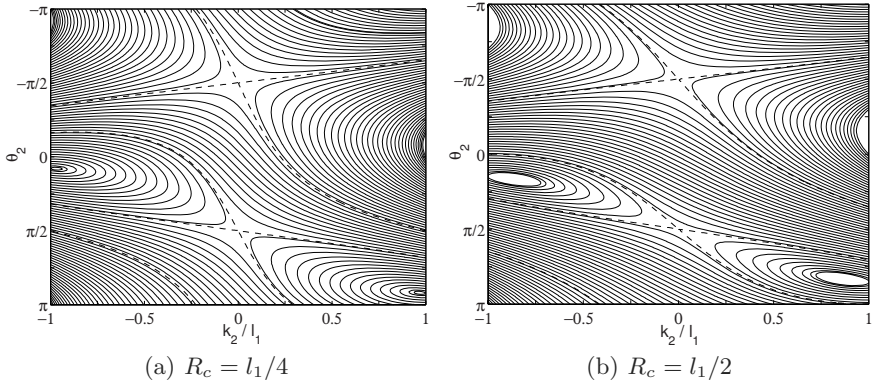


Fig. 4.25. Circular contact trajectories

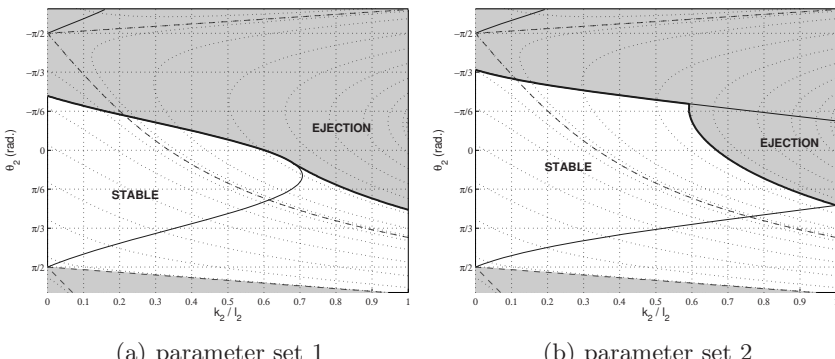


Fig. 4.26. Circular one-phalanx grasp stability. $R_c \equiv l_1/4$

result from the previous analyses: *usually*, a single point of contact is theoretically the worst case that can happen in terms of grasp stability, *except* when closing-ejection occurs. The latter noticeably increases unstable domains in the grasp-state plane for linear and circular contacts and is the main obstacle to grasp stability with practical objects. The method to study the grasp stability of an underactuated two-phalanx finger has been presented for different cases of contact geometry and hypotheses on the finger. However, in practice, a combination of these different parameters should more certainly be taken into account, as illustrated in Fig. 4.27. In Fig. 4.28 a brief illustration of the transformation between the Cartesian space shape of the object and its corresponding curve in the grasp-state space is illustrated. Basically, it should be verified that this curve intersects the equilibrium curve or the joint limit lines: this is a necessary but not sufficient condition for grasp stability. To obtain a decisive answer about the latter, the contact evolution on the curve should also be considered.

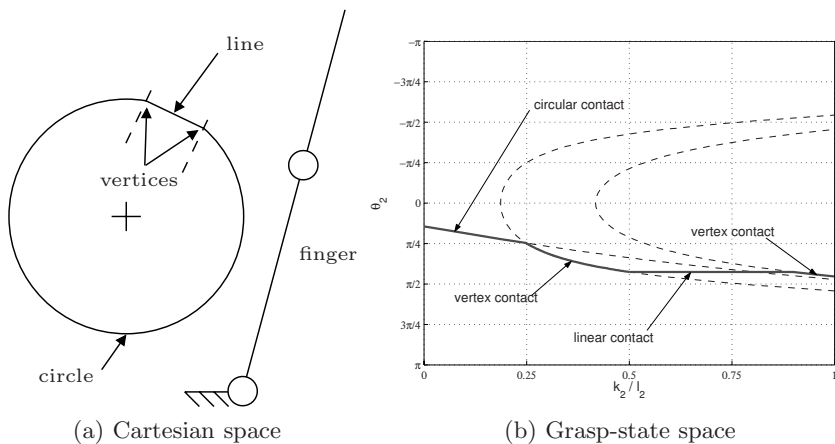


Fig. 4.27. Segmentation example

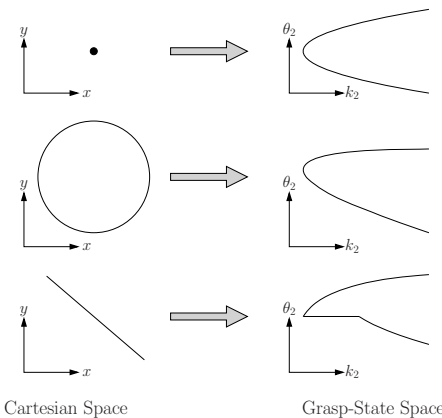


Fig. 4.28. Conversion chart between the Cartesian and grasp-state spaces

4.2.5 Application: Synthesis of an Optimally Unstable Finger

A method to obtain a finger design unable to grasp almost any object under normal conditions can be established using the results of this chapter. Although obtaining unstable fingers may seem useless, applications are presented at the end of this section. The first condition to synthesize an unstable gripper is to ensure that no initial grasp-state will generate a positive proximal contact, i.e., $f_1 < 0 \forall (k_2, \theta_2)$.

This condition can be developed using eq. (4.3), namely

$$k_2(1+R) + Rl_1G < 0 \quad (4.31)$$

by taking into account only the part of f_1 that can change sign. It is assumed that $-\pi < \theta_2 < \pi$ and $0 < k_2 < l_2$. Hence, one obtains a condition on the transmission factor R to ensure the negativity of f_1 , i.e.,

$$R < \frac{-k_2}{k_2 + l_1 G} = \frac{-1}{1 + \frac{l_1 G}{k_2}} \quad (4.32)$$

since $k_2 + l_1 G > 0$ assuming—initially—that $\mu = 0$. Considering eq. (4.32), it can be seen that the condition obtained on R cannot be satisfied for any value of the grasp-state unless $R \rightarrow -\infty$ for grasp-states defined by $(k_2, \arccos(-k_2/l_1))$. However, no transmission ratio is known to be function of the distal contact location k_2 , hence the condition

$$R \left[\arccos \left(-\frac{k_2}{l_1} \right) \right] \rightarrow -\infty \quad (4.33)$$

cannot be satisfied. Thus, one must restrict the range of values of θ_2 inside the workspace defined by $-\pi/2 < \theta_2 < \pi/2$ which yields that both $l_1 G$ and k_2 are positive. Therefore, a sufficient condition on R to satisfy eq. (4.32) is

$$R(\theta_2) < -1 \quad \forall \theta_2 \quad (4.34)$$

This condition is easily achievable in practice using $r_1 < r_2$ with tendon-driven fingers or $a < c$ with linkage-driven fingers. Thus, it could be assumed that an unstable design has been obtained. Indeed, if one considers the limit case $c = a$ with a linkage-driven finger only in contact with the object through the distal phalanx, the latter is subjected to three pure forces, two of them being parallel. The condition for equilibrium, namely that the three forces intersect in a common point, seems impossible to satisfy. Nevertheless, as discussed before this finger does have equilibrium configurations for $\theta_2 = \pm\pi/2$, i.e., at the limits of the workspace. Physically, these configurations correspond to the three forces intersecting *at infinity*. Furthermore, these limit values of θ_2 , which are equilibrium curves, cannot be dismissed as marginal because of the contact trajectories. Indeed, many contact trajectories corresponding to an initial contact location in the finger workspace will lead to $\theta_2 = \pi/2$ as illustrated in Fig. 4.29. Except for contact situations in the shaded area, any other initial grasp-state (between the contact asymptotes) will lead to a static equilibrium with $\theta_2 = \pi/2$.

Hence, considering only the sign of the contact forces is fundamentally incomplete and might be misleading in the analysis of the stability of underactuated fingers.

Back to the Grasp-State Plane

In order to synthesize unstable fingers, considering only the sign of the proximal contact forces is not sufficient and the grasp-state plane must be carefully analyzed. To obtain an unstable design, one has to ensure that for any initial grasp-state, the sliding motion on the associated contact trajectory will not converge to an equilibrium location. For this condition to be valid in any practical

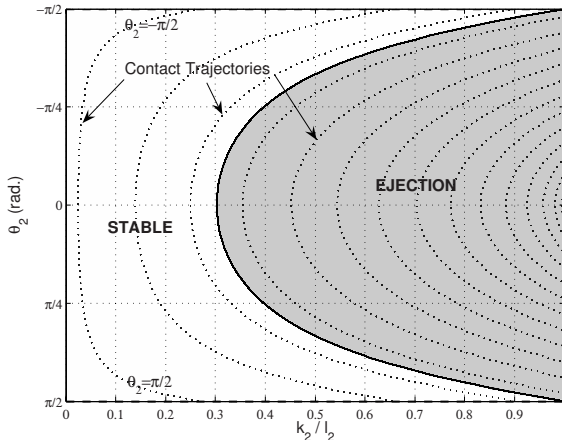


Fig. 4.29. Unstable design, contact trajectories and stability regions

initial condition ($-\pi/2 < \theta_2 < \pi/2$ and $0 < k_2 < l_2$), no contact trajectory must intersect an equilibrium curve. Graphically, no equilibrium curve should appear in the grasp-state plane between the two asymptotes of the contact trajectories as illustrated in Fig. 4.29. The latter intersect the equilibrium curve defined by $f_1 = 0$ in two points defined by $\theta_2 = \pm\pi/2$ and $k_2 = 0$ according to eq. (4.13) (except when friction is considered). Hence, in order for the equilibrium curve not to enter the central part of the grasp-state plane, two conditions are necessary:

1. the equilibrium location for $-\pi/2 < \theta_2 < \pi/2$ should be negative,
2. the slope of the equilibrium curve for $\theta_2 = \pm\pi/2$ should be greater than the slope of the respective trajectory asymptote.

The first condition can be easily related to the transmission ratio R using eq. (4.13), namely

$$e\left(\left[-\frac{\pi}{2}, \frac{\pi}{2}\right]\right) < 0 \Leftrightarrow R\left(\left[-\frac{\pi}{2}, \frac{\pi}{2}\right]\right) \notin [-1, 0]. \quad (4.35)$$

It should be noted that in order to create a closing motion of the distal phalanx, R has to be negative according to eq. (4.3). Hence, the previous condition can be reduced to $R < -1$, the condition obtained with the first method. The second and additional condition can be developed as

$$\left. \frac{\partial e}{\partial \theta_2} \right|_{\theta_2=\pi/2} > \left. \frac{\partial g}{\partial \theta_2} \right|_{\theta_2=\pi/2} \quad (4.36)$$

where the asymptotes are defined by $g = k_2 = -2l_1 \cos \theta_2$. Eq. (4.36) can be developed as

$$\frac{R(\pi/2)}{1 + R(\pi/2)} l_1 > 2l_1. \quad (4.37)$$

It should be noted that only $\theta_2 = \pi/2$ has been considered since the contact trajectories and asymptotes are symmetrical with respect to the axis $\theta_2 = 0$. Hence, eq. (4.37) is valid for both asymptotes.

Finally, one obtains

$$R(\pi/2) < -2. \quad (4.38)$$

Hence, a sufficient condition for the non-existence of an achievable equilibrium location between the contact trajectory asymptotes is $R(\theta_2) < -2$ in this area of the grasp-state plane. The condition obtained in the previous Section ($R < -1$) is incomplete as it only guarantees that the proximal contact force will be negative in the chosen workspace but the edges of this workspace are stable curves leading to a static equilibrium. On the other hand, if the conditions obtained with the analysis of the grasp-state plane are followed, the proximal contact force will be negative **and** ejection will occur for any grasp-state in this workspace. Similarly, mechanical limits should not be located between the asymptotes, as they also constitute equilibrium curves, i.e.,

$$\theta_{2max} > \arccos\left(\frac{-l_2}{2l_1}\right). \quad (4.39)$$

Fig. 4.30 shows different equilibrium curves with a constant transmission ratio R (tendon-driven fingers), the critical value of $R = -2$ is clearly illustrated (all curves are symmetrical with respect to the axis $\theta_2 = 0$).

Hence, a very simple design of unstable finger can be obtained using a tendon transmission by setting $r_2 = 2r_1$. Such a design is illustrated in Fig. 4.31. Notice that a stable design can be obtained by exchanging the distal and proximal pulleys, a simple inversion of the pulleys totally changes the behaviour of the finger with respect to grasp stability! Furthermore, it should also be noted that using the same pulleys for both locations is not a very good idea since it yields

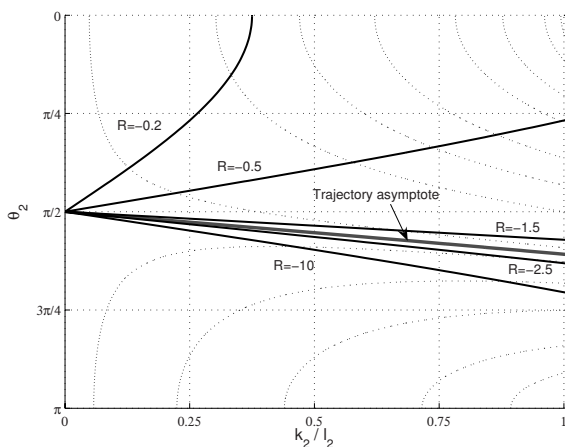


Fig. 4.30. Equilibrium curves for different values of R

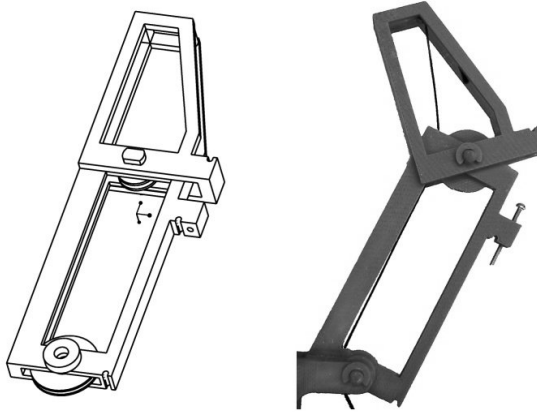


Fig. 4.31. Stable design (left) and unstable prototype (right) of two-phalanx underactuated finger

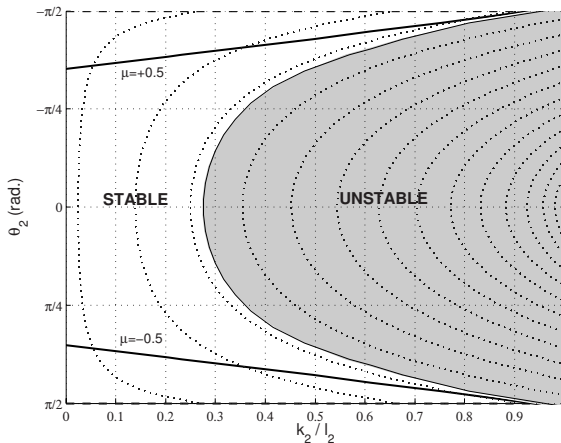


Fig. 4.32. Stability regions due to friction ($R = -5$, $\mu = \pm 0.5$)

$R = -1$ and therefore, the finger will always find itself in a configuration where $\theta_2 = \pi/2$. In this case, the shape adaptation is totally lost.

Friction can be considered in the analysis, but its influence is predictably stabilizing on the grasp. An example of stability regions taking into account a friction coefficient of 0.5 is presented in Fig. 4.32. Note that the grasp-state corresponding to a small value of k_2 will eventually reach the equilibrium curve indicated by $\mu = -0.5$.

Applications

Finally, potential applications of unstable grippers are discussed in this section. Unstable grippers are not usually particularly desirable unless as a *toy*. Indeed,



Fig. 4.33. A plastic toy imitating a robotic grasping hand



Fig. 4.34. A skill crane machine containing balls

one could imagine building plastic robotic hands such as the one illustrated in Fig. 4.33 to actually amuse children and/or trick people.

Another application of unstable grasping—albeit morally condemnable—is confidence games, e.g., skill crane machines. An example of such a machine—commonly found in fairs and commercial malls—is illustrated in Fig. 4.34. For a small fee, the player can control a crane equipped with a gripper to pick a gift, usually a plush or a small toy, and has to drop it in a place where he/she can grab

it. If such machines were equipped with a gripper designed using the analysis described in the previous section, the user's chance to actually obtain a gift is almost zero. Note that the objects to be grasped are a statistically predictable data, for instance, in Fig. 4.34, only balls with a certain diameter and friction coefficient are to be considered. This a priori data can be used to refine the design obtained in the previous section, for instance, contact trajectories corresponding to a circular object can be taken into account, c.f. Section 4.2.4.

However, the authors do not recommend to use the technique presented in this section to actually trick people out of their money. Prospective swindlers should meditate this advice from a distributor of skill crane machines:

*"You can have the best plush toys in the world in your equipment, but if your customers do not win often enough, the game will not be profitable.
[...] If you tighten your game up too much and no one wins, then everyone will find out and quit playing."*

4.2.6 Application: Design Validation

In order to validate the theoretical results of Sections 4.2–4.2.4, a model of one of the underactuated fingers (Laliberté and Gosselin 2003) built at Université Laval (SARAH) was exported to a dynamic simulation package. To obtain a two-phalanx finger, only the last two phalanges of the finger were considered (illustrated in Fig. 4.35). The actual prototype of the hand was built and is shown in Fig. 2.7(e). Obviously, the stability of the last two phalanges is not decisive in the case of a three-phalanx prototype since the “base joint” of the two-phalanx finger is moving on a circle in the three-phalanx case. However, as a first approximation, stability can be estimated using the method presented above.

To summarize, the virtual model includes: a non-negligible spring between the two phalanges, a non-zero constant thickness of the phalanges, and a circular contact, but with no friction. The resulting grasp-state plane, including the initial and final contact situations, measured from the dynamic simulation, as well as the equilibrium and contact curves is presented in Fig. 4.36. The final position of the finger corresponds to a contact situation indistinguishable from the predicted equilibrium position (numerical differences are less than 1% for both k_2 and θ_2).

The limits on angle θ_2 in Fig. 4.36 correspond to the actual mechanical limits of the finger, i.e., $-20^\circ < \theta_2 < 90^\circ$. It is also pointed out that these limits, corresponding to stable contact situations as previously discussed and the equilibrium curve associated with the finger, completely prevent any kind of ejection. The other contact trajectories presented in Fig. 4.36 correspond to other positions of the same circular object in the Cartesian space. Therefore, it can be stated that if contact is made between the finger and this object, the final grasp will be stable, even if the contact is only maintained with the distal phalanx. Also, it should be observed that a contact with only the distal edge (tip) of the distal phalanx is not considered with our model since the phalanx is assumed to be tangent to the object's local shape.

If a frictional contact is considered, the tangent distal force generates a moment in O_2 equal to $-f_{t2}\epsilon$. This moment is equivalent to a wrench with the same

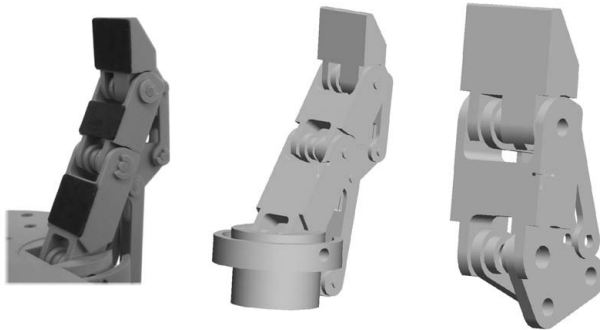


Fig. 4.35. Three-phalanx prototype, model and the last two phalanges

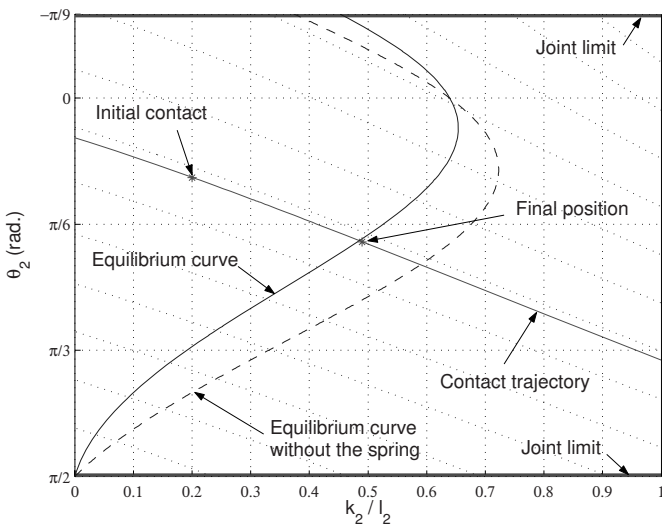


Fig. 4.36. Grasp-state plane for the grasp of the prototype finger

normal and tangent forces but with a torque τ_2 considering a zero thickness phalanx. Hence, one has $\tau_2 = \eta_2 f_2 = -f_{t2}\epsilon$, therefore the equivalent instantaneous rolling friction coefficient is $\eta_2 = -\epsilon\mu$. The latter coefficient must be added to the previous value of η_2 describing the contact friction (even if it is zero). This modification can be made directly in matrix \mathbf{J} in order to obtain the new expressions of the forces, which were verified using a static analysis (Birglen 2004).

4.2.7 On the Grasp-State Plane Necessity

Now that a thorough analysis and dedicated tools for underactuated grasp stability have been established, the next natural step is to determine if a design that always avoids ejection could be found. In order to do so, the best approach is to

design a finger that never loses contact with the object but “sticks” to it, i.e., a finger where both f_1 and f_2 are always positive. Unfortunately, it can be proved that no two-phalanx underactuated finger can guarantee a stable two-phalanx grasp in the whole workspace, at least with a frictionless single point of contact model.

To prove this assertion, one may consider a general underactuated finger design characterized by its transmission matrix \mathbf{T} :

$$\mathbf{T} = \begin{bmatrix} 1 & R(\theta_2) \\ 0 & 1 \end{bmatrix}, \quad (4.40)$$

where R is the transmission factor. If the spring and friction are neglected, the analytical expression of the contact forces can be obtained from eq. (4.3) as:

$$\mathbf{f} = \begin{bmatrix} \frac{k_2(1+R)+Rl_1 \cos \theta_2}{k_1 k_2} T_a \\ -\frac{R}{k_2} T_a \end{bmatrix}. \quad (4.41)$$

Assuming that $k_1 > 0$, $k_2 > 0$ and $T_a > 0$, to ensure that both components are positive, one has:

$$R(\theta_2) < 0, \quad \forall \theta_2. \quad (4.42)$$

From the definition of f_2 , and from the definition of f_1 , the following expression is obtained:

$$k_2(1 + R(\theta_2)) + R(\theta_2)l_1 \cos \theta_2 > 0. \quad (4.43)$$

Therefore,

$$\begin{cases} R(\theta_2) > \frac{-k_2}{k_2+l_1 \cos \theta_2} & \text{if } k_2 + l_1 \cos \theta_2 > 0 \\ R(\theta_2) < \frac{-k_2}{k_2+l_1 \cos \theta_2} & \text{otherwise.} \end{cases} \quad (4.44)$$

For $-\pi/2 < \theta_2 < \pi/2$, one obtains $R(\theta_2) > \frac{-k_2}{k_2+l_1 \cos \theta_2}$ for any k_2 . The limit case $k_2 = 0$ yields that $R(\theta_2) > 0$, this is in contradiction with eq. (4.42) and therefore $R(\theta_2)$ such that f_1 and f_2 are positive (for all possible values of k_2) does not exist at least for this range of angle θ_2 . Indeed, only the function $R(\theta_2) = 0$ satisfies the positiveness condition on f_1 and f_2 , however not strictly since in this case $f_2 = 0$ for any value of angle θ_2 . This paradox can be illustrated graphically using Figs. 4.3-4.5: the stable fully positive contact configurations are located on top of the equilibrium curve. If these stable areas are to correspond to the whole range of the contact location k_2 , the only possibility is an equilibrium value that is always zero. Since the latter is proportional to coefficient R (see eq. (4.13)), one obtains that R must also be zero. This proves that there is no design of underactuated finger that can provide a fully positive workspace, neglecting spring and friction, at least with our model of underactuated finger and for all possible values of the contact location. Therefore one **must** study the grasp-state plane characteristics to prevent ejection. Furthermore, a contact with the proximal phalanx cannot be ensured in all cases since it depends on the size and position of the object seized. Hence, the grasp stability in case of a pinch grasp should be guaranteed.

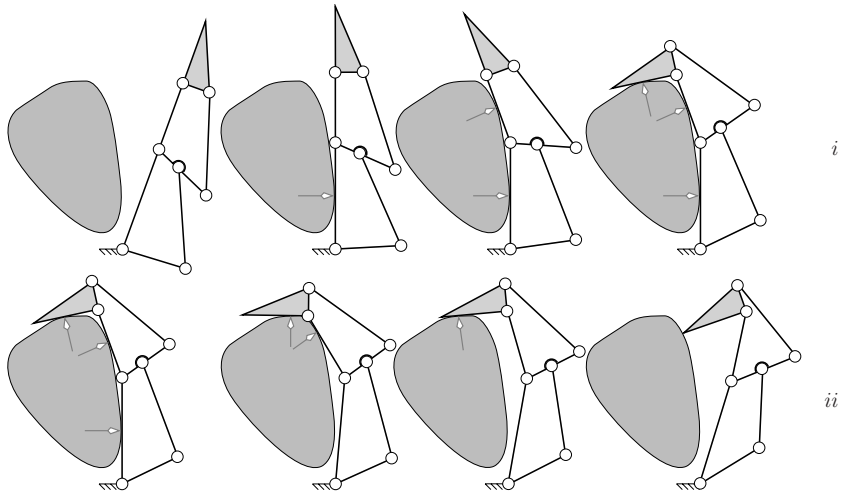


Fig. 4.37. Ideal grasping sequence (i) degenerating into ejection (ii)

4.3 Grasp Stability of Three-Phalanx Underactuated Fingers

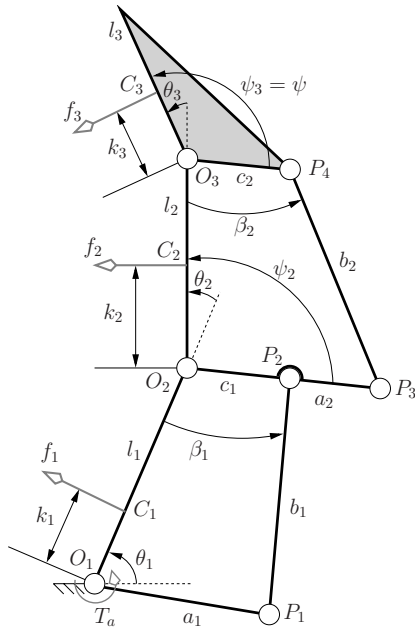
4.3.1 Three-Phalanx Underactuated Fingers Ejection Theory

It was shown in Section 4.2.7 that -no- two-phalanx underactuated finger can always apply forces on a fixed object and with all its phalanges, in all possible configurations. This strongly suggests that three-phalanx fingers may suffer from the same drawback. Hence, an ideal grasping sequence as illustrated in Fig. 4.37*i* might not always occur and some sequences may instead lead to the ejection phenomenon illustrated in Fig. 4.37*ii*. Indeed, n contacts are usually required in order to constrain a n -phalanx finger. However, $n - i$ contacts can be enough for the finger to be in static equilibrium, if certain geometric conditions are met. Thus, one can describe an i^{th} order equilibrium when i contacts are missing. In this section, the case for which $n = 3$ is studied and a particular emphasis is placed on the case for which $i = 1$. A discussion will be presented for $i = 2$, while the case $i = 0$ was presented in Section 3.5.

The objective of this section is to determine when a grasp is stable and if ejection can occur with a three-phalanx finger. Preliminary experiments with a dynamic simulation package, a commercial dynamic simulation package, suggest that, indeed, ejection can happen with a three-phalanx underactuated finger. However, this phenomenon does not occur very often and it is very likely favoured by particular conditions of the model used (e.g. single-point contacts, no friction). In this section, it is assumed that the initial configuration of the finger is the one depicted in the last schematic of the ideal grasping sequence (Fig. 4.37*i*). Thereupon, in this configuration, some forces may be negative. The case where the three forces are negative is not very likely to happen. In fact, with a tendon-driven

Table 4.2. Geometric parameters of linkage and pulley fingers

Set 1 (linkages)									
l_1	l_2	l_3	ψ	a_1	b_1	c_1	a_2	b_2	c_2
1	.67	.62	$\pi/2$.62	.95	.26	.62	.95	.26
Set 2 (pulleys)									
l_1	l_2	l_3	—	r_1	—	r_2	r_3	—	r_4
1	.67	.62	—	.62	—	.26	.62	—	.26

**Fig. 4.38.** Three-phalanx finger using linkages

underactuated finger, it is even impossible since the last phalanx force is *always* positive (Section 3.6.2). Furthermore, it contradicts the closing motion of the finger necessary to achieve the initial configuration. For linkage-driven fingers, particular configurations of the transmission linkages (where $h_i = 0$ and/or $h_j = -l_j$ with $i = 2, 3$) can correspond to a negative or zero distal phalanx force. These configurations correspond to a hyperflexion/hyperextension in the finger or to a singularity in the transmission linkages. They were studied in Sections 3.2 and 4.2.1. These situations will not be represented in the forthcoming figures for legibility purposes but should be taken into account. Numerical results and figures will be given for a finger with the geometric parameters listed in Table 4.2.

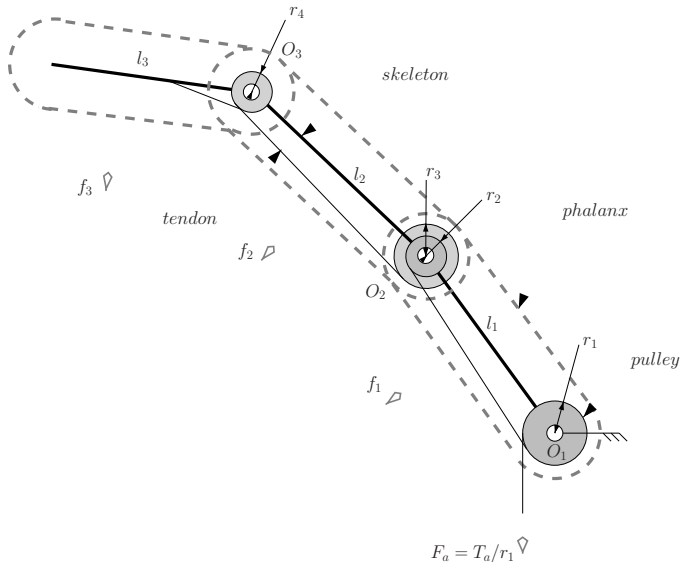


Fig. 4.39. Three-phalanx finger using tendons

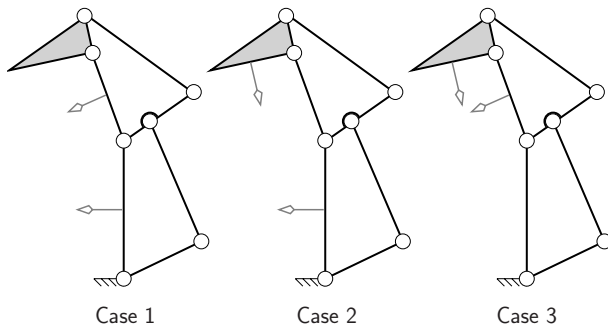


Fig. 4.40. Cases studied for ejection

Geometric details and nomenclature of the models are provided in Figs. 4.38 and 4.39. The equivalence between linkages and tendon transmissions was highlighted in Section 3.6.2, both types of transmission share similar properties.

If only one contact force is negative, the interesting cases reduce to only three, presented in Fig. 4.40. The equilibrium is achieved when the force on the phalanx with no contact (the initially negative force) increases to zero, while the others remain positive. The procedure to obtain an analytical expression of the normal contact forces was presented in Section 3.2. Basically, the contact forces can be expressed as:

$$\mathbf{f} = \mathbf{J}^{-T} \mathbf{T}^{-T} \mathbf{t}, \quad (4.45)$$

where $\mathbf{f} = [f_1 \ f_2 \ f_3]^T$ is the vector of the normal contact forces and \mathbf{J} is a lower triangular matrix characterizing the contact locations (and friction, if modelled) that can be expressed analytically. Neglecting friction, one has:

$$\mathbf{J} = \begin{bmatrix} k_1 & 0 & 0 \\ k_2 + l_1 \cos \theta_2 & k_2 & 0 \\ k_3 + l_1 \cos(\theta_2 + \theta_3) + l_2 \cos \theta_3 & k_3 + l_2 \cos \theta_3 & k_3 \end{bmatrix}, \quad (4.46)$$

Matrix \mathbf{T} characterizes the underactuation and for a finger using linkages as illustrated in Fig. 4.38, one has:

$$\mathbf{T} = \begin{bmatrix} 1 - \frac{h_2}{h_2 + l_1} - \frac{h_2 h_3}{(h_2 + l_1)(h_3 + l_2)} \\ 0 & 1 & 0 \\ 0 & 0 & 1 \end{bmatrix}, \quad (4.47)$$

where

$$h_i = c_{i-1} (\cos(\theta_i - \psi_i) - \sin(\theta_i - \psi_i) \cot \beta_{i-1}). \quad (4.48)$$

Angle ψ_i is the angle between $O_i P_{2i-2}$ and $O_i O_{i+1}$ for $i > 1$ (see eq. (3.29)). Thus, angle ψ_i can be expressed recursively with, initially, $\psi_3 = \psi$. For tendon-driven fingers, the expressions are simpler, i.e., one has

$$\mathbf{T} = \begin{bmatrix} 1 - \frac{r_2}{r_1} - \frac{r_2 r_4}{r_1 r_3} \\ 0 & 1 & 0 \\ 0 & 0 & 1 \end{bmatrix}, \quad (4.49)$$

where r_{2i-1} and r_{2i} for $i > 0$ are respectively the radius of the pulley located at the base and the end of the i^{th} phalanx (Fig. 4.39). Hence, the expressions of the contact forces are

$$f_1 = \frac{l_1 U T_a}{k_1 k_2 k_3 (h_2 + l_1)(h_3 + l_2)}, \quad (4.50)$$

$$f_2 = \frac{h_2 l_2 (k_3 - h_3 \cos \theta_3) T_a}{k_2 k_3 (h_2 + l_1)(h_3 + l_2)}, \quad (4.51)$$

$$f_3 = \frac{h_2 h_3 T_a}{k_3 (h_2 + l_1)(h_3 + l_2)}, \quad (4.52)$$

with

$$\begin{aligned} U = & k_2 k_3 h_3 + k_2 k_3 l_2 - h_2 k_3 l_2 \cos \theta_2 - h_2 h_3 k_2 \cos(\theta_2 + \theta_3) \\ & + h_2 h_3 l_2 \cos \theta_2 \cos \theta_3 \end{aligned} \quad (4.53)$$

for a linkage-driven finger, and

$$f_1 = \frac{U'T_a}{k_1 k_2 k_3 r_1 r_3}, \quad (4.54)$$

$$f_2 = \frac{-r_2(-k_3 r_3 + r_4 l_2 \cos \theta_3 + r_4 k_3) T_a}{k_2 k_3 r_1 r_3}, \quad (4.55)$$

$$f_3 = \frac{r_2 r_4 T_a}{r_1 r_3 k_3}, \quad (4.56)$$

with

$$\begin{aligned} U' = & l_1 r_2 \cos \theta_2 (r_4 l_2 \cos \theta_3 + (r_4 - r_3) k_3) - l_1 r_2 r_4 k_2 \cos(\theta_2 + \theta_3) \\ & + (r_1 - r_2) k_2 k_3 r_3 \end{aligned} \quad (4.57)$$

for a tendon-driven finger. In the next subsections, some assumptions are made on the finger architecture and the contact, namely negligible friction at the contacts and negligible spring torques between the phalanges (the latter assumptions correspond to the above expressions for the contact forces). The object will be assumed fixed with respect to the base of the finger and the local geometry of the contacts will also be neglected, i.e., a single fixed point of contact on each phalanx is assumed.

4.3.2 Loss of One Contact

Case 1

The first case in Fig. 4.40 is trivial, since the distal phalanx force is always positive except in rare hyperflexion/hyperextension configurations with mechanical transmissions and never with pulleys and tendons. Thus, in this very unlikely situation, equilibrium can only be achieved in rare configurations such as the one illustrated in Fig. 4.41. In fact an equilibrium is achieved if the last phalanx does not touch the object: this should be prevented as the finger may not be considered to sufficiently envelop the object for proper grasping. Indeed, in that case, the finger act as if it had only two phalanges, the last one remaining unused. Design rules of four-bar linkages should be used to prevent this situation from happening.

Case 2

In the second case of Fig. 4.40, the finger can be regarded as a two-phalanx finger. Indeed, if contact is established and maintained with the first phalanx, the resulting configuration (with no second phalanx contact) can be considered exactly like a two-phalanx finger during a sliding motion as extensively studied in Section 4.2—the last two phalanges constituting a two-phalanx finger. However, the contact trajectories should be examined in the $(\theta_2, \theta_3, k_3)$ space rather than just the two-phalanx grasp-state plane described by (θ_3, k_3) . Indeed, angle θ_2 is

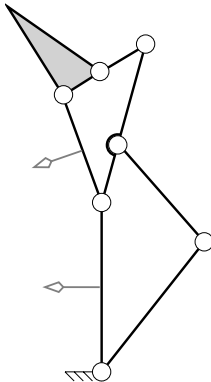


Fig. 4.41. Equilibrium configuration with no contact on the distal phalanx

required in order to establish the expression of the equilibrium surface in case of a linkage-driven finger (h_2 is a function of θ_2 and is present in the equilibrium expression, see eq. (4.61)). Furthermore, this angle could be required to establish the contact forces during the sliding process, as will be discussed in Section 4.3.4. In this grasp-state space, one obtains the equilibrium surface, mathematically defined by $f_2(\theta_2, \theta_3, k_3) = 0$. The plane $k_3 = l_3$ corresponds to the ejection situation (illustrated in Fig. 4.37ii) and will be referred to as the ejection surface. The contact trajectories describing the instantaneous grasp-state evolution of the finger, modified from Section 4.2.2 to include the variation of θ_2 , are

$$k_{3i}C_{\theta_{3i}} - k_3C_{\theta_3} = K, \quad (4.58)$$

$$l_2(1 - C_{\theta_{2i}-\theta_2}) + k_{3i}(C_{\theta_{3i}} - C_{\theta_2-\theta_{2i}-\theta_{3i}}) = K, \quad (4.59)$$

with

$$K = \frac{k_3^2 - k_{3i}^2}{2l_2}, \quad (4.60)$$

where C_α is a shorthand notation for $\cos \alpha$, $(\theta_{2i}, \theta_{3i}, k_{3i})$ is an arbitrary initial contact situation on the trajectory. Eqs. (4.58) and (4.59) mathematically imply a skewing of the trajectory plotted in Fig. 4.12 out of the (θ_3, k_3) plane, corresponding to the variation of θ_2 . Previously, in Section 4.2.2, this variation was disregarded, but it must be considered here in the three-phalanx case. Examples of contact trajectories with the associated equilibrium surfaces are presented in Figs. 4.42 and 4.43 with $(\theta_{2i}, \theta_{3i}, k_{3i}) = (\pi/4, \pi/4, 4/25)$. Once in an initial configuration, the grasp-state evolves following the trajectory until either a joint limit is attained (which can be represented by vertical planes in this space), or the equilibrium surface is attained, or ejection happens (top or bottom planes of the space represented, defined respectively by $k_3 = l_3$ and $k_3 = 0$). It should be noted that the direction in which the instantaneous contact state evolves along

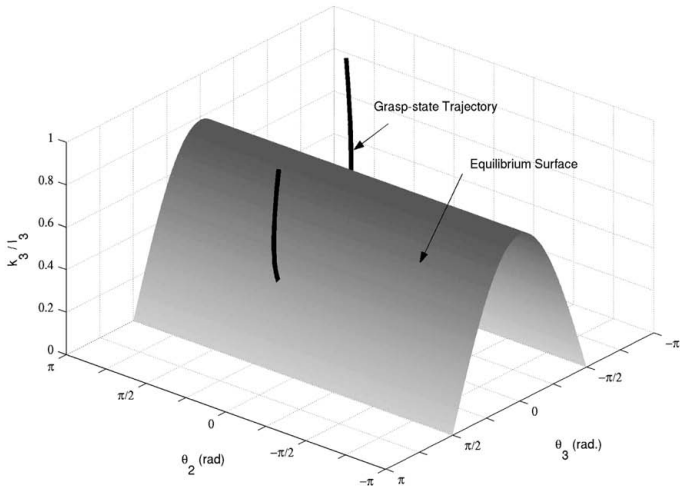


Fig. 4.42. Grasp-state trajectory and equilibrium surface (parameter set 2)

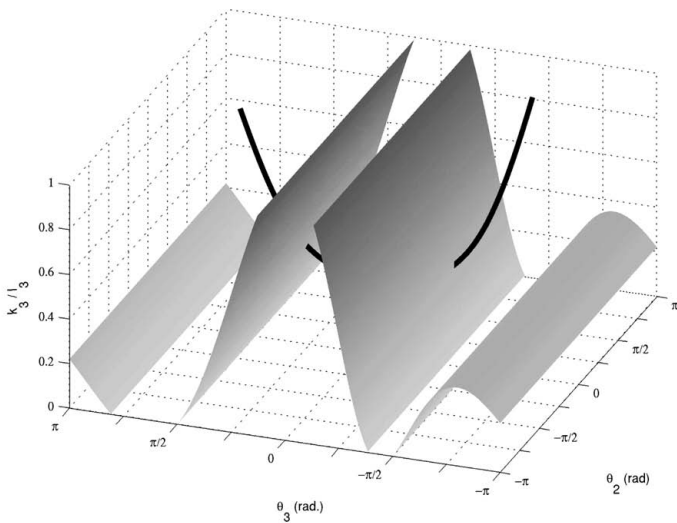


Fig. 4.43. Grasp-state trajectory and equilibrium surface (parameter set 1)

the trajectory depends on the side of the equilibrium surface on which this state is located, i.e., the sign of f_2 , similarly to the case of the two-phalanx finger.

Contact trajectories are obtained that can lead either to a static ($f_2(\theta_2, \theta_3, k_3) = 0$) or kinematic (joint limit) equilibrium, or to ejection ($k_3 > l_3$). The

expression of the equilibrium surface, defined by $f_2 = 0$, can be explicitly obtained and simplified—by taking into account only the part that can change sign—to

$$\begin{cases} h_2(h_3 \cos \theta_3 - k_3) = 0 & \text{for linkage-driven fingers} \\ (r_3 - r_4)k_3 - r_4 l_2 \cos \theta_3 = 0 & \text{for tendon-driven fingers.} \end{cases} \quad (4.61)$$

It is recalled that the surface defined by $h_2 = 0$ has not been plotted in Fig. 4.43 as stated in the introduction of this section. This case corresponds to both an equilibrium position and a singularity in the transmission linkage where points O_2 , P_2 and P_1 lie on the same line. Furthermore, in this configuration, both f_2 and f_3 become zero. Hence, this “equilibrium” surface should be avoided since the distal phalanx does not exert any grasping force on the object.

Case 3

The third case is the most interesting, since it is both particular to three-phalanx fingers and it is also the most complex of the three cases. Unfortunately, the problem becomes four-dimensional. Indeed, every time a phalanx is added to the finger, two grasp-state variables should be added (except for the first phalanx as shown in Section 3.5). Hence, two-phalanx fingers lead to two variables while three-phalanx fingers require **four** variables and n phalanx-fingers lead to $2(n-1)$ variables. Thus, contact trajectories and equilibrium surfaces cannot be easily visualized, as opposed to what was encountered in the two-phalanx case or in Case 2 above (where k_2 did not appear, leading to a simplified three-dimensional problem). However, by carefully studying the equations defining the grasp behaviour, a solution can be found in order to get some insight into this problem. First, consider the equations defining the contact trajectories, namely:

$$d_{oc_2}^2 = l_1^2 + k_2^2 + 2l_1 k_2 \cos \theta_2, \quad (4.62)$$

$$d_{c_2 c_3}^2 = (l_2 - k_2)^2 + k_3^2 + 2(l_2 - k_2)k_3 \cos \theta_3, \quad (4.63)$$

$$d_{oc_3}^2 = 2(l_1 + m_1)(k_3 + m_2) \cos(\theta_2 + \theta_3) + (l_1 + m_1)^2 + (k_3 + m_2)^2, \quad (4.64)$$

where d_{oc_2} , $d_{c_2 c_3}$, and d_{oc_3} are respectively the distances between the points $O_1 - C_2$, $C_2 - C_3$, and $O_1 - C_3$ (labeled in Fig. 4.38). These quantities are therefore constant (since the object is assumed to be fixed in space). Terms m_1 and m_2 are short notations for:

$$\begin{cases} m_1 = m \sin \theta_3 \\ m_2 = m \sin \theta_2 \end{cases} \quad \text{with } m = \frac{l_2 \sin(\theta_3 - \theta_2)}{\cos^2 \theta_2 - \cos^2 \theta_3}. \quad (4.65)$$

The equilibrium surface is defined as $U(\theta_2, \theta_3, k_2, k_3) = 0$, where U is the part of f_1 that can change sign, similarly to what was used in Case 2. For example, with a tendon-driven finger, one obtains:

$$\begin{aligned} U = & l_1 r_2 \cos \theta_2 (r_4 l_2 \cos \theta_3 + (r_4 - r_3)k_3) - l_1 r_2 r_4 k_2 \cos(\theta_2 + \theta_3) \\ & + k_2 k_3 (r_1 - r_2) r_3 \end{aligned} \quad (4.66)$$

and for linkage-driven finger:

$$U = h_2 l_2 \cos \theta_2 (h_3 \cos \theta_3 - k_3) - h_2 h_3 k_2 \cos(\theta_2 + \theta_3) + k_2 k_3 (h_3 + l_2), \quad (4.67)$$

where h_2 and h_3 are the complex functions of the configuration defined in eq. (4.48). First, it can be observed that in this form, the problem is decoupled. The first three equations, namely eqs. (4.62) to (4.64) depend only on the contact point locations while the last one, eq. (4.66) or (4.67), depends only on the transmission used. Now, one has four equations with four variables, the equilibrium being a hypersurface in the grasp-state space. However, visualization can be achieved by writing the three contact equations in a certain form. Namely, the form presented in eqs. (4.62) to (4.64). Indeed, there are numerous ways of writing the contact equations but only this form of the equations leads to a simplified visualization. By looking closely at eq. (4.62), it is observed that a one-to-one relationship is easily obtained from this equation between θ_2 and k_2 , provided that an estimated k_2 can be evaluated to choose one of the two solutions of this equation (for a known θ_2), namely

$$k_2 = -l_1 \cos \theta_2 + \delta \sqrt{d_{oc2}^2 - l_1^2 \sin^2 \theta_2}, \quad (4.68)$$

with $\delta = \pm 1$. The solution corresponding to $0 < k_2 < l_2$ must be chosen or, when both solutions meet this requirement, the solution closest to the preceding point on the contact trajectory should be used. This one-to-one relationship can be substituted in the three remaining equations, leading to a system of three equations and three variables that can be visualized in the resulting three-dimensional space, namely $(\theta_2, \theta_3, k_3)$. It is pointed out that the latter is the state space used in Case 2. This reduced grasp-state space is similar to the grasp-state plane (θ_2, k_2) for a two-phalanx finger and allows the visualization of contact trajectories as well as equilibrium and validity surfaces, and therefore can help to study the grasp stability of the fingers. As a result, to accurately describe the grasp-state trajectory, k_2 is not required, even in Case 3, where it actually exists and evolves during the grasp self-motion. This result was not intuitively expected. Furthermore, eq. (4.62) is the equation defining the contact trajectory in the plane (k_2, θ_2) for a two-phalanx finger, therefore the contact trajectory in Fig. 4.12 can be regarded as the projection in the plane (θ_3, k_3) of the four-dimensional trajectory. Examples of an equilibrium surface and a state trajectory are respectively presented in Figs. 4.44 and 4.45 with $(\theta_{2i}, \theta_{3i}, k_{2i}, k_{3i}) = (10^\circ, 70^\circ, 0.33, 0.31)$. Due to the complexity of the surface and the trajectory, they have been plotted separately for legibility purpose.

It should be noted that reducing the dimension of the grasp-state analysis is a technique that cannot be applied to the grasp-state plane thoroughly studied in Section 4.2. Indeed, in the two-phalanx case, the contact trajectories are defined by a single equation and therefore, no substitution can be made. Additionally, if one considers the equilibrium curve and substitutes one variable by a function of the other, it is simply equivalent to finding the intersection of the two curves. However, this is not particularly useful since an existing intersection is

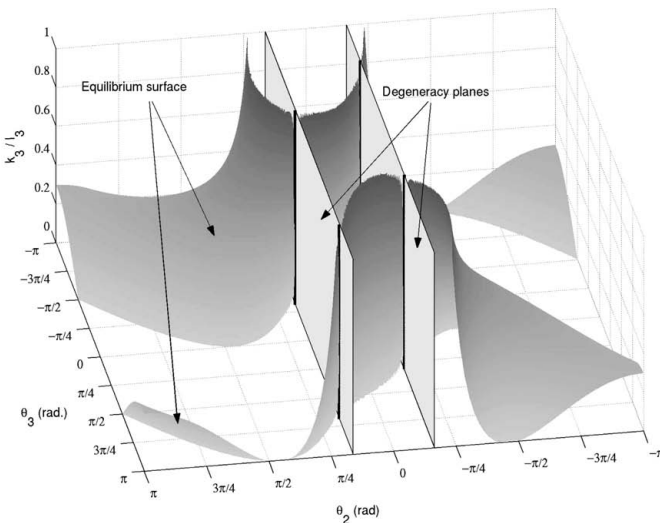


Fig. 4.44. Case 3 example of equilibrium surface (parameter set 2)

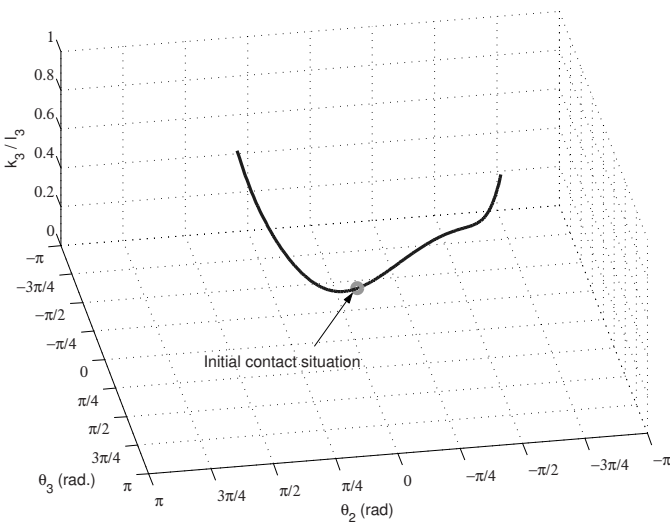


Fig. 4.45. Case 3 example of state trajectory (parameter set 2)

neither a necessary nor a sufficient condition for grasp stability. Indeed, one can achieve equilibrium with a mechanical limit and many trajectories intersecting the equilibrium curve actually lead to ejection because of the grasp-state evolution. Hence, reducing the grasp-state plane to a grasp-state “line” is not relevant. Similarly, reducing the already reduced grasp-state space to a grasp-state plane

is not useful neither. This reduction can be made but it implies a loss of generality as the obtained grasp-state plane is only valid for a particular initial grasp-state configuration (meaning a particular *object in a precise location*).

It is also noted that the words system of equations and “variables” have been used: we did not speak of “unknowns” since we are not interested in knowing if an intersection of the contact trajectory and the equilibrium surface exists. Indeed, a stable configuration can be achieved by attaining a joint limit. Thus, a real solution of this system is neither a sufficient nor a necessary condition for a stable grasp. It may seem peculiar that a four-dimensional problem can be reduced to a three-dimensional one. In fact, the problem is *still* four-dimensional, but a property of the system of equations was used in order to obtain a graphical visualization. Figs. 4.44 and 4.45 are indeed neither a projection, nor a section of this four-dimensional space. However, the equilibrium surface for *-this-* trajectory was drawn, which is obtained by substituting the solution of eq. (4.62) into the equilibrium equation.

For other trajectories, i.e., for other initial configurations in the $(\theta_2, \theta_3, k_3)$ space, the equilibrium surface even with the same finger will change, as illustrated in Figs. 4.46(a) and 4.46(b) (in which the other parameters are unchanged from Fig. 4.44). In fact, the surface will remain unchanged as long as the distance d_{oc_2} is the same. If the latter distance changes, eq. (4.62) also changes, therefore the substitution leads to different values and the surface is modified. Therefore, with this technique to allow visualization, one loses the decoupling of the problem initially present since now, the equilibrium surface is no longer only a function of the geometric configuration and architectural design parameters but also of the initial contact location on the phalanges, an acceptable tradeoff to obtain a clear and complete visualization.

4.3.3 Degeneracy Analysis

In Fig. 4.44, two planes are referred to as degeneracy planes. These planes correspond to a degeneracy in the equilibrium location, i.e., a situation where the equation $U(\theta_2, \theta_3, k_2, k_3) = 0$ is satisfied with k_3 going to infinity, i.e.,

$$k_3(U = 0) = \pm\infty. \quad (4.69)$$

These conditions were previously referred to—for a two-phalanx finger—as degeneracy conditions in Section 4.2.3. Indeed, if the grasp-state of the finger corresponds to one of the latter configurations, the contact location on the phalanx leading to a static equilibrium is pushed to infinity. The degeneracy itself can be either local, i.e., for a particular configuration of the finger (angles θ_2 and θ_3), or global, i.e., for all the finger’s configurations. This condition can be easily expressed analytically from eq. (4.66), for fingers using tendons:

$$k_2 r_3(r_1 - r_2) + r_2(r_4 - r_3)l_1 \cos \theta_2 = 0. \quad (4.70)$$

Since k_2 and θ_2 are also associated with eq. (4.62), this equation can be solved for θ_2 in order to obtain the angle θ_2 corresponding to these planes and examine

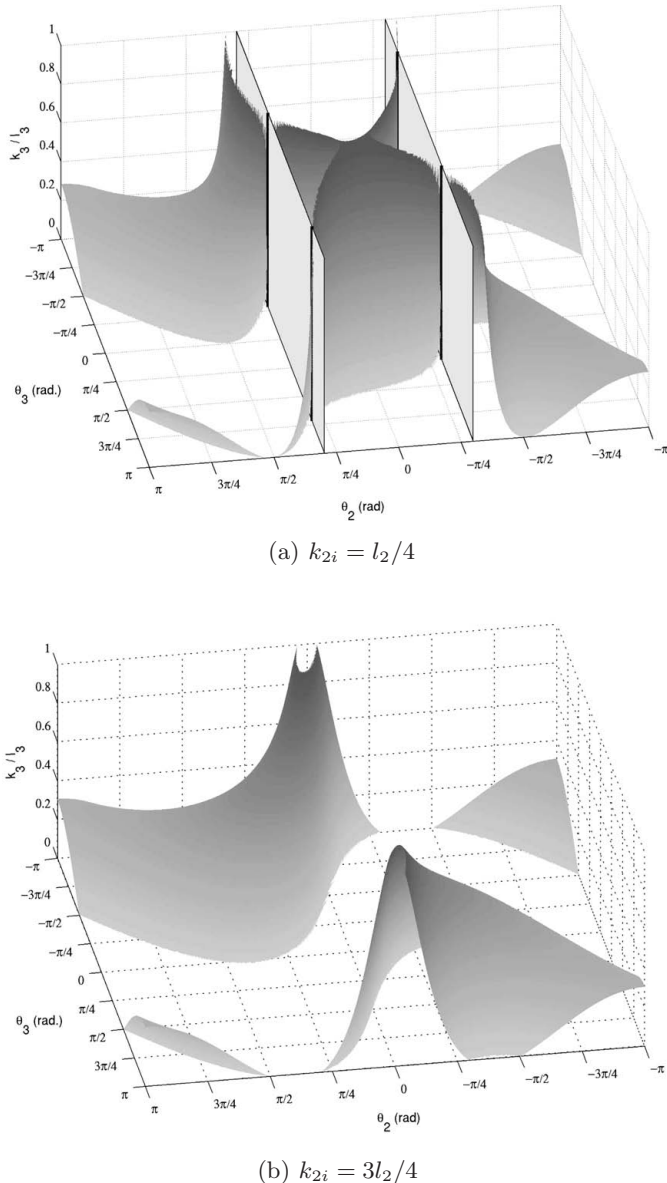


Fig. 4.46. Case 3 equilibrium surfaces with different values of k_{2i}

them in the reduced grasp-state space along with the equilibrium surface. It is noted that these degeneracy conditions are in fact a locus in the (k_2, θ_2) space and are only function of the design parameters of the finger, not the contact locations. Eq. (4.62) has only been used to draw the degeneracy condition in

the reduced grasp-state space. For linkage-driven fingers, the Case 3 degeneracy condition yields to

$$k_2(h_3 + l_2) - h_2 l_2 \cos \theta_2 = 0. \quad (4.71)$$

Similarly, eq. (4.62) can be used to obtain the angle θ_2 corresponding to a degeneracy configuration. However, it is recalled that h_2 and h_3 are complex functions of θ_2 and θ_3 . Therefore, degeneracy surfaces are obtained instead of degeneracy planes, since these configurations are now also functions of θ_3 . Nevertheless, the expression of these surfaces can be written analytically considering eqs. (4.48) and (3.29). Eq. (4.71) defines the degeneracy condition which is actually a surface in the $(k_2, \theta_2, \theta_3)$ space. Using eq. (4.62), the representation of the latter surface in the reduced grasp-state space $(\theta_2, k_3, \theta_3)$ can be obtained. An example of Case 3 degeneracy locus is presented in Fig. 4.47 for a linkage-driven finger. The solid curves represent the degeneracy locus as presented in eq. (4.71) while the dashed curves represent the locus of points where the degeneracy condition creates a paradoxical equilibrium, namely when

$$h_2 h_3 (k_2 \cos(\theta_2 + \theta_3) - l_2 \cos \theta_2 \cos \theta_3) = 0. \quad (4.72)$$

Indeed, a subset of these degenerate configurations contradicts the unstable behaviour and leads to a paradoxical equilibrium. Similarly to what was obtained for the two-phalanx finger, if the coefficient in the equilibrium equation U that does not depend on k_3 is also zero, *-any-* contact location leads to static equilibrium. This condition is defined by

$$l_2 \cos \theta_2 \cos \theta_3 - k_2 \cos(\theta_2 + \theta_3) = 0, \quad (4.73)$$

for a tendon-driven finger, a result very similar to eq. (4.72). Therefore, in order to define these equilibrium configurations, a set of two trigonometric nonlinear equations—the coefficient of k_3 and the other term in U (see eq. (4.66)) both equal to zero—must be solved for two unknowns (θ_2 and θ_3) using eq. (4.62). In these peculiar configurations, the equilibrium surface degenerates into two parallel straight lines. In Fig. 4.44, the four solutions (two solutions for θ_2 and for each one of the latter, two solutions for θ_3) of these equations are outlined in black. The two curves in Fig. 4.47 seem to coincide locally (for approx. $\theta_2 = 0$ and $\theta_3 = -\pi/2$) but in fact they do not, the two curves rather intersect in many points in this region of the (θ_2, θ_3) plane. The latter intersections correspond to paradoxical equilibria while there is no equilibrium possible between them, a peculiar behaviour.

By inspection of eq. (4.70), the conditions for a global (or architectural) degenerated design are obtained as: $r_1 = r_2$ and $r_3 = r_4$ (assuming $r_i > 0$) for tendon-driven fingers, which are also sufficient conditions for an architectural global Case 2 degeneracy! Indeed, such degeneracies can also happen in Case 2, but the conditions are simpler. Using eq. (4.61), one obtains

$$\begin{cases} h_3(\theta_3) = \pm\infty & \text{using linkages} \\ r_3 = r_4 & \text{using tendons.} \end{cases} \quad (4.74)$$

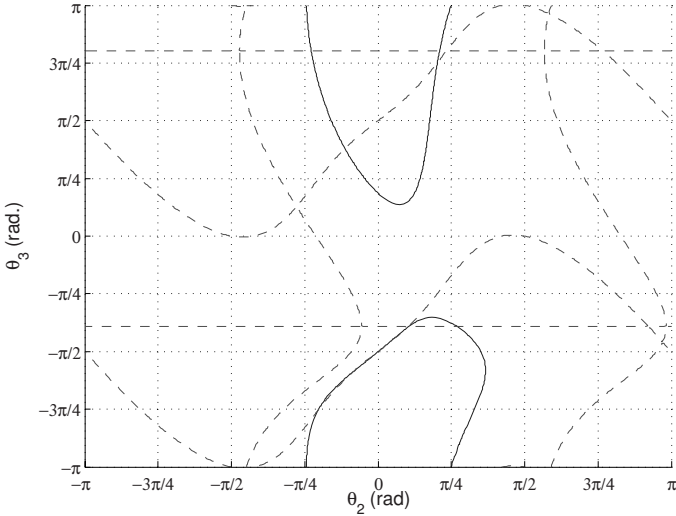


Fig. 4.47. Case 3 degeneracy analysis

Hence, with Case 2 and for tendon-actuated fingers, no local degeneracy is possible, only a global unstable design, defined with $r_3 = r_4$. The Case 2 degeneracy condition for linkage-driven fingers can be reduced to

$$\cot \beta_2 = \pm\infty, \quad (4.75)$$

since $\cot \beta_2$ can be expressed as a ratio—c.f. eq. (3.26)—equating its denominator to zero yields

$$(c_2 \cos(\theta_3 - \psi) + l_2) \sqrt{4a_2^2 b_2^2 - N^2} = M c_2 \sin(\theta_3 - \psi), \quad (4.76)$$

with

$$\begin{aligned} M &= -l_2(l_2 + 2c_2 \cos(\theta_3 - \psi)) + a_2^2 - b_2^2 - c_2^2, \\ N &= l_2(l_2 + 2c_2 \cos(\theta_3 - \psi)) - a_2^2 - b_2^2 + c_2^2. \end{aligned}$$

Hence, the Case 2 degeneracy condition for linkage-driven fingers is obtained. The degeneracy condition of eq. (4.76) can be solved for θ_3 in order to obtain the angle θ_3 corresponding to an impossible static equilibrium. Therefore, the Case 2 degeneracy surfaces are in fact, degeneracy planes but with θ_3 constant (as opposed to planes with θ_2 constant in Case 3 degeneracy condition for tendon transmission).

The contact trajectories themselves are not affected by the crossing of a degeneracy surface but no equilibrium is possible in these configurations, except the paradoxical equilibrium previously discussed and defined by eqs. (4.72) or (4.73). Since, close to these surfaces, the equilibrium location moves very quickly

to infinity, most of the configurations around these surfaces correspond to equilibrium positions far away from the real phalanx and are usually not physically achievable. In conclusion, these configurations are either undesirable (equilibrium point pushed to infinity, often) or ideal (any location leads to equilibrium, rare), but most certainly lead to a peculiar behaviour.

4.3.4 On the Validation Surfaces

The previous analyses relied on the assumption that during the sliding motion along the contact trajectories, the positive contact forces on the phalanges do not change sign. This hypothesis is not always satisfied since during the sliding motion of the phalanges on the object, one additional contact may be lost. The vanishing of the distal contact force f_3 can be dismissed as not likely to happen. Moreover, this condition contradicts the closing motion of the finger and in our quasi-static analysis: f_3 is always positive with tendon-driven fingers and can only be negative in a situation corresponding to a hyperflexion/hyperextension for linkage-driven fingers, as previously stated. These configurations are usually not physically achievable by design. However, both intermediate and proximal contact forces may be negative, since there is no provision to prevent them from changing sign in the above quasi-static analysis. In order to completely characterize the grasp-state space, the surface separating the valid part of the latter space from the invalid region—the one in which some contact forces are negative—should be determined. This validation surface can be expressed as $f_1 = 0$ for Case 2 and $f_2 = 0$ for Case 3. Since, in this case the sign of the force is required during the sliding motion, only a dynamic model of the finger can theoretically explicit this surface. However, under the hypothesis of a sliding motion relatively slow, which should be the case in most practical applications, especially due to friction, this dynamic behaviour can be approximated. For instance, in Case 2, a force μf_{3t} tangential to the distal phalanx surface can be introduced to model friction. Therefore, the finger is in static equilibrium provided that $\mu = 1$ and a certain value of f_{3t} is achieved. That value can be estimated using a quasi-static or static analysis. Once expressions for f_1 , f_3 and f_{3t} are obtained, and since there is an actual motion, f_1 during the latter can be estimated by imposing μ small, corresponding to a value of f_{3t} that does not lead to equilibrium, which is the case. The expression of the validation surfaces is therefore obtained

$$\begin{cases} V = (r_4 - r_3) \sin(\theta_2 + \theta_3) r_2 k_3 l_1 + l_1 \sin \theta_2 r_4 r_2 l_2 + (r_1 - r_2) \sin \theta_3 r_3 k_3 l_2, \\ V = (h_3 + l_2) \sin \theta_3 k_3 - h_2 k_3 \sin(\theta_2 + \theta_3) + h_2 h_3 \sin \theta_2, \end{cases} \quad (4.77)$$

respectively for tendon-driven and linkage-driven fingers. Note that the $f_{3t} = 0$ condition corresponds to the equilibrium condition proposed in Section 4.3.2. For Case 3, the same technique with an intermediate tangential phalanx force leads to

$$\begin{cases} V = (r_3 - r_4) k_3 - l_2 r_4 \cos \theta_3, \\ V = h_2(h_3 \cos \theta_3 - k_3), \end{cases} \quad (4.78)$$

respectively for tendon-driven and linkage-driven fingers. Note that the latter validation equations correspond to the equilibrium conditions of Case 2, i.e., $f_2 = 0$ without the intermediate contact, which was foreseeable. Similarly, the condition $f_{2t} = 0$ also corresponds to the equilibrium condition of Section 4.3.2. An example of Case 2 validation surface is illustrated in Fig. 4.48, examples of Case 2 validation surfaces have already been shown since they correspond to the Case 2 equilibrium surfaces. Note that the parameters adopted in Fig. 4.48 provide a satisfied validation condition ($f_1 > 0$) for almost all the common ranges of values for angles θ_2 and θ_3 , namely $0 < \theta_i < \pi$ ($i = 2, 3$). Obviously, this technique has its own limitations and will not lead to accurate results if the dynamics of the finger cannot be neglected. In the latter case, the dynamic behaviour of the finger must be considered (Higashimori et al. 2003).

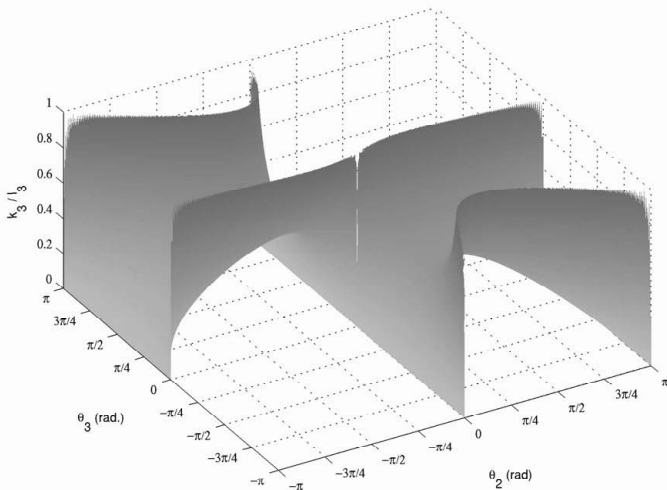


Fig. 4.48. Case 2 validation surface example (parameter set 2)

4.3.5 Loss of Two Contacts

In the case where two contacts are lost ($i = 2$), i.e., in the invalid part defined by the validation surface, the internal mobility of the finger is increased to 2-DOF. Hence, the contact situation evolves not along a contact trajectory but on a contact surface. If, as proposed in this chapter the distal phalanx force is assumed to remain positive in all configurations, this situation can only mean that the proximal and intermediate contacts are lost. The contact surface is therefore described by eq. (4.64). However, the exact contact evolution on the surface is unknown since the latter is dependent on the dynamics of the finger. Indeed, with two DOFs and one actuator, the general theory of underactuation should now be used to describe the system's state. Indeed, this time, a quasi-static technique cannot be used to obtain the grasp-state trajectory as in Section 4.3.4 since the

system has two DOFs. This particular situation is actually a connection between the concept of underactuation in robotic fingers and the theory of underactuation as used in robotics and commonly addressed in the literature. The equilibrium surface can also be described as

$$\begin{cases} f_1 = 0, \\ f_2 = 0. \end{cases} \quad (4.79)$$

Therefore, f_1 depends on k_2 , which does not exist (see also the discussion of Section 4.3.4). Hence, to evaluate the condition $f_1 = 0$ in terms of grasp-state variables, namely θ_2 , k_3 and θ_3 , it must be ensured that $f_1 = 0$ is actually true for any contact location k_2 , i.e., f_1 must be decomposed into two separate terms, namely

$$f_1 = a + b/k_2. \quad (4.80)$$

Then, both a and b are set to zero. It can also be proven that if $b = 0$ then either $f_2 = 0$ or $\cos \theta_2 = 0$, hence the condition for f_2 to become zero is “embedded” in the condition on f_1 (the proof is given in Appendix A.3). Hence, the following conditions must be satisfied

$$\begin{cases} a' = (r_1 - r_2)r_3k_3 - l_1r_2r_4 \cos(\theta_2 + \theta_3) = 0, \\ b' = (r_4 - r_3)k_3 + r_4l_2 \cos \theta_3 = 0 \text{ or } \cos \theta_2 = 0, \end{cases} \quad (4.81)$$

with tendon-driven fingers or

$$\begin{cases} a' = k_3(h_3 + l_2) - h_2h_3 \cos(\theta_2 + \theta_3) = 0, \\ b' = k_3 - h_3 \cos \theta_3 = 0 \text{ or } \cos \theta_2 = 0, \end{cases} \quad (4.82)$$

with linkage-driven fingers, where a' and b' are respectively the part of a and b that can become zero ($\cos \theta_2$ has been disregarded for b' in order to simplify the expressions). Hence, the equilibrium surface is defined by a set of two equations and three variables. It is therefore no longer an equilibrium surface but an equilibrium curve! The latter corresponds to the intersection of the equilibrium conditions for Case 2 and Case 3. As an implication, an equilibrium with contact only on the distal phalanx (without the help of a mechanical limit) is very rare. Nevertheless, ensuring the stability of the last phalanx of the finger might be a promising method to reduce the complexity of the grasp stability analysis of n -phalanx fingers with $n > 3$. Indeed, if the last phalanx is in equilibrium and internal motions of the finger are excluded, the grasp is stable in the sense proposed in this book, as previously discussed in Section 3.5.

4.4 Conclusions

In this chapter, the grasp stability of two- and three-phalanx underactuated fingers with a general architecture was discussed. Using a new grasp-state space

analysis technique, a method to obtain the condition for these fingers to be in equilibrium or to eject the object was presented. The equations of the contact trajectories defining the motion undergone by the fingers when one or more contacts are missing on the phalanges, was also discussed. One aim of this chapter is to acknowledge the impossibility for an underactuated finger to always apply forces on the object seized with all phalanges. If a situation where one or more phalanx forces are negative occurs, the motion undergone by the finger must then be studied because the latter can lead either to a stable grasp—where the finger is fully constrained by only the existing contacts—or to an ejection of the object. To ensure a stable grasp, ejection must be prevented. This chapter has given practical tools to study the finger behaviour, especially with two-phalanx fingers, considering a refined model including friction, springs, phalanx thickness, and also the local geometry of the object at the contact point. The results have been validated with a dynamic simulation package and applied to study a practical prototype. The grasp-state representation presented in this work allows the study of the properties of the grasp, as well as the determination of the finger behaviour.

However, this work is only the first step towards a more general grasp stability theory. Indeed, the model presented for the three-phalanx finger should be refined to include friction, local contact geometries, spring stiffnesses, if these characteristics are required for an accurate modelling. Furthermore, the grasp stability remains to be determined in the case where two contacts are lost, showing the limit of our approach that does not use a dynamic model. Additionally, the assumption on the initial configuration, namely that initially the finger closed all phalanges on the object as illustrated in Fig. 4.37*i*, does not necessarily hold since during the closing process, contact with the first phalanges could be lost. This again, illustrates the need to obtain a stability theory taking into account all contact situations, i.e., establishing the contact dynamics of the finger. Finally, the grasp stability of n -phalanx fingers with $n > 3$ remains a totally open problem despite the progresses reported in this chapter. The results presented in this chapter have been presented in (Laliberté et al. 2002; Birglen and Gosselin 2003; Birglen and Gosselin 2006b; Birglen and Gosselin 2006c; Birglen and Gosselin 2006d) and naturally lead to the next chapter, the optimal design of underactuated fingers.

5 Optimal Design of Underactuated Fingers

The hand that hath made you fair hath made you good.

William Shakespeare, *Measure for Measure*, Act 3 scene 1, 1623.

in which, using the results obtained in the previous analyses of the force properties and grasp stability of underactuated fingers, we propose to design optimal fingers. The aim of this chapter is to elaborate simple and practical design rules to obtain stable and optimal fingers.

5.1 Introduction

This chapter presents the optimal design of underactuated fingers considering several issues among which the force isotropy of the grasp, i.e., its ability to generate a uniform pressure on the object seized, its stability, and the Cartesian directions of contact forces. First, the force isotropy property is defined and a method to achieve the latter is presented. Its robustness with respect to undesired variations of the design parameters is also discussed. Second, guidelines to minimize or completely avoid ejection are presented as well as their influence on the desired optimality. The occurrence of the situations where one phalanx force is negative should be decreased (prevention is impossible as established in Section 4.2.7, at least with our model of underactuated fingers) and the ejection should be avoided.

In Section 5.2, the concept of isotropic grasp as an optimality criterion, and also, a method to either minimize or completely eliminate ejection if a limited range of motion is acceptable, are presented for two-phalanx fingers. It should be pointed out that the optimal ejection-free design method presented in this chapter differs from usual optimization, since a criterion is not maximized or minimized but matched exactly. The latter is therefore a constraint and not

a criterion per se. The designs resulting from the proposed method are force isotropic for a certain task *and* ejection free. Results are given for both tendon-pulley and linkage transmissions. Two considerations will form the guidelines of Section 5.2: first, the grasp must be stable in the sense that ejection should be prevented, second, differences between the phalanx forces should be kept to a minimum. If the proximal phalanx force is negative the latter phalanx will loose contact with the object and the distal phalanx corresponding to a positive force will slide on the object surface. This sliding process will continue until either a stable configuration is achieved (with a zero proximal phalanx force), or joint limits are met (stable situation, but the shape adaptation is less effective), or the last phalanx will curl away and loose contact with the object (ejection, illustrated in Figs. 4.1 and 4.15). If the distal phalanx force is negative (an impossible situation in the case of tendon-driven fingers), the finger's configuration corresponds to hyperflexion/hyperextension and the contact is lost with no stable grasp possible. However, these situations are usually made impossible by design and joint limits. Nevertheless, they should be taken into account. Considering this sliding motion and its characteristics, presented in the previous chapter, one shall design fingers preventing ejection.

In Section 5.3, a method for the optimal design of three-phalanx fingers is presented. It is noted that it could also easily be applied to two-phalanx fingers. The method introduces simple geometric relationships based on practical considerations in order to reduce the number of design parameters of the optimization to only two. A study is then performed on fingers obtained from the possible combination of parameters. For each finger, a series of grasps are performed on circular objects of different sizes and positions. The performance of the fingers is thereupon based on a global index defined by a combination of performance indices. These indices ensure that the sum of the forces applied by a finger on an object in each direction are correctly distributed in order to resist external forces, that the forces applied at the phalanges are well distributed in order to avoid large local forces and that the finger avoids ejection of the object. Finally, a second method based on a grasp-stability analysis is presented.

5.2 Optimal Design of Two-Phalanx Underactuated Fingers

5.2.1 Force Properties and Ejection

Force isotropy is defined as the property of a finger to generate equal contact forces on all its phalanges. This property is useful to prevent damages to the grasped object resulting from an unbalanced grasping force distribution. Since the ratio between the phalanx forces is independent from the control variables, this issue must be addressed at the design stage. For instance, the work presented in (Hirose and Umetani 1978), despite its importance (one of the first attempts with (Shimojima et al. 1987) to formalize underactuation for grasping), claimed that the optimal design proposed in the latter publication was force isotropic

while it is in fact force isotropic for one and only one configuration. Indeed, the isotropic configuration of (Hirose and Umetani 1978) is defined as

$$\begin{cases} \theta_i = 0 & i > 1 \\ \text{and } k_i = l_i/2 & i > 0 \end{cases} \quad (5.1)$$

with the convention used in this book. However, this shortcoming was known and verbally acknowledged by one of the authors of (Hirose and Umetani 1978). In fact, despite having correctly established, in a very elegant manner, the geometric condition for isotropy (a quadratic variation of the pulley radii), this optimal design is not isotropic because of the integer approximation as the authors established using the results of Chapter 3. It can be shown that this design generates an equal force but only on one every two phalanges. This result illustrates how a slight difference in the design parameters (presented in Fig. 5.1) can have a tremendous impact on the properties of the finger. As a numerical indication, the ratio between the area under the curves in Fig. 5.1 and the area between them is more than 20 to 1.

The above discussion highlights the need not only to focus on isotropy itself but also on its robustness with respect to the design parameters. Since a physical prototype matching exactly the optimal design is anyway impossible, the optimal design objective should also take into account robustness in the sense of obtaining geometric constraints that are as robust to errors as possible. Force design (Gosselin 1996; Herder and de Visser 2000) or kinematic design (Crisman et al. 1996) can be used for underactuated fingers, but

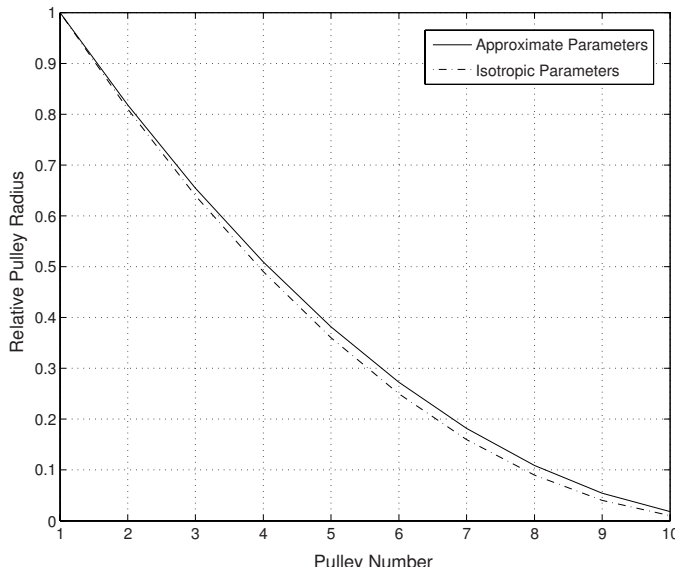


Fig. 5.1. Difference between exact and approximate design parameters

the former seems more promising. Indeed, the latter only aims at optimizing the finger workspace without any knowledge of force properties. Indices to characterize the finger properties inside the workspace have been proposed in the literature (Mason and Salisbury 1985; Imcaoudene and Gosselin 1994; Hunt et al. 1991; McAree et al. 1991). These indices are similar to those used in serial robot kinematics. Hence, they are not dedicated to finger design and thus may be inappropriate. Kinematic properties such as dexterity are almost irrelevant from a grasping point of view, where forces are the main focus. The approach in (Herder and de Visser 2000) is much more relevant and is based on the assumption that the finger motion itself is far less important than the finger force properties during the grasp:

“a joint, for example, is not considered as an element that provides rotational motion about an axis, but as a force generator that can be employed to achieve equilibrium.”

quoted from (Herder 2004). This chapter acknowledges this statement and follows the same philosophy.

Other considerations may also have a significant impact on the quality of the grasp. For example, bounds on the phalanx forces can be used to prevent the latter from being either too small or too large, despite being equal (isotropy). The Direct Optimal Problem (DOP) and the Inverse Optimal Problem (IOP) should also be precisely defined. The former problem consists in defining what state of a system is actually optimal with respect to a certain criterion. The latter consists in designing the system so that a particular task will be optimally performed. For robotic fingers, one aim is to have a force isotropic configuration corresponding to a set of grasped objects. Furthermore, the final stability of the grasp must be ensured. Combining stability, force isotropy and acceptable force range may not be simple. The analytical expression of the normal contact forces for a general two-phalanx underactuated finger was established in Chapter 3, namely

$$\mathbf{f} = \begin{bmatrix} \frac{k_2(1+R)+Rl_1 \cos \theta_2}{k_1 k_2} T_a - \frac{k_2+l_1 \cos \theta_2}{k_1 k_2} T_2 \\ -\frac{R}{k_2} T_a + \frac{1}{k_2} T_2 \end{bmatrix} \quad (5.2)$$

where $T_2 = K\theta_2 T_a$ is the spring torque, note that the spring stiffness has been related to the actuation torque T_a and a zero neutral position of the spring has been chosen.

Additionally,

$$\begin{cases} R = -r_2/r_1 & \text{with a tendon transmission} \\ R = -h/(h + l_1) & \text{with a linkage transmission} \end{cases} \quad (5.3)$$

where, as usual, h is the directed distance between point O_1 and the geometric intersection of lines (OO_1) and (P_1P_2) , i.e.,

$$h = c(\cos(\theta_2 - \psi) - \sin(\theta_2 - \psi) \cot \beta). \quad (5.4)$$

In the latter equation, $\cot \beta$ can be expressed analytically as shown in eq. (4.7).

5.2.2 Force Isotropic Design

In order to obtain a force isotropic design, the two phalanx forces must be equal. This property allows a precise control of the grasping pressure since all forces are equal. Otherwise, one phalanx might exert too large (or too small) forces in comparison with the other. Obviously, such a characteristic is only local, i.e., it depends on the finger configuration defined by the angle θ_2 and the contact locations k_1 and k_2 . Therefore, if the object is moved in the Cartesian space (with the exception of a rotation around the base joint), this property is no longer satisfied.

Furthermore, as noted verbally by Dr. Krut, relating the spring stiffness to the actuation torque to achieve isotropic designs yields a fundamental drawback: changing the actuation torque will modify the isotropic configuration of the finger. Hence, the actuation torque has to remain constant, or the spring must be neglected during the analysis.

For tendon-driven fingers, the equation $f_1 = f_2$ reduces to

$$r_1(k_2 - GK\theta_2) = r_2G \quad (5.5)$$

where $G = k_1 + l_1 \cos \theta_2 + k_2$. With $\alpha = r_2/r_1$, one obtains

$$\alpha = -K\theta_2 + \frac{k_2}{k_2 + l_1 \cos \theta_2 + k_1}. \quad (5.6)$$

This pulley radius ratio corresponds to a force isotropic contact situation (k_1, k_2, θ_2) .

For linkage-driven fingers, the force isotropy equation is

$$(h + l_1)(k_2 - GK\theta_2) = hG. \quad (5.7)$$

Hence, similarly, the optimal transmission coefficient in this case is

$$\frac{h}{h + l_1} = -K\theta_2 + \frac{k_2}{k_2 + l_1 \cos \theta_2 + k_1}. \quad (5.8)$$

However in this case, another step is necessary since h is a function of the design parameters and the angle θ_2 . Furthermore, many design variables are available to satisfy the latter equation, namely a , b , c , and ψ . Similarly, in the case of the tendon-driven finger, the ratio of the pulley radii was specified, not each radius independently. Therefore, additional constraints can be satisfied. For example, an upper bound on the dimensions, standard link lengths, commercially available pulleys, or machining simplicity. For instance, with a linkage-driven finger, if one arbitrarily chooses $a = b$, a known length c (e.g. resulting from minimal distance considerations) and $\psi = \pi/2$, a is completely defined as

$$a = \frac{2l_1 c \sin \theta_2 + c^2 + l_1^2}{2} \frac{\sqrt{A}}{B} \quad (5.9)$$

with

$$A = (C - 1)((C - 1)c^2 + 2cCl_1 \sin \theta_2) + C^2 l_1^2 \quad (5.10)$$

$$B = -c^2 + Cc^2 - l_1 c \sin \theta_2 + 2Cl_1 c \sin \theta_2 + Cl_1^2 \quad (5.11)$$

$$C = -K\theta_2 + \frac{k_2}{k_2 + l_1 \cos \theta_2 + k_1}. \quad (5.12)$$

As it can be seen the analytical force isotropy condition with linkages is much more complicated than with pulley-tendons. However, this condition can be obtained explicitly, as opposed to numerically, and the method in both cases is identical. These expressions allow one to solve the IOP, which is particularly useful when designing underactuated fingers. The solution of the DOP is simply defined by eqs. (5.5) and (5.7) respectively for each kind of transmission. The force isotropic configurations are defined by these equations for a particular set of design parameters, and define a 2D surface in the contact space (k_1, k_2, θ_2) , which will be referred to as the isotropic surface. Examples are illustrated in Figs. 5.2–5.3 for the geometric parameter set one and the *Soft Gripper* of Table 4.1.

This isotropic surface is the solution to the DOP, and is also related to the IOP that aims at finding the design parameters defining such a surface passing through a predefined point. In (Krut 2005), a fully force-isotropic finger was presented, where the contact forces at mid-phalanx of both phalanges are equal for any angle θ_2 . To achieve such a property, eq. (5.2) is considered. If the spring is neglected, equating both contact forces yields

$$k_2(1 + R) + Rl_1 \cos \theta_2 = -Rk_1. \quad (5.13)$$

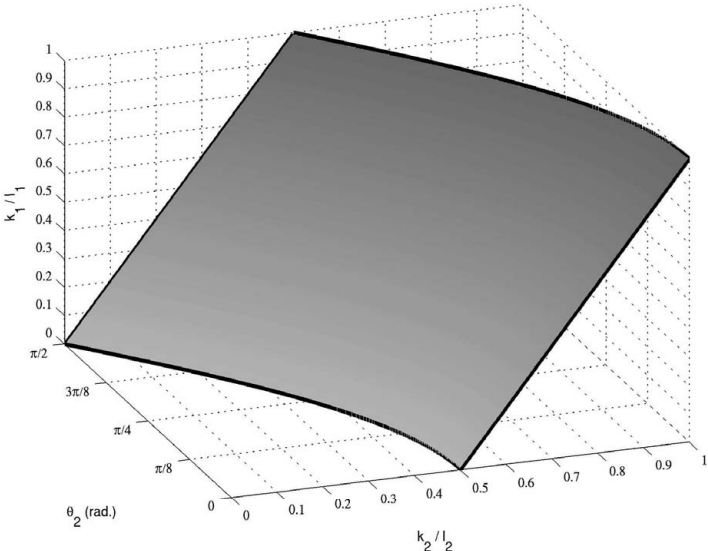


Fig. 5.2. Force isotropic locus for a *Soft Gripper* type finger

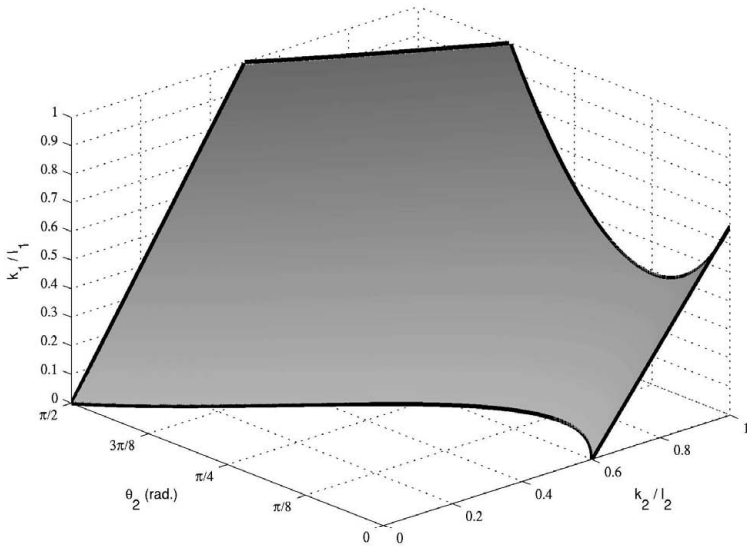


Fig. 5.3. Force isotropic locus for a linkage-driven finger (parameter set 1)

If the contacts are located at mid-phalanx, i.e., $k_1 = l_1/2$ and $k_2 = l_2/2$, one obtains

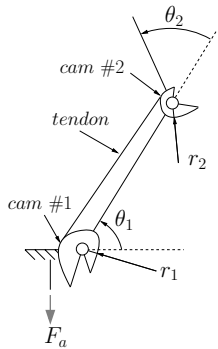
$$R = -\frac{l_2}{l_2 + l_1(1 + 2 \cos \theta_2)} \quad (5.14)$$

or, as established in (Krut 2005),

$$R = -\frac{1}{4 \cos^2(\frac{\theta_2}{2})} \quad (5.15)$$

when $l_1 = l_2$. If the transmission factor R satisfies eq. (5.14) then the finger is force-isotropic for any angle θ_2 . Using this equation, (Krut 2005) established the envelope curve corresponding to the profile of a cam located between the two phalanges. The tendon is then routed around the cam used as a variable radius pulley, illustrated in Fig. 5.4. It is noted that the proximal cam can be replaced by a constant radius pulley, eliminating θ_1 from the expression of the transmission factor.

It should also be pointed out that the equation giving the transmission factor in the case of a pulley transmission, i.e., $R = -r_2/r_1$ cannot be used directly in eq. (5.14) to compute the local cam radius, as properly shown in (Krut 2005). The force isotropic surface of this finger is depicted in Fig. 5.5, where it is noted that the surface passes through the line defined by $k_1 = l_1/2$, $k_2 = l_2/2$ (dashed black line) which corresponds to the desired isotropic configurations. An interesting characteristic of this surface is that it is a ruled surface, more precisely an helicoid whose axis is the line previously discussed. Because of its

**Fig. 5.4.** Cam-tendon transmission

ruled nature, the surface presents peculiar properties. For instance, if $\theta_2 = \pi/2$ then the force-isotropic condition is

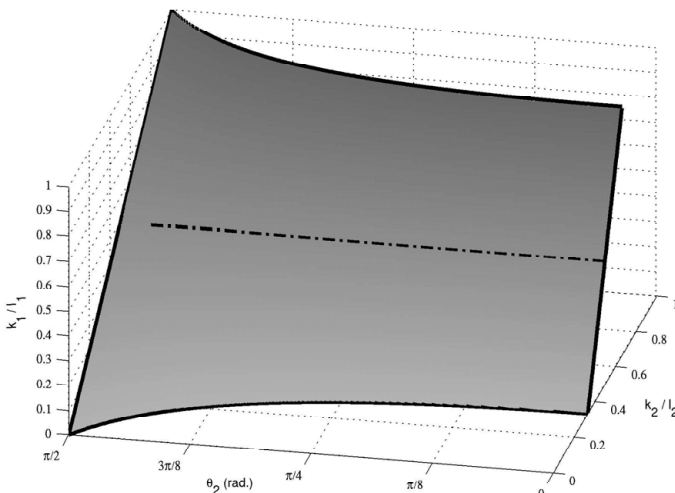
$$k_1 l_2 = k_2 l_1 \quad (5.16)$$

Hence, if $l_1 = l_2$, the forces distribution generated by both phalanges are strictly identical, i.e., the contact forces are the same on each phalanx if the contact locations are the same ($k_1 = k_2$). Therefore, and from an “applied force” point of view, both phalanges are identical.

It should be noted that the force-isotropic surface and this property itself are very sensitive to design parameter variations, one has

$$\frac{\partial(f_1/f_2)}{\partial\alpha} = -\frac{k_2}{k_1(\alpha + K\theta_2)^2} \quad (5.17)$$

for tendon-driven mechanisms. The same result holds for linkage transmissions by replacing α with $h/(h + l_1)$. Therefore, since k_1 and k_2 are usually of the

**Fig. 5.5.** Force isotropic locus for the cam-tendon finger

same order of magnitude, and since both α and K are usually small, a slight change in the transmission factor can lead to a significant change of the isotropic surface. For instance, if the same parameters that were used to plot Fig. 5.2 are used, the volume between the two surfaces defined by $f_1 = 0.9f_2$ and $f_1 = 1.1f_2$, i.e., a 10% tolerance on isotropy, is about 0.3% of the total volume of the plotting space. Therefore, isotropy is not very robust with respect to variations of the design parameters. The spring can help reduce this sensitivity by decreasing the factor established in eq. (5.17). However, the spring stiffness opposes the actuation torque and thus, the grasp forces, and a compromise must be found between isotropy and the magnitude of the contact forces (usually associated with a secure grasp). In (Hirose and Umetani 1978), the authors neglected the influence of the springs (a return cable in their case) when solving the IOP and this might explain the highly sensitive design that they obtain, as illustrated in Fig. 5.1.

In this section, the force isotropic design of a two-phalanx underactuated finger with either tendon or linkage transmissions was presented and studied. It should however be noted that the results given are valid only for a single point of contact on each phalanx (which can be the edges of a polygon or points on a cylinder). This is rather limitative but this method can be extended to a minimization of the deviation for a set of typical objects as will be discussed in Section 5.3.2.

5.2.3 Guidelines to Prevent Ejection

Another important property of underactuated fingers that should be analyzed is their robustness against ejection. Indeed, if one obtains an isotropic and therefore stable design for a particular contact set (k_1, k_2, θ_2) , it may be of interest that the finger also be robust with respect to ejection around this isotropic point, in order to ensure that a deviation from this configuration does not lead to an unstable grasp. The final aim is to guarantee stability for all grasps if possible and satisfy certain “quality” based indices like isotropy. Force isotropy and grasp stability are two distinct notions, and it is the authors’ opinion that the latter is the most critical while the former is useful but not necessary. An index that can be used to ensure the grasp stability, even if the proximal phalanx contact is lost is:

$$\mu^* = \frac{\int_W \delta^*(k_2, \theta_2) dk_2 d\theta_2}{\int_W dk_2 d\theta_2} \quad (5.18)$$

where $\delta^*(k_2, \theta_2)$ is also a Kronecker-like symbol for characterizing the stability of the contact situation:

$$\delta^*(k_2, \theta_2) = \begin{cases} 1 & \text{if the final grasp is stable} \\ 0 & \text{otherwise} \end{cases} \quad (5.19)$$

The above index μ^* is the ratio between the stable (clear) and unstable (grey shaded) areas in the grasp-state plane of the finger, illustrated in Figs. 4.12–4.14.

Other indices can characterize the ability of the finger to generate full-phalanx grasps, i.e., grasps with all phalanx forces positive, as presented in Section 3.5. Numerical values of the index μ^* are illustrated in Figs. 5.6 and 5.7 for a tendon-driven finger and linkage-driven finger respectively. As it can be seen on the figures, the two plots are very similar. General guidelines arise from these figures, e.g., for given phalanx lengths, there are typically two ratios r_2/r_1 leading to a given value of the performance index: the highest ratio corresponds to a finger exhibiting closing-ejection in the workspace while the smallest ratio leads to a finger exhibiting opening-ejection. In light of the results of Chapter 4.2, the smallest ratio should be preferred since opening-ejection is more easily prevented. The plots of Figs 4.12–4.14 can also be used to find the optimal pulley radius ratio for given phalanx lengths. It is noted that in these examples, the complete $[-\pi, \pi]$ range of motion of angle θ_2 was considered. If this range is not physically possible, it should be reduced accordingly and effects of the mechanical limits should be taken into account.

For instance, a two-phalanx version of the *Soft Gripper* (Hirose and Umetani 1978) achieves a score of 0.28 while with the same phalanx lengths a pulley ratio of 0.55 would increase the performance index to 0.45, a 60% gain. However, the authors of (Hirose and Umetani 1978) tried to obtain a force isotropic design and did not consider ejection: this fact explains such a difference. Furthermore, if mechanical limits restrain the achievable range of angle θ_2 between 0 and $\pi/2$, both designs obtain a perfect score of 1, illustrating that ejection can be eliminated in certain cases. This result does not hold for instance with a cylindrical contact. However, as discussed in Section 4.2.4, a single point of contact is a conservative assumption with respect to the grasp stability if closing-ejection is eliminated.

Conversely, for a given transmission factor, optimal phalanx lengths can be chosen to minimize ejection. If all geometric parameters are considered as design variables, a design procedure can be devised to completely avoid ejection (rather than minimizing it). The design procedure is based on the analysis of the grasp-state plane and can be described as follows.

To prevent opening-ejection, mechanical limits such as $0 < \theta_2$ must be used since the point of the contact trajectories with vertical tangent are defined by

$$\begin{cases} \theta_2 = 0 \\ k_2^2 - k_{2i}^2 + 2d_1(k_2 - k_{2i} \cos \theta_{2i}) = 0. \end{cases} \quad (5.20)$$

Furthermore, another limit, such as $\theta_2 < \pi/2$, can also be used since the contact trajectories may be unstable beyond their asymptotes. Since mechanical limits act like additional equilibrium curves—described by $\theta_2 = \text{constant}$ in the grasp-state plane—grasp-state trajectories that would normally cross them will result in stable grasps. Moreover, if joint limits are used, they act as stable limits (however not attractive). The large regions of instability in Figs. 4.12–4.14 should be moderated, because one should remember that, in the central zones of these figures (which correspond to the usual range of motion), unstable regions correspond to stable two-phalanx contact grasps. Each stability region is dual

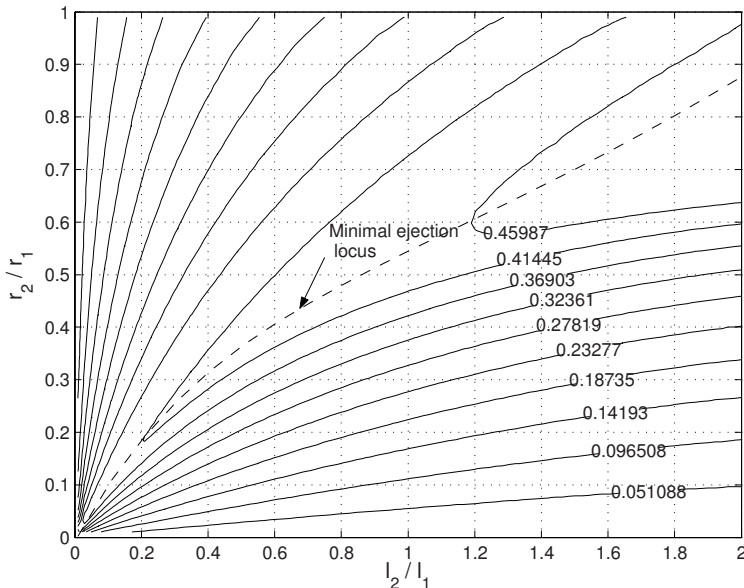


Fig. 5.6. Contour plot of μ^* with a tendon-driven finger

to the other. Hence, in most cases, i.e., when the contact is initially established with the proximal phalanx, the final grasp will be stable with the notable exception of the second type of unstable region discovered in Fig. 4.13, namely

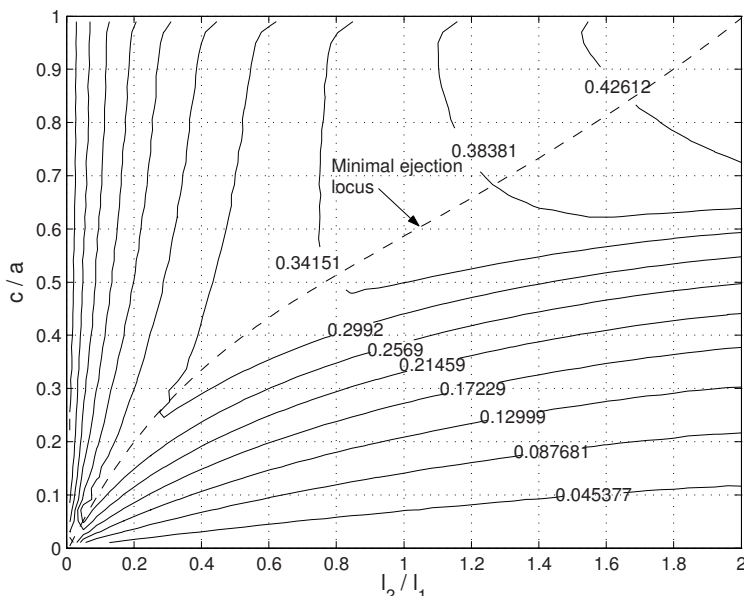


Fig. 5.7. Contour plot of μ^* with a linkage-driven finger ($b = 1$ and $\psi = \pi/2$)

closing-ejection. This type of instability is most insidious, as discussed in Section 4.2.4, and should therefore be avoided as much as possible through suitable design.

To prevent closing-ejection, the finger must be designed so that either the equilibrium curve is always physically on the phalanx as proposed in (Laliberté and Gosselin 1998), or both solutions of $e(\theta_2) = l_2$ —where e denotes the mathematical expression of the equilibrium curve—if they exist, correspond to $\theta_2 < 0$. More precisely, in (Laliberté and Gosselin 1998) the sign of f_1 for $k_2 = l_2$ in the possible range of θ_2 is obtained. If $f_1 > 0$ for any θ_2 , this means that the equilibrium curve is always on the physical phalanx. It should be noted that this verification corresponds to the analysis of the finger in a small portion of the grasp state plane, namely along the limit $k_2 = l_2$ and for an angle θ_2 between the mechanical limits. For tendon-driven fingers, since the solution of the equation $e(\theta_2) = l_2$ is

$$\theta_2 = \pm \arccos\left(\frac{l_2(1 - \alpha)}{l_1\alpha}\right), \quad (5.21)$$

the only solution to avoid closing-ejection is to ensure that $\max[e(\theta_2)] < l_2$. With linkage-driven fingers, the latter condition on angle θ_2 can be satisfied. Manipulation of the design parameters also permits to choose between two-phalanx grasps and one-phalanx pinching configurations. For instance, the design proposed in Table 5.1 (parameters have been approximated to the closest simple ratio) can always provide a stable grasp with an approximately equal probability of one- and two-phalanx contact, if joint limits are used to ensure that $0 < \theta_2 < \pi/2$. The corresponding grasp-state plane is presented in Fig. 5.8. The area under the equilibrium curve is maximized without generating additional unstable regions. Therefore, one can design a finger that eliminates ejection for a single point of contact.

Other contact conditions could also be of interest and are not covered here, namely the local geometry of the contact (circular, linear, etc.), friction, etc. If the aforementioned conditions cannot be met to prevent ejection, a minimization of this phenomenon, measured with the index μ^* through numerical or algebraic analysis should be performed. There is obviously a relationship between the condition on the equilibrium curve to eliminate closing-ejection and the optimal transmission ratio resulting from the previous section. It is possible that this optimal ratio corresponds to a finger presenting ejection in its workspace. To avoid this situation, the design of the finger should be decomposed in two consecutive steps:

1. choose α according to the force isotropic optimal criterion of eq. (5.5): this implies the choice of l_1 ,
2. choose l_2 in order for the equilibrium curve to stay on the phalanx, i.e.,

$$l_2 > \frac{\alpha}{1 - \alpha}l_1. \quad (5.22)$$

Table 5.1. Two-phalanx optimal geometric parameters

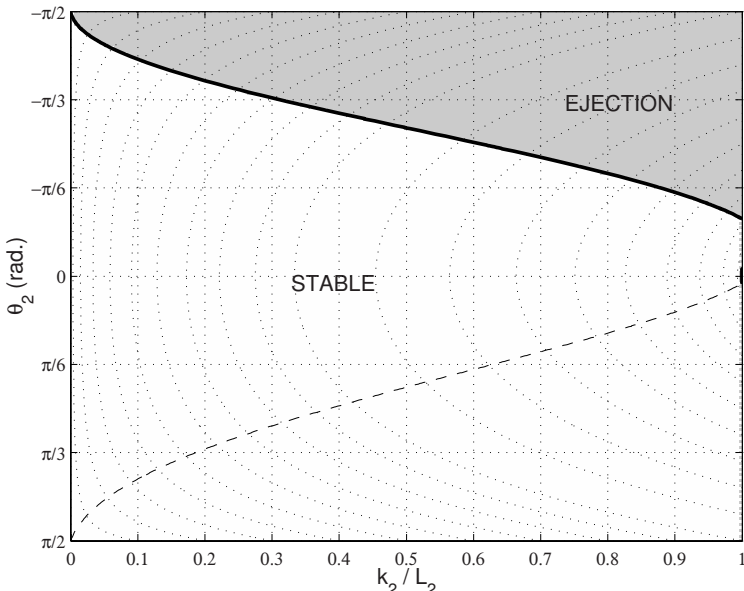
Set	l_1	l_2	ψ	a	b	c
3	1	3/4	54°	3/4	1	1/3

Usually, the ratio α is less than 0.5 which leads to phalanges of related proportions. A similar technique can be used for linkage-driven fingers, but again, the expressions are much more complicated. Basically, one has:

1. choose h according to the force isotropic optimal criterion of eq. (5.7): this also implies the choice of l_1 ,
2. choose a , b , c , ψ and l_2 in order for the equilibrium curve to stay on the phalanx, i.e., $e(\theta_2) < l_2 \mid \forall \theta_2$.

This last step cannot be given explicitly, since there are five available parameters and only one equation and one inequality to be satisfied. Therefore, some assumptions must be made on the parameters, e.g. $a = b$ and $\psi = \pi/2$, and the isotropic condition is then used to determine a as suggested in Section 5.2.2. Parameter l_2 is chosen such that $e(\theta_2) < l_2 \mid \forall \theta_2$. Because of the complexity of the equation of the equilibrium point, it is advisable to proceed numerically.

Plastic prototypes, replica of the mechanism presented in Fig. 2.5, have been built using Fused Deposition Modelling (Fig 5.9) to experiment the influence of the parameters on the grasp stability. Experimental results confirmed

**Fig. 5.8.** Grasp-state plane (optimal parameter set)

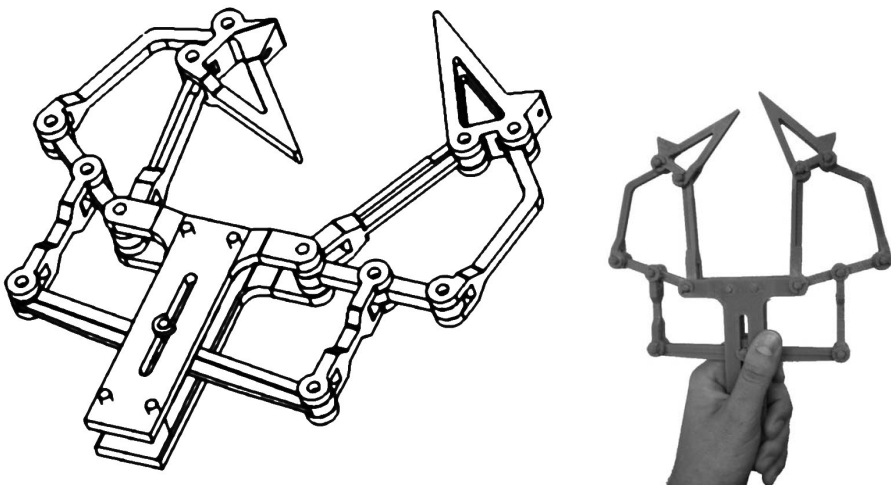


Fig. 5.9. CAD model and prototype of an underactuated gripper (design by Mathieu Goulet and Pierre-Luc Richard)

the theoretical behaviour of the fingers. Indeed, trajectories sliding toward an equilibrium (stable or unstable) configuration can be reproduced. Opening- and closing-ejection also happen and unstable fingers cannot grasp any object except when the distal joint is resting on the mechanical limit. Other transmission mechanisms have been tested and led to similar properties (illustrated in Fig. 5.10).

5.3 Optimal Design of Three-Phalanx Underactuated Fingers

5.3.1 Force Properties and Ejection

Surprisingly, the optimal design of three-phalanx underactuated fingers is relatively unexplored avenue in the context of design of self-adaptive hands. Because of the complexity of the contact force equations—cf. eqs. (4.50–4.52) or (4.54–4.56) for instance—the force-isotropic conditions have never been studied despite their practical importance. In fact, the force distribution of three-phalanx underactuated fingers at mid-phalanx as illustrated in Figs. 3.3, 3.8, or 3.12 has only been very recently revealed in (Birglen and Gosselin 2004a). Previously, designs have largely relied upon intuitive considerations with little or no regards to the contact forces generated with however a few notable exceptions (Hirose and Umetani 1978; Shimojima et al. 1987; Laliberté and Gosselin 1998; Herder and de Visser 2000). Underactuated fingers have often been designed as serial manipulators based on kinematic or dynamic considerations which are generally inappropriate for robotic grasping hands. Again, it is worth repeating that in robotic hands, the key issue is the generated contact forces (Herder and de Visser 2000) which should be studied

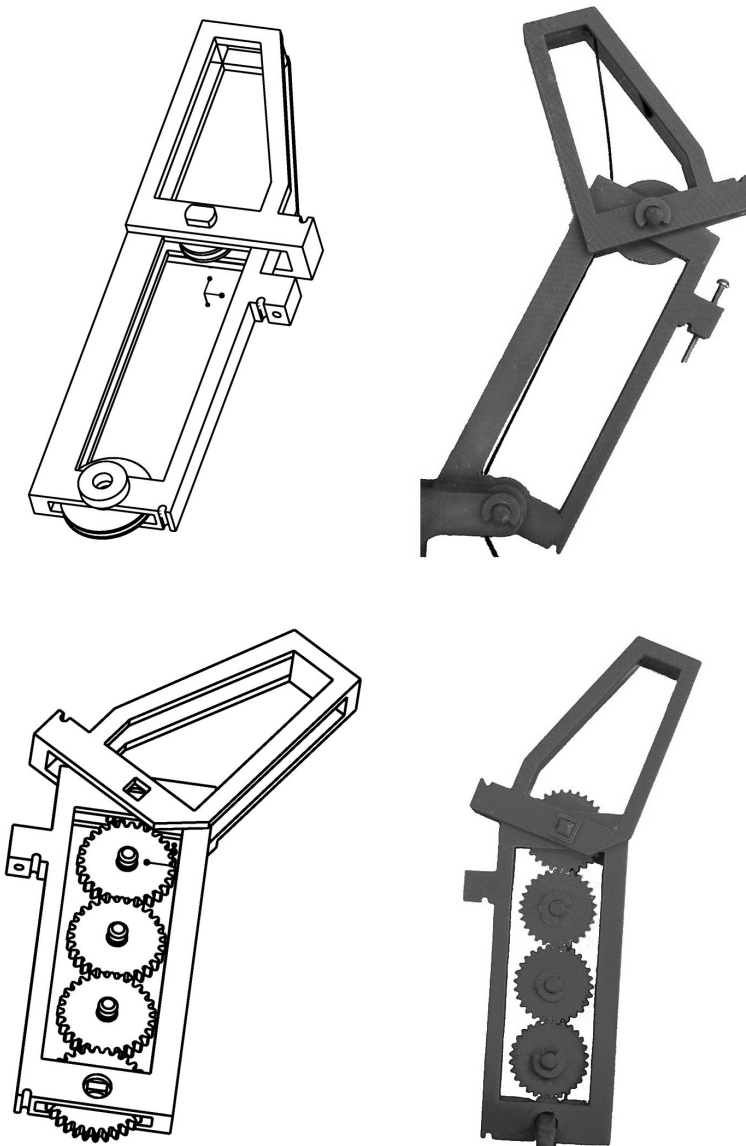


Fig. 5.10. Alternative transmissions using pulleys and gears

and optimized. Furthermore, the characteristics of the transmission used to distribute the actuation has to be taken into account since it dictates the behaviour of the fingers.

The ejection theory with three-phalanx underactuated fingers is even more difficult to study. As demonstrated in Section 4.3, the grasp-state space is of dimension four and even if a technique to reduce the dimension of the problem

is used—such as in Section 4.3.2—, generalizing the results to any architecture and obtaining design rules that eliminate ejection as in Section 5.2.3 remains a completely open problem. Although the techniques developed in this Section are applied to three-phalanx fingers, the basic principle can be used for an arbitrary number of phalanges.

5.3.2 Dimensional Analysis

This approach has been proposed in (Laliberté and Gosselin 2001b) to overcome the difficulties of a more complete and detailed optimization of the geometric parameters of three-phalanx underactuated fingers. This method is based on simple geometric relationships and has led to excellent practical designs of prototypes in the past (Gosselin and Laliberté 1996; Laliberté and Gosselin 2003). It should be noted for instance that while no theoretical proof of the absence of ejection is provided, this phenomenon was never observed in practice with the designs obtained with this method. A design is proposed in this section for linkage-driven architectures but, as usual, the methodology remains valid considering any type of transmission.

The length of the phalanges, i.e., l_i with $i = 1, \dots, 3$ are obtained from comparisons with other existing fingers, human fingers, and experiments performed with a finger model on objects to be grasped. The remaining design variables are a_i , b_i , c_i for $i = 1, 2$ and ψ . In order to introduce design constraints and to reduce the number of independent variables, some relationships between these parameters are imposed, reducing the number of variables to two.

It was pointed out in Section 4.2.3 for two-phalanx fingers and in (Laliberté and Gosselin 2001b) for three-phalanx fingers that the behaviour of linkage-driven underactuated fingers is mainly dictated by the ratios $R_i = c_i/a_i$ with $i = 1, 2$. In order to minimize the size of the finger, the length c_i should be chosen as small as possible but is limited by considerations on mechanical interference. Therefore, c_i is fixed to its smallest possible value. Hence, a_i is fixed for a given ratio. The ratios R_i are used as design parameters and optimized. However, the lengths b_i and the angle ψ also have to be selected. In order to obtain these parameters, design constraints are added to associate each of the ratios R_i with particular values of the parameters. These constraints are mostly empirical, for instance, in (Laliberté and Gosselin 2001b), it is argued that the performance of the finger regarding stability, mechanical interferences and internal forces is correct if the angle between the links a_i and b_i , as well as between the links c_i and b_i , is close to 90 degrees, in an average configuration.

A similar argument is used in (Jensen 1991) in the context of the design of four-bar linkages. In other words, this assumptions allows to minimize the variation of the ratio R over the practical range and keeps the mechanism away from the hyperflexion/hyperextension configurations. Also, it is noted that in this configuration, the geometry of the linkage is exactly the same as the geometry of a finger driven with tendons if the proximal and distal pulleys are respectively of radius a_i and c_i . In fact, the transmission angle is always 90° in tendon-driven fingers, which might explain their better performance. Finally,

it is noted that very good practical performances have been achieved with this method. Thereupon, the parameters b_i and ψ can be computed. First, the average configuration of the finger is defined as the configuration in which angles α_1 and α_2 are given by

$$\alpha_i = \frac{\min(\alpha_i) + \max(\alpha_i)}{2}, \quad i = 1, 2 \quad (5.23)$$

with

$$\alpha_i = \pi - \theta_{i+1} \quad i = 1, 2. \quad (5.24)$$

Then, the average angles β_1 and β_2 corresponding to the angles between l_1 and b_1 , and l_2 and b_2 respectively are defined as

$$\beta_i = \arcsin\left(\frac{a_i - c_i}{l_i}\right), \quad i = 1, 2 \quad (5.25)$$

which leads to the values of b_i with

$$b_i = l_i \cos \beta_i, \quad i = 1, 2 \quad (5.26)$$

and the value of ψ is given by

$$\psi = \frac{3\pi}{2} - \alpha_2 - \beta_2. \quad (5.27)$$

It is noted that in the original reference (Laliberté and Gosselin 1998), another angle, named ψ_1 is defined as

$$\psi_1 = \pi - \alpha_1 + \beta_2 - \beta_1 \quad (5.28)$$

and corresponds to a constant angle between links c_1 and a_2 . In our model, this angle is assumed to be zero. Using the above equations as design constraints, the performance indices can be computed as functions of only two design parameters, namely the ratios R_1 and R_2 .

A study is thereupon performed on fingers with different combinations of ratios R_i , giving an overview of possible fingers. To perform the study, a series of grasps are performed on circular objects of different sizes and at different positions, in order to simulate different sizes and shapes of objects. The latter correspond to grasp-states which can be used to compute the generated contact forces (cf. Chapter 3). Equivalently, results have been obtained in the literature either using a CAD package (Sie and Gosselin 2002; Myrand and Gosselin 2004) or a dedicated custom software (Laliberté and Gosselin 1998). The performance of the fingers is defined as a combination of four performance indices, each representing a particular point of interest in designing underactuated fingers. These indices, used to estimate the performance of the fingers are:

- the sum of the forces applied by each finger on the object, defined by a contact force vector $\mathbf{F} = [F_x \ F_y]^T$, must be directed towards the palm in order

to obtain a grasp securing the object, namely the component F_y must be negative. Also, the force components F_x should be larger than the components F_y in order to obtain balanced grasps, since the components F_y generated by each finger work in cooperation (towards the palm) whereas the components F_x work in opposition (against each other). Indeed, ideally $F_x = EF_y$, where the value of E is equal to the number of fingers grasping the object in order to apply a uniform pressure on the object.

These situations arise in symmetric grasp configurations. However, E actually depends on the position and shape of the object seized. In (Laliberté and Gosselin 2001b) E is assumed constant and equal to two which is a valid hypothesis for typical enveloping grasps. This index allows a hand to correctly resist external forces that are applied on a grasped object. These external forces, which occur from contacts with the environment and acceleration, can be of different amplitudes and directions. The performance index associated with the resulting forces is given by the sum of the smallest force for each of the m objects grasped, namely

$$I_{xy} = \frac{1}{m} \sum_{i=1}^m \frac{\min(F_{x,i}, EF_{y,i})}{T_a} \delta(F_{y,i}) \quad (5.29)$$

where $\delta(F_{y,i})$ is a Kronecker-like symbol (cf. Section 3.5) for the negativeness of F_y which results in the attribution of a zero score if $F_{y,i}$ is positive:

$$\delta(F_{y,i}) = \begin{cases} 1 & \text{if } F_{y,i} < 0, \\ 0 & \text{otherwise.} \end{cases} \quad (5.30)$$

The components F_x and F_y of the sum of the contact forces onto the axes x and y can be expressed as

$$\begin{bmatrix} F_x \\ F_y \end{bmatrix} = \mathbf{P} \mathbf{J}^{-T} \mathbf{T}^{-T} \mathbf{t} \quad (5.31)$$

using eq. (3.42), where \mathbf{P} is the projection matrix of the contact forces onto the axes, i.e., for an n -phalanx finger one has

$$\mathbf{P} = \begin{bmatrix} -\sin \theta_1 & -\sin(\theta_1 + \theta_2) & \dots & -\sin(\sum_{i=1}^n \theta_i) \\ \cos \theta_1 & \cos(\theta_1 + \theta_2) & \dots & \cos(\sum_{i=1}^n \theta_i) \end{bmatrix}. \quad (5.32)$$

Therefore, in the three-phalanx case, one has

$$\mathbf{P} = \begin{bmatrix} -\sin \theta_1 & -\sin(\theta_1 + \theta_2) & -\sin(\theta_1 + \theta_2 + \theta_3) \\ \cos \theta_1 & \cos(\theta_1 + \theta_2) & \cos(\theta_1 + \theta_2 + \theta_3) \end{bmatrix}. \quad (5.33)$$

- The forces should be well distributed among the phalanges in order to avoid large local forces on the object. The corresponding index is defined as the ratio of the total force on the three phalanges divided by the largest force, namely

$$I_{gs} = \frac{1}{m} \sum_{i=1}^m \frac{\sum_{j=1}^n f_{j,i}}{n \max_j(f_{j,i})} \quad (5.34)$$

where $f_{j,i}$ is the contact force generated by the j^{th} phalanx on the object i . The index I_{gs} is identical to the performance index defined in eq. (3.65) where the continuous grasp-state workspace W is replaced with a discrete set of grasp-states corresponding to the m user-defined typical objects and $\delta(\mathbf{k}^*, \boldsymbol{\theta}^*) = 1$ is assumed. This index favours force-isotropic configurations.

- The equilibrium curve obtained by considering the last two phalanges of the finger should physically stay on the distal phalanx in all configurations in order to ensure feasible stable grasps. This characteristic is known to eliminate closing-ejection with two-phalanx fingers as discussed in Section 5.2.3. This approximation was proposed in (Laliberté and Gosselin 1998) since no theory of ejection with three-phalanx fingers was available at the time. If the equilibrium location is always on the last physical phalanx, then $I_{eq} = 1$; if it is not, then $I_{eq} = 0$. Considering usual transmission mechanisms (linkage or tendon), this condition is equivalent to (friction is neglected to obtain a worst-case scenario)

$$\max_{\theta_3} \left(\frac{e}{l_3} \right) = \max_{\theta_3} \left(-\frac{l_2 R_2}{l_3(R_2 + 1)} \cos \theta_3 \right) < 1 \quad (5.35)$$

where R_2 is the transmission ratio between the intermediate and distal phalanges and therefore might be a function of angle θ_3 . A more restrictive but easier to handle expression of this criterion is

$$\max_{\theta_3} \left(\frac{-R_2}{R_2 + 1} \right) < \frac{l_3}{l_2}. \quad (5.36)$$

For instance, with a tendon-driven finger, one obtains the condition

$$\alpha < \frac{l_3}{l_2 + l_3} \quad (5.37)$$

where $\alpha = r_3/r_2$. Again, with linkage-driven fingers the expressions are much more complicated and a numerical procedure is advised. A more conservative approach could be to smooth the penalty of the maximal value of the equilibrium location when approaching the limit of the distal finger by using a sigmoid function, e.g.

$$I_{eq} = \frac{1}{1 + e^S} \quad (5.38)$$

with

$$S = S_1 \max(e) - S_2 l_3 \quad (5.39)$$

where $\max(e)$ is the maximal value of the equilibrium location and (S_1, S_2) are constants used to tune the penalty when $\max(e)$ tends to l_3 . The approach consisting in the analysis of only the last two phalanges to study the grasp stability of three-phalanx fingers has also been illustrated in Section 4.2.6. It should be noted that the design parameters used in Section 4.2.6 have been obtained using the procedure described in this section.

- The finger mechanism should be as compact as possible. If the finger is sufficiently compact, the index $I_c = 1$. Otherwise, the index is between 0 and 1.

The performance indices defined above are combined in order to obtain a global index defined as

$$I_G = I_{xy}^2 I_{gs} I_{eq} I_c \quad (5.40)$$

for each of the fingers. The index I_{xy} is squared since it is a more important criterion. An example of I_G as a function of R_1 and R_2 is presented in Figure 5.11. Approximately 30 cylindrical objects were considered in this example. An effective finger can then be chosen among the best values of I_G , for instance $R_1 \approx 0.4$ and $R_2 \approx 0.5$.

5.3.3 Grasp-Stability Analysis

The analysis described in Section 4.3 allows one to obtain the final stability of a grasp with respect to an initial configuration of the finger. For instance,

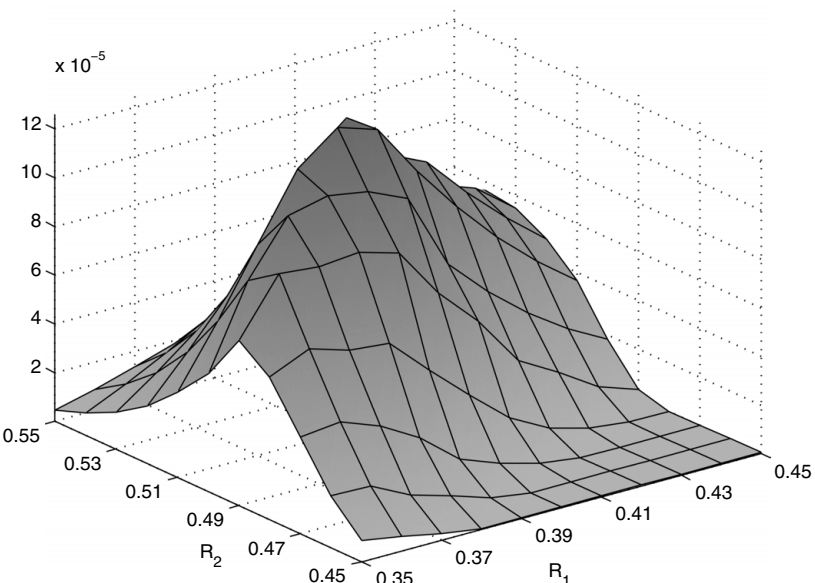


Fig. 5.11. Performance index of a three-phalanx finger with respect to its characteristic link length ratios

as assumed in Chapter 4, if in this initial configuration one force is negative, the study on the sliding motion of the finger can be performed in order to determine if a stable grasp will be achieved, if the latter uses the mechanical limits of the finger or not, or if the finger will eject the object. This technique can therefore be useful in the design of an underactuated finger that must grasp a certain set of typical objects. The robustness of the finger's stability with respect to design parameters can be studied, as illustrated in Fig. 5.12. In this figure, an underactuated finger using tendons is grasping an object with an initial configuration given by $(\theta_2, \theta_3, k_2, k_3) = (\pi/6, \pi/3, 0.5, 0.5)$, i.e., with a missing proximal contact, and the final stability of the grasp is presented with respect to the ratio of the transmission pulley radii. The phalanx lengths used are the same as in parameter set 2, and the full range of both angles, namely $-\pi < \theta_i < \pi$ with $i = 2, 3$ was used.

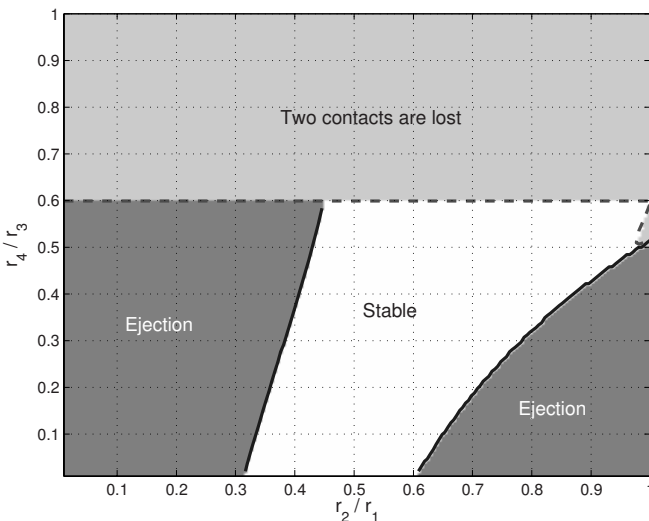


Fig. 5.12. Case 3 stability regions with respect to design parameters

In this figure, two distinct regions corresponding to an unstable grasp leading to ejection can be identified. The leftmost ejection region corresponds to what has been defined as opening-ejection. This kind of ejection is easily prevented using a mechanical limit on the joint of the finger. For instance, a limit on both angles such that $0 < \theta_i < \pi/2$ with $i = 2, 3$ completely stabilizes this region to a kinematic equilibrium. The rightmost ejection region corresponds to closing-ejection, a more insidious case of ejection that should be prevented by other techniques than mechanical limits (cf. Section 5.2.3), since this phenomenon can happen in the usual range of motion of the joint angles. The same technique can be used with a Case 1 grasp but the illustration is of less significance since in this case the final stability depends only on the ratio r_4/r_3 , the first stage of the finger being immobile.

However, it should be emphasized that this analysis is based on a particular example and no design rules are known to eliminate ejection with three phalanx fingers, as opposed to the two-phalanx case (cf. Section 5.2.3). This problem remains one important and yet unresolved issue with underactuated fingers.

5.4 Conclusions

In this chapter, procedures to optimally design two- and three-phalanx underactuated fingers were presented. The results obtained can be used to design fingers using any transmission mechanisms although the focus was placed on linkages and pulleys as transmission mechanisms. Two issues were considered: the contact force distribution of the grasp and the overall grasp stability of the finger with respect to ejection. The aim of this chapter is to provide practical tools for the design of underactuated fingers. Previously, this design was mainly driven by the designer's inspiration, which can result in very good designs but may also sometimes produce questionable results. If the rules presented in this chapter are followed, the optimality of the design with respect to the grasping characteristics can be ensured. With two-phalanx fingers, the stability and the local force-isotropic property of the grasps can be achieved perfectly, and therefore, the latter properties can be used as constraints rather than as criteria. Hence, one can obtain the design parameters ensuring stability and then, select a solution in this subset of the design parameter space that maximizes a certain criterion, such as robustness with respect to the contact force variation. With three-phalanx fingers, the complexity of the equations of both the contact forces and the grasp-state space elements has not yet allowed to obtain similar results. However, two approaches were proposed to obtain design parameters based on either a performance index composed of several sub-indices or a grasp-stability analysis. The results of this chapter have been published in (Laliberté and Gosselin 2001b; Birglen and Gosselin 2003; Birglen and Gosselin 2004b).

6 Underactuation between the Fingers

But when thou doest alms, let not thy left hand know what thy right hand doeth.

Gospel according to Matthew 6:3.

in which a methodology is proposed for the analysis of the force capabilities of mechanisms used to extend the principle of underactuation from the fingers to the hand itself. In the first part of the Chapter, several differential elements are presented and a simple matrix formulation is developed to obtain the relationship between the actuation and output forces of the devices. Then, a mathematical method to obtain the output force capabilities of connected differential mechanisms is presented. Finally, two examples are analyzed using the technique presented in the chapter.

6.1 Introduction

Common robotic hands do not usually comprise one single finger, except maybe in tentacle inspired systems. The prototypes presented in Table 2.1 have a number of fingers comprised between two and five, while over 50% have three fingers. It is therefore a natural step to extend the principle of underactuation to the hand itself in addition to individual fingers. The purpose of the underactuation between the fingers is to use the power of one actuator to drive the open/close motion of all the fingers of a robotic hand collectively. The transmission mechanism must be adaptive, i.e., when one or more fingers are blocked, the remaining finger(s) should continue to move. When all the fingers are blocked, the force should be well distributed among the fingers and it should be possible to apply large grasping forces while maintaining a stable grasp. Introducing underactuation between the fingers of a robotic hand allows to further reduce the complexity of the systems, from the actuation point of view.

The application of the principle of underactuation among fingers has been demonstrated with several prototypes (Rakic 1989; Guo et al. 1992; Fukaya et

al. 2000; Crowder 1991; Kennedy 2001; Laliberté and Gosselin 2003). The basic element commonly used to this end is the differential mechanism, as discussed in Section 2.2. As noted in the latter section and according to the IFToMM terminology (IFToMM 1991), a differential mechanism is a two-DOF mechanism that can resolve a single input into two outputs and vice versa. In underactuated grasping systems in the sense used in this book, a spring element is generally used to constrain kinematically the outputs of the differential mechanism during the pre-grasping phase. Usually, the spring is of negligible stiffness with respect to the actuation torque and used to keep both outputs in the same kinematic state (e.g., same angles or same positions). However, this is not obligatory, especially if multiple outputs are provided through stacked elements. It should also be noted that although differentials are the most commonly used elements in underactuation, they are not the only technological solution to achieve this property in grasping (Krut 2005).

In this chapter, several differential systems specifically used in robotic hands to provide underactuation between a certain number of fingers are presented. In the first part of the chapter, the focus is placed on the analysis of several common differential mechanisms modelled as basic force input/output cells (illustrated in Fig. 6.1). Several solutions are studied with respect to their force capabilities: the objectives and methods of this analysis are similar to those of Chapter 3 where phalanx forces were studied. Indeed, if underactuation can be used to drive several robotic fingers, it can also be used to drive several phalanges of these fingers with a single actuator as described in details in Chapter 3. Although similar in its approach, the force analysis of underactuation between the fingers is fundamentally different from the underactuation within the fingers as it will be shown. In the second part of this chapter, some mathematical tools are presented to analyze the force capabilities of connected differential mechanisms used to provide n outputs by stacking multiple elements. These tools also include a simple method to study the implications of the reversal principle of differential mechanisms. Examples are thereupon provided to clearly illustrate the results of the chapter and their application to the design of grasping devices. Finally, two non-standard solutions—i.e., not based on differential mechanisms—are presented and discussed in comparison with differential mechanisms. To the best of the authors' knowledge the force capabilities developed by connected differential mechanisms have never been mathematically studied, despite having been used in numerous occasions. The idea itself of connecting differential mechanisms to produce multiple output adaptive systems is however not new and should be attributed to Prof. Hirose (Hirose 1985; Hirose 1993).

6.2 Design Solutions

6.2.1 Movable Pulley

The movable pulley is perhaps the best known and most commonly used mechanical systems to distribute one actuation force to two outputs (Hirose 1985; Massa et al. 2002). Since a tendon is used, such a system can easily be employed

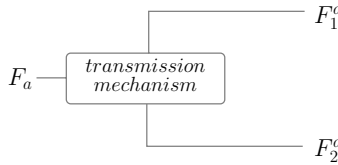


Fig. 6.1. Force transmission system used in underactuated mechanisms

to drive underactuated fingers which commonly use tendons for actuation transmission. In Fig. 6.2, for instance, two n -phalanx underactuated fingers are driven with one input through a movable pulley located inside the palm of the hand. Note that the fingers are themselves also underactuated since several phalanges are driven with a single tendon and since their motion is not coupled. The movable pulley can also drive fully-actuated fingers (using coupled rotations for example). More generally, this principle can be used to drive any mechanical system driven by two tendons and thereby provide adaptability. The notation pertaining to the analysis of the movable pulley presented in this section is shown in Fig. 6.3. It is pointed out that the two DOFs of the pulley are: a translation along the sliding guide and a rotation about an axis perpendicular to the plane of the figure. The input force is noted F_a while the two output forces are respectively F_1^a and F_2^a . A spring, modelled by the torque T^s , constrains the remaining DOF of the pulley. The purpose of this analysis is to obtain the actuation forces transmitted to the output as functions of the input forces—the spring is considered an input—, i.e.,

$$\mathbf{F} = \mathbf{T}^f \mathbf{t}^\diamond \quad (6.1)$$

with

$$\mathbf{F} = \begin{bmatrix} F_1^a \\ F_2^a \end{bmatrix} \quad \mathbf{t}^\diamond = \begin{bmatrix} F_a \\ T^s \end{bmatrix}. \quad (6.2)$$

Matrix \mathbf{T}^f , hereafter referred to as the force transmission matrix, characterizes the underactuation device used, similarly to the transmission matrix \mathbf{T} which characterizes the system used in the underactuation of the phalanges. However, one should note that \mathbf{T} relates velocities while \mathbf{T}^f relates forces and/or torques: these two matrices should not be confused. Referring to Fig. 6.3 and using a very simple static analysis, one readily obtains

$$\mathbf{T}^f = \frac{1}{c} \begin{bmatrix} r & \sin \alpha_2 \\ r & -\sin \alpha_1 \end{bmatrix} \quad (6.3)$$

where c is the sum of the respective distances from points A_1 and A_2 to the axis of the prismatic joint, i.e., $c = r(\sin \alpha_2 + \sin \alpha_1)$ and where α_1 and α_2 are

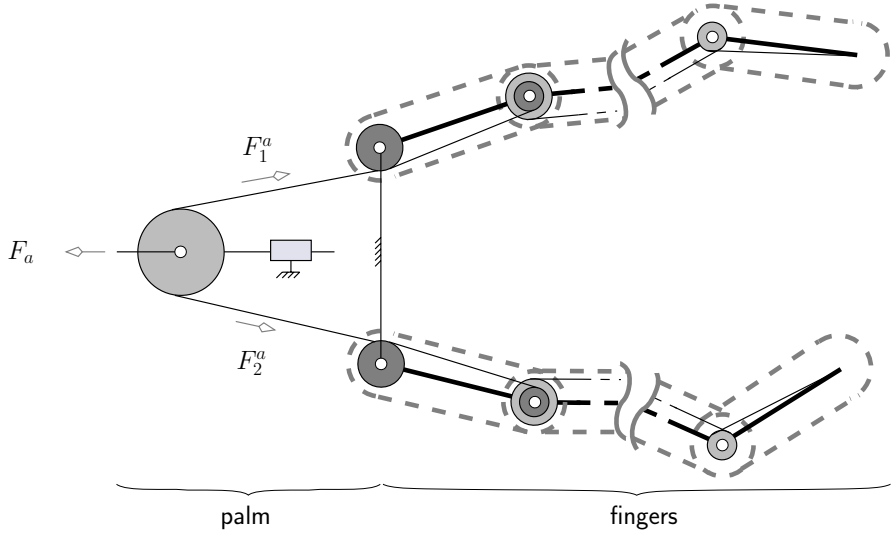


Fig. 6.2. Movable pulley driving two underactuated fingers

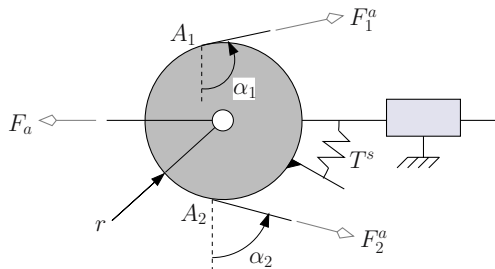


Fig. 6.3. Modelling of the movable pulley

defined in Fig. 6.3. It is noted that c cannot be negative for the device to work properly. If the stiffness of the spring is negligible, one obtains

$$F_1^a = F_2^a = \frac{F_a}{\sin \alpha_1 + \sin \alpha_2}. \quad (6.4)$$

An important property of the movable pulley is that it is force-isotropic, in the sense of the discussion of Section 5.2.2, i.e., the two output forces are equal. This result was to be expected since the tension in the common cable is constant. Furthermore, the system is *globally* force-isotropic since this property holds for any configuration, i.e., any value of α_1 and α_2 . The force transmission ratio F_i^a/F_a for $i = 1, 2$ is however significantly affected by the angles of the output tendons even over a limited range of the angular values, as illustrated in Fig. 6.4. The force transmission ratio F_i^a/F_a is sometimes designated as the *mechanical advantage* of the system.

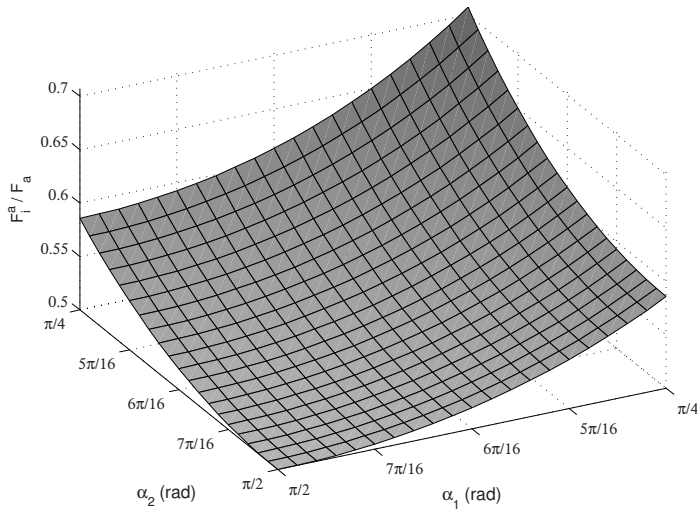


Fig. 6.4. Force transmission ratio as a function of the output tendon angles for the movable pulley

6.2.2 Seesaw Mechanism

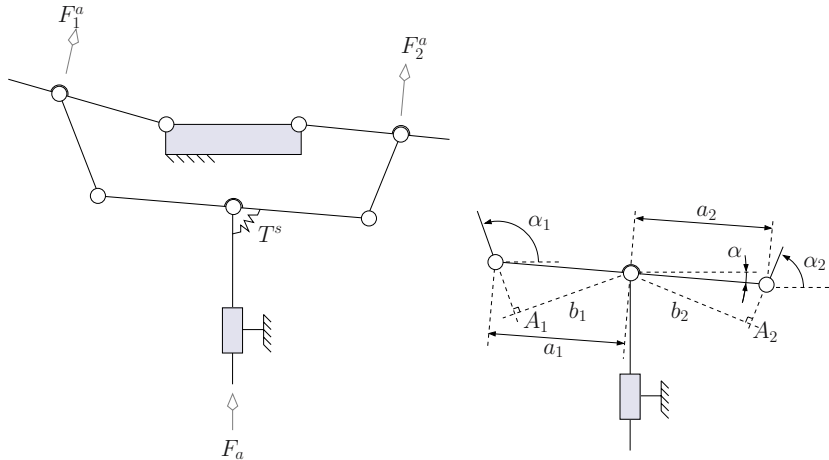
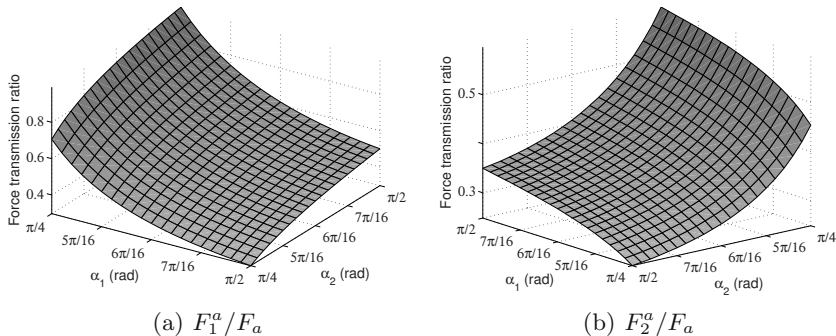
The principle of this device is to use a central seesaw bar whose translation in one direction is controlled while the other is prevented by design. The rotation of the bar is used to accommodate the difference of position between two output rods transmitting the motion. A seesaw mechanism driving two underactuated fingers is illustrated in Figs. 2.5 and 5.9. The notation pertaining to this mechanism is indicated in Fig. 6.5. Seesaw mechanisms have been successfully used in a number of underactuated hands. It is referred to as the “differential lever” in (Rakic 1989) or the “equalizing bar” in (Crowder 1991). In (Hirose et al. 1997), a double “rocker arm,” i.e., a rocker-bogie sole, was proposed as a terrain-adaptive sole, still based on the principle of the seesaw mechanism. This concept has been applied by the authors of the latter paper to a quadruped walking robot, the TITAN VII. Commercially available road profilographs also use a similar design. Several different names have been used in the literature to refer to the mechanism analyzed in this section. In this book, the denomination proposed in (Hirose 1985) is used, namely, seesaw mechanism.

The force transmission matrix of this mechanism can be written as

$$\mathbf{T}^f = \frac{1}{c} \begin{bmatrix} b_2 & \sin \alpha_2 \\ b_1 & -\sin \alpha_1 \end{bmatrix} \quad (6.5)$$

where, similarly to the movable pulley presented in Section 6.2.1, c is the sum of the respective distances from the axis of the prismatic joint to points A_1 and A_2 , i.e.,

$$c = b_1 \sin \alpha_2 + b_2 \sin \alpha_1 \quad (6.6)$$

**Fig. 6.5.** Seesaw mechanism**Fig. 6.6.** Force transmission ratios as a function of the output angles α_1 and α_2 for a seesaw mechanism defined by $a_1 = a_2 = 1$ and $\alpha = \pi/6$

with $b_i = a_i \sin(\alpha_i - \alpha)$ for $i = 1, 2$. Again, c has to be positive for the device to properly transmit forces. The similarity between the seesaw mechanism and the movable pulley is another illustration of the duality between tendon-driven and linkage-driven mechanisms, as previously discussed in Sections 3.6.2 and 4.2.3. Examples of the force transmission ratio F_1^a/F_a and F_2^a/F_a are illustrated in Figs. 6.6(a) and 6.6(b). Similarly to the case of the movable pulley, significant variations are observed even over a limited range of motion.

6.2.3 Fluidic T-Pipe

The simplest method to distribute one input towards two outputs may be to use a T-pipe scheme, as illustrated in Fig. 6.7. This fluidic stage is a differential mechanism, according to the IFToMM definition, and takes advantage of

the deformability of a fluid to separate its flow into two distinct streams. The force transmission matrix of a T-pipe can be readily written by expressing the conservation of pressure in the fluid.

One obtains

$$\begin{bmatrix} F_1^a \\ F_2^a \end{bmatrix} = \frac{F_a}{S_a} \begin{bmatrix} S_1^a \\ S_2^a \end{bmatrix} \quad (6.7)$$

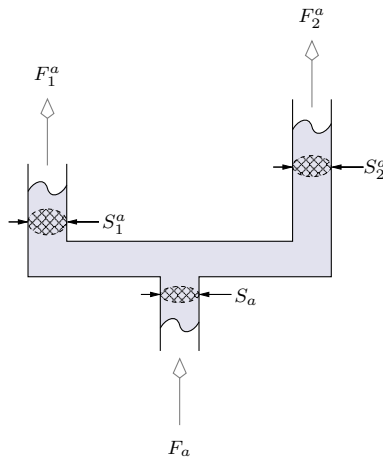
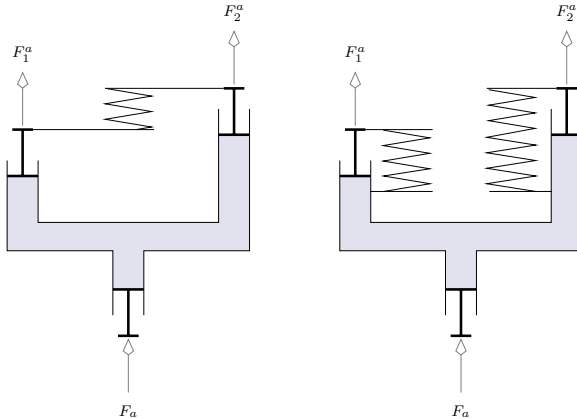
where S_a , S_1^a and S_2^a are the respective section areas of the input, primary and secondary output pipes. It is noted that in this case, instead of having a *matrix* characterizing the underactuation capability of the device, a vector is rather obtained. This is due to the fact that no return torque or force is usually embedded in the stage itself. Namely, the system is not fully constrained from a static point of view. However, in practical applications, a return spring is commonly found in the fluidic struts driven by this stage. When this system is used to drive robotic fingers, it is usually desired to keep both output states identical. In the latter case, if a spring opposes the difference between the two outputs, one obtains

$$\begin{bmatrix} F_1^a \\ F_2^a \end{bmatrix} = \begin{bmatrix} S_1^a/S_a & -1 \\ S_2^a/S_a & 1 \end{bmatrix} \begin{bmatrix} F_a \\ F^s \end{bmatrix} \quad (6.8)$$

where the force transmission matrix is readily recognizable. Alternatively, if two springs act on the outputs, the previous equation becomes

$$\begin{bmatrix} F_1^a \\ F_2^a \end{bmatrix} = \begin{bmatrix} S_1^a/S_a & 1 & 0 \\ S_2^a/S_a & 0 & 1 \end{bmatrix} \begin{bmatrix} F_a \\ F_1^s \\ F_2^s \end{bmatrix}. \quad (6.9)$$

Both cases are illustrated in Fig. 6.8. In the case where two springs are used, the force transmission matrix of the stage is not square, due to the fact that the device is overconstrained with respect to a static analysis. Indeed, a n -output m -input underactuated mechanism in the sense of this book requires $n - m$ springs in order to be statically determined. However, in the latter case, the two-output one-input device uses not one but two springs. This overconstraint may seem penalizing since it implies that for a desired output in force, an infinite number of solutions of the input force vector are possible. However, this is usually not true since the stiffness of the springs is fixed by design and therefore the only control variable available to the user is the input force. Namely, the force inputs of the springs are usually not controllable. Another characteristic of the T-pipe scheme is that the output forces are constant and independent from the output position (if the spring(s) is (are) negligible) with respect to the actuator torque. Furthermore, the force-isotropic property can be easily achieved with this device by making the output section areas equal.

**Fig. 6.7.** Fluidic stage**Fig. 6.8.** Possible designs for the fluidic stage

6.2.4 Planetary and Bevel Gear Differentials

The most common differential mechanisms are based on either planetary or bevel gear transmissions. Aside from automotive applications, gear differentials have also been used in underactuated hands. For instance, bevel gear differentials have been used in (Luo et al. 2004) to drive a copy of the SARAH hand (Laliberté and Gosselin 2003), while the latter uses planetary gear trains. In the planetary differential, for consistency, the input is chosen to be the carrier torque while the primary and secondary outputs are the sun and ring torque, as illustrated in Fig. 6.9(a).

Therefore, one obtains

$$\begin{bmatrix} T_1^a \\ T_2^a \end{bmatrix} = \mathbf{T}^f \begin{bmatrix} T_a \\ T^s \end{bmatrix} \quad (6.10)$$

with the force transmission matrix

$$\mathbf{T}^f = \begin{bmatrix} r_s/(r_s + r_c) & 1 \\ r_c/(r_s + r_c) & -1 \end{bmatrix} \quad (6.11)$$

where r_c and r_s are respectively the ring/annulus and sun pitch radii. Note that the authors use the term “force” transmission matrix even if only torques are considered. The number of teeth can be equivalently used in the above equation as in Section 3.6.3 since both quantities are related through the module of the gear train m , i.e., $2r_i = mN_i$, where N_i is the number of teeth of gear i .

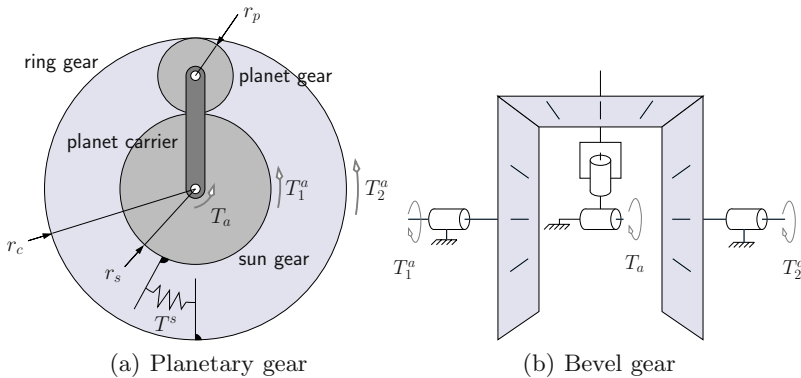


Fig. 6.9. Geared differential

By inspection of the planetary gear force transmission matrix it is clear that the output torques are constant and independent from the output position, similarly to what was observed in the T-pipe scheme presented in Section 6.2.3. Again, similarities between technological solutions stand out from the analysis. The independence of the output force from the output kinematic state can be of interest to ensure constant performances over the driven device’s workspace.

The bevel-gear differential (illustrated in Fig. 6.9(b)) is simply a particular case of the more general planetary gear differential. In this special case, both output torques are globally force-isotropic and are equal to one half of the input torque (if the spring is neglected). It is noted that force isotropy is impossible to achieve with a simple planetary gear differential because it would require a zero radius of the planet gear, according to eq. (6.11). However, particular planetary gears, where the planet consists of two rigidly connected gears instead of a single gear, have been used to overcome this problem. An example of such

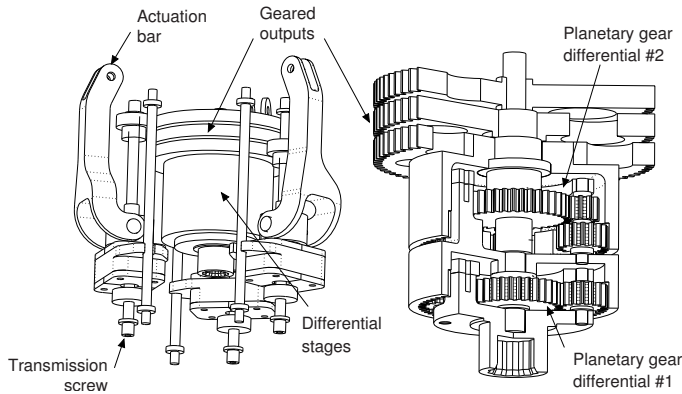


Fig. 6.10. One-input three-output differential system of the SARAH prototypes



Fig. 6.11. Picture of the SARAH-CSA differential stage

gear trains achieving force-isotropic outputs is used in the SARAH class prototypes (Laliberté and Gosselin 2003). The latter use one-input three-output devices based on two stacked planetary gear differentials, as illustrated in Figs. 6.10 and 6.11, to drive three underactuated fingers with one actuator.

6.3 Combining Multiple Stages

6.3.1 Transmission Tree Analysis

In order to obtain n outputs—typically three to four in robotic hands—multiple differential devices can be stacked, each stage adding one degree of freedom to

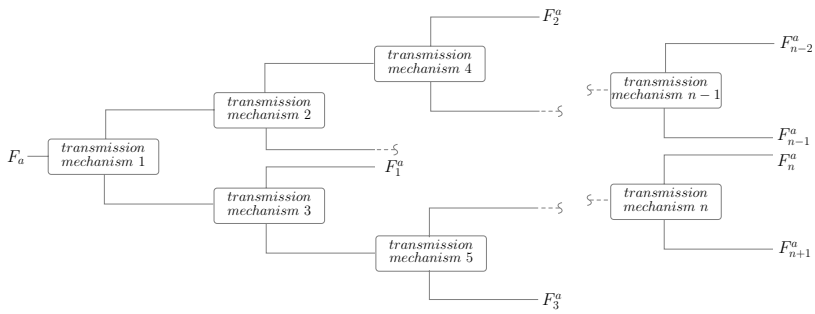


Fig. 6.12. Transmission tree to produce multiple outputs

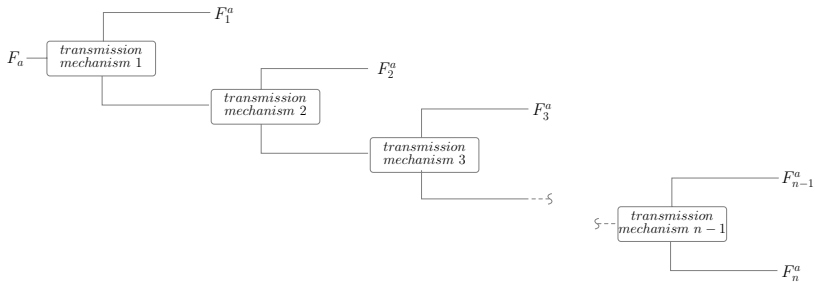


Fig. 6.13. Strictly serial transmission tree

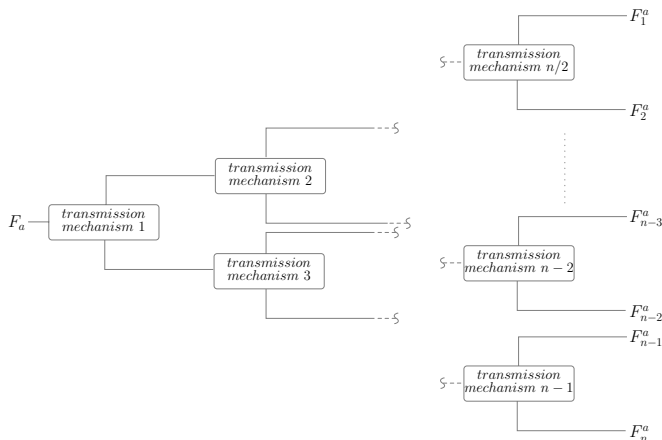


Fig. 6.14. Strictly symmetrical transmission tree

the system. Any layout tree may be used for the routing of the actuation, as illustrated in Fig. 6.12.

This tree is similar to the transmission architecture used in the conceptual underactuated finger presented in Fig. 3.1. However, in the latter case, the structure of the transmission tree was strictly serial. This simplification results from the physical layout of robotic fingers where rigid links (the phalanges) are connected to each other in series. Indeed, the serial architecture of the fingers naturally leads to a serial underactuated transmission. Nevertheless, this serial architecture is not necessary and is almost certainly not used if the driven system differs from a mechanical finger. Furthermore, the mechanical connection between the phalanges leads to peculiar phenomena, as discussed in Chapter 4.

To produce n outputs, $n - 1$ differential stages are required since each differential mechanism produces two outputs for one input. Each transmission stage can be described by its associated force transmission matrix, defined in eq. (6.1), hence $n - 1$ equations are obtained. Using a superscript i to indicate the i^{th} stage, one obtains

$${}^i \mathbf{F} = {}^i \mathbf{T}^f {}^i \mathbf{t}^\diamond \quad i = 1, \dots, n - 1. \quad (6.12)$$

Furthermore, the $n - 1$ equations can be combined in a single input-output relationship, namely

$$\begin{bmatrix} F_1^a \\ F_2^a \\ \vdots \\ F_n^a \end{bmatrix} = \mathbf{T}^f \begin{bmatrix} F_a \\ T_1^s \\ \vdots \\ T_{n-1}^s \end{bmatrix} \quad (6.13)$$

In this section, all the transmission matrices are assumed to be square. If this hypothesis cannot be satisfied—c.f. the discussion on the fluidic stage (Section 6.2.3)—the right-hand side vector should be modified accordingly. Non-square matrices do not prohibit the use of the method presented in this section since no matrix inversion is required. The form of this single input-output equation depends on the transmission tree layout. For example, if the latter is strictly serial, as illustrated in Fig. 6.13, one obtains

$$\begin{bmatrix} F_1^a \\ F_2^a \\ \vdots \\ F_n^a \end{bmatrix} = \left(\prod_{i=1}^{n-1} \begin{bmatrix} \mathbf{1}_{n-1-i} & \mathbf{0} \\ \mathbf{0} & {}^{n-i} \mathbf{T}^f \mathbf{1}_{i-1} \end{bmatrix} \right) \begin{bmatrix} F_a \\ T_1^s \\ \vdots \\ T_{n-1}^s \end{bmatrix}. \quad (6.14)$$

The matrices included in the above product are block diagonal, i.e., square diagonal matrices in which the diagonal elements are square matrices, and the off-diagonal elements are zero. The blocks on the diagonal are either the force transmission matrix of the associated stage or the identity matrix. Indeed, $\mathbf{1}_k$ indicates the identity matrix of dimension k . Note that, if one has $\mathbf{1}_0$, no

component exists. The derivation of equation (6.14) is given in Appendix A.4.1. On the other hand, if the tree is strictly symmetrical, as illustrated in Fig. 6.14, one has

$$\begin{bmatrix} F_1^a \\ F_2^a \\ \dots \\ F_n^a \end{bmatrix} = \left(\prod_{i=1}^{\frac{\log n}{\log 2}} \begin{bmatrix} {}^{2^{i-1}}\mathbf{T}^f & & & \\ & \ddots & & \mathbf{0} \\ & & {}^{2^{i-1}}\mathbf{T}^f & \\ \mathbf{0} & & & \mathbf{1}_{n-2^i} \end{bmatrix}^i \mathbf{B}_n \right) \begin{bmatrix} F_a \\ T_1^s \\ \dots \\ T_{n-1}^s \end{bmatrix}. \quad (6.15)$$

With this transmission tree, n must be a power of two, i.e., $n = 2^k$ $k \in \mathbb{N}$. The derivation of equation (6.15) is also given in Appendix A.4.2. Matrix ${}^i\mathbf{B}_k$ is the “bubble” matrix of rank i and dimension k . Its purpose is to re-order the terms resulting from the multiplication of the block diagonal matrix with the vector on the right hand side of the equation, i.e., to move upwards the components of the vector that are not in their final position (hence the name “bubble”). The elements of this matrix are defined as

$$\begin{aligned} {}^i b_n^{m,j} = 1 & \text{ if } \begin{cases} m = 2k & k = 1, \dots, 2^{i-1} \\ j = k + 2^{i-1} \end{cases} \\ \text{or} & \begin{cases} m = 2k - 1 & k = 1, \dots, 2^{i-1} \\ j = k \end{cases} \\ \text{or} & \begin{cases} m = k & k = 2^i, \dots, n \\ j = k \end{cases} \\ {}^i b_n^{m,j} = 0 & \text{ otherwise.} \end{aligned} \quad (6.16)$$

It is noted that ${}^1\mathbf{B}_n = \mathbf{1}_n$, i.e., the identity matrix of dimension n . The bubble matrices are tedious to express properly but are not complicated once their function is clearly understood.

Furthermore, matrices of higher dimensions can be written recursively, e.g.,

$${}^2\mathbf{B}_4 = \begin{bmatrix} 1 & 0 & 0 & 0 \\ 0 & 0 & 1 & 0 \\ 0 & 1 & 0 & 0 \\ 0 & 0 & 0 & 1 \end{bmatrix} \quad (6.17)$$

$${}^2\mathbf{B}_8 = \begin{bmatrix} {}^2\mathbf{B}_4 & \mathbf{0}_4 \\ \mathbf{0}_4 & \mathbf{1}_4 \end{bmatrix} \quad (6.18)$$

$${}^3\mathbf{B}_8 = \begin{bmatrix} 1 & 0 & 0 & 0 & 0 & 0 & 0 & 0 \\ 0 & 0 & 0 & 0 & 1 & 0 & 0 & 0 \\ 0 & 1 & 0 & 0 & 0 & 0 & 0 & 0 \\ 0 & 0 & 0 & 0 & 0 & 1 & 0 & 0 \\ 0 & 0 & 1 & 0 & 0 & 0 & 0 & 0 \\ 0 & 0 & 0 & 0 & 0 & 0 & 1 & 0 \\ 0 & 0 & 0 & 1 & 0 & 0 & 0 & 0 \\ 0 & 0 & 0 & 0 & 0 & 0 & 0 & 1 \end{bmatrix} \quad (6.19)$$

$${}^3\mathbf{B}_{16} = \begin{bmatrix} {}^3\mathbf{B}_8 & \mathbf{0}_8 \\ \mathbf{0}_8 & \mathbf{1}_8 \end{bmatrix}. \quad (6.20)$$

It should be noted that, for the typical three to four outputs (for robotic hands), the tree is either serial or symmetrical; no other layout is possible. For three outputs, only the serial layout is possible. Hence, if the differential stages are numbered as indicated in Fig. 6.13, one has

$$\begin{bmatrix} F_1^a \\ F_2^a \\ F_3^a \end{bmatrix} = \begin{bmatrix} 1 & \mathbf{0} \\ \mathbf{0} & {}^2\mathbf{T}^f \end{bmatrix} \begin{bmatrix} {}^1\mathbf{T}^f & \mathbf{0} \\ \mathbf{0} & 1 \end{bmatrix} \begin{bmatrix} F_a \\ T_1^s \\ T_2^s \end{bmatrix}. \quad (6.21)$$

Hence, the global transmission matrix is

$$\begin{bmatrix} {}^1T_{1,1}^f & {}^1T_{1,2}^f & 0 \\ {}^2T_{1,1}^f {}^1T_{2,1}^f & {}^2T_{1,1}^f {}^1T_{2,2}^f & {}^2T_{1,2}^f \\ {}^2T_{2,1}^f {}^1T_{2,1}^f & {}^2T_{2,1}^f {}^1T_{2,2}^f & {}^2T_{2,2}^f \end{bmatrix} \quad (6.22)$$

where ${}^kT_{i,j}^f$ is the component on the i^{th} line and j^{th} column of matrix ${}^k\mathbf{T}^f$. If the effect of the springs can be neglected, i.e., $T_1^s = T_2^s = 0$, the latter equation becomes

$$\begin{bmatrix} F_1^a \\ F_2^a \\ F_3^a \end{bmatrix} = \begin{bmatrix} {}^1T_{1,1}^f \\ {}^2T_{1,1}^f {}^1T_{2,1}^f \\ {}^2T_{2,1}^f {}^1T_{2,1}^f \end{bmatrix} F_a. \quad (6.23)$$

With four outputs, the tree layout can be either serial or symmetrical.

If the former case is chosen, one has

$$\begin{bmatrix} F_1^a \\ F_2^a \\ F_3^a \\ F_4^a \end{bmatrix} = \begin{bmatrix} 1 & 0 & \mathbf{0} \\ 0 & 1 & \mathbf{0} \\ \mathbf{0} & \mathbf{0} & {}^3\mathbf{T}^f \end{bmatrix} \begin{bmatrix} 1 & \mathbf{0} & 0 \\ \mathbf{0} & {}^2\mathbf{T}^f & \mathbf{0} \\ 0 & \mathbf{0} & 1 \end{bmatrix} \begin{bmatrix} {}^1\mathbf{T}^f & \mathbf{0} & \mathbf{0} \\ \mathbf{0} & 1 & 0 \\ \mathbf{0} & 0 & 1 \end{bmatrix} \begin{bmatrix} F_a \\ T_1^s \\ T_2^s \\ T_3^s \end{bmatrix} \quad (6.24)$$

and thus, the global transmission matrix is

$$\begin{bmatrix} {}^1T_{1,1}^f & {}^1T_{1,2}^f & 0 & 0 \\ {}^2T_{1,1}^f {}^1T_{2,1}^f & {}^2T_{1,1}^f {}^1T_{2,2}^f & {}^2T_{1,2}^f & 0 \\ {}^3T_{1,1}^f {}^2T_{2,1}^f {}^1T_{2,1}^f & {}^3T_{1,1}^f {}^2T_{2,1}^f {}^1T_{2,2}^f & {}^3T_{1,1}^f {}^2T_{2,2}^f & {}^3T_{1,2}^f \\ {}^3T_{2,1}^f {}^2T_{2,1}^f {}^1T_{2,1}^f & {}^3T_{2,1}^f {}^2T_{2,1}^f {}^1T_{2,2}^f & {}^3T_{2,1}^f {}^2T_{2,2}^f & {}^3T_{2,2}^f \end{bmatrix}. \quad (6.25)$$

If the effect of the springs is negligible, eq (6.24) becomes

$$\begin{bmatrix} F_1^a \\ F_2^a \\ F_3^a \\ F_4^a \end{bmatrix} = \begin{bmatrix} {}^1T_{1,1}^f \\ {}^2T_{1,1}^f {}^1T_{2,1}^f \\ {}^3T_{1,1}^f {}^2T_{2,1}^f {}^1T_{2,1}^f \\ {}^3T_{2,1}^f {}^2T_{2,1}^f {}^1T_{2,1}^f \end{bmatrix} F_a. \quad (6.26)$$

If a symmetrical layout is selected, one obtains

$$\begin{bmatrix} F_1^a \\ F_2^a \\ F_3^a \\ F_4^a \end{bmatrix} = \begin{bmatrix} {}^2\mathbf{T}^f & \mathbf{0} \\ \mathbf{0} & {}^3\mathbf{T}^f \end{bmatrix} \begin{bmatrix} 1 & 0 & 0 & 0 \\ 0 & 0 & 1 & 0 \\ 0 & 1 & 0 & 0 \\ 0 & 0 & 0 & 1 \end{bmatrix} \begin{bmatrix} {}^1\mathbf{T}^f & \mathbf{0} \\ \mathbf{0} & 1 \end{bmatrix} \begin{bmatrix} F_a \\ T_1^s \\ T_2^s \\ T_3^s \end{bmatrix} \quad (6.27)$$

and the global transmission matrix is

$$\begin{bmatrix} {}^2T_{1,1}^f {}^1T_{1,1}^f & {}^2T_{1,1}^f {}^1T_{1,2}^f & {}^2T_{1,2}^f & 0 \\ {}^2T_{2,1}^f {}^1T_{1,1}^f & {}^2T_{2,1}^f {}^1T_{1,2}^f & {}^2T_{2,2}^f & 0 \\ {}^3T_{1,1}^f {}^1T_{2,1}^f & {}^3T_{1,1}^f {}^1T_{2,2}^f & 0 & {}^3T_{1,2}^f \\ {}^3T_{2,1}^f {}^1T_{2,1}^f & {}^3T_{2,1}^f {}^1T_{2,2}^f & 0 & {}^3T_{2,2}^f \end{bmatrix}. \quad (6.28)$$

In this case, if the effect of the springs is negligible, eq (6.27) becomes

$$\begin{bmatrix} F_1^a \\ F_2^a \\ F_3^a \\ F_4^a \end{bmatrix} = \begin{bmatrix} {}^2T_{1,1}^f & {}^1T_{1,1}^f \\ {}^2T_{2,1}^f & {}^1T_{1,1}^f \\ {}^3T_{1,1}^f & {}^1T_{2,1}^f \\ {}^3T_{2,1}^f & {}^1T_{2,1}^f \end{bmatrix} F_a. \quad (6.29)$$

If the transmission tree is neither serial nor symmetrical, the analysis should be performed considering the particular layout of the tree and using eq. (6.12).

6.3.2 Performance Evaluation of the Transmission Tree

Usually, for robotic hands, two different cases of force transmission between the fingers are of interest. Namely, either all outputs of the system should be close to being equal, or one output should be close to the sum of all the others. The former case arises when all the fingers are identical and when the grasp configuration is symmetrical, e.g., in pinch or spherical grasps. The latter case implies that one finger is working against all the others, this is usually the case in humanoid hands where a thumb is in opposition to the three or four other fingers. This case can also happen in particular grasp configurations, even for non-anthropomorphic hands, e.g., in the cylindrical configuration where one finger faces the others.

In the previous sections, it was shown that the force transmission of the mechanical system resolving a single input into multiple outputs may depend on the output states (e.g. movable pulley, seesaw mechanism) or may be constant by design (e.g. fluidic T-pipe, gear trains). Although a constant output solution may be preferred, design constrains such as size, complexity or actuation energy might prevent their effective use. Therefore, the other solutions are not to be neglected.

Furthermore, as discussed in Section 6.3, in order to achieve multiple outputs using strictly two output devices, the layout of the transmission tree should be considered. Combining all these aspects might not be trivial for the designer. However, some indices to be optimized arise from this discussion. For instance, in the two typical cases arising in robotic hands—i.e., identical fingers or “thumb” layout—, achieving identical outputs, i.e., force-isotropy, is crucial. Indeed, if this goal is obvious in the case of identical fingers in a symmetrical grasp configuration, for a thumb-based layout, one shall also consider keeping the fingers opposing the thumb with an identical input. Furthermore, an obvious transmission tree that can achieve such property consists of a first stage with identical outputs, one of which is directly connected to the thumb, while the other output is directed to another transmission tree whose outputs are the other fingers and should be force-isotropic. Hence, even in this case, the problem can be separated into two force-isotropy sub-problems.

The force-isotropic condition can be mathematically evaluated and an index can be computed, similarly to eq. (3.65) for the phalanx forces, i.e.,

$$I_f = \frac{\int_W U \, d\boldsymbol{\theta}^a}{\int_W n \, d\boldsymbol{\theta}^a} \quad (6.30)$$

with

$$U = \frac{\sum_{i=1}^n T_{i,1}^f}{\max_i(T_{i,1}^f)} \quad (6.31)$$

for a n -output transmission tree, where W is the workspace of the device parameterized with the output state vector $\boldsymbol{\theta}^a$, similarly to eq. (3.65) and $T_{i,1}^f$ is the component on the first column and i^{th} row of the global transmission matrix. It is noted that these components are positive for all the devices presented in Section 6.2. Also, in this section, the spring forces or torques are assumed to be small with respect to the actuation torque and thus, neglected. If this condition is not met, the components of the transmission matrix should be replaced by the complete expressions of the forces, including the springs.

Similarly to what was done in Section 3.5, one can calculate a “distance” from the vanishing of the smallest component, c.f. eq. (3.64), namely,

$$\sigma_f = \frac{\int_W \min_i(T_{i,1}^f) \, d\boldsymbol{\theta}^a}{\int_W F_a \, d\boldsymbol{\theta}^a} \quad (6.32)$$

which indicates a singularity in the transmission tree. If isotropy is inherent to the device (e.g. movable pulley), it can be of interest to keep the transmission ratio $\sum_{i=1}^n F_i^a / F_a$ as close as possible to one in order to maintain the correspondence between the magnitudes of the input actuation force and the actual forces distributed to the fingers. One mathematical expression of such an index is

$$I_f^* = \frac{\int_W \prod_{i=1}^n e^{n \frac{F_i^a}{F_a} (2 - n \frac{F_i^a}{F_a})} \, d\boldsymbol{\theta}^a}{\int_W e^n \, d\boldsymbol{\theta}^a} \quad (6.33)$$

where e is the exponential function. This index spans the range $[0, 1]$, where a value of 1 indicates that the system always satisfies $nF_i^a = F_a \forall i$, i.e., a constant force transmission ratio equal to unity over the whole workspace. It is noted that in this particular case, the force-isotropy condition is also satisfied.

6.4 Exchanging Inputs and Outputs

In the previous analysis, certain input/outputs of the mechanisms were arbitrarily chosen. While for the movable pulley and the seesaw mechanism one

particular branch of the system stands out and was naturally identified as the input of the system, other transmissions such as the T-pipe or the gear differential do not present such a particularity. Indeed, our choice of input and outputs was empirical and even for the devices where one branch was immediately identified with the input, nothing prevents the designer from using the latter as an output. However, the behaviour of the differential mechanism has to be carefully verified. Indeed, if a planetary gear train is chosen for instance, and if the ring gear is chosen as an input, then if the carrier gear is blocked, the sun gear will turn in the opposite direction of the ring gear. This change of direction may force the designer to choose the planetary gear as an input, depending on the application considered. Therefore, the behaviour obtained when the input and outputs are exchanged should be analyzed for the sake of completeness.

This analysis is rather simple since the basic equations describing the static equilibrium—i.e., the input/output relations—still hold with any set of input/outputs. Therefore, the equations described using the force transmission matrix still hold and only a re-arranging of the terms is required to obtain a new force transmission matrix. Assume a transmission stage characterized by its force transmission matrix \mathbf{T}^f . If the force output F_1^a is now the input, the new transmission matrix is

$$\begin{bmatrix} F_a \\ F_2^a \end{bmatrix} = \frac{1}{T_{1,1}^f} \begin{bmatrix} 1 & -T_{1,2}^f \\ T_{2,1}^f & \det \mathbf{T}^f \end{bmatrix} \begin{bmatrix} F_1^a \\ T^s \end{bmatrix}. \quad (6.34)$$

And conversely, if F_2^a is now the input, one obtains

$$\begin{bmatrix} F_a \\ F_1^a \end{bmatrix} = \frac{1}{T_{2,1}^f} \begin{bmatrix} 1 & -T_{2,2}^f \\ T_{1,1}^f & -\det \mathbf{T}^f \end{bmatrix} \begin{bmatrix} F_2^a \\ T^s \end{bmatrix}. \quad (6.35)$$

6.5 Applications

6.5.1 Underactuated Gripper

The design considered in this section is illustrated in Figs. 6.15 and 6.16. Similar underactuated grippers were presented in Figs. 2.5 and 5.9. Two underactuated linkage-driven fingers consisting of two phalanges are actuated through a seesaw mechanism as presented in Section 6.2.2.

Force-Isotropic Design

Seesaw mechanisms usually provide different values of force outputs, i.e., no force-isotropy except possibly in isolated configurations. However, this characteristic can be of use to obtain force-isotropic grasps in non-symmetrical situations. Indeed, if the typical object to be grasped is not symmetrical and/or the contact points are not symmetrically located with respect to the axis of the gripper, the contact forces will not be equal if the actuation torque induced at the base of each finger is identical. Hence, to generate a force-isotropic grasp

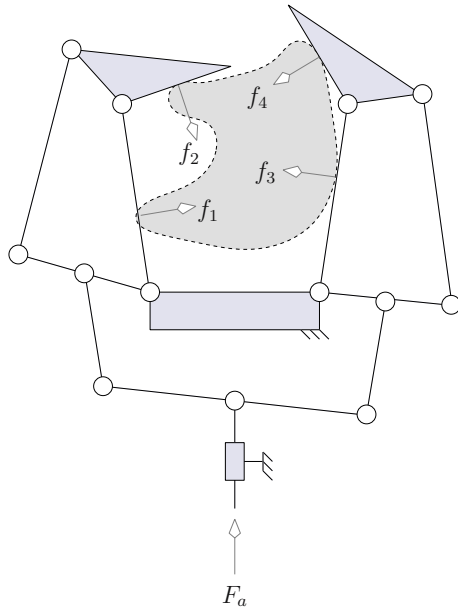


Fig. 6.15. Underactuated gripper

where all contact forces are equal, the outputs of the differential stage should not be force-isotropic. This seemingly surprising statement arises from the fact that the grasp configurations are not symmetric.

The first step to achieve a force-isotropic design is identical to the procedure presented in Section 5.2.2. Indeed, the force-isotropic condition, namely

$$f_1 = f_2 = f_3 = f_4 \quad (6.36)$$

includes the force-isotropic condition in each finger, i.e., $f_1 = f_2$ and $f_3 = f_4$. The details of the method having already been presented, it is assumed here that the geometric parameters of both fingers are known to satisfy a force-isotropic configuration defined by

$$(k_1, k_2, k_3, k_4, \theta_1, \theta_2, \theta_3, \theta_4) \quad (6.37)$$

and the contact forces (f_1, f_2, f_3, f_4) are therefore defined as functions of the actuation torque at the base of each finger. However, if this contact situation is not symmetrical, i.e., $k_1 \neq k_3$, $k_2 \neq k_4$, $\theta_1 \neq \theta_3$, or $\theta_2 \neq \theta_4$, it implies that $f_1 \neq f_3$ and $f_2 \neq f_4$ if the actuation torques transmitted to the fingers are identical.

To ensure that the final contact configuration is actually force-isotropic, the output force of the differential stage should satisfy

$$\frac{d_2 F_2^a}{d_1 F_1^a} = \frac{f_1}{f_3} \quad (6.38)$$

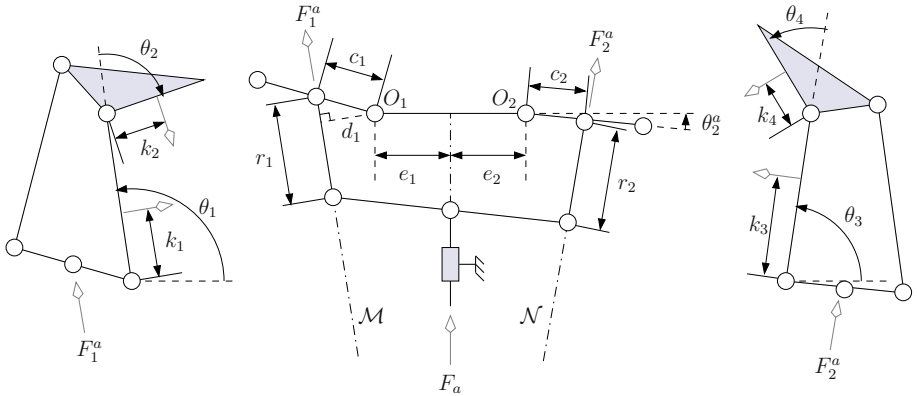


Fig. 6.16. Details of the underactuated gripper

where $d_1 F_1^a$ and $d_2 F_2^a$ are the torques generated by the output forces F_1^a and F_2^a with respect to points O_1 and O_2 respectively (see Fig. 6.16). Thus, d_1 and d_2 are respectively the distances from line \mathcal{M} to point O_1 and from line \mathcal{N} to point O_2 , i.e., the output force lines of action with respect to the associated finger. Hence, with the definition of the force transmission matrix of the seesaw mechanism, eq. (6.5), the differential stage has to satisfy

$$\frac{d_2 b_1}{d_1 b_2} = \frac{d_2 a_1 \sin(\alpha_1 - \alpha)}{d_1 a_2 \sin(\alpha_2 - \alpha)} = \frac{f_1}{f_3} \quad (6.39)$$

to generate a force-isotropic grasp (the springs in the differential stage are neglected in this section), with

$$d_i = c_i \sin(\alpha_i - \theta_i^a) \quad i = 1, 2. \quad (6.40)$$

Therefore one can choose a set of geometric parameters for the seesaw mechanism—including the location of the attachment of the output rods to the base of the fingers c_1 and c_2 —that satisfies the previous relationship, and obtain a force-isotropic grasp. For instance, let us suppose that the desired force-isotropic configuration is

$$(k_1, k_2, k_3, k_4, \theta_1, \theta_2, \theta_3, \theta_4) = (33/128, 1/2, 2/3, 1/2, \pi/2, -\pi/6, \pi/3, \pi/3) \quad (6.41)$$

considering a unitary proximal phalanx length. In order to simplify the example, these parameters have been chosen so that they correspond to the same force-isotropic finger defined by the following geometric parameters:

$$(l_1, l_2, \psi, a, b, c) = (1, 2/3, \pi/2, 6/5, 6/5, 1/3). \quad (6.42)$$

These parameters were obtained using the procedure described in Section 5.2.2. In this case, one can obtain geometric parameters that lead to a force-isotropic design, e.g.,

$$(e_1, e_2, c_1, c_2, r_1, r_2, a_1, a_2) = (1/2, 1/2, 1/3, 1/3, 1, 1, 17/20, 17/20). \quad (6.43)$$

Global Optimization

A fundamental drawback of the above method is that it requires a priori knowledge of the grasped object which might not be available. Furthermore, force-isotropy for typical objects might not be mandatory or difficult to obtain with reasonable geometric parameters. Alternatively, global performance indices can be defined using the definition of the stage force transmission ratio given in eq (6.5). The contact forces generated by the actuation force can easily be computed by combining the results of Chapter 3 and Section 6.2. Hence, performance indices based on the output forces are defined. One has

$$\begin{bmatrix} f_1 \\ f_2 \\ f_3 \\ f_4 \end{bmatrix} = \begin{bmatrix} \mathbf{J}_L^{-T} \mathbf{T}_L^{-T} \mathbf{d}_L & \mathbf{0} \\ \mathbf{0} & \mathbf{J}_R^{-T} \mathbf{T}_R^{-T} \mathbf{d}_R \end{bmatrix} \begin{bmatrix} b_2/c & (\sin \alpha_2)/c \\ b_1/c & -(\sin \alpha_1)/c \end{bmatrix} \begin{bmatrix} F_a \\ T^s \end{bmatrix} \quad (6.44)$$

which is the equation defining the contact forces as functions of the input actuation force F_a . Matrices \mathbf{J}_L and \mathbf{J}_R are the Jacobian matrices of the grasp (c.f. Section 3.2) for, respectively, the left and right finger. Similarly, \mathbf{T}_L and \mathbf{T}_R are the transmission matrices of the left and right fingers. Vectors \mathbf{d}_L and \mathbf{d}_R are defined as

$$\mathbf{d}_L = \begin{bmatrix} d_1 \\ T_L^s \end{bmatrix}, \quad \mathbf{d}_R = \begin{bmatrix} d_2 \\ T_R^s \end{bmatrix}. \quad (6.45)$$

The torques of the spring of the left and right fingers are respectively denoted by T_L^s and T_R^s . An index of interest could thereupon be defined as the ratio of the total grasp force to the actuation force, namely

$$I = \frac{\int_W \left(\sum_{i=1}^4 f_i \right) d\boldsymbol{\theta}^a}{\int_W F_a d\boldsymbol{\theta}^a}. \quad (6.46)$$

Note that the workspace W of the gripper is defined as the set of all contact configurations, described by $\boldsymbol{\theta}_a = [k_1 \ k_2 \ k_3 \ k_4 \ \theta_1 \ \theta_2 \ \theta_3 \ \theta_4]^T$, where all contact forces are positive. This index is the average mechanical advantage of the gripper as a whole. It has been shown (Herder 1998) that a value close to one is of the utmost importance for instance in the case of a manually driven surgical gripper. Indeed, this property allows the perception of the pulse of an artery and the stiffness differences between diseased and healthy tissues by the handler of the instrument without complex electronic feedback (Herder 1998). An analytical expression of this index can be computed, provided that a few assumptions on the gripper design and contact locations are made, namely,

1. both fingers are identical, i.e., $l_1 = l_3$ and $l_2 = l_4$
2. the springs are neglected

3. the contact points are located at mid-phalanx, i.e., $k_1 = k_3 = l_1/2$ and $k_2 = k_4 = l_2/2$
4. the range of motion for the angles are $\pi/4 < \theta_1, \theta_3 < 3\pi/4$ and $0 < \theta_2, \theta_4 < \pi/2$.

If the latter hypotheses are satisfied, one obtains

$$I = \int_W I^* d\boldsymbol{\theta} \quad (6.47)$$

where $\boldsymbol{\theta} = [\theta_1 \ \theta_2 \ \theta_3 \ \theta_4]^T$ and with

$$I^* = \frac{32}{l_2 c \pi^4} [A + B] \quad (6.48)$$

with

$$A = b_2 d_1 \frac{(l_2 - 2h_1 \cos \theta_2) + h_1}{h_1 + l_1} \quad (6.49)$$

$$B = b_1 d_2 \frac{(l_2 - 2h_2 \cos \theta_4) + h_2}{h_2 + l_1}. \quad (6.50)$$

For instance, if the geometric parameter set 1 of Table 4.1 is chosen for the fingers, the differential stage can be optimized accordingly. If further parameters are chosen, e.g. $e_1 = e_2 = c_1 = c_2 = 1/2$ and $r_1 = r_2 = 1$, the value of I can be computed as a function of $a^* = a_1 = a_2$. Index I is plotted as a function of a^* in Fig. 6.17. It can be seen in this Figure that the optimal value of a^* is approximately 1.40 with respect to this index. If this length is chosen, the average force applied by the user (e.g. a surgeon) in the gripper's previously defined workspace is the same as the force exerted on the object seized. Hence, the total squeezing force applied to the object is globally neither amplified, nor diminished, allowing the user to finely control the grasping force.

An example of an underactuated gripper using a design similar to that of Fig. 6.15 is presented in (Boudreault and Gosselin 2006) and in Fig. 6.18. The gripper is built using compliant hinges due to its small size (less than 10 mm) and is machined from a single block of NiTiNol, a nickel-titanium bio-compatible shape memory alloy with remarkable elastic characteristics. However, it should be noted that this preliminary prototype has not been designed using the methodology discussed above, but only considering fingers individually.

6.5.2 Multiple Pulley Routing

Two combinations of several movable pulleys that can be used to drive four outputs with one input are illustrated in Fig. 6.19. The first routing is serial according to the definition used in Section 6.3.1, meaning that one output of each stage is directly used to generate one of the final output forces while the other is propagated to the next stage of the transmission tree. The second routing is fully symmetrical, again using the definition given in Section 6.3.1, namely all

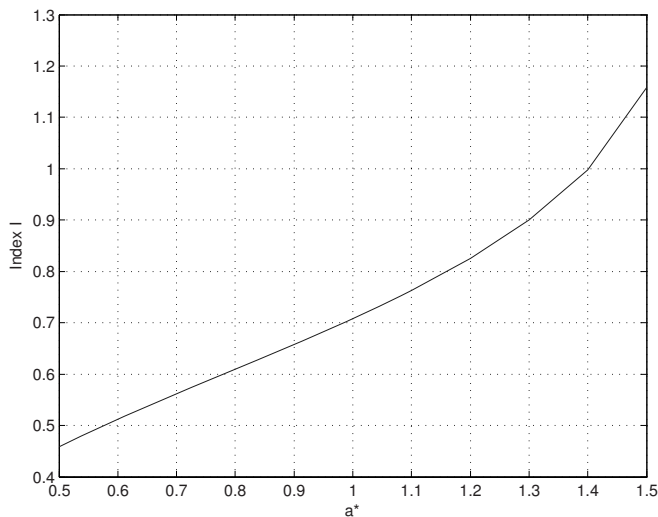


Fig. 6.17. Performance index I as a function of a^*



Fig. 6.18. Compliant sub-centimetre surgical gripper (from (Boudreault and Gosselin 2006))

outputs of each layer of the transmission tree are used to propagate the input except for the last layer whose outputs are the final force outputs. As discussed previously, with four outputs, these two transmission trees are the only possible routing.

The cables used in the serial routing are indicated by solid lines (between the pulleys), the output forces of this layout are F_i^a with $i = 2, \dots, 5$. In the symmetrical layout, the cables are indicated by dashed lines and the associated output forces are F_i^a with $i = 1, \dots, 4$. In order to simplify the expressions of the associated transmission matrices, it is assumed that the distance between two

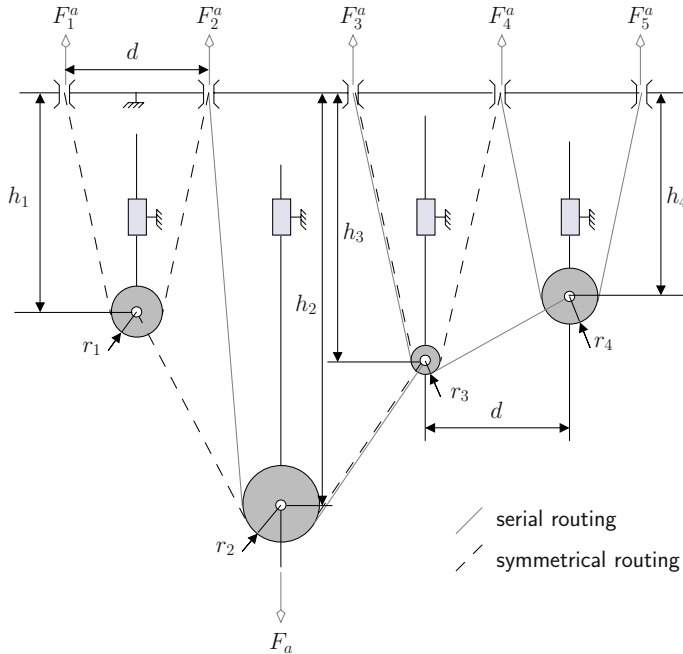


Fig. 6.19. Multiple pulley serial/symmetrical routing

consecutive force outputs are identical and the same as the distance between two consecutive axes of the movable pulleys. Nevertheless, the method presented is general and can easily be extended to more general cases.

6.5.3 Serial Routing

Using the results of Section 6.3.1, the global transmission matrix of the system with this routing is

$$\mathbf{T}^f = \begin{bmatrix} \frac{r_2}{c_2} & \frac{\sin \alpha_4}{c_2} & 0 & 0 \\ \frac{r_3 r_2}{c_3 c_2} & -\frac{r_3 \sin \alpha_3}{c_3 c_2} & \frac{\sin \alpha_6}{c_3} & 0 \\ \frac{r_4 r_3 r_2}{c_4 c_3 c_2} - \frac{r_4 r_3 \sin \alpha_3}{c_4 c_3 c_2} - \frac{r_4 \sin \alpha_5}{c_4 c_3} & \frac{\sin \alpha_8}{c_4} \\ \frac{r_4 r_3 r_2}{c_4 c_3 c_2} - \frac{r_4 r_3 \sin \alpha_3}{c_4 c_3 c_2} - \frac{r_4 \sin \alpha_5}{c_4 c_3} & -\frac{\sin \alpha_7}{c_4} \end{bmatrix} \quad (6.51)$$

with

$$\begin{cases} c_2 = r_2(\sin \alpha_3 + \sin \alpha_4) \\ c_3 = r_3(\sin \alpha_5 + \sin \alpha_6) \\ c_4 = r_4(\sin \alpha_7 + \sin \alpha_8) \end{cases} \quad (6.52)$$

where α_{2i-1} and α_{2i} , for $i = 2, 3, 4$, are respectively the left and right output angles of the pulley of radius r_i . These angles can be expressed as functions of the pulley positions h_i which are easier to measure, i.e.,

$$\begin{cases} \alpha_{2i} = \frac{\pi}{2} - 2 \arctan \left(\frac{-(h_i - h_{i+1}) + \sqrt{(2d)^2 - r_i^2 + (h_i - h_{i+1})^2}}{2d + r_i} \right) & i = 2, 3 \\ \alpha_8 = \frac{\pi}{2} - 2 \arctan \left(\frac{-h_4 + \sqrt{d^2 - r_4^2 + h_4^2}}{d + r_4} \right) \end{cases} \quad (6.53)$$

and

$$\alpha_{2i-1} = \frac{\pi}{2} + 2 \arctan \left(\frac{-h_i + \sqrt{d^2 - r_i^2 + h_i^2}}{d + r_i} \right) \quad i = 2, 3, 4. \quad (6.54)$$

If the springs are neglected, relatively simple expressions of the output forces can be obtained, namely

$$F_2^a = \frac{r_2}{c_2} F_a, \quad F_3^a = \frac{r_3 r_2}{c_3 c_2} F_a, \quad F_4^a = \frac{r_4 r_3 r_2}{c_4 c_3 c_2} F_a, \quad F_5^a = \frac{r_4 r_3 r_2}{c_4 c_3 c_2} F_a. \quad (6.55)$$

It is readily observed that the force transmission ratio of one stage also appears in the force transmission ratio of all the next stages. This characteristic is typical of a serial transmission tree. The main drawback of the serial routing arises from this coefficient propagation. Since generally $c_i > r_i$, the ratio r_i/c_i is smaller than one and hence the output forces tend to decrease when the number of stages increases. Consequently, in underactuated fingers, the distal phalanx is usually much weaker than the proximal phalanx. Therefore force-isotropy cannot be achieved with such a layout. However, this characteristic can be of use if a thumb-based layout is desired. Indeed, if the cable connected to the thumb corresponds to F_2^a , the coefficients r_i/c_i for $i = 3, 4$ can be adjusted to ensure

$$F_2^a = \sum_{i=3}^5 F_i^a \Rightarrow \frac{r_3}{c_3} \left(1 + 2 \frac{r_4}{c_4} \right) = 1. \quad (6.56)$$

Hence, the fingers opposing the thumb balance the force generated by the latter. However, this characteristic is generally only local since the coefficients c_i are functions of the kinematic state of the outputs.

6.5.4 Symmetrical Routing

The expression of the global transmission matrix for a symmetrical routing is

$$\mathbf{T}^f = \begin{bmatrix} \frac{r_1 r_2}{c_1 c_2} & \frac{r_1 \sin \alpha_4}{c_1 c_2} & \frac{\sin \alpha_2}{c_1} & 0 \\ \frac{r_1 r_2}{c_1 c_2} & \frac{r_1 \sin \alpha_4}{c_1 c_2} & -\frac{\sin \alpha_1}{c_1} & 0 \\ \frac{r_3 r_2}{c_3 c_2} - \frac{r_3 \sin \alpha_3}{c_3 c_2} & 0 & \frac{\sin \alpha_5}{c_3} \\ \frac{r_3 r_2}{c_3 c_2} - \frac{r_3 \sin \alpha_3}{c_3 c_2} & 0 & -\frac{\sin \alpha_5}{c_3} \end{bmatrix} \quad (6.57)$$

where the notation used is the same as in the previous case. Angles α_i can again be expressed as functions of the pulley positions h_i but since the routing is different, the expressions also differ, i.e.,

$$\begin{cases} \alpha_{2i-1} = \frac{\pi}{2} + 2 \arctan \left(\frac{-h_i + \sqrt{d^2 - r_i^2 + h_i^2}}{d+r_i} \right) \\ \alpha_{2i} = \frac{\pi}{2} - 2 \arctan \left(\frac{-(h_i - h_{i+1}) + \sqrt{(2d)^2 - r_i^2 + (h_i - h_{i+1})^2}}{2d+r_i} \right) \end{cases} \quad i = 1, 3 \quad (6.58)$$

and

$$\begin{cases} \alpha_3 = \frac{\pi}{2} + 2 \arctan \left(\frac{-(h_2 - h_1) + \sqrt{(2d)^2 - r_2^2 + (h_2 - h_1)^2}}{2d+r_2} \right) \\ \alpha_4 = \frac{\pi}{2} - 2 \arctan \left(\frac{-(h_2 - h_3) + \sqrt{(2d)^2 - r_2^2 + (h_2 - h_3)^2}}{2d+r_2} \right) \end{cases} \quad (6.59)$$

If the springs are neglected, the expressions of the output forces are

$$F_1^a = \frac{r_1 r_2}{c_1 c_2} F_a, \quad F_2^a = \frac{r_1 r_2}{c_1 c_2} F_a, \quad F_3^a = \frac{r_2 r_3}{c_2 c_3} F_a, \quad F_4^a = \frac{r_2 r_3}{c_2 c_3} F_a. \quad (6.60)$$

With this routing, it can be observed that the force transmission ratio of each output is the product of the force transmissions of both the stage located immediately before the output and the input stage. Hence, in this case, force-isotropy is possible and easily achievable. Namely, the transmission is force-isotropic if and only if

$$\frac{r_1}{c_1} = \frac{r_3}{c_3}. \quad (6.61)$$

However, this property is once more only local. Since force-isotropy can be achieved with such a layout, it can readily be applied to non-anthropomorphic, spherical grippers.

An example of a prosthetic hand built with Fused Deposition Modelling (FDM) rapid-prototyping technology and using a multiple pulley routing is presented in Fig. 6.20. A single tendon is used to drive five fingers with one thumb opposing the four other fingers. The four fingers are driven through a fully symmetrical transmission tree while the thumb is directly connected to the

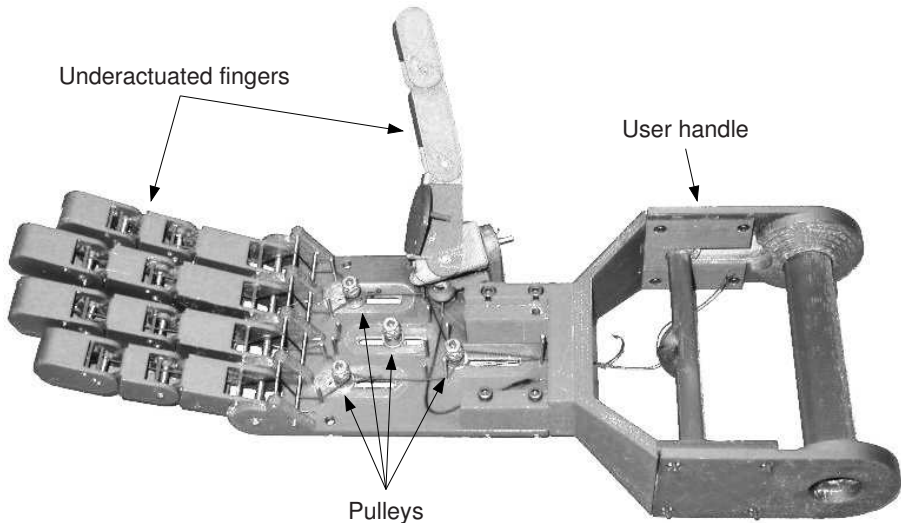


Fig. 6.20. Prosthetic hand using a multiple pulley routing (from (Gosselin et al. 2008))

driving cable. The hand therefore provides 15 DOFs and self-adaptability to the various shapes of seized objects with only one actuator.

6.6 Other Transmission Solutions

While not strictly based on differential mechanisms, other transmission mechanisms have been proposed to generate multiple outputs. Indeed, as discussed in the introduction, differential mechanisms are only one class of mechanisms that can be used for underactuation (Krut 2005). In this section, a brief discussion is proposed to discuss the advantages and drawbacks of these transmissions in comparison with differential mechanisms.

6.6.1 The Floating Platform

The principle of this solution, illustrated in Fig. 6.21 is similar to the seesaw mechanism presented in Fig. 2.5 but extended to three fingers. Instead of using the central seesaw linkage, an additional output is provided by using the third dimension of the Cartesian space. In this case, a floating platform is free to rotate around two intersecting axes. The motion of the centre of rotation is induced by a prismatic joint and the power is transmitted through the vertices of a triangular platform. The distribution of the forces is governed by the shape of the triangle. The closer a vertex of the triangle is to the centre, the larger is the force transmitted to the corresponding output.

The main difficulty with this solution is that, depending on the geometry of the grasp, the distribution of the forces should be different. Therefore, the

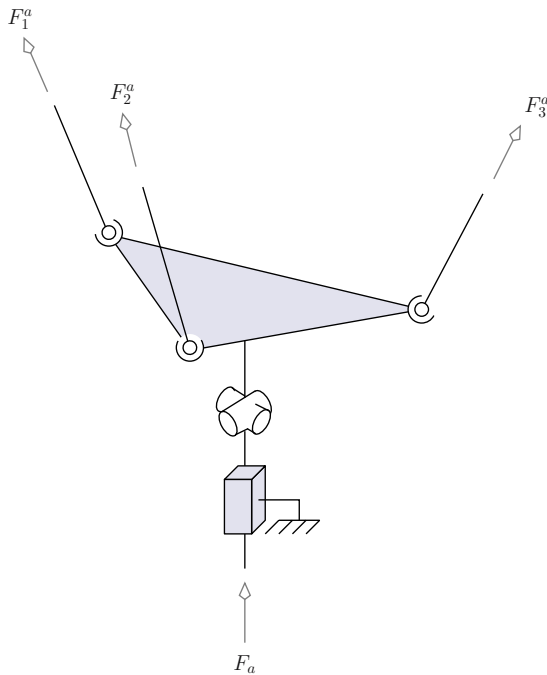


Fig. 6.21. Schematic representation of the floating platform

shape of the triangular platform should adapt to the geometry of the grasp or correspond to a selected compromise. In practice however, the shape of the platform can only be partially adapted.

Finally, since the platform undergoes complex three-dimensional movements, its behaviour is difficult to predict. Also, a large number of kinematic joints (pin, Hooke and spherical joints) is necessary to implement this mechanism. Furthermore, stacking up floating platforms to generate a n -output mechanism requires a complicated design and seems unpractical. Currently, only dynamic models have been using this kind of mechanism for underactuation between the fingers (Myrand and Gosselin 2004). However, it should be noted that a similar mobile platform has been proposed and used in (Herder and de Visser 2000) with tendon-driven fingers.

6.6.2 The Spring-Loaded Slider

The spring-loaded slider illustrated in Fig. 6.22 and proposed in (Massa et al. 2002), consists of a slider whose translation in the plane is controlled by an actuation cable (input force F_a). Three cables are also attached to the slider but through compression springs that allow the slider to resume its motion if one (or two) cable(s) is (are) blocked. The stiffness of the springs can be individually adjusted to differentiate the outputs. In this section, a version of the mechanism in which the three outputs are identical is studied rather than the

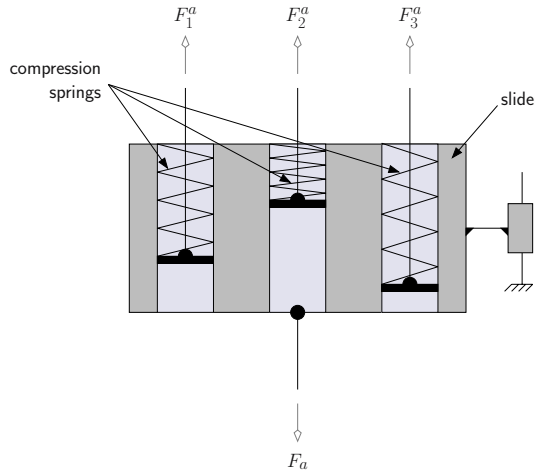


Fig. 6.22. Spring-loaded three-output slider

solution presented in (Massa et al. 2002). In the latter reference, one output was directly attached to the slider. This implementation can be analyzed by setting the associated spring stiffness to infinity in the model developed here. One particularly attractive feature of this device is that the mechanism can be very easily extended to provide n outputs, by including additional springs.

The force equations of the three-output device can be written as

$$\begin{bmatrix} F_1^a \\ F_2^a \\ F_3^a \end{bmatrix} = \begin{bmatrix} 1 & 0 & -1 & -1 \\ 1 & -1 & 0 & -1 \\ 1 & -1 & -1 & 0 \end{bmatrix} \begin{bmatrix} F_a \\ F_1^s \\ F_2^s \\ F_3^s \end{bmatrix}. \quad (6.62)$$

But, in this case, the force transmission matrix can be equivalently written as

$$\mathbf{T}^f = \begin{bmatrix} 0 & 1 & 0 & 0 \\ 0 & 0 & 1 & 0 \\ 0 & 0 & 0 & 1 \end{bmatrix}. \quad (6.63)$$

In fact, each row of any of the matrices can be used in the other matrix to write the force transmission matrix, e.g.,

$$\mathbf{T}^f = \begin{bmatrix} 0 & 1 & 0 & 0 \\ 0 & 0 & 1 & 0 \\ 1 & -1 & -1 & 0 \end{bmatrix}. \quad (6.64)$$

is also valid. This device is peculiar in many ways. For instance, it cannot be assumed that the springs are negligible because, with this assumption, the transmission does not work properly. Indeed, if one (or more) spring is negligible, the corresponding output disappears since the position of the latter is directly proportional to the spring stiffness according to Hooke's law. On the other hand, if more than one spring has an infinite stiffness (i.e., the corresponding cables are directly attached to the slider), the adaptability of the mechanism is reduced since if one of these cables is stopped, it will also prevent the slider from moving and thus, the other fingers will be blocked. Hence, only one cable can be attached to the slider even if multiple outputs are considered. Without any loss of generality, it can be assumed that the last cable is attached to the slider and, in this case, the force equation of the three-output device becomes

$$\begin{bmatrix} F_1^a \\ F_2^a \\ F_3^a \end{bmatrix} = \begin{bmatrix} 0 & 1 & 0 \\ 0 & 0 & 1 \\ 1 & -1 & -1 \end{bmatrix} \begin{bmatrix} F_a \\ F_1^s \\ F_2^s \end{bmatrix}. \quad (6.65)$$

Note that in this case, the force transmission matrix is square and uniquely defined. However, this arrangement suffers from a practical drawback penalizing its use in practice. Indeed, attaching one cable directly to the slider prevents the adjustment of the grasping force with the actuator. Therefore, the fingers cannot be force controlled. Indeed, referring to eq. (6.65), the output forces of the cables not connected to the slider are independent from the input force. This can be explained from a practical point of view: if the device is in static equilibrium, the cables attached to the slider are locked. Hence, the position of the slider is also fixed. In this position, if the input force changes, only the output force corresponding to the cable attached to the slider is modified. Since the slider position does not change, the deformation of the other springs is also constant. Thus, the associated output forces cannot be changed. By eliminating the rigid attachment of one cable to the slider, the position of the latter can be changed even if all cable lengths are fixed and thus, the output forces can be controlled. This control is limited since the force in the springs is dependent on the displacement of the springs, i.e., if a finger is stopped before another, the force in the first one will be larger. Also, the stiffness of the grasp is limited by the stiffness of the springs, which is limited in order to allow adaptability. However, architectures with a tendon attached to the slider have been used for prosthetic devices (Massa et al. 2002) (specifically, the thumb). The authors conjecture that this choice was dictated by the need to secure a mobile object inside the hand with several fingers acting against the thumb.

6.7 Conclusions

In this chapter, a methodology was proposed for the analysis of the force capabilities of common differential mechanisms used to extend the principle of

underactuation from the fingers to the hand itself. In the first part of the chapter, several differential systems, most commonly used in robotic hands to provide underactuation between a certain number of fingers, were presented. A simple matrix formulation was developed to obtain the relationship between the actuation and output forces of the devices. Then, a mathematical method to obtain the output force capabilities of connected differential mechanisms was presented. The application of the method to the analysis of strictly serial and fully symmetrical transmission trees was presented and completed with the definition of performance indices. Two examples were then analyzed using the technique presented in the Chapter: first an underactuated gripper and second a multiple pulley routing. Finally, two non-standard solutions were discussed in the light of the results. The mathematical expressions of the transmission tree characterizing the underactuated system considered are fundamentally different from the transmission matrix arising when one considers underactuation in the fingers instead of between them. Similarly to what was mentioned in the discussion proposed in the conclusion of Chapter 3, the authors believe that the tools presented in this chapter can help refining the design of an underactuated transmission. The material presented in this chapter was published in (Birglen and Gosselin 2006a).

7 Design and Control of the Laval Underactuated Hands

I hope tonight's story isn't as boring as last night's was. It put me right to sleep. - Don't worry. This story will keep you up all night. - Really? What is it? - It's called "The Disembodied Hand That Strangled People." - Gosh, this is great! How creepy! I never get a scary story! A disembodied hand! Wow! - And you know what's really scary? They never found it! To this day, nobody knows where the hand is! In fact, the hand could... OH NO! THERE IT IS! IT'S GOT ME!! GAKK!!

Bill Watterson, *The Authoritative Calvin and Hobbes*, 1990.

in which the design and control of several prototypes of underactuated hands built at Université Laval are presented and discussed. The taxonomy of the grasps is reviewed in order to select an optimal geometry for the architecture of the hands. Following this selection, a parallel precision grasp mechanism is introduced to allow the performance of pinch grasps. Subsequently, the MARS and SARAH-class hands are presented and discussed. The control algorithms used with these hands are detailed and experiments with simple control schemes are discussed. If finer force control is required, the advantages of using tactile sensors and fuzzy logic are exposed and supported with experimental results.

7.1 Introduction

Following the analyses and optimizations discussed in the preceding chapters, practical aspects are now discussed in the context of design and control of underactuated hands. Several prototypes of underactuated hands built at Université Laval are extensively presented in this chapter. The analysis and optimization of underactuated fingers (Chapters 3–5) as well as the available techniques to extend the underactuation between the fingers (Chapter 6), naturally lead to the design and control of actual prototypes. Such prototypes demonstrate the behaviour and capabilities of this technology. First and foremost, in an underactuated hand, several fingers are required to grasp an arbitrary object. Hence,

the first section of this chapter focuses on selecting the necessary number of fingers and their relative positions. The hands presented in this chapter are mainly intended for use in hazardous environments, e.g. in space. Successful grasping in a spatial environment is an important issue addressed in the literature. More specifically, in (Foster and Akin 2001), a study of the different grasping requirements for 242 existing crew aids and tools as well as during extravehicular activities (EVA) showed that over 50% of the grasps were cylindrical and three-fingered hands achieve over 90% of the required tasks. The results presented in the latter reference were used to orient the design choices presented in the subsequent sections.

7.2 Design of Laval Underactuated Hands

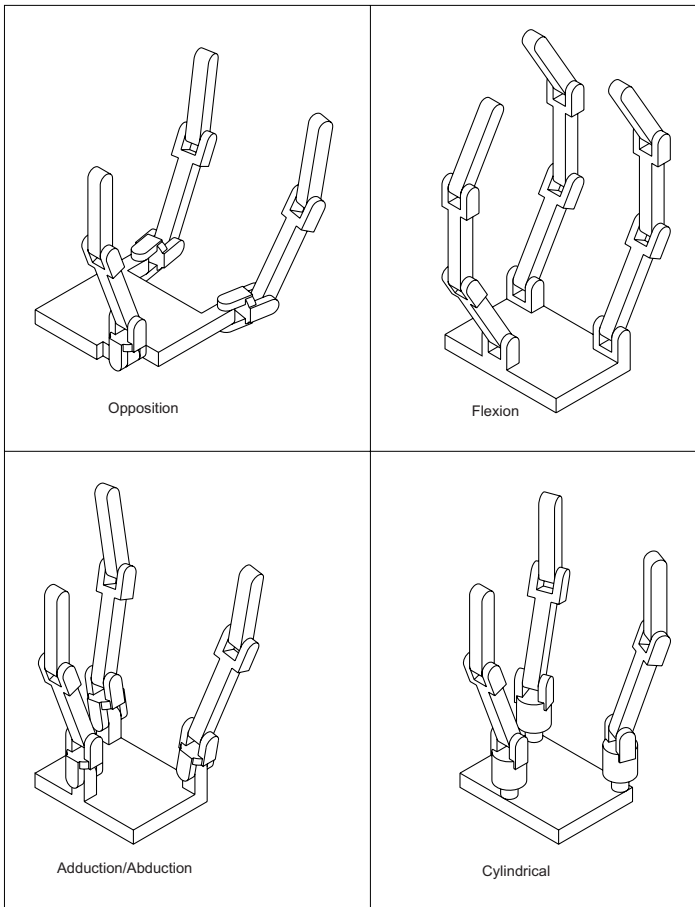
7.2.1 Location and Orientation of the Fingers

The relative orientations of the fingers allow different classes of grasps to be performed and are usually termed accordingly. Reportedly, in (Schlesinger 1919), six classes of grasps are distinguished: cylindrical, tip, hook, palmar, spherical and lateral. According to (Landsmeer 1962), these classes can be further separated into two main categories, namely power grasps (cylindrical, spherical, hook) and pinch or precision grasps (palmar, tip, lateral). Power grasps are associated with large grasping forces and with contact zones which are located along the phalanges and the palm, thereby enveloping the object. On the other hand, precision grasps are generally associated with small grasping forces and with contacts at the fingertips. The latter grasps are generally used in manipulation. This classification is closely related to the behaviour of each of the fingers. Additionally, it can be noted that the orientation of the forces on each of the fingers allows the determination of the geometry of the grasps as defined in (Schlesinger 1919). Indeed, a grasp is said to be cylindrical when all the forces are directed towards a line, spherical when all the forces are directed towards a point and planar when two fingers are in opposition. This geometry of the grasp characterizes the relative arrangement of the fingers in the hand. Classifying common grasp geometries is very useful in designing artificial hands or grippers since it allows the characterization of the capabilities necessary to achieve the desired tasks. A classification of the grasps identified above is presented in Table 7.1 with examples. It should be noted that more refined classifications exist and have been proposed in the literature, depending mostly on the applications, e.g. (Iberall and Lyons 1984; Cutkosky 1989). To be able to perform a maximal number of grasps, robotic hands have generally adopted an anthropomorphic design. However, if some classes of grasps are deemed unnecessary (e.g. hook grasp), other topologies can be employed as discussed in Section 2.1.

Similar classifications based on geometry can also be used to characterize robotic hands themselves. For instance, in (Reynaerts 1995), several families of robotic hand architectures are differentiated based on the relative configuration of the fingers: opposition, flexion, abduction, or cylindrical, as illustrated in Fig. 7.1.

Table 7.1. Grasp classification with examples

	Power	Precision
Cylindrical	wrap (e.g. hammer)	palmar (e.g. pencil)
Spherical	ball	marble
Planar	“task specific grippers”	tip or lateral (e.g. paper sheet)
Nonprehensile	hook (e.g. suitcase)	platform (e.g. service plate)

**Fig. 7.1.** Classification of dexterous hands (courtesy of Prof. Reynaerts)

In this chapter, three identical underactuated fingers are used in the design of underactuated robotic hands. Using three fingers seems a good compromise between complexity and capability for grasping since it is the minimum number

of fingers required to successfully accomplish many grasps, especially in spatial environments as discussed in the introduction of the chapter. Moreover, the three fingers are chosen identical and mounted on an additional revolute joint whose axis is located on the vertex of an equilateral triangle and oriented normal to the plane of the triangle (i.e., the palm of the hand). This arrangement corresponds to the cylindrical configuration presented in Fig. 7.1. However, this adjective should not be confused with the grasp classification, i.e., a cylindrical hand can perform other types of grasps than cylindrical. With additional revolute joints mounted at the base of the fingers, the hands can be reconfigured by modifying the orientation of the fingers in order to adapt to the general geometry of the object to be grasped. This feature is widely used in the literature (Ulrich 1988; Bartholet 1992; Guo et al. 1995) with several different implementations.

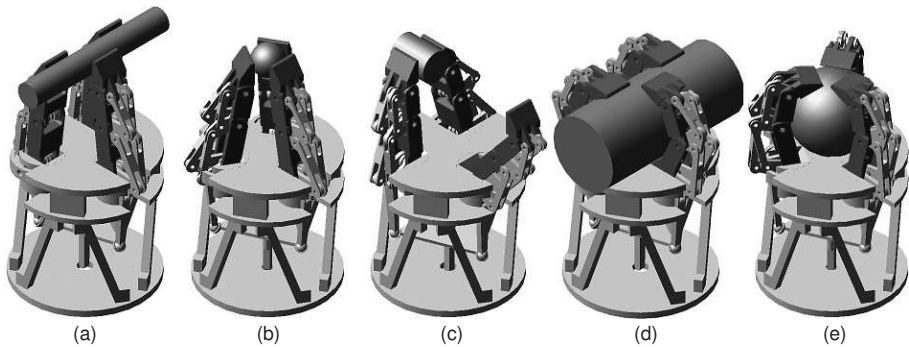


Fig. 7.2. Typical grasps (from (Myrand and Gosselin 2004)): (a) precision cylindrical, (b) precision spherical, (c) precision planar, (d) power cylindrical, (e) power spherical

The main grasping configurations of the fingers available are thereupon: cylindrical, spherical and planar, illustrated in Fig. 7.2 from (Myrand and Gosselin 2004). In the cylindrical configuration, two fingers point in the same direction while the third one points in the opposite direction and moves between the other two. This is the preferred configuration to grasp cylindrical/prismatic objects or objects where one dimension is significantly larger than those of the hand. In the spherical configuration, the three fingers are oriented towards the centroid of the triangle formed by the base joints of the fingers. This configuration is the preferred choice to perform enveloping grasps of objects with sizes close to the size of the hand or with no distinct particular axis. In the planar configuration, two fingers are directly facing each other and the third finger is not used. This configuration is used for pinch grasps, usually of objects with small dimensions. The implementation of these configurations will be illustrated for the robotic hands presented in the chapter.

The distance between the base of each of the fingers, or the size of the palm, raises issues which are similar to what must be considered when choosing the lengths and length ratios of the phalanges. A large palm allows the grasping of relatively large objects while a small palm allows the grasping of relatively small objects. Knowing the size of the objects to be grasped, the size of the palm

can be determined by simulation. Also, the minimum and maximum size of the objects that can be grasped can be computed from geometric relationships. A reasonable size of the palm can also be estimated from a review of the dimensions of robotic hands presented in the literature, i.e., one can obtain an average value leading to a reasonable choice. For instance, in (Laliberté and Gosselin 1998), a ratio of approximately 0.56 between the size of the palm and the lengths of the fingers was found. Hence, with fingers 10 cm long, the distance between the fingers should be from 5 to 6 cm.

7.2.2 Pinch Grasp Mechanism

Underactuated fingers cannot usually perform precision or pinch grasps, since maintaining the distal phalanges parallel to each other with objects of different sizes is not possible with the mechanisms previously presented in the book. Nevertheless, this feature is highly desirable since it allows secure grasps when only the tips of the fingers are used. It also allows the grasping of very small objects. Please note that the adjective “secure” as used in this chapter refers to a grasp which is both stable in the sense of the book and force-closed. Pinching is a simple feature often feasible (or even standard) with simple mechanical grippers. A two-phalanx three-finger underactuated hand, namely Bartholet’s hand (Bartholet 1992), illustrated in Fig. 7.3, resolved this issue with a very ingenious mechanism. This solution is based on a disengaging cam mechanism, presented in Fig. 7.4. The cam 81 is maintained in contact with the roller 112 during the pre-grasping motion of the finger and during pinch grasp. However, in power grasps, this contact can be broken allowing the distal phalanx to close on the object seized.

A mechanism achieving a similar behaviour with the distal phalanx of a three-phalanx underactuated finger was developed in (Gosselin and Laliberté 1996) and is illustrated in Fig. 7.5. It is composed of two parallelograms mounted in series. This mechanism is coupled to the phalanges of the finger but not to the other links of the shape adaptation mechanism (it is moving on a parallel yet distinct plane). Its aim is to constrain the orientation of the distal phalanx relatively to the palm until contact is made with the object, without sensors to detect this contact. If the latter happens with the distal phalanx itself, the finger is fixed (assuming that the object is seized). On the other hand, if contact is made with the proximal or intermediate phalanx, the mechanism is automatically disengaged and the distal phalanx can close on the object. Two mechanical limits with springs at the top and bottom ends of the mechanism allow precision grasps to be performed while maintaining the shape adaptation capability for power grasps if necessary.

Referring to Fig. 7.5: the finger is shown in (a) in its initial configuration, the parallel pinch mechanism is in plain lines while the usual transmission linkage is represented with dashed lines, both are moving in parallel planes. Note that only the usual transmission mechanism is actuated, the parallel precision grasp mechanism is passive. In configuration (b), a parallel motion of the distal phalanx is accomplished ending in a pinch grasp of an object, the parallelogram mechanism

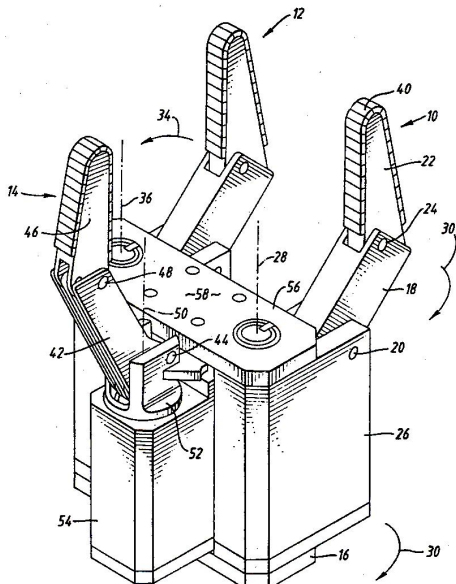


Fig. 7.3. Bartholet's hand

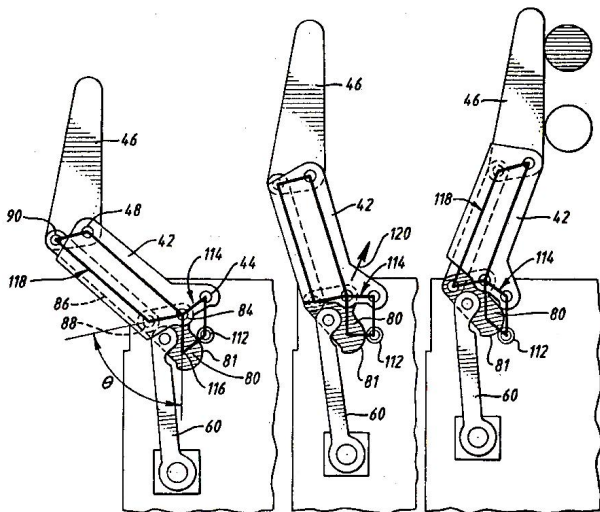


Fig. 7.4. Bartholet's parallel cam-linkage for pinch grasps

is maintained on its mechanical limits. In (c), a power grasp is performed with contacts on all phalanges. In this case, the parallelogram mechanism is moved away from its mechanical limits and the distal phalanx is no longer maintained perpendicular to the palm in order to close on the object. This mechanism will be used with all the subsequent prototypes of underactuated hands presented in this chapter.

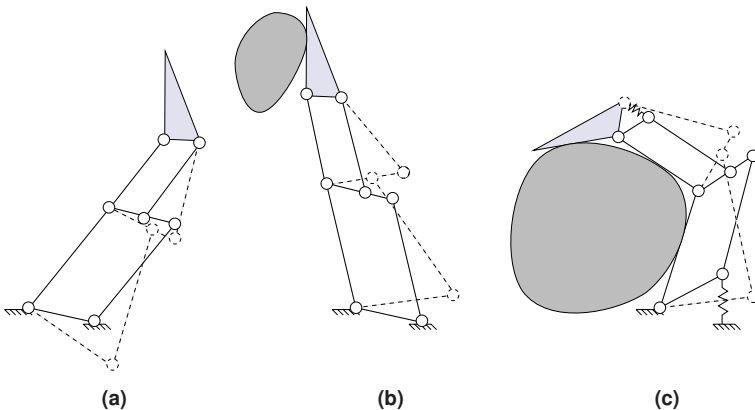


Fig. 7.5. The parallel precision grasp mechanism (plain lines)

7.2.3 The MARS Hand

This first underactuated hand built at Université Laval was the MARS hand (Gosselin and Laliberté 1996), an acronym for “Main Articulée Robuste Sous-actionnée” or “Minimally Actuated Robotic System.” This prototype was built in 1996 as a testbed in order to experiment underactuation in fingers and study grasping strategies (Gosselin et al. 1998). This prototype is illustrated in Fig. 7.6. The surface of the fingers is flat since this is simple to machine and well suited for grasping. The tip of the fingers is not rounded—as it is often seen in other robotic hands—in order to allow the grasping of small objects on a flat surface during pinch grasps, cf. Section 7.2.2. The fingers have a total length of 16.5 cm from the first joint to the tip, and a width of 4 cm. The length of the phalanges are respectively, from base to tip: 7 cm, 5 cm and 4.5 cm. The lengths of the transmission linkages have been optimized using the technique described in Section 5.3.2 and illustrated in Fig. 5.11. The distance from the centroid to the vertices of the equilateral triangle constituting the palm is 6 cm. Each of the three fingers is mounted on top of an actuation module. These modules are mounted on a mainframe and can be independently rotated in order to obtain different grasp configurations, as illustrated in Fig. 7.7.

The actuation module comprises an actuator (a DC brushless motor) driving the opening and closing motion of a finger. The transmission of the actuator to the finger is composed of a ballscrew in order to obtain large forces, and a timing belt in order to obtain compact modules and allow the modification of the transmission ratio. Note that since a ballscrew is used, the fingers are backdrivable. Each module also comprises a small gearmotor to drive the orientation of the finger. The transmission is performed via a gear attached to the actuator and another attached to the mainframe. The three fingers can be rotated by 60 degrees, as illustrated in Fig. 7.7. Infinitely many configurations can be obtained, including the three main configurations previously introduced in Section 7.2.1.

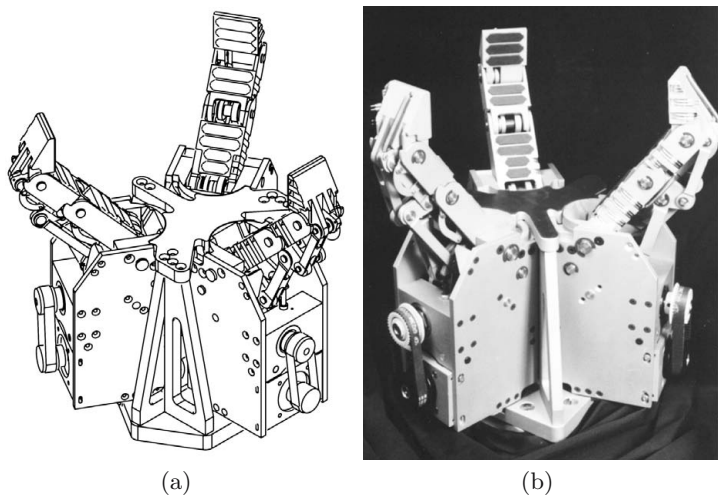


Fig. 7.6. CAD model and picture of the 12-DOF 6-DOA MARS hand

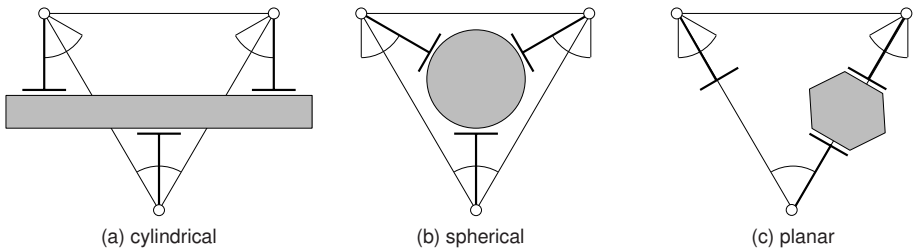


Fig. 7.7. MARS finger orientations

Since each finger is driven by two actuators—one to drive the phalanges and one to change the orientation of the finger—the hand has a total of six actuators. Each finger has three grasping DOF and one orientation DOF for a total of 12 DOF for the hand. The total mass of the hand is approximately 9 kg. The parts are made of aluminum, the shafts and screws are made of steel and the bushings are made of reinforced nylon. The design of the MARS hand is protected by US (US 5,762,390) and Canadian (CA 2,209,863AA) patents.

7.2.4 The SARAH Hands

In order to further reduce the number of actuators and hence decrease the complexity of the controller required, underactuation can be introduced not only into the fingers but also among them, with the technique presented in Section 6.2.4, namely a geared differential (termed the “hyperdifferential”). Also, by keeping only the most useful finger orientations with respect to the base, cf. Fig. 7.7,

it is possible to couple the orientation of the fingers. Several prototypes of underactuated hands, the SARAH-class hands, have been built based on these two improvements. SARAH is an acronym for Self-Adaptive Robotic Auxiliary Hand. In addition to using underactuation in the fingers, introducing underactuation among them and coupling the orientation of the fingers leads to a robotic hand with ten DOFs and only two actuators (two DOAs). One actuator is used to drive the underactuation system which controls the opening/closing of all three fingers. The second actuator is used to drive the orientation of the fingers. The possible grasps are essentially the same as with the MARS hand. The only previously validated task not possible is the grasp and activation of a screwdriver.

To ensure secure grasps and high stiffness, the transmission should not be backdrivable. Indeed, if each finger is self-locking (not backdrivable), the grasp will be secured independently of the position or shape of the object. This is especially of interest during cylindrical grasps where two fingers are opposing a single one. With the MARS hand, it was possible to control the actuation torque of each finger independently and thus, ensure force-closure. However, with the SARAH hands, only one actuator is available for the closing of all fingers and this might be problematic when a single finger opposes the other two. The mechanism used to ensure non backdrivability with the SARAH hands is based on ACME screws which require a rotating motion as input. It should be noted that this is not compatible with the floating platform, cf. Section 6.6.1, which could have been used to drive the three fingers but has mainly a linear output. The three outputs of the hyperdifferential drive three ACME screws and each finger is directly attached to one of these screws. The hyperdifferential is mainly composed of two stages of planetary gears. Its behaviour corresponds to required properties, the adaptability of the fingers is good and the force available is maximized. However, the mechanism involves a large number of gears (16) which complexifies the design and assembly. The coordination of the unconstrained fingers results from the fact that the stages of the differential tend to stay synchronized when the fingers are unconstrained. When the thumb is constrained, the other two fingers move at the same speed (1.5 times the unconstrained speed). When one of the fingers is constrained, the other finger will go twice the unconstrained speed and the thumb at the unconstrained speed. When any two fingers are constrained, the other finger will move three times the unconstrained speed.

The main configurations of the fingers are obtained by orienting two of the fingers within a range of 90 degrees, as illustrated in Fig. 7.8. The rotation of the two fingers is coupled by a geared mechanism, shown in Fig. 7.9. The two sections of gears are attached to the two orientable fingers. In the planar configuration, where the third finger is not used, its closing motion is blocked at the hyperdifferential level by a stopper activated by the orientation mechanism. The purpose of the orientation transmission is to use one actuator to drive the two rotating fingers. This rotation is synchronized by the gearing system and the fingers rotate in opposite directions. The input gear, attached to the input shaft, directly drives the finger 1 gear. The second finger gear, driven via a free

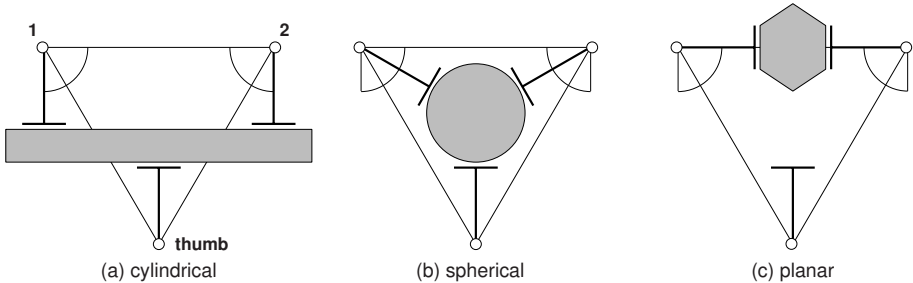


Fig. 7.8. SARAH finger orientations

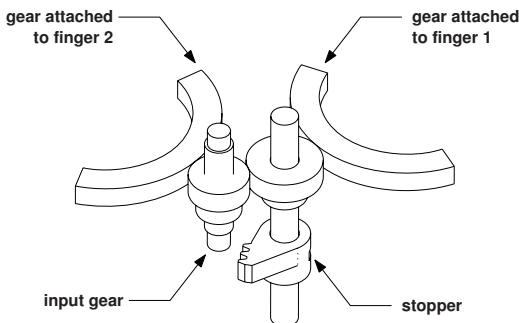


Fig. 7.9. The orientation mechanism

gear, is attached to a free shaft to obtain a rotation of the second finger in a direction opposite from that of the first finger.

In some versions of SARAH, a four-position Geneva mechanism is used between the actuator axis and the input shaft, illustrated in Fig. 7.10. Because of this mechanism, discrete positions, with 90 degrees between each of them, are obtained. At the finger level, it is desired to obtain cylindrical, spherical and planar orientations. The cylindrical and spherical orientations are separated by 30 degrees (cf. Fig. 7.8). The spherical and planar orientations are separated by 60 degrees. With an intermediate orientation, termed elliptical, between spherical and planar, we obtain four useful configurations separated by 30 degrees each. To convert the 90 degrees steps of the input shaft to the 30 degrees steps of the fingers, the ratio between the input gear and each of the finger gears is 1/3.

When the fingers are oriented in the planar configuration, the two rotating fingers are facing each other and the third finger should not be involved in the grasp. Therefore, this third finger should be kept opened only in this case. In order to obtain this behaviour, a stopper part, equipped with teeth compatible with the teeth of the output gears of the hyperdifferential, is attached to the orientation shaft (cf. Fig. 7.9). The teeth of the stopper part engage with the output gear of the hyperdifferential corresponding to the finger to stop only when the orientation shaft is in the planar position.

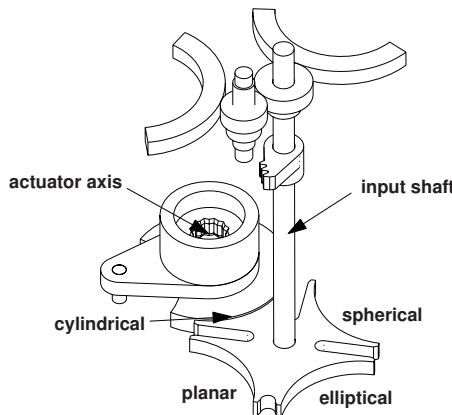


Fig. 7.10. Geneva mechanism used to select the orientation of the fingers

When the Geneva mechanism is in the moving phase, the pin of the Geneva input is in one of the four slots of the Geneva output. During this phase, the Geneva input moves the Geneva output by 90 degrees. When the Geneva mechanism is in the dwell phase, the Geneva output is locked by the locking disk of the Geneva input and the Geneva input is free to rotate allowing some tolerance in the actuator shaft orientation. During this phase, the fingers are locked in their orientation. In order to restrain the orientation of the fingers in the four positions, one of the slots of the Geneva output is filled to stop the rotation of the Geneva mechanism. In general, this mechanism allows self-locking of the fingers even if they are not driven, allows positioning errors of the Geneva input and free motion of the Geneva input during the dwell phase.

The design of the SARAH hands is protected by a US patent (US 6,505,870), a Canadian patent (CA 2,406,921) as well as by a pending WIPO patent (WO2001/091979). A summary of the characteristics of the MARS and SARAH hands is presented at the end of this section, in Table 7.2¹.

SARAH M1

The prototype M1 of the SARAH class hands has been developed as a collaborative effort between MD Robotics Limited (now MDA Space Missions) and Université Laval (Rubinger et al. 2001; Rubinger et al. 2002). This hand is adapted as an end-effector to the Special Purpose Dextrous Manipulator (SPDM) of the Canadian Space Arm (a.k.a. SSRMS) used in the International Space Station (ISS), illustrated in Fig. 7.11. Note that while SARAH M1 is a realistic proof of concept, a space qualified version, including correct materials, lubricants, etc., is still to be developed.

In this case, the power is provided by the socket torque and advance available at the end of the SPDM. The socket advance has only limited power and

¹ Size ratio with respect to the human hand.

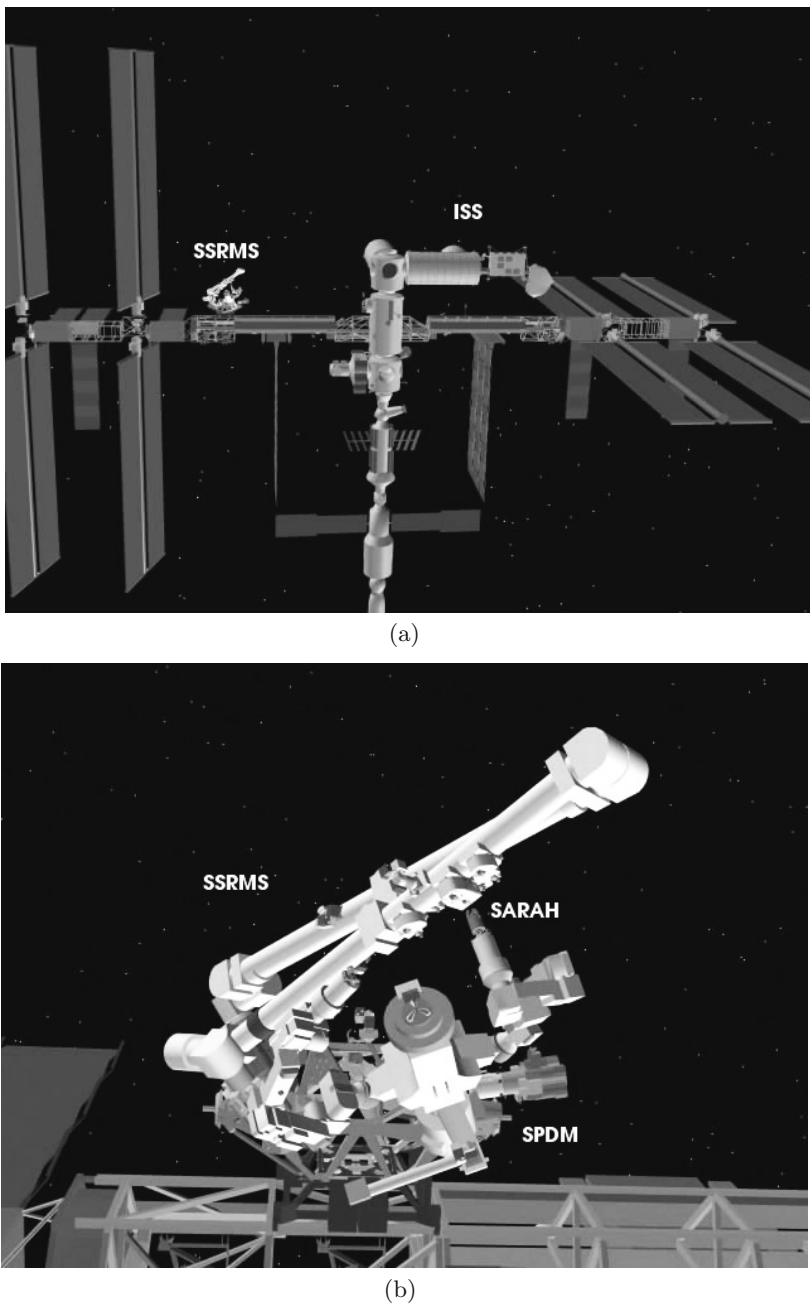


Fig. 7.11. SARAH M1 used as an effector on the International Space Station (courtesy of MDA Space Missions)

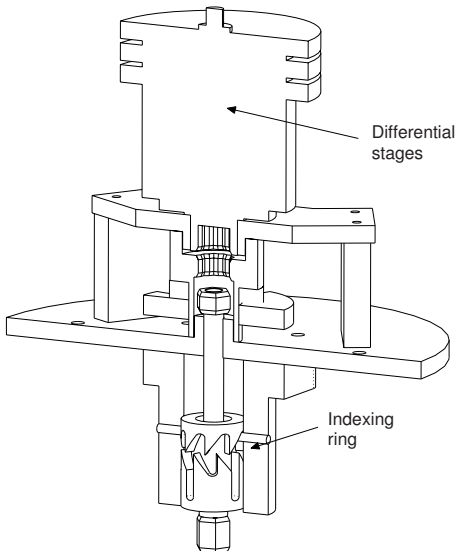
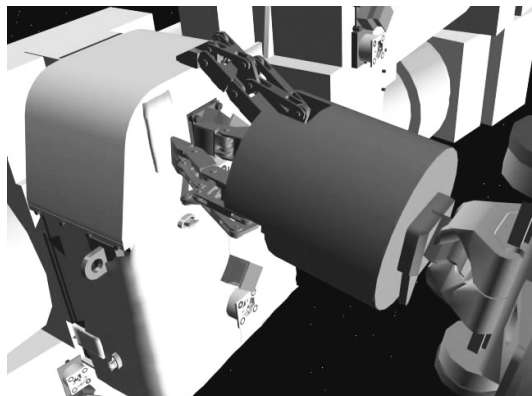


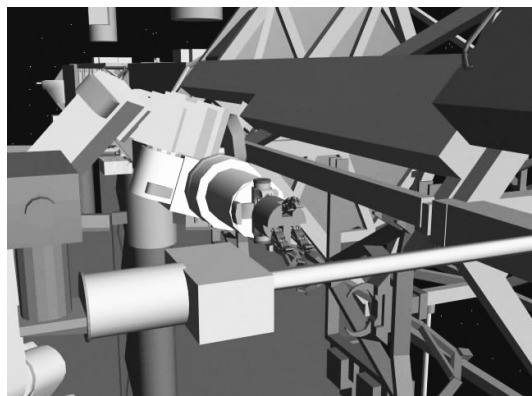
Fig. 7.12. Switching mechanism

control possibilities, therefore the two tasks (open/close and orientation) must be actuated by the powerful and controllable socket torque. The switching of the power of the socket torque between the two tasks is performed by the socket advance with the help of an indexing mechanism, illustrated in Figure 7.12. The power of the socket torque is transmitted to the sockets of the differential or orientation mechanism through the main shaft. It is free to rotate and translate in the hole of the bottom plate, and includes nuts at its ends. An indexing ring is free to rotate but fixed in translation on the main shaft. Indexing pins are attached to the interface and are inserted in the grooves of the indexing ring in order to guide the motion of the indexing ring. A compression spring is inserted on the main shaft, between the bottom plate and a shoulder on the main shaft, in order to keep the main shaft backwards. In this position, no mechanism sockets are engaged. When the socket pushes on the main shaft, it advances against the spring. This advance is stopped by the indexing pins up to a position that engages the main shaft on one of the two mechanism sockets, depending on the length of the groove engaged. Then, if the socket torque is activated, the corresponding mechanism is activated. Each time the socket is released and advanced, the power is switched between the two mechanism sockets.

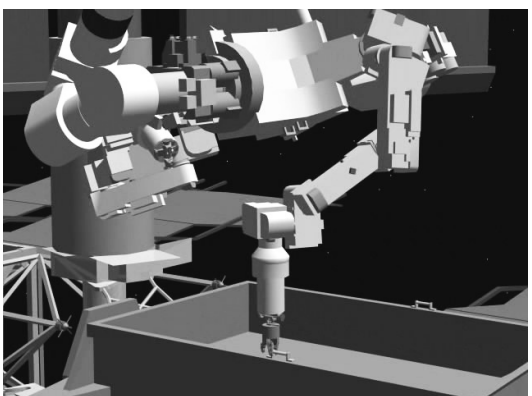
The key feature of SARAH M1 is that it is a completely self-contained, passive mechanism requiring only the existing SPDM driving unit to actuate its fingers. Hence, this hand has neither actuators nor sensors which are difficult to operate in space. The overall envelope of SARAH M1 is similar to that of an astronaut glove. Furthermore, SARAH M1's force capabilities are similar to those applied by an astronaut in a typical EVA activity. Several possible Extra Vehicular Robotics (EVR) operations for SARAH M1 have been identified and



(a) Thermal blanket removal



(b) Camera relocation



(c) SPDM stabilization

Fig. 7.13. Applications of SARAH M1 on the International Space Station (courtesy of MDA Space Missions)

include: SPDM stabilization when operating on the end of the SSRMS in an unplanned environment, thermal blanket manipulation, electrical/fluid connector actuation, Articulating Portable Foot Restraint (APFR) and re-locatable cameras installation/removal, and the manipulation of Orbital Replacement Units (ORU) with crew handling features such as handholds. Illustrations of these applications are presented in Fig. 7.13.

SARAH M1 would allow the robotic exchange of many of the current EVA ORU leading to a further reduction in crew time spent on station maintenance. In addition, for ORU that remain exclusively EVA, the SPDM equipped with SARAH M1 could be used to set up the worksite before the crew arrives and tear down the worksite after the crew is finished. This robotic support allows the crew to focus on high value added tasks which leaves more time to do more important functions like science.

SARAH M1 is a realistic proof of concept of the application of underactuation to grasping tasks and its great potential, especially in hazardous environment. SARAH M1 is built mainly of anodized aluminium for better surface resistance, shafts are made of steel, joints are made of reinforced nylon bushings, and gears of brass or steel. The surface of the fingers is covered by rubber to increase the friction. SARAH M1 is illustrated in Fig. 7.14

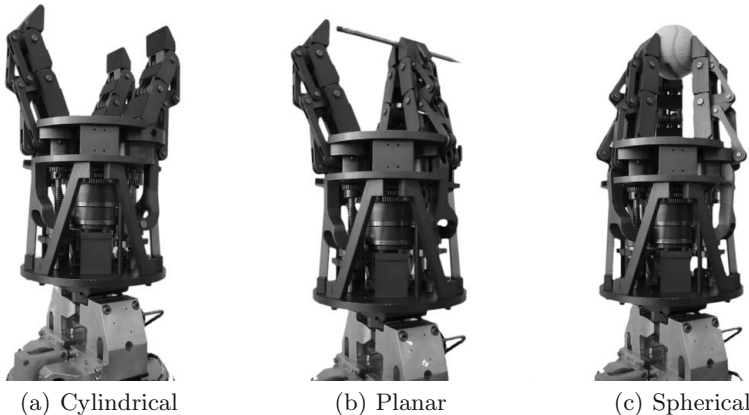


Fig. 7.14. Grasp configuration examples with SARAH M1

SARAH P1

The prototype SARAH P1 is a replica of SARAH M1 made of plastic with the help of a rapid prototyping machine. The purpose of the P1 prototype was to rapidly validate the mechanisms chosen and the global concept. It is also often used as a simple tool for demonstration.

The use of rapid prototyping is very efficient since a prototype can be obtained rapidly and soon in the design process. On the other hand, since it is made of deposited plastic, it is much less robust than the metal version. Also, the

precision of the plastic parts is rather limited. Hence, in order to ensure the functionality of the prototype, the most critical parts are made of metal, e.g., the transmission screws and the input shaft. Nevertheless, SARAH P1 can only be driven manually or with an electric screwdriver.

Even if the plastic prototype is not an exact copy of the metal prototype, it provides an effective means of qualitatively evaluating the real system. The functionalities of SARAH have been validated. All the functions of SARAH P1 were shown to work properly, including: the fingers, the underactuation between the fingers, the transmission screws, the orientation mechanism and the switching mechanism. The forces that SARAH P1 can sustain are 2.0 kg in cylindrical power mode and 0.5 kg in planar precision mode.

SARAH CSA

The SARAH CSA hand, developed for the Canadian Space Agency, is shown in Fig. 7.15. This hand has been mounted on the tip of one of the two arms of the CSA Automation and Robotic Testbed (CART). The size and configuration of the CART are similar to those of the SPDM (Rubinger et al. 2002). While the CART is a research facility, it is also used for astronaut training. With SARAH CSA mounted on the CART, the ability to perform a number of EVA operations was demonstrated. Among others, SARAH CSA was used as the grabber in a simulation of satellitic capture, where one arm of the CART was the chasing satellite and the other the target satellite. The CART is also equipped with a teleoperation facility that allows emulating control of a space robot from the ground.

By contrast with SARAH M1, the CART version is a stand-alone end-effector that has its own actuators. One interesting feature of the installation of SARAH on CART is the use of a high-speed data bus to control the hand. CSA is currently working on the utilization of the hand through teleoperation and through autonomous control. In this last mode, the planning of grasping poses needs to be included. Using a dragonfly camera, illustrated in Fig. 7.16, an automated grasp planner has been proposed (Boivin et al. 2004; Boivin and Sharf 2005) taking into account the particular geometry of the SARAH hands. The algorithm presented was dedicated to the grasping of planar (pinch or precision grasps) and revolute (power grasps) objects. Experiments reported successes for the majority of objects, even with unpredicted and peculiar shapes (e.g. a glue gun).

Since the prototype of this version of the hand was designed to be mounted on the CART, it is scaled by a factor of 0.7 compared to SARAH M1 and its weight is 3.2 kg.

Pneumatic SARAH

One of the most complex parts of the SARAH hands is the gear differential mechanism that provides the underactuation between the fingers. A much simpler substitute of this differential could be used in the case of pneumatic or hydraulic actuation, namely a distributor constituted of two T-pipe connections

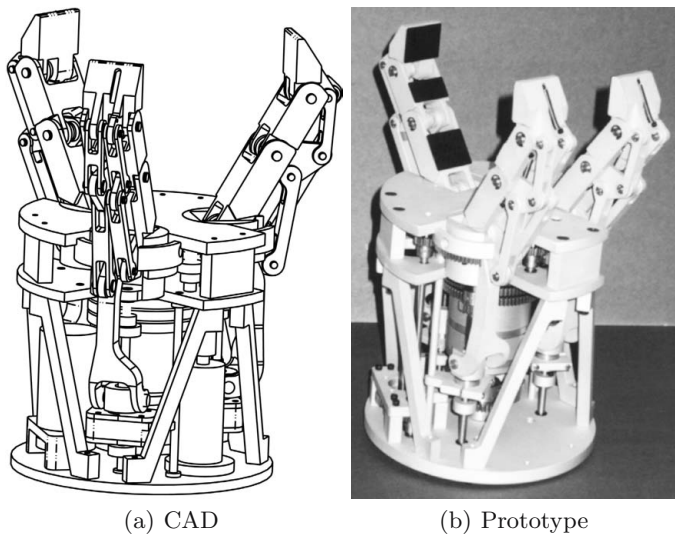


Fig. 7.15. The SARAH CSA hand

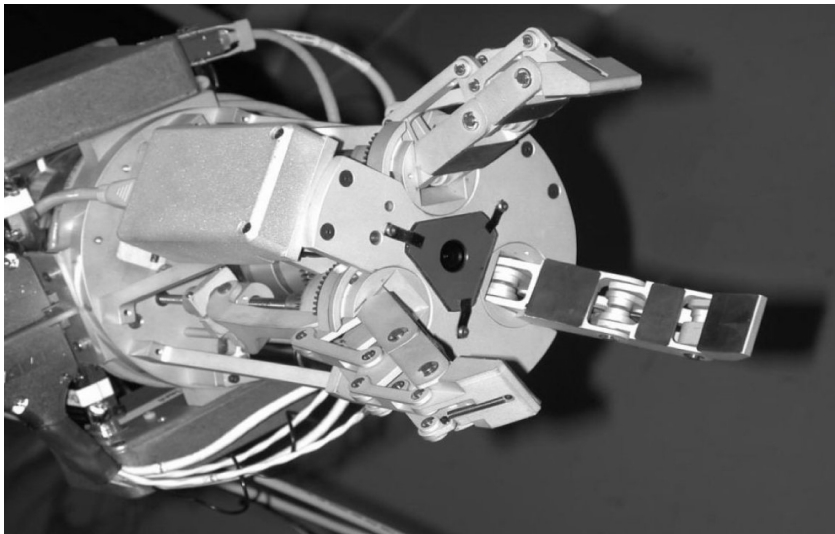


Fig. 7.16. SARAH CSA mounted on the CART and equipped with a camera (courtesy of Prof. I. Sharf)

in series as discussed in Section 6.2.3. This simple scheme produces three outputs with one input. Furthermore, in many applications, hydraulic or pneumatic actuation is standard and therefore, a prototype taking advantage of the latter is a great substitute to standard grippers.

A plastic model, named Pneumatic SARAH (a.k.a. Air SARAH), was built using a rapid prototyping machine, similarly to SARAH P1. This hand is the smallest of all the SARAH class underactuated hands. Three pneumatic cylinders are used for closing the fingers in combination with three flow control valves. The valves are manually adjusted to set the closing speed of the fingers. The force of the fingers can be controlled by the air pressure of the first air supply. A push button is used to let the air flow that closes the fingers.

Two other pneumatic cylinders are used for orienting the fingers and a three-position switch is used to direct the flow to one of the cylinders or to disrupt it, thus selecting one of the three grasp configurations. The result is a relatively low-cost multi-functional underactuated robotic hand that can fit onto an industrial robot, if an appropriate interface and compressed air are supplied. One pressure-regulated source is sufficient in addition to several binary outputs. Its functionalities, size, and lightweight make this hand a good demonstration towards a potential replacement for current prosthetic hands driven by linkages. Air SARAH is illustrated in Fig. 7.17

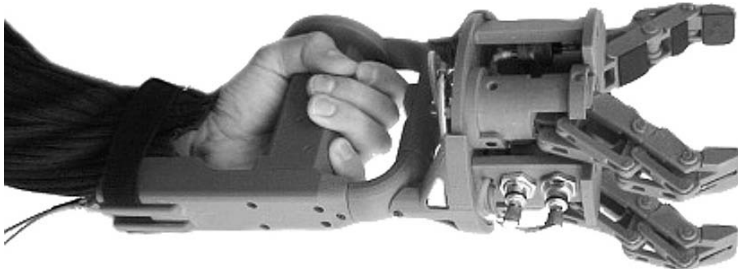


Fig. 7.17. Pneumatic SARAH

SARAH UKAEA

This robotic hand was developed for the United Kingdom Atomic Energy Authority (UKAEA). The main business of UKAEA is the clean-up of nuclear sites. One of their tasks is to retrieve radio-active waste or contaminated material from old storing sites in order to package and store it in safer conditions. The retrieval of contaminated material is a timely and complex task. The objects to be collected consist mainly of cans and a variety of debris. Presently, several grippers are used, each one being adapted to a specific type of object. Unfortunately, the changeout of the grippers is time consuming. The use of a more flexible gripper that can replace several specialized grippers facilitates and accelerates the retrieval process.

This flexible gripper is adapted from the SARAH class hands. In order to satisfy the requirements of the material retrieval tasks, several components were redesigned. Among others, SARAH UKAEA has a significantly larger payload (100 kg) and is adapted to a radio-active environment. Also, the tip of the fingers is manually reconfigurable between a standard tip and a 'hook' tip. This allows

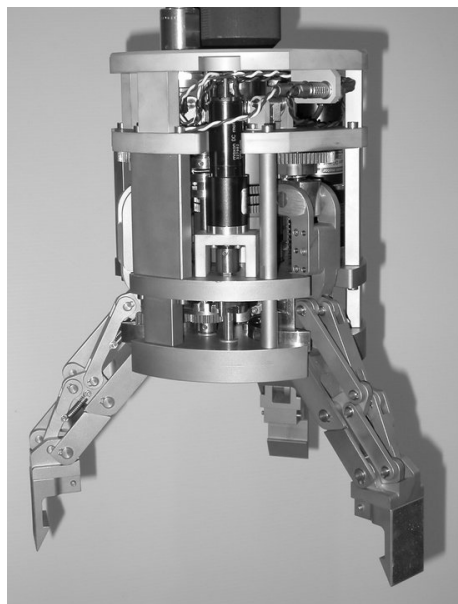


Fig. 7.18. SARAH UKAEA

the grasping of heavy cans located in confined spaces as well as the handling of a variety of objects. SARAH UKAEA, illustrated in figure 7.18, began to be used for radio-active material retrieval in 2007.

7.3 Control and Experimentation of the Laval Underactuated Hands

7.3.1 Hybrid Control of the MARS Hand

Before performing a grasp, the geometry of the object should be determined and the hand should adjust itself to this geometry by orienting the fingers. To orient the fingers, a simple trajectory is generated to a prescribed position and the servomotors follow this trajectory with a PD or PID position control.

When the grasp is to be performed, a closing trajectory is generated up to a fully closed position. The closing trajectory is followed by the closing actuator using again a PD position control loop. The position of the motors is obtained from optical encoders. In order to limit the grasping force applied on the object, a maximum motor torque is set to a desired value. The relationship between the force on the object and the torque of the motor can be obtained either by using the results of Chapter 3 or by calibration. To set the maximum torque of the motor, it is assumed that the voltage is proportional to the current in the motor—which is true when the motor is stalled, i.e., when a grasp is performed—and that the current at the motor is proportional to the torque generated. When the

Table 7.2. Main characteristics of the Laval underactuated hands

	MARS	SARAH P1	SARAH M1	SARAH CSA	Air SARAH	SARAH UKAEA
Year	1996	1999	2000	2001	2002	2006
Size ratio	1.6	1.4	1.4	1.2	1	1.8
Weight (kg)	9	1.6	5	3.3	1	25
Actuation	3 DC 3 BL	2 (external)	2 (external)	2 DC	5 pneumatic cylinders	2 DC
Finger DOF	3	3	3	3	3	3(4)
Orientation DOF	3	1	1	1	1	1
Total DOF	12	10	10	10	10	10(13)
Payload (kg)	70	n.a.	23	7	n.a.	100
Sensors	position tactile	none	none	position	none	none
Patent	US5762390	US6505870	US6505870	US6505870	US6505870	US6505870
Note		built with FDM rapid-prototyping	SPDM end-effector	CART end-effector	built with FDM, hand-held	Nuclear waste retrieval

grasp is performed, since the PD position control tries to reach the fully closed position, the force on the fingers corresponds to the maximum voltage set due to the large values of the gains.

The forces generated at the phalanges are not known accurately since no exact information on the configuration of the finger or contact locations is used in this position control technique. The grasping force is therefore a coarse approximation depending on the maximal torque imposed by the controller, it can be considered light (30% of the maximum torque), average (50%), large (70%) or very large (90%). This approximation is sufficient in most practical cases. Overall, the control strategy uses a closed-loop position control cascaded with a saturating open-loop force control. Hence, the final controller is very simple and computationally efficient. With this control scheme, the grasping forces are set and the resulting forces on the object is zero. If external forces are applied on the object they must be compensated for. This compensation is handled differently with the MARS and SARAH hands. With the MARS hand, the basic principle is to provide additional force to the fingers that are being pushed against by the external force and leave the force on the other fingers unchanged. To implement this functionality, an additional PD position control loop reacts only when a finger moves backwards from the initial grasping position. This PD control can be adjusted to yield a more or less stiff reaction to the external perturbations on the object.

If the hand loses the object, the fingers will suddenly close—the fingers will reach high velocities—since the fingers are very far from their prescribed position. This has two consequences: first, the loss of the object is immediately perceived and second, the high speed of the fingers could damage the hand or the object. Therefore, the velocity of the finger should be limited to a given maximum speed. To achieve this, the voltage at the actuator is set to zero when the velocity exceeds the given limit. This will not stop the finger but will ensure that the speed limit is not exceeded.

Since the hand has six actuators, an interface was developed to integrate the commands of each of the fingers. Each of the fingers can be controlled separately in position, velocity and force, but it is also possible to use the simple commands such as “close” and “open” for the whole hand. For the orientation, it is possible to prescribe a general orientation to each of the fingers independently, but also to prescribe directly the type of geometry of the grasp (spherical, cylindrical, planar) and the orientation of each of the fingers is automatically generated. The appropriate finger positions and relative forces will be set automatically depending on the orientation of the fingers. With position control, for a planar grasp, the finger not involved in the grasp will not move. As an example, to achieve force-closure, the finger opposing the other two in the cylindrical grasp must be set to twice the force of the others. Therefore, when the “close” command is given, the hand behaves properly.

In order to eventually develop and study finer force control as will be developed in Section 7.3.2, other sensors were added. Two potentiometers are mounted in each of the fingers in order to measure the position of the intermediate and

distal joint angles, giving the configuration of the fingers. Also, tactile sensors placed along the fingers, give the position of the contact points and provide information on the force at these contacts. It should be noted that none of these sensors were used in the control technique discussed in the present section.

The hand was tested on a GMF-S300 manipulator as illustrated in Fig. 7.19. The objective of the experimentation was to confirm the variety of shapes and sizes of objects that can be successfully grasped, the weight of these objects and the ability of the hand to grasp objects lying on a flat surface. Also, the characterization of the hand and the experimental validation of the control scheme were important issues.

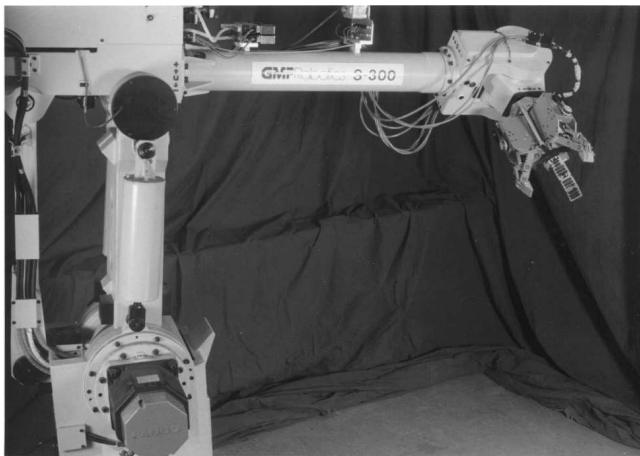


Fig. 7.19. The MARS hand mounted on a GMF-S300

In order to test the adaptability of the hand, a wide range of objects were grasped. The objects are first placed manually in the hand to show the ability to grasp virtually any object in many orientations. Then, objects are grasped from a flat surface. The pinch grasp mechanism has shown to be very useful in this situation. The smallest sphere grasped is a marble (approx. 1 cm diameter) and the largest is a volleyball (approx. 21 cm diameter). The smallest object grasped using a power grasp is a cylinder (2.5 cm diameter). Other objects grasped include a box, a chair, a disk, a tube, a boot, a baseball glove, a wooden bar, a screwdriver, a hammer, a barbell, a tennis ball, and a sheet of paper. Generally, the MARS hand performed extremely well and is able to grasp several objects with complex shapes without any problem. Examples of grasps are shown in Fig. 7.20.

To test the power of the hand, heavy objects were grasped and lifted. The ultimate test was to lift a person. The hand first grasped a steel bar and then a person was suspended from the steel bar. The combined weight was 70 kg. Note that this mass is more than seven times the mass of the hand itself. The

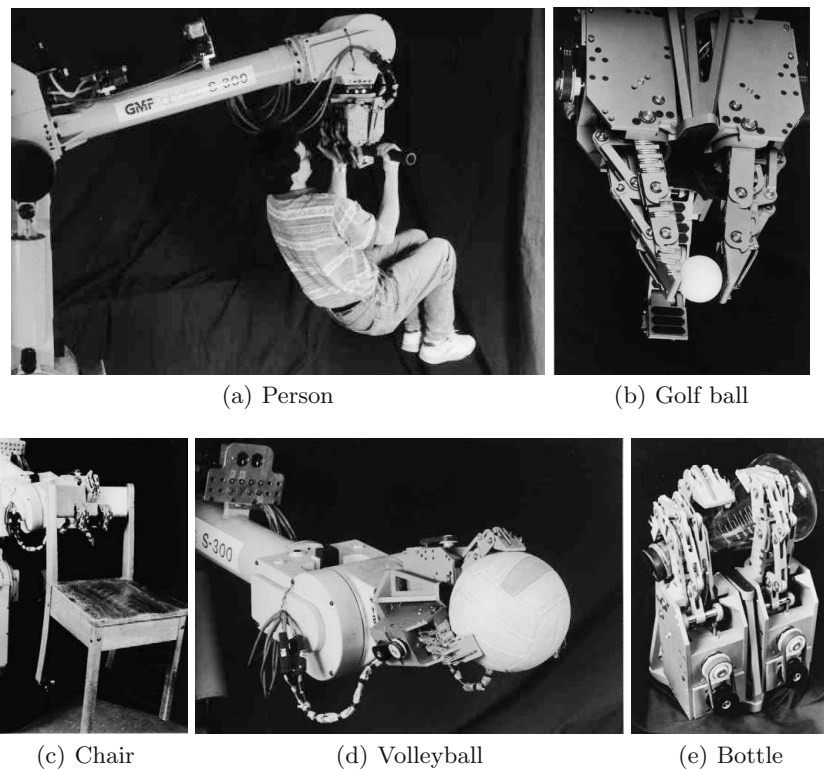


Fig. 7.20. Examples of grasps performed with the MARS hand

mechanical structure of the hand was designed to securely lift 90 kg in any orientation.

A special task successfully performed was to use a first object (a tool) to lift a second object. An example was to grasp a hammer and to lift the chair with the hook of the hammer. Another special task was to grasp an electric screwdriver with two fingers and to use the third finger to push the button and activate the screwdriver. This worked in two different configurations: in a power grasp and in a pinch grasp. The power grasp is more stable but the pinch grasp is more flexible, the axis of the screwdriver being normal to the palm. The width of the fingers and the size of the hand may make it cumbersome in constrained situations. For example, the handle of a suitcase is usually too small to be grasped with a power grasp and a different grasp must be used. Experiments performed without the use of the tactile sensors tend to show that these sensors are not required in many grasping tasks. However, the hand could not grasp very fragile objects, and the information on the grasp is limited since there is no sensorial feedback except for the position of the actuator axes. In that case, visual feedback is very useful, if available.

7.3.2 Force Control of the MARS Hand

The phalanges of the MARS hand are equipped with Force Sensing Resistors (FSR, see Fig. 7.21)—three for the proximal phalanx, two for the intermediate phalanx, and three for the distal phalanx—to allow experimental testing of the relevance of tactile sensing to control underactuated hands.

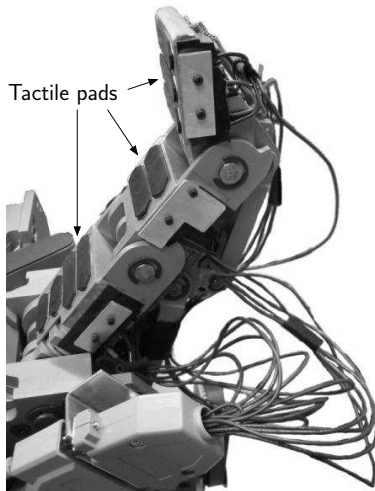


Fig. 7.21. MARS finger equipped with tactile sensors

Tactile sensors are devices providing pressure data and often distribution of the latter on the sensors. These sensors are intended to provide robots with the sense of touch and generally use matrix technology. Such devices have numerous applications for robotic hands (Liu et al. 1995; Son and Howe 1996; Maekawa et al. 1996; Choi et al. 1998; Zhang and Chen 2000; Maeno et al. 2000): slip-page detection, friction coefficient estimation, vibration detection, internal efforts control, contact geometry estimation, grasp stability enhancement, mechanical impedance control, etc. However, tactile sensors have been reported to be prone to noise and to have a limited range of measure. With the MARS hand, the limited amount of control available over the behaviour of the hand is penalizing from a control point of view. Nevertheless, with additional sensors, one can try to make the control more intelligent without becoming too complicated. Indeed, the complexity involved in controlling multifingered fully-actuated robotic hands, as discussed in Chapter 2, is usually linked to the number of actuators required. Our approach is not to complexify the control architecture, or at least not much, but to use the sensors data to improve the performance of the control of the only closing actuator available.

Using Tactile Sensors with Underactuated Hands

The only particularity that differentiates the MARS hand experimentally used in this section from previous tactile experiments, is that this hand is underactuated, i.e., the freedom of movement available with other robotic hands is not available. In simple terms, underactuated fingers can only press harder or lighter. The equations of the contact forces have been established in Chapter 3, and allow the determination of the contact point on each phalanx using a recursive scheme, provided that the geometric configuration of the finger is known and that the magnitude of the normal forces is measured. Tactile sensors can be used to ensure the homogeneity of the grasp by measuring the location of the contact and using eq. (3.42) to infer the magnitude of the force. Furthermore, they can be used to ensure that the grasp is successful, a very useful information in practice! Typical variations on the contact force generated by the finger on the object are from 1 to 20 depending on the location of the contact on the phalanx. However, the scarcity of sensors and their lack of precision do not allow to obtain the reliable data required with this method.

It should be pointed out that tactile sensing requires electronics to be embedded (at least partially) in the finger, which departs from the prototypes described in this chapter. Furthermore, if the presence of electronics in the fingers is not an obstacle, including rotational encoders (or potentiometers) should also be considered as with the MARS hand. With both types of sensors, one can establish a basic scheme for automatic object recognition for instance. Using the information on the contact location, different typical objects can be recognized. This information can be used to obtain an *a priori* knowledge of the friction coefficient for example, if tangential grasp force measurements are not available.

Electronic Design of the Controller

In order to use FSRs, the first step is to translate the change of resistance of the sensor into a voltage that can be acquired and processed using a digital acquisition board on a computer. This has been referred to as the “tactile data inversion” problem. Several techniques exist to do this, e.g., a voltage divider circuit, a Wheatstone bridge, or an operational amplifier circuit. The voltage divider is the simplest technique but is not the recommended choice since it is inaccurate and sensitive to noise. The Wheatstone bridge is the most precise method but requires several components for each FSR, an expensive current monitor and a most tedious calibration procedure. Therefore, an operational amplifier circuit was used. The manufacturer of the FSR used, namely Interlink ElectronicsTM, proposes several circuits to perform this translation. A layout based on an inverting operational amplifier has been adopted (presented in Fig. 7.22).

The circuit has been modified by the addition of another feedback resistor with an analog switch provided by a CMOS 4066 chip. This circuit allows to switch the gain of the amplifier between two predefined values. Indeed, by using such a circuit, one maps the 0 – 5 V delivered by the amplifier to two different ranges of

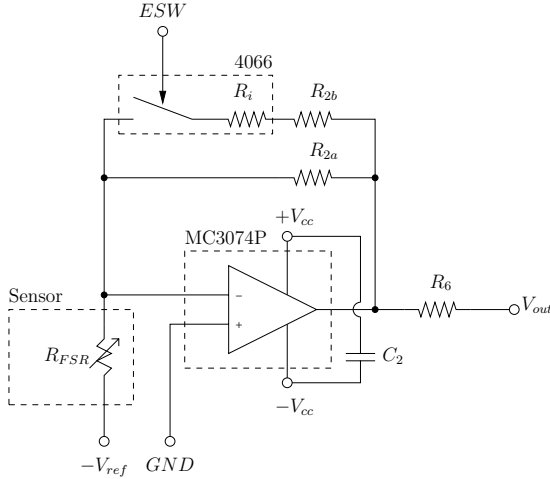


Fig. 7.22. Basic circuit cell

pressure values. For instance, with the MARS hand, values have been chosen to allow the mapping of the voltage to approximately either 0 – 2 kg or 0 – 10 kg. Thus, the sensitivity is improved for light duty grasps, which correspond to less than 2 kg maximal forces. This is inspired from the grasp classification proposed in (Landsmeer 1962) and discussed in Section 7.2.1. Therefore, such an adaptive range mapping takes advantage of the grasping configurations of the MARS hand.

It should be noted that the three phalanges do not have the same resistor values: this choice has been made in order to further enhance the sensitivity of the last phalanx of the finger. According to the theory presented in Chapter 3 and to previous practical experiments, the contact forces on the last phalanx of the finger are always much smaller than the forces on the other two. Additionally, two potentiometers allowing to measure angles θ_2 and θ_3 were also connected to this board, using a non-inverting circuit. The choice between inverting and non-inverting circuits depends on the expected sensor behaviour. If the resistance change is expected to be a linear function (or close to linear) of the data measured, one should select the non-inverting circuit which provides a linear relationship between the resistor and the voltage output. In the case of the FSR, the resistor is expected to be close to an inverse function of the payload applied (or the grasp force in our case). Therefore, an inverting circuit is particularly well suited for this task, the output voltage being:

$$V_{out} = -\frac{R_2}{R_{measured}} V_{ref}, \quad (7.1)$$

where in this case, $R_{measured}$ is the input resistor (FSR) and R_2 is the feedback resistor. Furthermore, one could use the negative power supply required by the

amplifier to provide a steady V_{ref} . Using the double gain circuit previously presented, one obtains:

$$V_{out} = \frac{R_{2a}(R_{2b} + R_i)}{R_{measured}(R_{2a} + R_{2b} + R_i)} V_{cc} \text{ if the switch is closed,} \quad (7.2)$$

$$V_{out} = \frac{R_{2a}}{R_{measured}} V_{cc} \quad \text{otherwise} \quad (7.3)$$

with R_i being the internal resistance of the analog switch (Motorola MC14066B chips were used with a typical resistance of 1050 Ω). This value should be the lowest possible in order to be neglected or else taken into account when calculating the gain value. This technique of double gain can be extended by using a voltage controlled resistor created with a FET, but this exceeds our needs. Powerful operational amplifiers have also been used to reduce parasites, namely the Motorola MC34074P, which has been specially designed for this purpose. Digital filters are used to process the data. In our case, fourth order elliptic filters were designed, allowing a lag time typically smaller than 20 ms. Combining these techniques, the measurement noise was reduced by a factor of 15.

The angles measured by the potentiometers are directly angles θ_2 and θ_3 (with a simple bias). However, angle θ_1 , which is required to estimate the Cartesian position of the finger is not directly measured but is a complex function of the motor's encoder position, the potentiometers' angles, and the transmission linkage used to transform the motor torque into the actuation torque T_a (Fig. 7.23). This transmission mechanism is based on two separate stages: a slider-crank and a four-bar linkage. However, its kinematic model was derived and implemented in the control scheme, allowing its real-time evaluation. The input-output equation of the slider-crank mechanism is

$$s^2 - (2r \sin \phi)s + (r^2 + e^2 - 2er \cos \phi - L^2) = 0. \quad (7.4)$$

Hence

$$\phi = 2 \arctan \left(\frac{A + B}{C} \right) \quad (7.5)$$

with

$$A = 4rs \quad (7.6)$$

$$B = 2\sqrt{-(e^2 + s^2 - L^2 - r^2 + 2Lr)(e^2 + s^2 - L^2 - r^2 - 2Lr)} \quad (7.7)$$

$$C = 2(r^2 + e^2 + 2er + s^2 - L^2). \quad (7.8)$$

The input variable s is defined using the pitch of the lead screw attached to the actuator, i.e., $s = p(\Phi - \Phi_{initial})$ where Φ is the actuator angle. The output of this slider-crank mechanism is the angle ϕ which is itself the input angle of another four-bar mechanism similar to the mechanism used in the underactuated finger with linkages, commonly found in this book and introduced in Fig. 3.2. The latter input-output equation is easily found in the literature as well as its derivative with respect to time, referred to as Kennedy's Theorem, as discussed in Section 3.2.

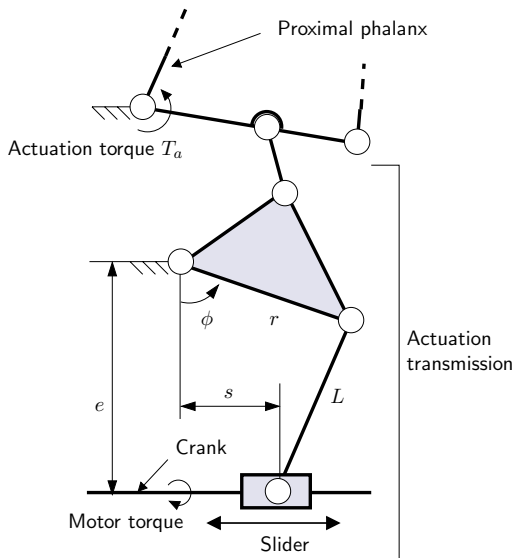


Fig. 7.23. Actuator transmission

Fuzzy Force Control

Preliminary experiments were conducted in force control to ensure that the grasping force can be controlled using tactile feedback. However, experimental results prove to be very deceptive. Maintaining the grasping force in the neighbourhood of the prescribed force (command) is very difficult with a simple force control scheme, using a PID for instance. Experimental results indicate that this is mainly due to the friction in the numerous joints of the finger and actuation transmission mechanism that make the actuation almost not-backdrivable. In other words, the grasping forces can only be increased and not decreased. An illustration of this phenomenon is available in Fig. 7.30(b) at approximately $t = 67$ s. At this time, the actuation torque is zero. However the grasping force F_7 is not zero as it should be, but almost 50% of its previous value. In practical terms, this means that even by stopping the actuator, the finger will continue applying forces on the object. The phalanx forces are not sufficient to counter the friction in the joints, thus forces are applied but no motion is produced. This is similar to what happens when one pushes a box lying on the ground: until the applied force overcomes the tangential friction force, no motion is possible. This hysteresis phenomenon was foreseeable but its magnitude was not. In fact, firm grasps can be achieved with the actuator turned off. Therefore, if one wants to fine tune the grasp force, one must develop other more advanced control schemes dedicated to the management of large friction.

Two different approaches are possible to overcome this problem, i.e., either a friction compensation scheme or an intelligent control scheme. Friction compensation is not very attractive since it requires precise friction modelling which

depends on the seized object. An intelligent control approach seems more promising, like for instance sliding modes or fuzzy logic. Using such schemes, it is possible to fully exploit tactile sensors. A closed loop force control scheme can be designed and, for example, detect if the grasping forces are on the edge of vanishing, resuming the grasping actuation.

Hence, and since PID control was proven to be unsatisfactory, a fuzzy logic approach was taken, the latter having been reported successful in controlling underactuated fingers (Dubey et al. 1999). In our case, the idea to control the finger using fuzzy logic is to increase/decrease the actuator torque, hence the contact force, until the objective contact force is attained. Therefore, the input of the fuzzy controller might be the contact force error while its output will be the actuator torque variation. The fuzzy error force is defined as

$$\epsilon_F(t) = F_d(t) - F^*(t) \quad (7.9)$$

where F_d is the desired distal phalanx total force and F^* is the distal phalanx force evaluated as the moving average on four values of the absolute total distal error measures, i.e.,

$$F^*(t) = \sum_{k=0}^3 \frac{1}{4} \sqrt{\left(\sum_{i=7}^9 F_i(t - k\Delta t) \right)^2} \quad (7.10)$$

where Δt is the sampling period (1 ms with our prototype), and F_7 , F_8 , and F_9 are the distal phalanx measured forces. The controller uses only the last phalanx contact force information but can be extended to include all phalanx forces. The fuzzy membership functions associated to the force error are illustrated in Fig. 7.24.

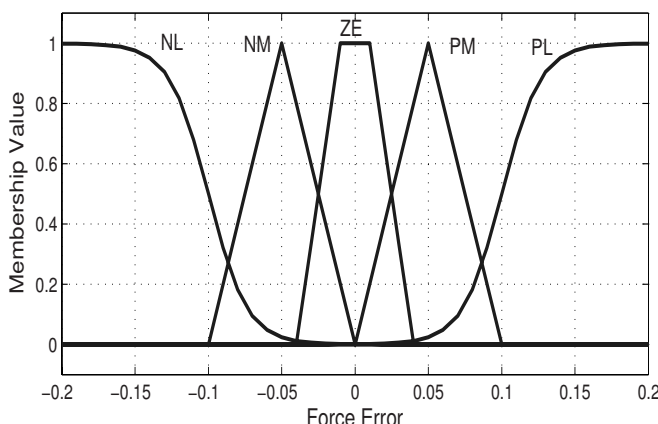


Fig. 7.24. Membership functions of the force error

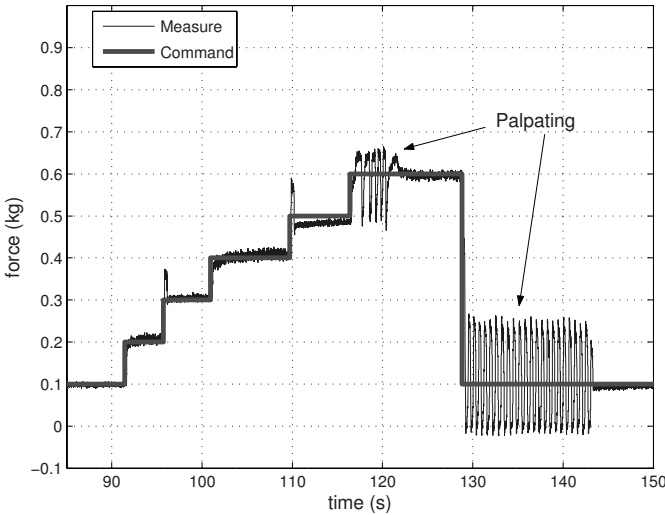


Fig. 7.25. Palpation phenomenon

Experiments show that these rules are not sufficient, since the contact force tends to oscillate around the desired input. This oscillation creates the impression that the finger is “palpating” the object and is illustrated in Fig. 7.25. A solution to prevent this phenomenon is to add another fuzzy input, namely the measured force derivative, to slow down the grasping force increase (or decrease) when the error force is small, i.e., add some damping to the system, but not always. A PID controller would not allow such finesse. The force differential dF is defined as the moving average on a hundred values of the total distal phalanx force derivative, i.e.,

$$dF(t) = \sum_{k=0}^{99} \frac{1}{100} \frac{d \left(\sum_{i=7}^9 F_i(t - k\Delta t) \right)}{dt} \quad (7.11)$$

and its respective membership functions are illustrated in Fig. 7.26. The final resulting fuzzy control surface itself is illustrated in Fig. 7.27 with the fuzzy association memory (FAM) bank which define all cases of “if-and-then” rules. The nomenclature is found in Table 7.3. The minimum function is associated with the fuzzy “and” operator while a centroid defuzzification method was chosen. A typical example of force control result is presented in Fig. 7.28: the oscillations are considerably attenuated. A square wave was chosen to illustrate the repeatability of the experiments, as well as the similar behaviour during increase and decrease of the command. However, it has been experimentally found that some oscillations may transitorily subsist in the case of overcompliant contacts, i.e., locally deformable objects. Nevertheless, the latter can be eliminated by increasing the damping of the controller, without a significant decrease of the settling time since the damping only acts when the error is small. The resulting controller

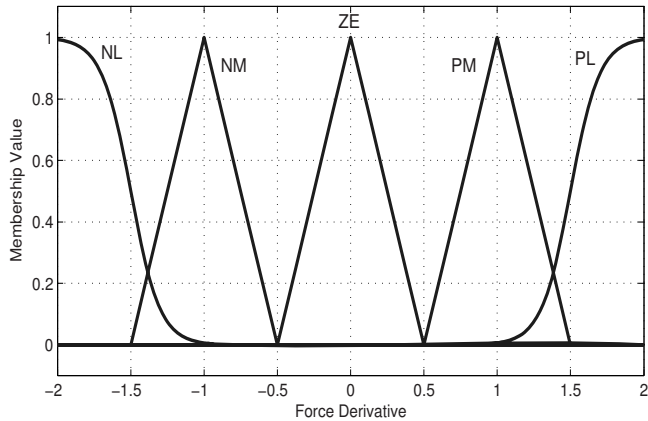


Fig. 7.26. Membership functions of the derivative of the force

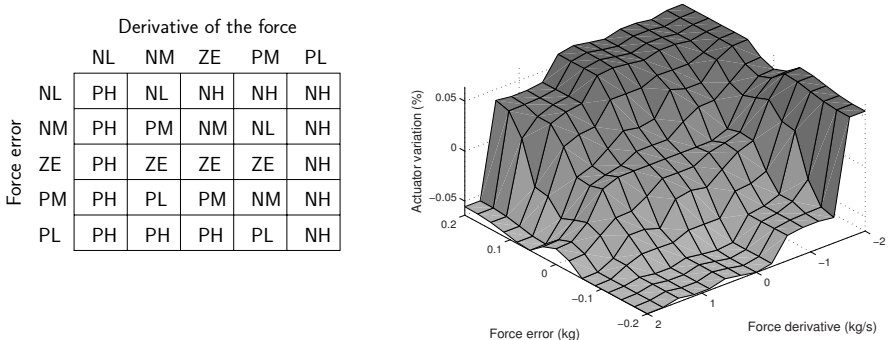


Fig. 7.27. FAM bank and associated fuzzy control surface

behaves extremely well and is able to seize fragile objects, in collaboration with a human as illustrated in Fig. 7.29.

Slippage detection *should* not be possible with the kind of sensors used here. Indeed, the FSR can only measure pure normal forces, no tangential information of any kind is theoretically available. However, slippage can be detected as it has been concluded experimentally. Experimental examples of slippage measures are presented in Figs. 7.30(a) and 7.30(b), these figures being typical of what was observed. As it can be observed on these graphs, one can note a very significant variation in the magnitude of normal force when slippage occurs (Fig. 7.30(b)), zoom on the slipping event presented in Fig. 7.31(a)). This variation comes without any motion of the finger itself (Fig. 7.30(a)) which is thus still grasping what appears to be a motionless object. Furthermore, no change in actuator torque was requested. Thus, one has the situation of a motionless object, grasped with a constant actuator torque but the tactile sensor of the finger records a quick change of the force applied.

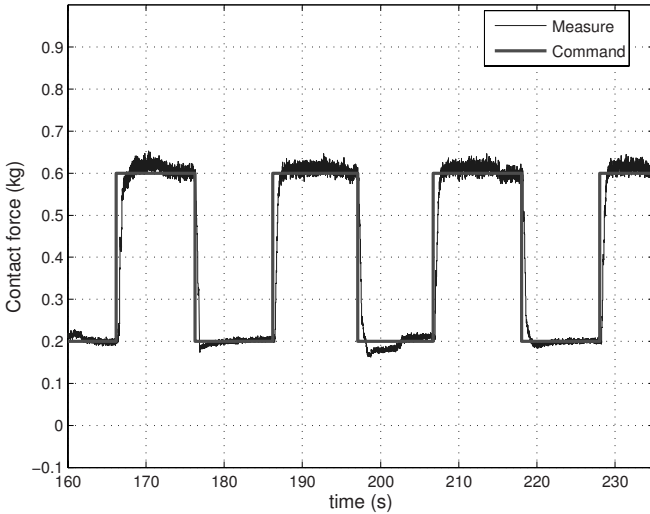


Fig. 7.28. Fuzzy force control experimental data

Table 7.3. Membership symbols

NH	negative huge
NL	negative large
NM	negative medium
ZE	zero
PM	positive medium
PL	positive large
PH	positive huge

It is noted that the increase of one sensed force in Fig. 7.30(b) seems to indicate a variation in the force distribution along the phalanx, while the overall forces keep the finger in static equilibrium. This phenomenon can only be explained either by a local deformation of the object or by slippage. Both cases require a different handling. For instance if the object is locally starting to deform, it means that the object is breaking down, the grasping forces should therefore be decreased. On the contrary, if the object is slipping, grasping forces should be increased to keep the object from escaping. In fact, this dilemma is not solvable without *a priori* knowledge or extra information. The same happens when a human tries to seize an egg and the latter begins to crack, the first reaction of the human is to grasp more firmly the egg to prevent it from falling but this tends to break it even further. Nevertheless, from an experimental point of view, slippage is detectable, even with cheap off-the-shelf sensors like FSRs. An example of slippage with a power grasp is illustrated in Fig. 7.31(b). It is noted that the forces measured by the sensors after the slippage are usually not the same as before the slippage.

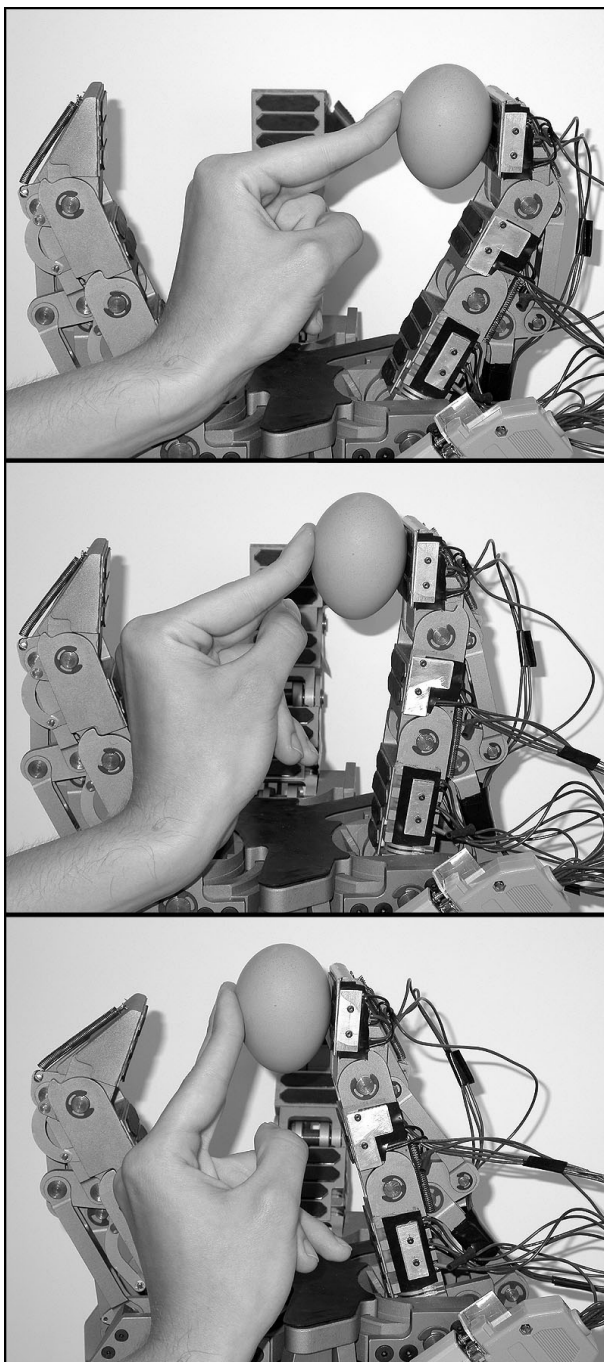


Fig. 7.29. Force control during a collaborative handling

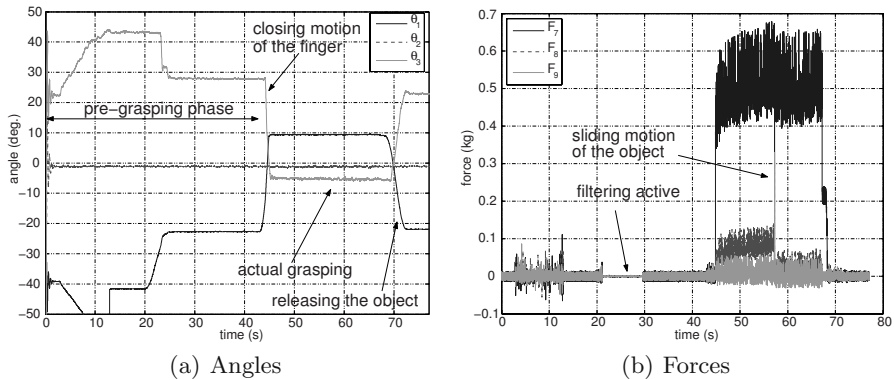


Fig. 7.30. Slippage detection during a pinch grasp

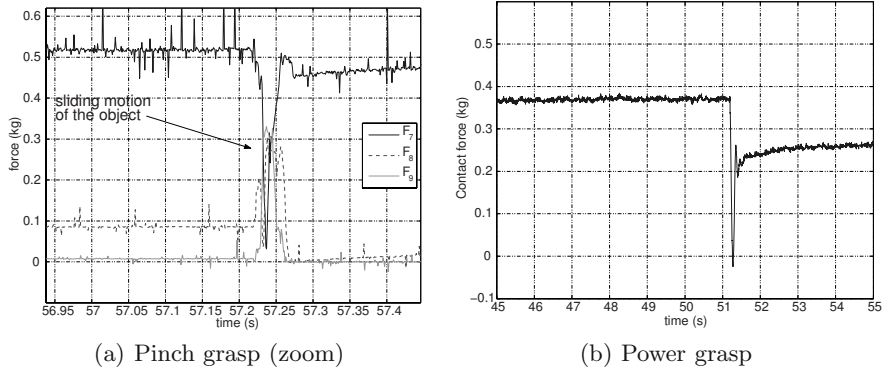


Fig. 7.31. Typical slippage signals

To summarize, the event “slippage” can be described as corresponding to: a short-time variation of the phalanx forces, a constant actuation torque, no motion of the finger. The latter condition however needs to be relaxed since small vibrations can happen during slippage. Furthermore, to detect the motion of the finger, one has to use the data provided by the potentiometers and the actuator’s encoder. Indeed, the latter data is not sufficient to detect a motion of the finger since the finger can move with its actuator locked—this feature being mandatory to obtain the shape adaptation behaviour. Hence, data from the potentiometers is necessary to detect slippage. In response to this event, an anti-slippage scheme was implemented that increases the actuation torque as soon as these characteristic conditions are fulfilled. This increase has been experimentally determined to be a jerk increase of 10%, mimicking the reflex action of a human being, and is added to the force control component of the command. This superposition of the commands has also been reported to be the

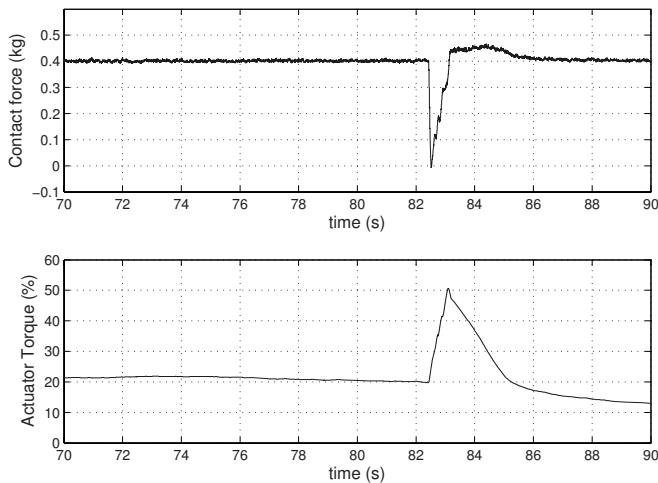


Fig. 7.32. Fuzzy force control reaction during slippage

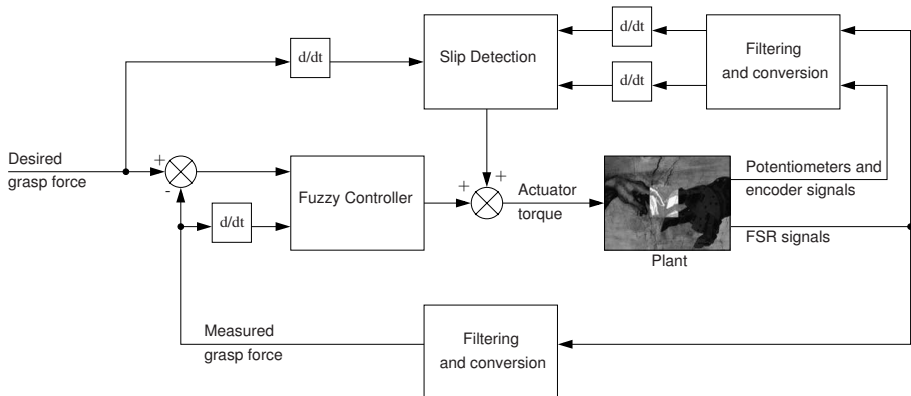


Fig. 7.33. Control scheme of the finger

principle behind human prehension (Zatsiorsky et al. 2004). Since both commands are to be added, the influence of the fuzzy force controller should be taken into account. Indeed, the force controller detects the decrease of the grasping force and tries to counter the latter, as illustrated in Fig. 7.32 (the controller output is a variation of the actuator torque, expressed as a percentage of the maximal admissible torque). The fuzzy force controller is however too slow to actually prevent slippage. A block diagram of the complete control scheme is presented in Fig. 7.33: it is implemented in real-time. Such an impulse control technique has also been suggested to be well suited for plants subject to

Table 7.4. Hardware costs

Item	Units	Price (US\$)
FSR	8	28
DB cables	3	40
electronic board	1	15
components (IC, resistors, etc.)	-	10
connectors	6	10
power supply	1	20
Total		≤ 125

uncharacterized but large friction (Rathbun et al. 2004a; Rathbun et al. 2004b). One should note that the total cost of the hardware required to achieve tactile sensing and an intelligent behaviour is very affordable and negligible compared to the machining cost of a finger (see Table 7.4).

7.3.3 Control of the SARAH hands

Since there are only two motors, the control of the SARAH hand is simple. No grasping coordination is needed by the control algorithm since the grasping of the fingers is again mechanically coordinated by the differential, which tends to keep the forces on the fingers equal. If a grasp requires more force at one of the fingers—such as in the cylindrical grasp—the finger will naturally compensate when pushed backwards because of the self-locking feature. The planar grasp is the only one that requires different finger positions and it is managed mechanically by the stopper previously described. No reconfiguration coordination is needed since the orientation of the fingers is coupled mechanically.

If external forces are applied on the grasped object, they must be compensated for. Because of the transmission screws, the fingers are self-locking and they will naturally compensate for external forces. Therefore, the simple initial control scheme can be used. In fact, since there is only one motor driving the closing of the three fingers, the force at each finger cannot be controlled independently. Therefore, a modified version of the control algorithm for the MARS hand could not be used and self-locking of the fingers is essential.

The use of tactile and position sensors could be useful to obtain information on the grasp performed, as the forces applied, and the position and shape of the object. This could help to confirm the quality of a grasp if visual confirmation is not available. If a grasp is not correct and if it is possible to release the object, it is then grasped again in order to obtain a better grasp.

7.4 Conclusions

The design of several underactuated hands developed at Université Laval was presented in this chapter. After reviewing the taxonomy of the grasps, a geometry for the architecture of the hands was chosen. Following this selection, an additional DOF either for each finger (MARS) or for the hand (SARAH) is provided to widen the range of possible grasps. To further increase this range, a parallel precision grasp mechanism was also added to the fingers. This mechanism keeps the distal phalanx of the fingers perpendicular to the palm allowing efficient pinch grasps. During power grasps, this mechanism is automatically disengaged without any controller or sensors to properly envelop the object seized. Different prototypes of underactuated hands have been thereupon built at Université Laval. The MARS hand with six DOA requires some simple motor coordination while the SARAH class hands with two DOA requires only minimum control algorithms—similarly to simple grippers—and has grasping capabilities comparable to the MARS hand. The SARAH class hands introduced underactuation between the fingers in addition to the underactuation in the fingers. Furthermore, the relative orientation of the fingers is mechanically predetermined. Moreover, with the use of a Geneva mechanism, only the four discrete most useful orientations were kept. Therefore, for most applications the SARAH class hands obtain outstanding results with a simple control scheme. If a more precise force control is required, tactile sensors can be used. Promising experiments were reported that clearly demonstrate that the behaviour of underactuated fingers can be enhanced using tactile information. Underactuated fingers may even be a predilection type of hands to use tactile sensing since the simplicity of the initial controller leaves significant computation time available to process the tactile data in real-time. Experimental force control was implemented with very good results using a fuzzy logic controller and prevention of slippage was included in the controller. The results of this chapter have been published in (Laliberté et al. 2002; Birglen and Gosselin 2005).

8 Conclusion

*iza saraba
ware mo kaeran
aki no kure*

*it is finished
I also have to go now
the autumnal dusk*

Ryōkan.

in which a brief summary of the book is presented and the methodology that has guided this work along its main contributions is emphasized. Finally, perspectives on underactuation in robotic grasping are discussed.

8.1 Summary and Contributions of the Book

This book is an attempt to lay the fundamental bases for the use of underactuation in grasping robotic hands and to summarize more than a decade of research. It covers a broad spectrum ranging from the analysis of theoretical properties of underactuation in grasping to the actual design and control of prototypes. In the introduction of the book, a survey of current architectures of robotic hands was presented. Then, the principle of underactuation, i.e., using fewer actuators than DOFs, was presented as well as how it can be used to drive robotic hands. Several prototypes, some of them century-old, were pointed out from the literature. Although underactuation is a very old technique, it has only very recently attracted the attention of the research community. Beside this introductory survey, the first contribution of the book is the definition of two matrices—termed Jacobian and Transmission matrices—allowing immediate characterization of the force capabilities of a robotic finger. These matrices provide the analytical expressions of contact forces developed by a finger of arbitrary design and with any number of phalanges. The only limitation of the

method presented is that abduction/adduction actuation should not participate in the grasp effort. Analyzing these matrices and the resulting contact forces expressions lead to considerations on equilibrium, and can also provide practical tools for the designer to compare between different solutions.

The acknowledgment that some phalanx forces may become negative with underactuated robotic fingers leads to the definition of a method to analyze the grasp stability of these fingers based on a newly defined grasp-state space. This hyperspace includes state trajectories as well as stable/unstable hypersurfaces, and clearly constitutes the second contribution of the book. In the case of two-phalanx fingers, the grasp-state space becomes a grasp-state plane which accurately depicts a finger's tendency to either converge to a static equilibrium or to lead to unstable grasps, namely ejection. The grasp-state plane elements and curves can be refined to meet an arbitrary level of complexity in order to consistently reflect a real finger's behaviour. Most noticeably in the book, contact properties such as friction and design parameters' influences were considered. This analysis was subsequently extended to three-phalanx fingers, although the complexity of the grasp stability problem in this case left unresolved questions. Indeed, the analysis in its present state is still incomplete and the model discussed should be refined to include friction, local contact geometries, spring stiffnesses, etc. A dynamic modelling will also be useful to obtain the exact behaviour of three-phalanx fingers in the case of two lost contacts, i.e., obtain the exact validity surfaces. As clearly stated in the introduction, substantial work remains to be completed and this book constitutes nothing more than a work in progress. Especially in the three-phalanx case, many points require more attention, and the need to obtain a stability theory taking into account more refined contact situations is evident. Furthermore, once ejection is prevented using an accurate modelling, other important aspects may be taken into account like the grasp isotropy.

The natural extension of the first part of the book was to use the results obtained in the previous chapters to build optimal robotic fingers with respect to the generated contact forces and grasp stability. With two-phalanx fingers, the design of optimal underactuated fingers is fairly simple and adequately documented. The understanding of the nature of the grasp-state plane and its related elements with their physical "real-life" equivalent phenomena led to simple and practical rules to obtain ejection-free two-phalanx underactuated fingers. It was also shown that such fingers can even satisfy additional performance criteria like force isotropy. With three-phalanx fingers, since the modelling of the elements of the grasp-state space is not as complete as in the two-phalanx case, optimal design relies more on a numerical procedure based on the combination of several criteria. In this case, the intuition of the designer in combining the criteria and weigh their importance becomes more predominant. However, this approach has lead to designs with much practical success and therefore should be acknowledged.

Following the discussions on theoretical aspects and the design of underactuated fingers, a methodology was proposed for the analysis of the force capabilities

of common differential mechanisms. These mechanisms are used to extend the principle of underactuation from the fingers to the hand itself, leading to designs with numerous fingers and DOFs driven by as few as one actuator. Several differential elements, commonly used in robotic hands were analyzed. A simple matrix formulation was developed to obtain the relationship between the actuation and output forces of these devices. Then, a mathematical method to obtain the output force capabilities of connected differential mechanisms was presented. By connecting differential mechanisms using a properly designed scheme, one can obtain systems with an arbitrary large number of outputs. Two examples were then analyzed using the technique presented: first, an underactuated gripper and second, a multiple pulley routing. Actual prototypes of the latter examples were illustrated, i.e., a surgical compliant gripper and a prosthetic hand. The mathematical expressions of the transmission tree characterizing the underactuated system considered are fundamentally different from the Transmission matrix arising when one considers underactuation in the fingers instead of between them. Similarly to the discussion in the conclusion of Chapter 3, the authors believe that the tools presented in Chapter 6 can help refining the design of an underactuated transmission.

Finally, practical issues in the design and control of the prototypes of underactuated robotic hands developed at Université Laval were presented. After reviewing the taxonomy of the grasps, a geometry for the architecture of the hands was chosen to extend as much as possible the range of possible grasps. A parallel precision grasp mechanism was also added to the fingers, to keep the distal phalanx of the fingers perpendicular to the palm, allowing pinch grasp. During power grasps, this mechanism is automatically disengaged without any controller or sensors to properly envelop the object seized. Thereupon, several prototypes built at Université Laval were presented with their respective characteristics. The latest class of prototypes, termed SARAH class of hands, is able to grasp most irregularly shaped objects with a simple control scheme, obtaining outstanding results. If a more precise force control is required, tactile sensors can be used. Promising experiments were reported in order to demonstrate that the behaviour of underactuated fingers can be enhanced using tactile information. Underactuated fingers may even be a predilection type of hands to use tactile sensing since the simplicity of the controller leaves significant computation time available to process the tactile data in real-time. Experimental force control was implemented with very good results using a fuzzy logic controller and prevention of slippage was included in the controller.

8.2 Perspectives

It has been noted (Bar-Cohen and Breazal 2003) that we are at the dawn of a new era in robotic systems. Initially, human technological systems tended to be large, stiff, with right angles. Nowadays, new developments, especially in soft materials and actuators, tend to favour compliant designs with many sensors. Underactuation in grasping, with its inherent compliance allowing shape adaptation, belongs

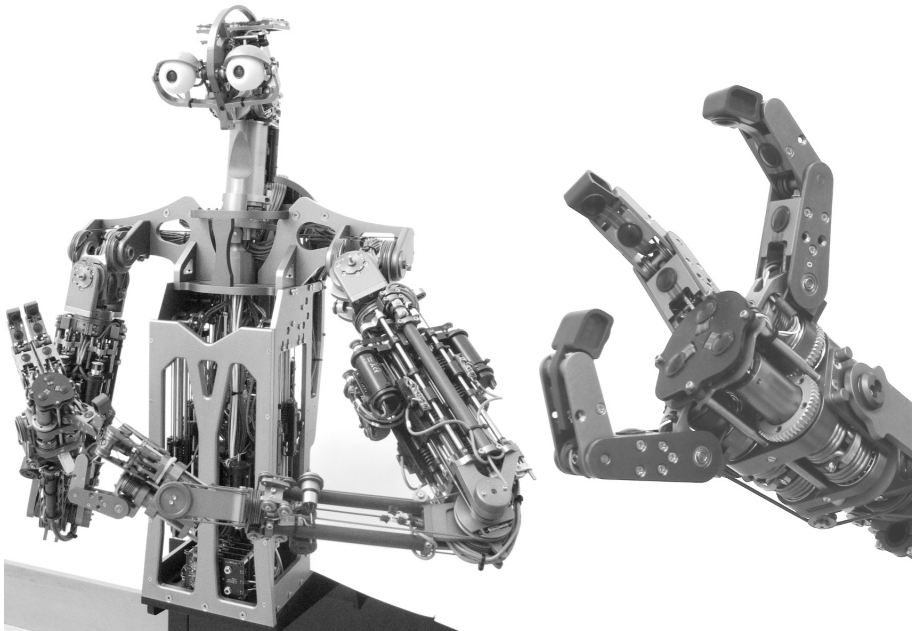


Fig. 8.1. The DOMO humanoid robot and a close-up of its compliant hand (courtesy of Dr. Aaron Edsinger)

to this new trend. However, it is only one member of a vast family of solutions, even in grasping. For instance, the compliance can be displaced from the finger to the actuators as illustrated in Fig. 8.1 (Edsinger-Gonzales 2004) using series elastic actuators (SEA) (Pratt and Williamson 1995; Williamson 1995). This actuation technology inserts a compliance directly on the actuator axis. Such systems allow to command the impedance of the actuator and the elasticity can store and release energy if desired, without any explicit control. Although a certain shape adaptation is indeed achieved, the aim is not, conversely to traditional underactuated hands, to realize enveloping grasps since the rotations of the finger joints are coupled and do not depend on the object to be seized. Furthermore, SEA technology is close but distinct from underactuation as discussed in this book. By introducing an elastic element between the actuator and joint axes, one adds an extra DOF to the system while keeping the same number of actuators. This addition leads some people to classify systems using SEA as underactuated, since they have fewer actuators than DOFs. However, the authors disagree with this point as the added DOF is internal to the actuation module, the system considered is not by itself underactuated and there are no transmission mechanisms. Hence, SEA are an actuation technology but do not make the driven system underactuated.

Underactuation in robotic grasping hands offers tremendous possibilities, and is one of the promising new techniques in robotics emerging—again—in this new century. Until very recently, underactuation in grasping was a chaotic subject

where a few designs were periodically “discovered” but with little, if any, knowledge of the principles behind these mechanisms. As noted throughout the book, despite many recent contributions to the theory of underactuation grasping, little is known actually and many theoretical issues are left unresolved. In the authors’ opinion, so many aspects of underactuation analysis remain to be discovered and studied that it is both enthusing and depressing at the same time! Enthusiasm springs from the remaining amount of work which is a promise of years of exciting research to come. Depression comes from exactly the same fact: a foreseen Herculean amount of work, which might require more than a lifetime.

Challenging issues will be addressed in the future and the practical impact of this subject is expected to be significant. Underactuated self-adaptive grippers are likely to be the preferred solution for the next generation of end effectors for space, prosthetic, and surgical applications. Additionally, according to the *U.N. World Robotics Survey 2004*, service robotics is expected to be the most successful area in robotics for the next decade and double digit growths are expected. Industrial applications such as inspection in unstructured and/or hazardous environments can also benefit from underactuated grasping. It is the profound belief of the authors that underactuation in robotic hands is a technology that has so much potential that it must and will be investigated.

A Mathematical Proofs

A.1 Influence of the Base Joint Spring

If a spring is located in the base point O_1 between the first phalanx and the fixed frame, the expression of vector \mathbf{t} and $\boldsymbol{\omega}_a$ should be modified to

$$\mathbf{t} = \begin{bmatrix} T_a \\ T_1 = -K_1 \Delta\theta_1 \\ \dots \\ T_n = -K_n \Delta\theta_n \end{bmatrix}, \quad \boldsymbol{\omega}_a = \begin{bmatrix} \dot{\theta}_{a_1} \\ \dot{\theta}_1 \\ \dots \\ \dot{\theta}_n \end{bmatrix}, \quad (\text{A.1})$$

to include the contribution of this spring to the total virtual work. From Chapter 3, one has

$$\dot{\theta}_{a_1} = \dot{\theta}_1 - X_2 \dot{\theta}_2 - \dots - X_n \dot{\theta}_n \quad (\text{A.2})$$

where X_i are characteristic coefficients of the transmission, defined in the latter reference. Hence, one can define an extended transmission matrix as $\boldsymbol{\omega}_a = \mathbf{T}^* \dot{\boldsymbol{\theta}}$, i.e.,

$$\begin{bmatrix} \dot{\theta}_{a_1} \\ \dot{\theta}_1 \\ \dots \\ \dot{\theta}_n \end{bmatrix} = \begin{bmatrix} 1 & X_2 & \dots & X_n \\ 1 & 0 & \dots & 0 \\ \dots & \dots & \dots & \dots \\ 0 & 0 & \dots & 1 \end{bmatrix} \begin{bmatrix} \dot{\theta}_1 \\ \dot{\theta}_2 \\ \dots \\ \dot{\theta}_n \end{bmatrix}. \quad (\text{A.3})$$

Eq. (4.2) therefore becomes

$$\mathbf{f} = \mathbf{J}^{-T} \mathbf{T}^{*T} \mathbf{t}. \quad (\text{A.4})$$

It should be noted that this extended transmission matrix is not inverted as it is not square. The contribution of the base spring, namely T_1 , is the second component of vector \mathbf{t} . Since matrix \mathbf{J} is lower triangular, its inverse is upper triangular and the first component of this inverse is simply $1/k_1$. Given the particular form of matrix \mathbf{T}^* , only this component is multiplied by T_1 . Hence,

the base spring only contributes to the expression of f_1 and the latter can be expressed as T_1/k_1 .

A.2 Influence of k_1

The general form of the transmission matrix is:

$$\mathbf{T} = \begin{bmatrix} 1 & X_2 & \dots & X_n \\ 1 & 0 & \dots & 0 \\ \dots & \dots & \dots & \dots \\ 0 & 0 & \dots & 1 \end{bmatrix} \begin{bmatrix} \dot{\theta}_1 \\ \dot{\theta}_2 \\ \dots \\ \dot{\theta}_n \end{bmatrix} \quad (\text{A.5})$$

and the actuation torque vector is

$$\mathbf{t} = \begin{bmatrix} T_a \\ T_2 \\ \dots \\ T_n \end{bmatrix}. \quad (\text{A.6})$$

Hence, one has

$$\mathbf{T}^{-T} \mathbf{t} = \begin{bmatrix} T_a \\ X_2 T_a + T_2 \\ \dots \\ X_n T_a + T_n \end{bmatrix}. \quad (\text{A.7})$$

The Jacobian matrix of the grasp is

$$\mathbf{J} = \begin{bmatrix} k_1 & 0 & 0 & \dots & 0 \\ \mathbf{r}_{12}^T \mathbf{x}_2 & k_2 & 0 & \dots & 0 \\ \dots & \dots & \dots & \dots & \dots \\ \mathbf{r}_{1n}^T \mathbf{x}_n & \mathbf{r}_{2n}^T \mathbf{x}_n & \mathbf{r}_{3n}^T \mathbf{x}_n & \dots & k_n \end{bmatrix}. \quad (\text{A.8})$$

Because of the particular expressions of the terms of this matrix, described in eq. (3.20), k_1 only appears in the upper left corner. The inverse of this matrix can be written as (Strang 1986)

$$\mathbf{J}^{-1} = \frac{1}{\det \mathbf{J}} \mathbf{C} \quad (\text{A.9})$$

where \mathbf{C} is the cofactor matrix of \mathbf{J}^T . The determinant of the latter matrix is simple, since it is triangular, i.e.,

$$\det \mathbf{J} = \prod_{i=1}^n k_i = \Delta. \quad (\text{A.10})$$

Then, each component of matrix \mathbf{K} can be expressed as

$$C_{ij} = (-1)^{i+j} \det \mathbf{M}_{ji} \quad (\text{A.11})$$

where \mathbf{M}_{ij} is formed by deleting row j and column i of \mathbf{J} and where C_{ij} represents the (i, j) entry of matrix \mathbf{C} . One has

$$J_{ij}^{-1} = 0 \quad \text{for } j > i \quad (\text{A.12})$$

where J_{ij}^{-1} stands for the (i, j) entry of matrix \mathbf{J}^{-1} . Hence, the first line of \mathbf{J}^{-1} contains only zeros, except for the very first entry which is Δ/k_1 , since \mathbf{J} is lower triangular. Let \mathbf{J}_{*i}^{-1} denotes the i^{th} column of \mathbf{J}^{-1} , one has

$$\mathbf{J}_{*1}^{-1} = \frac{1}{\Delta} \mathbf{C}_{*1} \quad (\text{A.13})$$

where \mathbf{C}_{*j} denotes the j^{th} column of \mathbf{C} . From eq. (A.11), one has that each entry of the latter column does not depend on k_1 , since k_1 does not appear in any entry of \mathbf{J} outside the first column. The other components of \mathbf{J}^{-1} can be written as

$$J_{ij}^{-1} = \frac{1}{\Delta} C_{ij} \quad j > 1 \quad (\text{A.14})$$

and the cofactor C_{ij} can be expressed as

$$(-1)^{i+j} \begin{vmatrix} J_{1,1} & 0 & 0 & 0 & 0 & 0 & 0 & 0 & 0 & \dots & 0 \\ J_{2,1} & J_{2,2} & 0 & 0 & 0 & 0 & 0 & 0 & 0 & \dots & 0 \\ J_{3,1} & J_{3,2} & J_{3,3} & 0 & 0 & 0 & 0 & 0 & 0 & \dots & 0 \\ \dots & \dots \\ J_{j-1,1} & \dots & J_{j-1,i-1} & J_{j-1,i+1} & \dots & J_{j-1,j-1} & 0 & \dots & 0 & \dots & 0 \\ J_{j+1,1} & \dots & J_{j+1,i-1} & J_{j+1,i+1} & \dots & J_{j+1,j-1} & J_{j+1,j} & J_{j+1,j+1} & 0 & \dots & 0 \\ \dots & \dots \\ J_{n,1} & \dots & J_{n,n} \end{vmatrix} \quad (\text{A.15})$$

with $J_{i,i} = k_i$. This determinant is obviously factorable by k_1 . Hence k_1 is a common factor for all components C_{ij} with $j > 1$. Therefore, since

$$\Delta = k_1 \prod_{i=2}^n k_i \quad (\text{A.16})$$

k_1 only appears as a factor in the denominator of the first column of \mathbf{J}^{-1} or the first line of \mathbf{J}^{-T} . Hence, with eqs. (A.7) and (3.42), this k_1 factor only appears in the denominator of f_1 . Therefore the signs of components of \mathbf{f} are independent from k_1 .

A.3 Relationship between Proximal and Intermediate Forces

Let us assume a finger with a general transmission, described by a matrix \mathbf{T} having the form:

$$\mathbf{T} = \begin{bmatrix} 1 & X_2 & X_3 \\ 0 & 1 & 0 \\ 0 & 0 & 1 \end{bmatrix}. \quad (\text{A.17})$$

The contact forces can then be expressed using eq. (3.42), if springs are neglected,

$$f_1 = -\frac{((1-X_2)k_3 - l_1 X_3 \cos(\theta_2 + \theta_3))}{k_1 k_3} T_a + \frac{l_1 \cos \theta_2 [(X_2 - X_3)k_3 - X_3 l_2 \cos \theta_3]}{k_1 k_2 k_3} T_a \quad (\text{A.18})$$

$$f_2 = \frac{(X_3 - X_2)k_3 + X_3 l_2 \cos \theta_3}{k_2 k_3} T_a \quad (\text{A.19})$$

$$f_3 = -\frac{X_3}{k_3} T_a. \quad (\text{A.20})$$

Therefore, one has

$$f_1 = \frac{(X_2 - 1)k_3 + l_1 X_3 \cos(\theta_2 + \theta_3)}{k_1 k_3} T_a - \frac{f_2 l_1 \cos \theta_2}{k_1} \quad (\text{A.21})$$

and hence k_2 appears only in the denominator of the second part of f_1 .

QED.

A.4 Transmission Tree Formulae

A.4.1 Serial Transmission Tree

A serial transmission tree according to the definition given in Section 6.3.1 and illustrated in Fig. 6.13 is studied. The formula defined in eq. (6.14) is to be proven by induction. Each transmission stage is described by its associated force transmission matrix, i.e.,

$${}^i \mathbf{F} = {}^i \mathbf{T}^f {}^i \mathbf{t}^\diamond \quad i = 1, \dots, n-1. \quad (\text{A.22})$$

Heredity

Let us suppose a serial transmission tree with $n - 1$ stages and described by eq. (6.14), i.e.,

$$\begin{bmatrix} F_1^a \\ F_2^a \\ \vdots \\ F_n^a \end{bmatrix} = \left(\prod_{i=1}^{n-1} \begin{bmatrix} \mathbf{1}_{n-1-i} & \mathbf{0} \\ & {}^{n-i}\mathbf{T}^f \\ \mathbf{0} & \mathbf{1}_{i-1} \end{bmatrix} \right) \begin{bmatrix} F_a \\ T_1^s \\ \vdots \\ T_{n-1}^s \end{bmatrix}. \quad (\text{A.23})$$

If another stage is added to the tree, accordingly to the definition given in Section 6.3.1, i.e., keeping the tree strictly serial, one has

$$\begin{bmatrix} {}^nF_1^a \\ {}^nF_2^a \end{bmatrix} = {}^n\mathbf{T}^f \begin{bmatrix} {}^{n-1}F_2^a \\ T_n^s \end{bmatrix} \quad (\text{A.24})$$

which describes the last stage of the transmission tree. Since the transmission tree has one more stage than previously, eq. (A.23) should be modified, i.e.,

$$\begin{bmatrix} F_1^a \\ F_2^a \\ \vdots \\ F_{n-1}^a \\ {}^{n-1}F_2^a \end{bmatrix} = \left(\prod_{i=1}^{n-1} \begin{bmatrix} \mathbf{1}_{n-1-i} & \mathbf{0} \\ & {}^{n-i}\mathbf{T}^f \\ \mathbf{0} & \mathbf{1}_{i-1} \end{bmatrix} \right) \begin{bmatrix} F_a \\ T_1^s \\ \vdots \\ T_{n-1}^s \end{bmatrix} \quad (\text{A.25})$$

which can be expanded to include the spring of the last stage, i.e.,

$$\begin{bmatrix} F_1^a \\ F_2^a \\ \vdots \\ F_{n-1}^a \\ {}^{n-1}F_2^a \\ T_n^s \end{bmatrix} = \left(\prod_{i=1}^{n-1} \begin{bmatrix} \mathbf{1}_{n-1-i} & \mathbf{0} \\ & {}^{n-i}\mathbf{T}^f \\ \mathbf{0} & \mathbf{1}_i \end{bmatrix} \right) \begin{bmatrix} F_a \\ T_1^s \\ \vdots \\ T_{n-1}^s \\ T_n^s \end{bmatrix} \quad (\text{A.26})$$

since

$$\begin{aligned} \prod_{j=1}^m \begin{bmatrix} \mathbf{A}_j & \mathbf{0} \\ \mathbf{0} & \mathbf{1} \end{bmatrix} &= \begin{bmatrix} \mathbf{A}_1 & \mathbf{0} \\ \mathbf{0} & \mathbf{1} \end{bmatrix} \begin{bmatrix} \mathbf{A}_2 & \mathbf{0} \\ \mathbf{0} & \mathbf{1} \end{bmatrix} \cdots \begin{bmatrix} \mathbf{A}_m & \mathbf{0} \\ \mathbf{0} & \mathbf{1} \end{bmatrix} \\ &= \begin{bmatrix} \prod_{j=1}^m \mathbf{A}_j & \mathbf{0} \\ \mathbf{0} & \mathbf{1} \end{bmatrix} \end{aligned} \quad (\text{A.27})$$

if \mathbf{A}_j , $\forall j$ is square. It is noted that the index of the lower right identity matrix in the product of eq. (A.26) has been changed to account for the increased dimension. Eq. (A.24) can also be expanded to include all output forces, namely

$$\begin{bmatrix} F_1^a \\ F_2^a \\ \dots \\ F_n^a \\ F_{n+1}^a \end{bmatrix} = \begin{bmatrix} \mathbf{1}_{n-2} & \mathbf{0} \\ \mathbf{0} & {}^n\mathbf{T}^f \end{bmatrix} \begin{bmatrix} F_1^a \\ F_2^a \\ \dots \\ {}^{n-1}F_2^a \\ T_n^s \end{bmatrix}. \quad (\text{A.28})$$

Therefore, combining eqs. (A.26) and (A.28), one obtains

$$\begin{bmatrix} F_1^a \\ F_2^a \\ \dots \\ F_n^a \\ F_{n+1}^a \end{bmatrix} = \begin{bmatrix} \mathbf{1}_{n-2} & \mathbf{0} \\ \mathbf{0} & {}^n\mathbf{T}^f \end{bmatrix} \left(\prod_{i=1}^{n-1} \begin{bmatrix} \mathbf{1}_{n-1-i} & \mathbf{0} \\ \mathbf{0} & {}^{n-i}\mathbf{T}^f \\ & \mathbf{1}_i \end{bmatrix} \right) \begin{bmatrix} F_a \\ T_1^s \\ \dots \\ T_{n-1}^s \\ T_n^s \end{bmatrix} \quad (\text{A.29})$$

or equivalently, by changing the index in the second matrix,

$$\begin{bmatrix} F_1^a \\ F_2^a \\ \dots \\ F_n^a \\ F_{n+1}^a \end{bmatrix} = \begin{bmatrix} \mathbf{1}_{n-2} & \mathbf{0} \\ \mathbf{0} & {}^n\mathbf{T}^f \end{bmatrix} \left(\prod_{i=2}^n \begin{bmatrix} \mathbf{1}_{n-i} & \mathbf{0} \\ \mathbf{0} & {}^{n+1-i}\mathbf{T}^f \\ & \mathbf{1}_{i-1} \end{bmatrix} \right) \begin{bmatrix} F_a \\ T_1^s \\ \dots \\ T_{n-1}^s \\ T_n^s \end{bmatrix}. \quad (\text{A.30})$$

Therefore, one has

$$\begin{bmatrix} F_1^a \\ F_2^a \\ \dots \\ F_{n+1}^a \end{bmatrix} = \left(\prod_{i=1}^n \begin{bmatrix} \mathbf{1}_{n-i} & \mathbf{0} \\ \mathbf{0} & {}^{n+1-i}\mathbf{T}^f \\ & \mathbf{1}_{i-1} \end{bmatrix} \right) \begin{bmatrix} F_a \\ T_1^s \\ \dots \\ T_n^s \end{bmatrix} \quad (\text{A.31})$$

which is the result predicted by eq. (6.14),

QED.

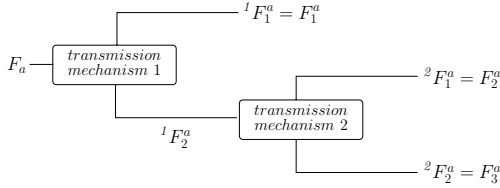


Fig. A.1. Strictly serial transmission tree for $n = 3$

Initialization

If $n = 2$, the proof of eq. (6.14) is trivial. If another stage is added, i.e., for $n = 3$ (illustrated in Fig. A.1), one has

$$\begin{bmatrix} {}^1F_1^a \\ {}^1F_2^a \end{bmatrix} = \begin{bmatrix} F_1^a \\ {}^1F_2^a \end{bmatrix} = {}^1\mathbf{T}^f \begin{bmatrix} F_a \\ T_1^s \end{bmatrix} \quad (\text{A.32})$$

$$\begin{bmatrix} {}^2F_1^a \\ {}^2F_2^a \end{bmatrix} = \begin{bmatrix} F_2^a \\ F_3^a \end{bmatrix} = {}^2\mathbf{T}^f \begin{bmatrix} {}^1F_2^a \\ T_2^s \end{bmatrix}. \quad (\text{A.33})$$

Hence,

$$\begin{bmatrix} F_1^a \\ F_2^a \\ F_3^a \end{bmatrix} = \begin{bmatrix} 1 & \mathbf{0} \\ \mathbf{0} & {}^2\mathbf{T}^f \end{bmatrix} \begin{bmatrix} F_1^a \\ {}^1F_2^a \\ T_2^s \end{bmatrix} \quad (\text{A.34})$$

where the left hand side vector of eq. (A.32) can be readily identified. Therefore, one obtains

$$\begin{bmatrix} F_1^a \\ F_2^a \\ F_3^a \end{bmatrix} = \begin{bmatrix} 1 & \mathbf{0} \\ \mathbf{0} & {}^2\mathbf{T}^f \end{bmatrix} \begin{bmatrix} {}^1\mathbf{T}^f & \mathbf{0} \\ \mathbf{0} & 1 \end{bmatrix} \begin{bmatrix} F_a \\ T_1^s \\ T_2^s \end{bmatrix} \quad (\text{A.35})$$

which is the result obtained by setting $n = 3$ in eq. (6.14).

A.4.2 Symmetrical Transmission Tree

A symmetrical transmission tree according to the definition given in Section 6.3.1 and illustrated in Fig. 6.14 is studied. The formula defined in eq. (6.15) is to be proven by induction. Similarly to what was presented in the previous section, each transmission stage is described by its associated force transmission matrix, i.e.

$${}^i\mathbf{F} = {}^i\mathbf{T}^f {}^i\mathbf{t}^\diamond \quad i = 1, \dots, n - 1. \quad (\text{A.36})$$

Heredity

Let us suppose a symmetrical transmission tree with $n - 1$ stages (and thus, n force outputs) described by eq. (6.15), i.e.,

$$\begin{bmatrix} F_1^a \\ F_2^a \\ \dots \\ F_n^a \end{bmatrix} = \left(\prod_{i=1}^{\frac{\log n}{\log 2}} \begin{bmatrix} {}^{2^{i-1}}\mathbf{T}^f & & & & \mathbf{0} \\ & \ddots & & & \\ & & {}^{2^{i-1}}\mathbf{T}^f & & \\ & & & \mathbf{0} & \mathbf{1}_{n-2^i} \\ & & & & \end{bmatrix} {}^i\mathbf{B}_n \right) \begin{bmatrix} F_a \\ T_1^s \\ \dots \\ T_{n-1}^s \end{bmatrix}. \quad (\text{A.37})$$

If n supplementary stages are added to the transmission tree, accordingly to Fig. A.2 to keep the tree strictly symmetrical, one has

$$\begin{cases} \begin{bmatrix} {}^i F_1^a \\ {}^i F_2^a \end{bmatrix} = {}^i\mathbf{T}^f \begin{bmatrix} {}^{i/2} F_1^a \\ T_i^s \end{bmatrix} & i = 2k \\ \begin{bmatrix} {}^i F_1^a \\ {}^i F_2^a \end{bmatrix} = {}^i\mathbf{T}^f \begin{bmatrix} {}^{(i-1)/2} F_2^a \\ T_i^s \end{bmatrix} & i = 2k + 1 \end{cases} \quad \text{for } k = n/2, \dots, n-1 \quad (\text{A.38})$$

with

$$\begin{bmatrix} {}^i F_1^a \\ {}^i F_2^a \end{bmatrix} = \begin{bmatrix} F_{2(i-n)+1}^a \\ F_{2(i-n)+2}^a \end{bmatrix} \quad i = n, \dots, 2n-1. \quad (\text{A.39})$$

Note that the n supplementary stages have indices n to $2n-1$ and their associated force outputs have indices 1 to $2n$. Hence,

$$\begin{bmatrix} F_1^a \\ F_2^a \\ F_3^a \\ \dots \\ F_{2n-1}^a \\ F_{2n}^a \end{bmatrix} = \begin{bmatrix} {}^n\mathbf{T}^f & & & & & \\ & {}^{n+1}\mathbf{T}^f & & & & \mathbf{0} \\ & & \ddots & & & \\ & & & \mathbf{0} & & {}^{2n-1}\mathbf{T}^f \\ & & & & & \end{bmatrix} \begin{bmatrix} {}^{n/2} F_1^a \\ T_n^s \\ {}^{n/2} F_2^a \\ T_{n+1}^s \\ \dots \\ T_{2n-1}^s \end{bmatrix}. \quad (\text{A.40})$$

Re-ordering the components in the right hand side vector, one has

$$\begin{bmatrix} {}^{n/2} F_1^a \\ T_n^s \\ {}^{n/2} F_2^a \\ T_{n+1}^s \\ \dots \\ T_{2n-1}^s \end{bmatrix} = \begin{bmatrix} 1 & 0 & 0 & \dots & 0 & | & 0 & 0 & 0 & \dots & 0 \\ 0 & 0 & 0 & \dots & 0 & | & 1 & 0 & 0 & \dots & 0 \\ 0 & 1 & 0 & \dots & 0 & | & 0 & 0 & 0 & \dots & 0 \\ 0 & 0 & 0 & \dots & 0 & | & 0 & 1 & 0 & \dots & 0 \\ \dots & \dots \\ 0 & 0 & 0 & \dots & 0 & | & 0 & 0 & 0 & \dots & 1 \end{bmatrix} \begin{bmatrix} {}^{n/2} F_1^a \\ \dots \\ {}^{n-1} F_2^a \\ T_n^s \\ \dots \\ T_{2n-1}^s \end{bmatrix} \quad (\text{A.41})$$

where the bubble matrix ${}^n\mathbf{B}_{2n}$ can be readily recognized. Hence, eq. (A.40) can be written as

$$\begin{bmatrix} F_1^a \\ F_2^a \\ F_3^a \\ \dots \\ F_{2n-1}^a \\ F_{2n}^a \end{bmatrix} = \begin{bmatrix} {}^n\mathbf{T}^f & & & & & \\ & {}^{n+1}\mathbf{T}^f & & \mathbf{0} & & \\ & & \ddots & & & \\ & & & \mathbf{0} & {}^{2n-1}\mathbf{T}^f & \\ & & & & & \end{bmatrix} {}^n\mathbf{B}_{2n} \begin{bmatrix} {}^{n/2}F_1^a \\ \dots \\ {}^{n-1}F_2^a \\ T_n^s \\ \dots \\ T_{2n-1}^s \end{bmatrix} \quad (\text{A.42})$$

where eq. (A.37) which characterizes the initial transmission tree can be readily recognized. Therefore, one obtains

$$\begin{bmatrix} F_1^a \\ F_2^a \\ F_3^a \\ \dots \\ F_{2n-1}^a \\ F_{2n}^a \end{bmatrix} = \begin{bmatrix} {}^n\mathbf{T}^f & & & & & \\ & {}^{n+1}\mathbf{T}^f & & \mathbf{0} & & \\ & & \ddots & & & \\ & & & \mathbf{0} & {}^{2n-1}\mathbf{T}^f & \\ & & & & & \end{bmatrix} {}^n\mathbf{B}_{2n} \times \quad (\text{A.43})$$

$$\begin{bmatrix} \prod_{i=1}^{\frac{\log n}{\log 2}} & \begin{bmatrix} {}^{2^{i-1}}\mathbf{T}^f & & & & & \\ & \ddots & & \mathbf{0} & & \\ & & {}^{2^{i-1}}\mathbf{T}^f & & & \\ & & & \mathbf{0} & \mathbf{1}_{n-2^i} & \\ & & & & & \mathbf{0} \end{bmatrix} & {}^i\mathbf{B}_n & \mathbf{0} & \begin{bmatrix} F_a \\ T_1^s \\ \dots \\ \dots \\ T_{2n-1}^s \end{bmatrix} \end{bmatrix}.$$

Using eq. (A.27) and the definition of the bubble matrices in eq. (6.16), one has

$$\begin{bmatrix} F_1^a \\ F_2^a \\ F_3^a \\ \dots \\ F_{2n-1}^a \\ F_{2n}^a \end{bmatrix} = \begin{bmatrix} {}^n\mathbf{T}^f & & & & & \\ & {}^{n+1}\mathbf{T}^f & & \mathbf{0} & & \\ & & \ddots & & & \\ & & & \mathbf{0} & {}^{2n-1}\mathbf{T}^f & \\ & & & & & \end{bmatrix} {}^n\mathbf{B}_{2n} \times \quad (\text{A.44})$$

$$\begin{bmatrix} \prod_{i=1}^{\frac{\log n}{\log 2}} & \begin{bmatrix} {}^{2^{i-1}}\mathbf{T}^f & & & & & \\ & \ddots & & \mathbf{0} & & \\ & & {}^{2^{i-1}}\mathbf{T}^f & & & \\ & & & \mathbf{0} & \mathbf{1}_{2n-2^i} & \\ & & & & & \mathbf{0} \end{bmatrix} & {}^i\mathbf{B}_{2n} & \begin{bmatrix} F_a \\ T_1^s \\ \dots \\ \dots \\ T_{2n-1}^s \end{bmatrix} \end{bmatrix}.$$

Hence, one finally obtains

$$\begin{bmatrix} F_1^a \\ F_2^a \\ F_3^a \\ \dots \\ F_{n-1}^a \\ F_n^a \end{bmatrix} = \prod_{i=1}^{\frac{\log 2n}{\log 2}} \begin{bmatrix} {}^2\mathbf{T}^f & & & & & \\ & \ddots & & & & \\ & & {}^i\mathbf{B}_{2n} & & & \\ & & & \mathbf{0} & & \\ & & & & {}^{2^i-1}\mathbf{T}^f & \\ & & & & & \mathbf{0} \end{bmatrix} \begin{bmatrix} F_a \\ T_1^s \\ \dots \\ \dots \\ T_{2n-1}^s \end{bmatrix} \quad (\text{A.45})$$

which is the result predicted by eq. (6.15).

Initialization

For $n = 2$, illustrated in Fig. A.2, one has

$$\begin{bmatrix} {}^1F_1^a \\ {}^1F_2^a \end{bmatrix} = \begin{bmatrix} F_1^a \\ F_2^a \end{bmatrix} = {}^1\mathbf{T}^f \begin{bmatrix} F_a \\ T_1^s \end{bmatrix} \quad (\text{A.46})$$

which is the result anticipated by eq. (6.15). If two supplementary stages are added to the transmission tree (i.e. $n = 4$), and accordingly Section 6.3.1 to keep the tree symmetrical, one has

$$\begin{bmatrix} {}^1F_1^a \\ {}^1F_2^a \end{bmatrix} = {}^1\mathbf{T}^f \begin{bmatrix} F_a \\ T_1^s \end{bmatrix} \quad (\text{A.47})$$

$$\begin{bmatrix} {}^2F_1^a \\ {}^2F_2^a \end{bmatrix} = \begin{bmatrix} F_1^a \\ F_2^a \end{bmatrix} = {}^2\mathbf{T}^f \begin{bmatrix} {}^1F_1^a \\ T_2^s \end{bmatrix} \quad (\text{A.48})$$

$$\begin{bmatrix} {}^3F_1^a \\ {}^3F_2^a \end{bmatrix} = \begin{bmatrix} F_3^a \\ F_4^a \end{bmatrix} = {}^3\mathbf{T}^f \begin{bmatrix} {}^1F_2^a \\ T_3^s \end{bmatrix}. \quad (\text{A.49})$$

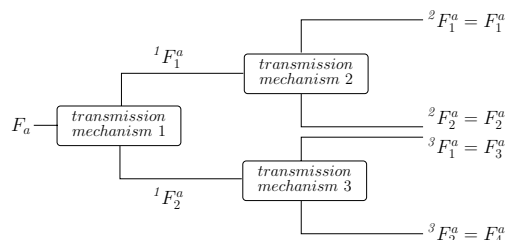


Fig. A.2. Symmetrical transmission tree for $n = 3$

Hence, by combining eqs. (A.48) and (A.49), one obtains

$$\begin{bmatrix} F_1^a \\ F_2^a \\ F_3^a \\ F_4^a \end{bmatrix} = \begin{bmatrix} {}^2\mathbf{T}^f & \mathbf{0} \\ \mathbf{0} & {}^3\mathbf{T}^f \end{bmatrix} \begin{bmatrix} {}^1F_1^a \\ T_2^s \\ {}^1F_2^a \\ T_3^s \end{bmatrix}. \quad (\text{A.50})$$

Re-ordering the components in the right hand side vector yields

$$\begin{bmatrix} F_1^a \\ F_2^a \\ F_3^a \\ F_4^a \end{bmatrix} = \begin{bmatrix} {}^2\mathbf{T}^f & \mathbf{0} \\ \mathbf{0} & {}^3\mathbf{T}^f \end{bmatrix} \begin{bmatrix} 1 & 0 & 0 & 0 \\ 0 & 0 & 1 & 0 \\ 0 & 1 & 0 & 0 \\ 0 & 0 & 0 & 1 \end{bmatrix} \begin{bmatrix} {}^1F_1^a \\ {}^1F_2^a \\ T_2^s \\ T_3^s \end{bmatrix} \quad (\text{A.51})$$

where the bubble matrix ${}^2\mathbf{B}_4$ can be readily recognized. Thereupon, one can use eq. (A.46) to obtain

$$\begin{bmatrix} F_1^a \\ F_2^a \\ F_3^a \\ F_4^a \end{bmatrix} = \begin{bmatrix} {}^2\mathbf{T}^f & \mathbf{0} \\ \mathbf{0} & {}^3\mathbf{T}^f \end{bmatrix} {}^2\mathbf{B}_4 \begin{bmatrix} {}^1\mathbf{T}^f & \mathbf{0} \\ \mathbf{0} & \mathbf{1}_2 \end{bmatrix} \begin{bmatrix} F_a \\ T_1^s \\ T_2^s \\ T_3^s \end{bmatrix} \quad (\text{A.52})$$

which is the result predicted by eq. (6.15).

References

- Akin, D.L., Carignan, C.R., Foster, A.W.: Development of a four-fingered dexterous robot end effector for space operations. In: Proceedings of the 2002 IEEE International Conference on Robotics and Automation, Washington, DC, USA, pp. 2302–2308 (2002)
- Alfieri, V.: La mano di collins per gli amputati di arto superiore. *Minerva Ortopedica* 21(1), 47–50 (1970)
- Antonelli, K., Immega, G.: An extensible robotic tentacle. *Industrial Robot* 24(4), 423–427 (1997)
- Bar-Cohen, Y., Breazal, C.: Biologically Inspired Intelligent Robots. SPIE-The International Society for Optical Engineering (2003)
- Bartholet, S.J.: Reconfigurable End Effector. US Patent No. 5 108 140 (1992)
- Bekey, G.A., Tomovic, R., Zeljkovic, I.: Control Architecture for the Belgrade/USC Hand in Dextrous Robot Hands. Springer, New York (1999)
- Bergevin, R., Mokhtari, M.: Multiscale contour segmentation and approximation: An algorithm based on the geometry of regular inscribed polygons. *Computer Vision and Image Understanding* 71(1), 55–73 (1998)
- Biagiotti, L., Melchiorri, C., Vassura, G.: Control of a robotic gripper for grasping objects in no-gravity conditions. In: Proceedings of the 2001 IEEE International Conference on Robotics and Automation, Seoul, Korea, pp. 1427–1432 (May 21–26, 2001)
- Bicchi, A.: Hands for dexterous manipulation and powerful grasping: A difficult road towards simplicity. *IEEE Transactions on Robotics and Automation* 16(6), 652–662 (2000)
- Bicchi, A., Kumar, V.: Robotic grasping and contact: A review. In: Proceedings of the IEEE International Conference on Robotics and Automation, San Francisco, CA, USA, pp. 348–353 (April 24–28, 2000)
- Birglen, L.: Analysis and Control of Underactuated Robotic Hands. Ph. D. thesis, Faculté des sciences et de génie, Université Laval, Québec, Canada (October 2004)
- Birglen, L.: An introduction to the analysis of linkage-driven compliant underactuated fingers. In: 2006 ASME International Design Engineering Technical Conferences, Philadelphia, PA, USA (September 10–13, 2006)
- Birglen, L., Gosselin, C.: On the force capabilities of underactuated fingers. In: Proceedings of the 2003 IEEE International Conference on Robotics and Automation, Taipei, Taiwan, pp. 1139–1145 (September 14–19, 2003)

- Birglen, L., Gosselin, C.: Kinetostatic analysis of underactuated fingers. *IEEE Transactions on Robotics and Automation* 20(2), 211–221 (2004a)
- Birglen, L., Gosselin, C.: Optimal design of 2-phalanx underactuated fingers. In: Proceedings of 2004 International Conference on Intelligent Manipulation and Grasping, Genova, Italy, pp. 110–116 (July 1-2, 2004b)
- Birglen, L., Gosselin, C.: Fuzzy enhanced control of an underactuated finger using tactile and position sensors. In: Proceedings of the 2005 IEEE International Conference on Robotics and Automation, Barcelona, Spain, pp. 2331–2336 (April 2005)
- Birglen, L., Gosselin, C.: Force analysis of connected differential mechanisms: Application to grasping. *International Journal of Robotics Research* 25(10), 1033–1046 (2006a)
- Birglen, L., Gosselin, C.: Geometric design of three-phalanx underactuated fingers. *ASME Journal of Mechanical Design* 128(2), 356–364 (2006b)
- Birglen, L., Gosselin, C.: Grasp-state plane analysis of two-phalanx underactuated fingers. *Mechanism and Machine Theory* 41(7), 807–822 (2006c)
- Birglen, L., Gosselin, C.: Optimally unstable underactuated gripper: Synthesis and applications. In: 2006 ASME International Design Engineering Technical Conferences, Philadelphia, PA, USA (September 10-13, 2006d)
- Boivin, E., Sharf, I.: Optimum grasp planner and vision-guided grasping using a three-finger hand. *Industrial Robot* 32(1), 35–42 (2005)
- Boivin, E., Sharf, I., Doyon, M.: Optimum grasp of planar and revolute objects with gripper geometry constraints. In: Proceedings of the 2004 IEEE International Conference on Robotics and Automation, New Orleans, LA, USA, pp. 326–332 (April 2004)
- Boudreault, E., Gosselin, C.: Mechanically intelligent grippers for telemedicine. In: Poster presented at the 15th Annual Canadian Conference on Intelligent Systems, Quebec City, Canada (June 5-7, 2005)
- Boudreault, E., Gosselin, C.: Design of sub-centimetre underactuated compliant grippers. In: 2006 ASME International Design Engineering Technical Conferences, Philadelphia, PA, USA (September 10-13, 2006)
- Bulich, C., Klein, A., Watson, R., Kitts, C.: Characterization of delay-induced piloting instability for the triton undersea robot. In: Proceedings of the 2004 IEEE Aerospace Conference (2004)
- Butterfass, J., Grebenstein, M., Liu, H., Hirzinger, G.: Dlr-hand ii: Next generation of a dexterous robot hand. In: Proceedings of the 2001 IEEE International Conference on Robotics and Automation, Seoul, Korea, pp. 109–114 (May 21-26, 2001)
- Cabas, R., Cabas, L.M., Balaguer, C.: Optimized design of the underactuated robotic hand. In: Proceedings of the 2006 IEEE International Conference on Robotics and Automation, Orlando, FL, USA, pp. 982–987 (May 2006)
- Carrozza, M.C., Cappiello, G., Stellin, G., Zaccone, F., Vecchi, F., Micera, S., Dario, P.: A cosmetic prosthetic hand with tendon driven under-actuated mechanism and compliant joints: Ongoing research and preliminary results. In: Proceedings of the 2005 IEEE International Conference on Robotics and Automation, Barcelona, Spain, pp. 2672–2677 (April 2005)
- Carrozza, M.C., Massa, B., Micera, S., Lazzarini, R., Zecca, M., Dario, P.: The development of a novel prosthetic hand — ongoing research and preliminary results. *IEEE/ASME Transactions on Mechatronics* 7(2), 108–114 (2002)

- Carrozza, M.C., Suppo, C., Sebastiani, F., Massa, B., Vecchi, F., Lazzarini, R., Cutkosky, M.R., Dario, P.: The spring hand: Development of a self-adaptive prosthesis for restoring natural grasping. *Autonomous Robots* 16, 125–141 (2004)
- Carrozza, M.C., Vecchi, F., Sebastiani, F., Cappiello, G., Roccella, S., Zecca, M., Lazzarini, R., Dario, P.: Experimental analysis of an innovative prosthetic hand with proprioceptive sensors. In: Proceedings of the IEEE International Conference on Robotics and Automation, Taipei, Taiwan, pp. 2230–2235 (September 14–19, 2003)
- Ceccarelli, M.: A historical perspective of robotics toward the future. *Journal of Robotics and Mechatronics* 13(3), 299–313 (2001)
- Chen, F.Y.: Gripping mechanisms for industrial robots. *Mechanism and Machine Theory* 17(5), 299–311 (1982)
- Choi, H., Koc, M.: Design and feasibility tests of a flexible gripper based on inflatable rubber pockets. *International Journal of Machine Tools and Manufacture* 46(12–13), 1350–1361 (2006)
- Choi, K.K., Jiang, S.L., Li, Z.: Multifingered robotic hands: Contact experiments using tactile sensors. In: Proceedings of the 1998 IEEE International Conference on Robotics and Automation, Leuven, Belgium (May 1998)
- Chua, P.Y., Ilschner, T., Caldwell, D.G.: Robotic manipulation of food products - a review. *Industrial Robot* 30(4), 345–354 (2004)
- Crisman, J.D., Kanojia, C., Zeid, I.: Graspar: A flexible, easily controllable robotic hand. *IEEE Robotics and Automation Magazine*, 32–38 (June 1996)
- Crowder, R.M.: An anthropomorphic robotic end effector. *Robotics and Autonomous Systems* 7(4), 253–268 (1991)
- Cutkosky, M.R.: On grasp choice, grasp models, and the design of hands for manufacturing tasks. *IEEE Transactions on Robotics and Automation* 5(3), 269–279 (1989)
- Dale, F.L.: Artificial Hand. US Patent No. 2 457 305 (1948)
- Dechev, N., Cleghorn, W.L., Naumann, S.: Multiple finger, passive adaptive grasp prosthetic hand. *Mechanism and Machine Theory* 36, 1157–1173 (2001)
- Diftler, M.A., Ambrose, R.O.: Robonaut: A robotic astronaut assistant. In: Proceedings of the 6th International Symposium on Artificial Intelligence and Robotics and Automation in Space: i-SAIRAS 2001, Saint-Hubert, QC, Canada (June 18–22, 2001)
- Dilibal, S., Guner, E., Akturk, N.: Three-finger sma robot hand and its practical analysis. *Robotica* 20(2), 175–180 (2002)
- Dollar, A.M., Howe, R.D.: A robust compliant grasper via shape deposition manufacturing. *IEEE/ASME Transactions on Mechatronics* 11(2), 154–161 (2006)
- Doshi, R., Yeh, C., Leblanc, M.: The design and development of a gloveless endoskeletal prosthetic hand. *Journal of Rehabilitation Research and Development* 35(4) (1998)
- Dubey, V.N., Crowder, R.M.: A finger mechanism for adaptive end effectors. In: Proceedings of 2002 ASME Design Engineering Technical Conferences, Montreal, Canada (September 29–October 2, 2002)
- Dubey, V.N., Crowder, R.M., Chappell, P.H.: Optimal object grasp using tactile sensors and fuzzy logic. *Robotica* 17(6), 685–693 (1999)
- Edsinger-Gonzales, A.: Design of a compliant and force sensing hand for a humanoid robot. In: Proceedings of the 2004 International Conference on Intelligent Manipulation and Grasping, Genova, Italy, pp. 291–295 (July 1–2, 2004)
- Figliolini, G., Ceccarelli, M.: A novel articulated mechanism mimicking the motion of index fingers. *Robotica* 20(1), 13–22 (2002)
- Figliolini, G., Principe, M., Rea, P.: Mechatronic design of ca.u.m.ha (cassino-underactuated-multifinger-hand). In: Proceedings of RAAD 2003, 12th International Workshop on Robotics in Alpe-Adria-Danube Region, Cassino, Italy (May 7–10, 2003)

- Fischer, T., Woern, H.: Structure of a robot system: Karlsruhe dexterous hand ii. In: Proceedings of the 1998 Mediterranean Conference on Control and Systems (1998)
- Fite, K.B., Withrow, T.J., Wait, K.W., Goldfarb, M.: Liquid-fueled actuation for an anthropomorphic upper extremity prosthesis. In: Proceedings of the 28th Annual International Conference of the IEEE Engineering in Medicine and Biology Society, New-York, USA, pp. 5638–5642 (August 2006)
- Foster, A.W., Akin, D.L.: A set of grasp requirements for a dexterous robot hand based on existing crew aids, tools and interfaces. In: Proceedings of the 6th International Symposium on Artificial Intelligence and Robotics & Automation in Space: i-SAIRAS 2001, Saint-Hubert, QC, Canada (June 18-22, 2001)
- Fukaya, N., Toyama, S., Asfour, T., Dillmann, R.: Design of the tuat/karlsruhe humanoid hand. In: Proceedings of 2000 IEEE/RSJ International Conference on Advanced Robotics, Takamatsu, Japan, vol. 3, pp. 1754–1759 (October 30–November 5, 2000)
- Gazeau, J.P., Zeghloul, S., Arsicault, M., Lallemand, J.P.: The lms hand: Force and position control in the aim of the fine manipulation of objects. In: Proceedings of the 2001 IEEE International Conference on Robotics and Automation, Seoul, Korea, pp. 2642–2648 (May 21–26, 2001)
- Goertz, R.C.: Fundamentals of general-purpose remote manipulators. *Nucleonics* 10(11), 36–45 (1952)
- Gosselin, C.: Analysis and synthesis of underactuated force generating mechanisms. In: Proceedings of the 1996 ASME Design Engineering Technical Conference and Computers in Engineering Conference, Irvin, CA, USA (August 18–22, 1996)
- Gosselin, C.: Adaptive robotic mechanical systems: A design paradigm. *ASME Journal of Mechanical Design* 128(1), 192–198 (2006)
- Gosselin, C., Angeles, J.: Singularity analysis of closed-loop kinematic chains. *IEEE Transactions on Robotics and Automation* 6(3), 281–290 (1990)
- Gosselin, C., Laliberté, T.: Underactuated mechanical finger with return actuation. US Patent No. 5 762 390 (1996)
- Gosselin, C., Laliberté, T., Degou lange, E.: Underactuated robotic hand. In: Video Proceedings of the 1998 IEEE International Conference on Robotics and Automation, Leuven, Belgium (May 1998)
- Greiner, H.: Passive and active grasping with a prehensile robot end-effector. Master's thesis, Massachusetts Institute of Technology, Artificial Intelligence Laboratory, Boston, MA, USA (May 1990)
- Guo, G., Qian, X., Gruver, W.A.: A single-dof multi-function prosthetic hand mechanism with an automatically variable speed transmission. In: Proceedings of the 1992 ASME Biennial Mechanisms Conference, Phoenix, AZ, pp. 149–154 (September 1992)
- Guo, G., Qian, X., Gruver, W.A.: Multi-function mechanical hand with shape adaptation. US Patent No. 5 378 033 (1995)
- Hannan, M.W., Walker, I.D.: The 'elephant trunk' manipulator, design and implementation. In: Proceedings of 2001 IEEE/ASME International Conference on Advanced/Intelligent Mechatronics, Como, Italy, pp. 14–19 (July 2001)
- Henning, F.C.: Artificial Hand. US Patent No. 1 298 502 (1919)
- Herder, J.: Energy-free Systems; Theory, Conception and Design of Statically Balanced Spring Mechanisms. Ph. D. thesis, Delft University of Technology, Delft, The Netherlands (2001)

- Herder, J.L.: Force directed design of laparoscopic forceps. In: Proceedings of the 1998 ASME Design Engineering Technical Conferences, Atlanta, GA, USA (September 1998)
- Herder, J.L.: Clinically driven design in rehabilitation and minimal access surgery. Technical report, Business Briefing: Medical Device Manufacturing and Technology (2004)
- Herder, J.L., de Visser, H.: Force directed design of a voluntary closing hand prosthesis. In: Proceedings of the 2000 ASME Design Engineering Technical Conferences, Baltimore, MD, USA, pp. 1–8 (September 2000)
- Higashimori, M., Kaneko, M., Ishikawa, M.: Dynamic preshaping for a robot driven by a single wire. In: Proceedings of the IEEE International Conference on Robotics and Automation, Taipei, Taiwan, pp. 1115–1120 (September 14–19, 2003)
- Hirose, S.: Connected differential mechanism and its applications. In: Proceedings of 1985 International Conference on Advanced Robotics, Tokyo, Japan, pp. 319–325 (September 1985)
- Hirose, S.: Biologically Inspired Robotics, translated by P. Cave and C. Goulden. Oxford University Press, Oxford (1993)
- Hirose, S., Umetani, Y.: The development of soft gripper for the versatile robot hand. Mechanism and Machine Theory 13, 351–358 (1978)
- Hirose, S., Yoneda, K., Tsukagoshi, H.: Titan vii: Quadruped walking and manipulating robot on a steep slope. In: Proceedings of the 1997 IEEE International Conference on Robotics and Automation, Albuquerque, NM, USA (April 1997)
- Hunt, K.H.: Kinematic Geometry of Mechanisms. Oxford University Press, Oxford (1978)
- Hunt, K.H., Samuel, A.E., McAree, P.R.: Special configurations of multi-finger multi-freedom grippers - a kinematic study. International Journal of Robotic Research 10(2), 123–133 (1991)
- Iberall, T., Lyons, D.: Towards perceptual robotics. In: Proceedings of the 1984 International Symposium on Systems, Man, Cybernetics, Halifax, Canada (October 9–12, 1984)
- IFToMM: Terminology for the theory of machines and mechanisms. Mechanism and Machine Theory 26(5), 435–539 (1991)
- Imcaoudene, B., Gosselin, C.: Application of dexterity indices to spatial articulated hands. Advances in Robot Kinematics and Computationed Geometry, 201–208 (1994)
- Itoh, H.: Mechanical Hand. US Patent No. 3 927 424 (1975)
- Jacobsen, S.C., Iversen, E.K., Knutti, D.F., Johnson, R.T., Biggers, K.B.: Design of the utah/mit dextrous hand. In: Proceedings of the 1986 IEEE International Conference on Robotics and Automation, San Francisco, CA, USA, pp. 1520–1532 (April 1986)
- Jensen, P.W.: Classical and Modern Mechanisms for Engineers and Inventors. Marcel Dekker, New-York (1991)
- Jiang, L., Jin, M.H., Gao, X.H., Xie, Z.W., Yang, L., He, P., Lie, Y.W., Wei, R., Cai, H.G., Liu, H., Seitz, N., Grebenstein, M., Hirzinger, G.: Multisensory hit/dlr dexterous robot hand. In: Proceedings of the 2003 IEEE/ASME International Conference on Advanced Intelligent Mechatronics, Kobe, Japan, vol. 1, pp. 76–81 (July 20–24, 2003)
- Kaneko, M., Hayashi, T.: Standing-up characteristic of contact force during self-posture changing motions. In: Proceedings of the IEEE International Conference on Robotics and Automation, pp. 202–208 (1993)

- Kaneko, M., Higashimori, M., Takenaka, R., Namiki, A., Ishikawa, M.: The 100 g capturing robot — too fast to see. *IEEE/ASME Transactions on Mechatronics* 8(1), 37–44 (2003)
- Kaneko, M., Tanie, K.: Contact point detection for grasping of an unknown object using self-posture changeability (spc). In: Proceedings of the IEEE International Conference on Robotics and Automation, pp. 864–869 (1990)
- Kato, I.: Mechanical Hands Illustrated. Survey Japan (1982)
- Kawasaki, H., Komatsu, T., Uchiyama, K.: Dexterous anthropomorphic robot hand with distributed tactile sensor: Gifu hand ii. *IEEE/ASME Transactions on Mechatronics* 7(3), 296–303 (2002)
- Kennedy, B.: Three-fingered robot hand with self-adjusting grip. *Nasa Tech Briefs* 25(12), 59 (2001)
- Kennedy, B., Agazarian, H., Cheng, Y., Garrett, M., Hickey, G., Huntsberger, T., Magnone, L., Mahoney, C., Meyer, A., Knight, J.: Lemur: Legged excursion mechanical utility rover. *Autonomous Robots* 11, 201–205 (2001)
- Koganezawa, K.: Artificial finger with shape-fitting mechanism. In: Proceedings of the 2004 International Conference on Intelligent Manipulation and Grasping, Genova, Italy, pp. 103–109 (July 2004)
- Koustoumpardis, P.N., Aspragathos, N.A.: A review of gripping devices for fabric handling. In: Proceedings of 2004 International Conference on Intelligent Manipulation and Grasping, Genova, Italy, pp. 229–234 (July 1-2, 2004)
- Krut, S.: A force-isotropic underactuated finger. In: Proceedings of the 2005 IEEE International Conference on Robotics and Automation, Barcelona, Spain, pp. 2325–2330 (April 2005)
- Kyberd, P.J., Light, C., Chappel, P.H., Nightingale, J.M., Whatley, D., Evans, M.: The design of an anthropomorphic prosthetic hands: A study of the southampton hand. *Robotica* 19(6), 593–600 (2001)
- Laliberté, T., Birglen, L., Gosselin, C.: Underactuation in robotic grasping hands. *Japanese Journal of Machine Intelligence and Robotic Control, Special Issue on Underactuated Robots* 4(3), 77–87 (2002)
- Laliberté, T., Gosselin, C.: Simulation and design of underactuated mechanical hands. *Mechanism and Machine Theory* 33(1/2), 39–57 (1998)
- Laliberté, T., Gosselin, C.: Development of a three-dof underactuated finger. In: Proceedings of the 2001 CCToMM Symposium on Mechanisms, Machines, and Mechatronics, Saint-Hubert, QC, Canada (June, 2001a)
- Laliberté, T., Gosselin, C.: Underactuation in space robotic hands. In: International Symposium on Artificial Intelligence, Robotics and Automation in Space, Montréal, Canada, pp. 18–21 (June 18–21, 2001b)
- Laliberté, T., Gosselin, C.: Actuation System for Highly Underactuated Gripping Mechanism. US Patent No. 6 505 870 (2003)
- Landsmeer, J.M.F.: Power grip and precision handling. *Annals of the Rheumatic Diseases* 21, 164–169 (1962)
- Lane, D.M., Davies, J.B.C., Casalino, G., Bartolini, G., Cannata, G., Veruggio, G., Canals, M., Smith, C., O'Brien, D.J., Pickett, M., Robinson, G., Jones, D., Scott, E., Ferrara, A., Angelletti, D., Cocco, M., Bono, R., Virgili, P., Pallas, R., Gracia, E.: Amadeus: Advanced manipulation for deep underwater sampling. *IEEE Robotics and Automation Magazine* 37, 34–45 (1997)
- Liu, H., Meusel, P., Butterfass, J., Knoch, A., Hirzinger, G.: Dlr's multisensory articulated hand part i-ii. In: Proceedings of the 1998 IEEE International Conference on Robotics and Automation, Leuven, Belgium, pp. 2087–2093 (May 1998)

- Liu, H., Meusel, P., Hirzinger, G.: A tactile sensing system for the dlr three-finger robot hand. In: Proceedings of the 1995 International Symposium on Measurement and Control in Robotics, Bratislava, Slovak Republic, pp. 91–96 (June 1995)
- Lotti, F., Tiezzi, P., Vassura, G., Biagotti, L., Palli, G., Melchiorri, C.: Development of ub hand 3: Early results. In: Proceedings of the 2005 IEEE International Conference on Robotics and Automation, Barcelona, Spain, pp. 4499–4504 (April 2005)
- Lotti, F., Vassura, G.: A novel approach to mechanical design of articulated fingers for robotic hands. In: Proceedings of the 2002 IEEE/RSJ International Conference on Intelligent Robots and System, vol. 2, pp. 1687–1692 (September 30–October 5, 2002)
- Luo, M., Mei, T., Wang, X., Yu, Y.: Grasp characteristics of an underactuated robot hand. In: Proceedings of the 2004 IEEE International Conference on Robotics and Automation, New Orleans, LA, USA, pp. 2236–2241 (April 2004)
- Maekawa, H., Tanie, K., Komoriya, K.: Dynamic grasping force control using tactile feedback for grasp of multifingered hand. In: Proceedings of the 1996 IEEE International Conference on Robotics and Automation, Minneapolis, MN, USA, pp. 2462–2469 (April 1996)
- Maeno, T., Hiromitsu, S., Kawai, T.: Control of grasping force by detecting stick/slip distribution at the curved surface of an elastic finger. In: Proceedings of the 2000 IEEE International Conference on Robotics and Automation, San Francisco, CA, USA, pp. 3896–3901 (April 24–28, 2000)
- Mason, M.T., Salisbury, J.K.: Robot Hands and the Mechanics of Manipulation. The MIT Press, Cambridge (1985)
- Massa, B., Roccella, S., Carrozza, M.C., Dario, P.: Design and development of an underactuated prosthetic hand. In: Proceedings of the 2002 IEEE International Conference on Robotics and Automation, Washington, DC, USA, pp. 3374–3379 (May 2002)
- McAree, P.R., Samuel, A.E., Hunt, K.H., Gibson, C.G.: A dexterity measure for the kinematic control of a multifinger, multidegree-of-freedom robot hand. International Journal of Robotic Research 10(5), 439–453 (1991)
- McCarthy, J.M.: Geometric Design of Linkages. Springer, Heidelberg (2000)
- Mochiyama, H., Hiramatsu, S., Mori, Y.: The frenet-serret manipulator. In: Proceedings of the IEEE/ASME International Conference on Advanced Intelligent Mechatronics, Como, Italy, pp. 20–25 (July 2001)
- Mosher, R.: Force reflection electrohydraulic servo manipulator. Electro-Technology (December 1960)
- Mullen, J. F.: Mechanical Hand. US Patent No. 3 694 021 (1972)
- Myrand, M., Gosselin, C.: Dynamic simulation of an underactuated hand for space applications. In: Proceedings of the 15th CISM-IFTOMM Symposium on Robot Design, Dynamics and Control, Montreal, Canada (June 14–18, 2004)
- Nasser, S., Rincon, D., Rodriguez, M.: Design of an anthropomorphic underactuated hand prosthesis with passive-adaptive grasping capabilities. In: Proceedings of the 2006 Florida Conference on Recent Advances in Robotics and Robot Showcase, Miami, FL, USA (May 25–26, 2006)
- Norton, R.L.: Design of Machinery. McGraw-Hill, Inc., New York (1992)
- Okada, T.: Computer control of multijointed finger system for precise object-handling. IEEE Transactions on Systems, Man and Cybernetics 12(3), 289–299 (1982)
- Olfati-Saber, R.: Nonlinear Control of Underactuated Mechanical Systems with Application to Robotics and Aerospace Vehicles. Ph. D. thesis, Massachusetts Institute of Technology, Boston, MA, USA (2001)

- Paulos, E.: Trends in grasping. Robotics Grasping Literature Overview (1998)
- Pratt, G.A., Williamson, M.M.: Series elastic actuators. In: Proceedings of the 1995 IEEE/RSJ International Conference on Human Robot Interaction and Cooperative Robots, Pittsburgh, PA, USA, vol. 1, pp. 399–406 (August 5-9, 1995)
- Pringle, A.: Artificial Hand. US Patent No. 1 324 564 (1919)
- Rakic, M.: Multifingered robot hand with selfadaptability. *Robotics and Computer-integrated Manufacturing* 3(2/3), 269–276 (1989)
- Rathbun, D.B., Berg, M.C., Buffinton, K.W.: Piecewise-linear-gain pulse width control for precise positioning of structurally flexible systems subject to stiction and coulomb friction. *ASME Journal of Dynamic Systems, Measurement, and Control* 126(1), 139–143 (2004a)
- Rathbun, D.B., Berg, M.C., Buffinton, K.W.: Pulse width control for precise positioning of structurally systems subject to stiction and coulomb friction. *ASME Journal of Dynamic Systems, Measurement, and Control* 126(1), 131–138 (2004b)
- Reuleaux, F.: The kinematics of machinery. In: Kennedy, A.B.W. (ed.) *Outlines of a theory of machines*, Dover Publications, New-York (1963)
- Reynaerts, D.: Control Methods and Actuation Technology for Whole-Hand Dexterous Manipulation. Ph. D. thesis, Faculty of Engineering, Dept. of Mechanical Engineering, Katholieke Universiteit Leuven, Heverlee, Belgium (May 1995)
- Robinson, G., Davies, J.B.C.: The amadeus project: an overview. *Industrial Robot* 24(4), 290–296 (1997)
- Rosheim, M.E.: *Robot Evolution: The Development of Anthrobotics*. John Wiley and Sons, Inc., Chichester (1994)
- Rovetta, A.: On functionality of a new mechanical hand. *ASME Journal of Mechanical Design* 103, 277–280 (1981)
- Rovetta, A., Franchetti, I., Vicentini, P.: Multi-Purpose Mechanical Hand. US Patent No. 4 351 553 (1982)
- Rubinger, B., Brousseau, M., Lymer, J., Gosselin, C., Laliberté, T., Piedboeuf, J.-C.: A novel robotic hand-sarah for operations on the international space station. In: ASTRA 2002. Proceedings of the 7th Workshop on Advanced Space Technologies for Robotics and Automation, Noordwijk, The Netherlands (November 19-21, 2002)
- Rubinger, B., Fulford, P., Gregoris, L., Gosselin, C., Laliberté, T.: Self-adapting robotic auxiliary hand (sarah) for spdsm operations on the international space station. In: i-SAIRAS 2001. Proceedings of the 6th International Symposium on Artificial Intelligence and Robotics and Automation in Space, Saint-Hubert, QC, Canada, pp. 18–22 (June 18-22, 2001)
- Saliba, M.A., de Silva, C.W.: An innovative robotic gripper for grasping and handling research. In: Proceedings of the 1991 International Conference on Industrial Electronics, Control and Instrumentation, Kobe, Japan, pp. 975–979 (November 1991)
- Salisbury, J.K., Craig, J.J.: Articulated hands: Force control and kinematic issues. *The International Journal of Robotics Research* 1(1), 4–17 (1982)
- Salisbury, K.: Whole arm manipulation. In: Proceedings of the 4th International Symposium on Robotics Research, Santa Cruz, CA, USA, pp. 183–189 (August 9-14, 1987)
- Schlesinger, G.: *Ersatzglieder und Arbeitshilfen*. Springer, Heidelberg (1919)
- Schulz, S., Pylatiuk, C., Bretthauer, G.: A new ultralight anthropomorphic hand. In: Proceedings of the 2001 IEEE International Conference on Robotics and Automation, Seoul, Korea, pp. 2437–2441 (May 21-26, 2001)

- Shimojima, H., Yamamoto, K., Kawakita, K.: A study of grippers with multiple degrees of mobility. *JSME International Journal* 30(261), 515–522 (1987)
- Sie, L., Gosselin, C.: Dynamic simulation and optimization of underactuated robotic fingers. In: Proceedings of the 2002 ASME Design Engineering Technical Conference and Computers in Engineering Conference, Montreal, Canada (September 29–October 2, 2002)
- Son, J.S., Howe, R.D.: Tactile sensing and stiffness control with multifingered hands. In: Proceedings of the 1996 IEEE International Conference on Robotics and Automation, Minneapolis, MN, USA, pp. 3228–3233 (April 1996)
- Spellerberg, E.: Artificial Arm. US Patent No. 42 515 (1864)
- Strang, G.: Linear Algebra and its Applications. Harcourt Brace Jovanovich College Publishers (1986)
- Tanikawa, T., Arai, T.: Development of a micro-manipulation system having two-fingered micro-hand. *IEEE Transactions on Robotics and Automation* 15(1), 152–162 (1999)
- Townsend, W.: The barrett hand grasper - programmably flexible part handling and assembly. *Industrial Robot* 27(3), 181–188 (2000)
- Tubiana, R., Thomine, J.-M.: La main, anatomie fonctionnelle et examen clinique. Masson, Paris (1990)
- Ullmann, E., Cepolina, F., Zoppi, M.: Upper limb prosthetics for developing countries. In: Proceedings of the 2004 International Conference on Intelligent Manipulation and Grasping, Genova, Italy, pp. 225–226 (July 2004)
- Ulrich, N., Kumar, V.: Grasping using fingers with coupled joints. *ASME Trends and Developments in Mechanisms* 3, 201–207 (1988)
- Ulrich, N.T.: Methods and Apparatus for Mechanically Intelligent Grasping. US Patent No. 4 957 320 (1988)
- Williamson, M.M.: Series elastic actuators. Master's thesis, Massachusetts Institute of Technology, Artificial Intelligence Laboratory, Boston, MA, USA (February 1995)
- Yang, J., Abdel-Malek, K., Pitarch, E.P.: Design and analysis of a cable actuated hand prosthesis. In: Proceedings of the 2004 ASME Design Engineering Technical Conference and Computers in Engineering Conference, Salt Lake City, UT, USA (September 28–October 2, 2004)
- Yang, J., Pitarch, E.P., Abdel-Malek, K., Patrick, A., Lindkvist, L.: A multi-fingered hand prosthesis. *Mechanism and Machine Theory* 39(6), 555–581 (2004)
- Yoshida, K., Nakanishi, H.: The tako (target collaborativize) flyer: a new concept for future satellite servicing. In: i-SAIRAS 2001. Proceedings of the 6th International Symposium on Artificial Intelligence and Robotics & Automation in Space, Saint-Hubert, QC, Canada (June 18–22, 2001)
- Yoshikawa, T.: Control algorithm for grasping and manipulation by multifingered robot hands using virtual truss model representation of internal force. In: Proceedings of the 2000 IEEE International Conference on Robotics and Automation, San Francisco, CA, USA, pp. 369–376 (April 24–28, 2000)
- Zatsiorsky, V.M., Latash, M.L., Gao, F., Shim, J.K.: The principle of superposition in human prehension. *Robotica* 22(2), 231–234 (2004)
- Zecca, M., Cappiello, G., Sebastiani, F., Roccella, S., Vecchi, F., Carrozza, M.C., Dario, P.: Experimental analysis of the proprioceptive and exteroceptive sensors of an underactuated prosthetic hand. *International Journal of Human-friendly Welfare Robotic Systems* 4(4), 2–6 (2003)

- Zhang, H., Chen, N.N.: Control of contact via tactile sensing. *IEEE Transactions on Robotics and Automation* 16(5), 482–495 (2000)
- Zhang, Y., Han, H., Zhang, H., Shang, X., Wang, T., Guo, W., Gruver, W.A.: Design and control of the buaa four-fingered hand. In: Proceedings of the 2001 IEEE International Conference on Robotics and Automation, Seoul, Korea, pp. 2517–2522 (May 21–26, 2001)
- Zhao, J., Xie, Z., Jiang, L., Cai, H., Liu, H., Hirzinger, G.: Levenberg-marquardt based neural network control for a five-fingered prosthetic hand. In: Proceedings of the 2005 IEEE International Conference on Robotics and Automation, Barcelona, Spain, pp. 4493–4498 (April 2005)

Index

- Abduction/adduction, 34, 39, 172, 210
- ABS, 17
- Anthropomorphic, 2, 4, 8, 11, 12, 31
- Argonne Laboratory, 8
- Arm/Gripper Coupling Mechanism, 18
- Asymptote, 72, 84, 87, 90–92, 127
- Bartholet, Stephen J., 175, 176
- Base spring, 215, 216
- Bekey, George A., 20
- Bio-compatible, 160
- Biologically-inspired, 11, 14
- Biomimetic, 10, 62
- Bubble matrix, 151, 223, 225
- Calibration, 190, 195
- Canadarm, 25, 181
- Canadian Space Agency, 25, 186, 187
- Carrozza, Maria C., 19, 21
- Chopstick, 8
- Circuit, 17, 195–197
- Classification, 173, 196
- Closing sequence, 15, 23, 34, 49, 61, 67, 72, 75, 83, 91, 99, 112, 115, 139, 177, 179, 190, 206
- Codex Atlanticus, 29, 55
- Cofactor, 46, 217
 - matrix, 217
- Compliant, 2, 11, 22, 23, 160, 161, 200, 211, 212
- Conic, 71
- Conjecture, 74, 168
- Control, 1, 3–5, 8, 10, 13, 14, 26, 53, 65, 94, 118, 143, 145, 166, 168, 171, 178, 179, 181, 186–188, 190–192, 194, 195, 197–200, 204–207, 209, 211, 212
- Damping, 200
- Flow, 188
- Force, 4, 34, 75, 121, 160, 168, 171, 191, 194, 198–200, 203, 205, 207, 211
- Friction, 53, 198
- Fuzzy logic, 4, 198–202, 205, 207, 211
- Impedance, 194
- Impulse, 206
- PID, 190, 198–200
- Position, 190, 191
- Voltage controlled resistor, 197
- Conversion chart, 89
- Cosmetic glove, 22
- CSA Automation and Robotic Testbed, 25, 186, 187, 189
- Cyberhand Consortium, 17
- Da Vinci, Leonardo, 28–31, 55–58
- Dale, Frank L., 26
- Davies, Bruce J.C., 21
- Degeneracy, 77, 81, 108, 110
 - analysis, 108, 111
 - condition, 81, 108–111
 - local, 81, 111
 - location, 82
 - locus, 110
 - non-degeneracy, 77
 - planes, 108, 111

- spring condition, 77, 82
- surfaces, 110, 111
- Design rules, 3, 5, 62, 102, 117, 131, 137, 138, 210
- Dexterity, 8, 23, 34, 120
- Differential systems, 1, 3, 11, 16, 17, 24, 25, 139, 140, 143, 144, 146–148, 150, 152, 156–158, 160, 165, 168, 169, 178, 179, 183, 187, 206
- Dilemma, 4, 7, 10, 13, 202
- Dillmann, Rüdiger, 21
- Direct optimal problem, 120, 122
- Disengaging cam mechanism, 23, 175, 176
- Double gain, 197
- Double-stage mechanism, 50, 51, 54, 58
- Edsinger, Aaron, 212
- Ejection, 4, 5, 34, 61–63, 70, 72, 75, 81–83, 85, 87, 92, 95–98, 100, 103, 104, 115, 117, 118, 125, 126, 128, 130, 131, 137, 138, 210
- Closing-ejection, 77, 82, 85, 87, 88, 126–128, 130, 135, 137
- Opening-ejection, 75, 81, 82, 85, 87, 107, 115, 126, 127, 130, 137
- prevention guidelines, 117, 125, 126
- Elephant trunks, 14
- Elliptic filters, 197
- Equilibrium, 36, 47, 48, 59, 61, 68, 70, 73, 75, 81, 83, 97, 100, 102, 103, 107, 112, 114, 115, 120, 130, 210
- condition, 59, 90, 112–114
- configuration, 48, 75, 90, 103, 110
- curve, 74, 75, 78–84, 87, 88, 90–93, 95, 97, 106, 107, 114, 127–129, 135
- equation, 72, 77, 80, 81, 108, 110
- hypersurface, 74, 106
- impossible, 77, 81, 87, 111
- kinematic, 104, 137
- limit, 75
- location, 75, 77, 82, 85, 90–92, 108, 111, 135
- locus, 77, 78, 80, 82
- order, 61, 98
- paradoxical, 82, 110, 111
- peculiar, 3, 110
- point, 68, 69, 72, 74, 75, 77, 129
- position, 47, 68, 70, 72, 81–84, 95, 105, 112
- situation, 61, 66, 72
- state, 78
- static, 45, 61, 62, 64, 79, 81, 90, 92, 98, 108, 110, 112, 156, 168, 202, 210
- surface, 3, 103–110, 113, 114
- Evil twin, 53, 81
- Extravehicular activities, 172, 183, 185, 186
- Faraday, Michael, 28
- Feedback
 - electronic, 159
 - perceptual, 8
 - resistor, 195, 196
 - sensorial, 193
 - tactile, 8, 198
 - visual, 8, 193
- Field effect transistor, 197
- Floating platform, 165, 166
- Force design, 119
- Force isotropy, 117–125, 128–130, 138, 142, 145, 147, 148, 154–159, 163, 164, 210
 - configuration, 119–123, 135, 157
 - design, 121, 125, 126, 156–158
 - equation, 121
 - grasp, 117
 - point, 125
 - surface, 122–125
- Force sensing resistors, 194–196, 201, 202, 206
- Force-closure, 45, 64
- Form-closure, 45, 64
- Four-bar linkage, 26, 28, 40, 54, 55, 75, 102, 132, 197
- Frenet-Serret manipulators, 14
- Friction, 10, 14, 37, 39, 44, 45, 60, 65, 67, 68, 78–82, 91, 93, 95–98, 101, 102, 112, 115, 128, 135, 185, 198, 206, 210
 - coefficient, 37, 39, 79, 93, 95, 96, 194, 195
 - compensation, 198
 - cone, 36, 37, 79
- Frontier
 - attractive, 72, 74, 75, 81, 127
 - repulsive, 72, 74, 81
- Fused deposition modelling, 17, 129, 164, 189

- Gazeau, Jean-Pierre, 12
 Gears, 2, 10, 14, 17, 24–26, 41, 54, 55, 58,
 131, 146–148, 154, 156, 177–180,
 185, 187
 Gordian knot, 13
 Grasp matrix, 43
 Grasp-state, 45, 46, 48, 49, 58, 65, 71, 72,
 74, 75, 83, 84, 86, 90, 92, 93, 103,
 106–108, 115, 121, 125, 133, 135,
 157, 159, 210
 line, 107
 plane, 65, 79, 81–83, 87, 88, 90–92,
 95–97, 102, 106–108, 125, 127–129,
 210
 reduced, 106
 space, 3, 45, 46, 61, 75, 88, 89, 103,
 106, 107, 109, 110, 112, 114, 131,
 135, 138, 210
 trajectory, 3, 49, 61, 66, 70, 72–75,
 80–84, 86–88, 90–92, 95, 102–108,
 111–113, 115, 127, 130, 210
 variable, 83, 105, 114
- Hand
 100G, 18, 19
 AMADEUS, 8, 9, 21
 ASI, 9, 13, 14
 BarrettHand, 8, 9, 20
 Beijing, 9
 Belgrade/USC, 8, 9, 17, 20, 25
 Bologna, 9, 12, 21
 Cassino, 14
 Cyberhand, 18, 21
 DLR, 8–10, 12
 DOMO, 212
 Gifu, 9
 Goldfinger, 9, 13
 JPL LEMUR, 17, 20, 23
 Karlsruhe, 8, 9, 21
 LAR-DEIS, 9
 LMS, 9, 12
 MARS, 9, 20, 23, 25, 171, 177–179,
 181, 189–196, 206, 207
 MEL, 8
 Odetics, 23
 Okada, 8, 9
 Omni-Hand, 9, 12
 Robonaut, 9, 12
 RTR, 9, 17, 19
 Salisbury, 8–10, 12
- SARAH, 9, 17, 20, 24, 95, 171,
 178–191, 206, 207, 211
 Shadow, 9, 12
 Soft Gripper, 9, 17–19, 26, 51, 56–58,
 67, 74, 122, 126
 Southampton, 25
 SPRING, 9, 17, 19
 SSL, 14
 TAKO, 18, 21
 TBM, 25
 TUAT, 17, 28
 TU Delft, 19
 Utah/MIT, 8–10, 12
- Handyman, 8
 Henning, Frederick C., 27
 Herder, Just L., 19
 Hirose, Shigeo, 11, 19
 Hirzinger, Gerhard, 12
 Holy Grail, 8
 Hyper-configuration, 70, 82
 Hyper-parallelepiped, 46
 Hyperbola, hyperbolic, 71, 83, 84
 Hyperbox, 50
 Hyperdifferential, 178–180
 Hyperextension, 15, 68–70, 72, 84, 85, 99,
 102, 112, 118, 132
 Hyperflexion, 68–70, 72, 84, 99, 102, 112,
 118, 132
 Hypersurface, 46, 210
- Indices, 2, 34, 49, 50, 58, 60, 120, 125
 Inertia, 15, 73
 Input resistor, 196
 Institute of Electrical and Electronics
 Engineers, 11
 Interlink Electronics, 195
 International Federation for the Theory
 of Machines and Mechanisms, 11,
 16, 140, 144
 International Space Station, 25, 181, 182,
 184
 Inverse optimal problem, 120, 122, 125
- Jacobian matrix, 2, 43, 59, 159, 209, 216
 Jacquot-Droz, Pierre, 8
 Jerk increase, 205
- Kaneko, Makoto, 19
 Kennedy's Theorem, 40, 197
 Kinematic design, 119

- Kronecker symbol, 49, 125, 134
 Krut, Sébastien, 121
- Lag time, 18, 197
 Lyapunov
 potential function, 74
 stability theory, 74
- Machinery's Handbook, 79
 MDA Space Missions, 25, 181, 182, 184
 Mechanical intelligence, 1, 14
 Melchiorri, Claudio, 12, 13
 Mono-directionality, 10, 22, 67
 Mosher, Ralph, 8
 Motorola, 197
 Musicienne, La, 8
- Negative-stiffness spring, 22
 NiTiNol, 160
 Noise, 194, 195, 197
 Non-backdrivable, 179, 198
- Object recognition, 195
 Operational amplifier, 195–197
 Orbital Replacement Unit, 185
- Palpation, 200
 Paradoxical point, 74
 Potentiometers, 195–197, 204
 Pringle, Alexander, 24, 31
 Prosthetics, 11, 17, 18, 21, 22, 25, 26, 28,
 53, 164, 165, 168, 188, 211, 213
- Quadratic, 119
 Quartic, 86
 Quasi-static, 112, 113
- Real-time, 4, 197, 207, 211
 Reciprocal screw product, 35
 Reflex, 205
 Release tendon, 63
 Renaissance, 28
 Return cable, 28, 63, 125
 Reynaerts, Dominiek, 173
 Roll-back phenomenon, 49
 Rosheim, Mark, 12
- Salisbury, J. Kenneth, 12
 Screw theory, 2, 34
 Seesaw mechanism, 17, 18, 25, 28, 143,
 144, 154–156, 158, 165
- Segmentation technique, 89
 Self-posture changeability, 62, 72
 Serial architecture/manipulator, 8, 43,
 120
- Series elastic actuators, 212
 Shape adaptation, 1, 4, 7, 14, 15, 17, 22,
 23, 28, 49, 60, 61, 81, 118, 176, 204,
 211, 212
- Shape memory alloy, 160
 Sharf, Inna, 187
 Singular configurations, 58, 59, 99, 105
 Skill crane machine, 94
 Slider-crank linkage, 197
 Slippage, 4, 194, 201, 202, 204, 205, 207,
 211
- Snake robots, 2, 14
 Space Station Remote Manipulator
 System, 181, 183
- Special Purpose Dextrous Manipulator,
 25, 181, 183, 185, 186, 189
- Spellerberg, Edward, 27
 Spring-loaded slider, 166, 167
 SSRMS, 25
 Stability region, 46, 63, 66, 67, 73, 74, 79,
 82, 84, 85, 88, 127, 128, 137
- Swiss Army knife, 23
- T-pipe scheme, 17, 25, 144, 145, 147, 154,
 156
- Tactile sensor, 4, 79, 171, 189, 191,
 193–195, 199, 201, 206, 207, 211
 data inversion, 195
- Telemanipulation/telemanipulator, 8
- Tentacle manipulators, 2, 14
- Thickness, 39, 79, 80, 95, 96, 115
- TITAN VII, 143
- Townsend, William T., 20
- Transmission
 angle, 132
 coefficient, 81, 121, 215
 design, 34
 equivalence, 53–55, 57, 139
 factor, 63, 65, 90, 97, 123, 125, 127
 force matrix, 141, 143, 145, 147, 150,
 152, 153, 155, 156, 158, 161, 162,
 164, 167, 168, 218, 221
- force ratio, 142–144, 155, 159, 163, 164
- matrix, 2, 3, 41, 44, 59, 97, 141, 159,
 169, 209, 211, 215, 216

- mechanism, 34, 37, 40, 41, 50, 58, 130, 135, 138, 177, 197, 198, 212
principle, 40
ratio, 41, 77, 90–92, 128, 135, 177
stage, 40, 56, 150, 156, 218, 221
tree, 3, 148–151, 154, 155, 160, 161, 163, 164, 169, 211, 218, 219, 221–224
Twist, 35, 36
United Kingdom Atomic Energy Authority, 188
Validation/validity surfaces, 106, 112, 113, 210
Vassura, Gabriele, 12, 13, 21
Virtual power, 34, 215
Walker, Ian D., 13
Walker, Rich, 12
Wheatstone bridge, 195
Whole-arm manipulation, 14
Whole-hand grasping, 34, 50
Windsor Royal Collection Folios, 30
Wrench, 14, 33, 35, 37, 43, 95
Wrist, 8
Wrist-bracing, 17
Yoshida, Kazuya, 21

Springer Tracts in Advanced Robotics

Edited by B. Siciliano, O. Khatib and F. Groen

- Vol. 40:** Birglen, L.; Laliberté, T.; Gosselin, C.
Underactuated Robotic Hands
241 p. 2008 [978-3-540-77458-7]
- Vol. 39:** Khatib, O.; Kumar, V.; Rus, D. (Eds.)
Experimental Robotics
563 p. 2008 [978-3-540-77456-3]
- Vol. 38:** Jefferies, M.E.; Yeap, W.-K. (Eds.)
Robotics and Cognitive Approaches to
Spatial Mapping
328 p. 2008 [978-3-540-75386-5]
- Vol. 37:** Ollero, A.; Maza, I. (Eds.)
Multiple Heterogeneous Unmanned Aerial
Vehicles
233 p. 2007 [978-3-540-73957-9]
- Vol. 36:** Buehler, M.; Iagnemma, K.;
Singh, S. (Eds.)
The 2005 DARPA Grand Challenge – The Great
Robot Race
520 p. 2007 [978-3-540-73428-4]
- Vol. 35:** Laugier, C.; Chatila, R. (Eds.)
Autonomous Navigation in Dynamic
Environments
169 p. 2007 [978-3-540-73421-5]
- Vol. 34:** Wisse, M.; van der Linde, R.Q.
Delft Pneumatic Bipeds
136 p. 2007 [978-3-540-72807-8]
- Vol. 33:** Kong, X.; Gosselin, C.
Type Synthesis of Parallel
Mechanisms
272 p. 2007 [978-3-540-71989-2]
- Vol. 32:** Milutinović, D.; Lima, P.
Cells and Robots – Modeling and Control of
Large-Size Agent Populations
130 p. 2007 [978-3-540-71981-6]
- Vol. 31:** Ferre, M.; Buss, M.; Aracil, R.;
Melchiorri, C.; Balaguer C. (Eds.)
Advances in Telerobotics
500 p. 2007 [978-3-540-71363-0]
- Vol. 30:** Brugali, D. (Ed.)
Software Engineering for Experimental Robotics
490 p. 2007 [978-3-540-68949-2]

- Vol. 29:** Secchi, C.; Stramigioli, S.; Fantuzzi, C.
Control of Interactive Robotic Interfaces – A
Port-Hamiltonian Approach
225 p. 2007 [978-3-540-49712-7]
- Vol. 28:** Thrun, S.; Brooks, R.; Durrant-Whyte, H.
(Eds.)
Robotics Research – Results of the 12th
International Symposium ISRR
602 p. 2007 [978-3-540-48110-2]
- Vol. 27:** Montemerlo, M.; Thrun, S.
FastSLAM – A Scalable Method for the
Simultaneous Localization and Mapping
Problem in Robotics
120 p. 2007 [978-3-540-46399-3]
- Vol. 26:** Taylor, G.; Kleeman, L.
Visual Perception and Robotic Manipulation – 3D
Object Recognition, Tracking and Hand-Eye
Coordination
218 p. 2007 [978-3-540-33454-5]
- Vol. 25:** Corke, P.; Sukkarieh, S. (Eds.)
Field and Service Robotics – Results of the 5th
International Conference
580 p. 2006 [978-3-540-33452-1]
- Vol. 24:** Yuta, S.; Asama, H.; Thrun, S.;
Prassler, E.; Tsubouchi, T. (Eds.)
Field and Service Robotics – Recent Advances in
Research and Applications
550 p. 2006 [978-3-540-32801-8]
- Vol. 23:** Andrade-Cetto, J.; Sanfeliu, A.
Environment Learning for Indoor Mobile Robots
– A Stochastic State Estimation Approach
to Simultaneous Localization and Map Building
130 p. 2006 [978-3-540-32795-0]
- Vol. 22:** Christensen, H.I. (Ed.)
European Robotics Symposium 2006
209 p. 2006 [978-3-540-32688-5]
- Vol. 21:** Ang Jr., H.; Khatib, O. (Eds.)
Experimental Robotics IX – The 9th International
Symposium on Experimental Robotics
618 p. 2006 [978-3-540-28816-9]
- Vol. 20:** Xu, Y.; Ou, Y.
Control of Single Wheel Robots
188 p. 2005 [978-3-540-28184-9]

- Vol. 19:** Lefebvre, T.; Bruyninckx, H.; De Schutter, J. Nonlinear Kalman Filtering for Force-Controlled Robot Tasks 280 p. 2005 [978-3-540-28023-1]
- Vol. 18:** Barbagli, F.; Prattichizzo, D.; Salisbury, K. (Eds.) Multi-point Interaction with Real and Virtual Objects 281 p. 2005 [978-3-540-26036-3]
- Vol. 17:** Erdmann, M.; Hsu, D.; Overmars, M.; van der Stappen, F.A (Eds.) Algorithmic Foundations of Robotics VI 472 p. 2005 [978-3-540-25728-8]
- Vol. 16:** Cuesta, F.; Ollero, A. Intelligent Mobile Robot Navigation 224 p. 2005 [978-3-540-23956-7]
- Vol. 15:** Dario, P.; Chatila R. (Eds.) Robotics Research – The Eleventh International Symposium 595 p. 2005 [978-3-540-23214-8]
- Vol. 14:** Prassler, E.; Lawitzky, G.; Stopp, A.; Grunwald, G.; Hägele, M.; Dillmann, R.; Iossifidis, I. (Eds.) Advances in Human-Robot Interaction 414 p. 2005 [978-3-540-23211-7]
- Vol. 13:** Chung, W. Nonholonomic Manipulators 115 p. 2004 [978-3-540-22108-1]
- Vol. 12:** Iagnemma K.; Dubowsky, S. Mobile Robots in Rough Terrain – Estimation, Motion Planning, and Control with Application to Planetary Rovers 123 p. 2004 [978-3-540-21968-2]
- Vol. 11:** Kim, J.-H.; Kim, D.-H.; Kim, Y.-J.; Seow, K.-T. Soccer Robotics 353 p. 2004 [978-3-540-21859-3]
- Vol. 10:** Siciliano, B.; De Luca, A.; Melchiorri, C.; Casalino, G. (Eds.) Advances in Control of Articulated and Mobile Robots 259 p. 2004 [978-3-540-20783-2]
- Vol. 9:** Yamane, K. Simulating and Generating Motions of Human Figures 176 p. 2004 [978-3-540-20317-9]
- Vol. 8:** Baeten, J.; De Schutter, J. Integrated Visual Servoing and Force Control – The Task Frame Approach 198 p. 2004 [978-3-540-40475-0]
- Vol. 7:** Boissonnat, J.-D.; Burdick, J.; Goldberg, K.; Hutchinson, S. (Eds.) Algorithmic Foundations of Robotics V 577 p. 2004 [978-3-540-40476-7]
- Vol. 6:** Jarvis, R.A.; Zelinsky, A. (Eds.) Robotics Research – The Tenth International Symposium 580 p. 2003 [978-3-540-00550-6]
- Vol. 5:** Siciliano, B.; Dario, P. (Eds.) Experimental Robotics VIII – Proceedings of the 8th International Symposium ISER02 685 p. 2003 [978-3-540-00305-2]
- Vol. 4:** Bicchi, A.; Christensen, H.I.; Prattichizzo, D. (Eds.) Control Problems in Robotics 296 p. 2003 [978-3-540-00251-2]
- Vol. 3:** Natale, C. Interaction Control of Robot Manipulators – Six-degrees-of-freedom Tasks 120 p. 2003 [978-3-540-00159-1]
- Vol. 2:** Antonelli, G. Underwater Robots – Motion and Force Control of Vehicle-Manipulator Systems 268 p. 2006 [978-3-540-31752-4]
- Vol. 1:** Caccavale, F.; Villani, L. (Eds.) Fault Diagnosis and Fault Tolerance for Mechatronic Systems – Recent Advances 191 p. 2003 [978-3-540-44159-5]